



**HAL**  
open science

# Matrix-bound delivery of BMP-2 from a biomimetic film : protein structure, long-term stability and cellular uptake

Flora da Silva Gilde

## ► To cite this version:

Flora da Silva Gilde. Matrix-bound delivery of BMP-2 from a biomimetic film : protein structure, long-term stability and cellular uptake. Other. Université de Grenoble, 2014. English. NNT : 2014GRENI083 . tel-01389964

**HAL Id: tel-01389964**

**<https://theses.hal.science/tel-01389964v1>**

Submitted on 31 Oct 2016

**HAL** is a multi-disciplinary open access archive for the deposit and dissemination of scientific research documents, whether they are published or not. The documents may come from teaching and research institutions in France or abroad, or from public or private research centers.

L'archive ouverte pluridisciplinaire **HAL**, est destinée au dépôt et à la diffusion de documents scientifiques de niveau recherche, publiés ou non, émanant des établissements d'enseignement et de recherche français ou étrangers, des laboratoires publics ou privés.

## THÈSE

Pour obtenir le grade de

### DOCTEUR DE L'UNIVERSITÉ DE GRENOBLE

Spécialité : **Matériaux, Mécanique, Génie civil, Electrochimie**

Arrêté ministériel : 7 août 2006

Présentée par

**Flora da Silva Gilde**

Thèse dirigée par **Catherine PICART**

préparée au sein du **Laboratoire des Matériaux et du Génie Physique**  
dans l'**École Doctorale I-MEP<sup>2</sup> : Ingénierie – Matériaux, Mécanique, Environnement, Energétique, Procédés, Production**

## Présentation de la BMP-2 par un film biomimétique : structure de la protéine, stabilité à long terme et internalisation cellulaire

Thèse soutenue publiquement le **25 Novembre 2014**,  
devant le jury composé de :

**Mr Pierre LAYROLLE**

Directeur de Recherche, INSERM, Nantes

Rapporteur

**Mr Josep SAMITIER**

Professor, University of Barcelona, Espagne

Rapporteur

**Mme Corinne ALBIGÈS-RIZO**

Directrice de Recherche, CNRS, Grenoble

Président du jury

**Mr Thomas MUELLER**

Professor, University of Wuerzburg, Allemagne

Examineur

**Mme Delphine LOGEART-AVRAMAGLOU**

Chargée de Recherche, CNRS, Paris

Examineur

**Mr Oommen VARGHESE**

Assitant Professor, Uppsala University, Suède

Examineur

**Mme Catherine PICART**

Professeur des Universités,  
Institut Polytechnique de Grenoble, Grenoble

Directeur de Thèse





**Matrix-bound delivery of BMP-2 from a biomimetic film:  
protein structure, long-term stability and cellular uptake**





## Acknowledgments

I first thank my advisor, Pr Catherine Picart, for the patient guidance, encouragement and advice she has provided throughout the three past years. I must say that I have been extremely lucky to have a supervisor who cared so much about my work, and who responded to my questions and queries so promptly.

I would like to thank Dr Pierre Layrolle and Dr Josep Samitier for the honor they made me by accepting to evaluate my work, and Dr Delphine Logeart-Avramoglou, Dr Corinne Albigès-Rizo, Dr Thomas Mueller and Dr Oommen Varghese, for accepting to participate in the thesis committee.

I also thank Corinne for her precious advices and collaboration in this work. I am equally grateful to Dr Thomas Boudou and Dr Olivier Destaing for the fruitful discussions and advice.

I recognize that this research would not have been possible without the financial assistance of the European Commission via an ERC Starting grant 2010 (GA 259370, BIOMIM) and the ANR-EmergenceBIO grant (ANR-09-EBIO-012-01). I thank Virginie Charrière, Josiane Viboud, Michèle San Martin and Nicole Douard for their administrative assistance.

I would like to thank three great engineers, Isabelle Paintrand, Fabien Dalonneau and Raphael Guillot, from who I learned a lot and for providing an excellent technical/scientific support to my work. I am deeply grateful to Dr Laure Fourel, Dr Ofélia Maniti and Dr Thomas Crouzier who guided me in the beginning of my work giving me the opportunity to learn from them. In particular, Laure provided great help in the last part of the work, namely with the cell transfections with siRNA.

I am really grateful to all the extraordinary colleagues I have met in the lab, not only for the scientific exchanges but also for the excellent work environment. A special thank you to Clairette, Fabien, Claire, Jorge, Colette, Sofia, Xiqiu, Benoit, Quentin, Naresh, Pauline, Seb, Sophie, Marie, Nick, Thomas, Lijie, Anne, Laure, Mélanie, Varvara, Louis and Lucile. I also had the pleasure to collaborate with Takaharu Okada from Japan and I thank him for his help in my work.

I must express my gratitude to all my family, in particular to my parents, Elisabete and Nelson, and to my brother Rafael that even being far away they have supported me in the ups and downs of my life. A special thank you to my partner, Raph, for the kind and continuous support, patience and encouragement. Thank you for being always there for me.

Finally, I thank my beloved friends from more or less far away: Sara, Liz, Ana Sofia, Helena, Vanessa, Marta and Paula. Thank you for making so many ordinary moments, extraordinary!



## Abbreviations

### Materials / Chemicals

Al<sub>2</sub>O<sub>3</sub>: Alumina  
BCP: Biphasic Calcium Phosphate  
Bioglass: Bioactive glass  
CPZ: Chlorpromazine  
CaP: Calcium Phosphate  
Co-Cr: Cobalt-Chromium alloys  
DMSO: Dimethylsulfoxide  
DYN: Dynasore  
EDC: 1-Ethyl-3-(3-dimethylamino-propyl) carbodiimide  
FBS: Fetal Bovine Serum  
GST: Genistein  
HA: Hyaluronic Acid or sodium hyaluronate  
HAP: Hydroxyapatite  
HEPES: 4-(2-Hydroxyethyl)-1-piperazine ethane sulfonic acid  
LbL: Layer-by-Layer  
MβCD: Methyl-β-cyclodextrin  
NaCl: Sodium Chloride  
NYS: Nystatin  
PBS: Phosphate buffered saline  
PCL: Polycaprolactone  
PE: Polyethylene  
PEEK: Polyetheretherketone  
PEI: Poly(ethylenimine)  
PEM: Polyelectrolyte multilayer films  
PGA: Polyglycolic acid  
PLA: Polylactic acid  
PLL: Poly(L-lysine)  
PLGA: Poly(lactic-co-glycolic acid)  
PMMA: Polymethyl meta acrylate  
PTFE: Poly Tetra Fluorethylene  
S-NHS: N-hydroxysulfo succinimide  
TBS: TRIS-Buffered Saline  
TCP: Tricalciumphosphate  
Ti: Titanium  
TiO<sub>2</sub>: Titanium Oxide  
Ti6Al4V: Titanium-aluminum-vanadium alloy

TRIS: 2-Amino-2-hydroxymethyl-propane-1,3-diol

ZrO<sub>2</sub>: Zirconia

### Techniques and equipment

CLSM: Confocal Laser Scanning Microscopy  
FRAP: Fluorescence Recovery after Photobleaching  
FTIR: Fourier Transform Infrared spectroscopy  
SEM: Scanning Electron Microscopy

### Proteins and cells

ALP: Alkaline Phosphatase  
BMP: Bone Morphogenic Protein  
BSA: Bovine Serum Albumin  
Cav-1: Caveolin-1  
CCPs: Clathrin-coated pits  
CHC: Clathrin Heavy-Chain  
DM: Differentiation Medium  
DMEM: Dulbecco's Modified Eagle's Medium  
Dyn-2: Dynamin-2  
ECM: Extracellular Matrix  
FBS: Fetal Bovine Serum  
GF: Growth Factor  
GM: Growth Medium  
MSC: Mesenchymal Stem Cells  
PM: Plasma Membrane  
RGD: Arginine - Glycine – Asparagine  
rhBMP-2: Human Recombinant Bone Morphogenic Protein-2  
siRNA: Small Interfering RNA  
TGF: Transforming Growth Facto



## Glossary

**Collagen:** the main structural protein of the various connective tissues in animals, being the most abundant protein in mammals. Fibrous protein found in bone, cartilage, skin, and other connective tissue. Collagens have great tensile strength, and provide these body structures with the ability to withstand forces that stretch them. Collagens consist of three polypeptide chains arranged in a triple helix, and are bundled together in fibers.

**Elastic Modulus,  $E_0$**  (Young's modulus in Pascal): it represents the stiffness of a material. It is defined as the ratio of tensile stress to tensile strain. It is the tendency of an object to deform along an axis when opposing forces are applied along that axis.

**Glycosaminoglycans, GAGs:** the most abundant heteropolysaccharides in the body. These molecules are long unbranched polysaccharides containing a repeating disaccharide unit. GAGs are highly negatively charged molecules with extended conformation. GAGs are located primarily on the surface of cells or in the extracellular matrix (ECM). Along with the high viscosity of GAGs solution comes low compressibility, which makes these molecules ideal for a lubricating fluid in the joints. At the same time, their rigidity provides structural integrity to cells and provides passageways between cells, allowing for cell migration. The specific GAGs of physiological significance are hyaluronic acid (the only non-sulfated GAG), dermatan sulfate, chondroitin sulfate, heparin, heparan sulfate, and keratan sulfate.

**Osteoconduction:** means that bone grows on a surface. An osteoconductive material supports bone growth and encourages the ingrowth of surrounding bone. It allows bone growth not only on its surface but down into pores, channels or pipes.

**Osteoinduction:** the process by which osteogenesis is induced. Growth factors trigger the differentiation of mesenchymal stem cells or muscle precursors into osteoblastic lineages.

**Osteointegration:** stable anchorage of an implant achieved by new bone formation around the implant resulting in direct bone-to-implant contact.

**Phosphoproteins:** conjugated proteins in which phosphoric acid is esterified with a hydroxy amino acid.

**Sialoproteins:** glycoproteins containing sialic acid.



## Table of contents

<b>Acknowledgments.....</b>	<b>5</b>
<b>Abbreviations.....</b>	<b>7</b>
<b>Table of contents.....</b>	<b>14</b>
<b>Glossary.....</b>	<b>9</b>
<b>Chapter I: Introduction.....</b>	<b>15</b>
I.A. BIOMATERIALS FOR BONE REGENERATION .....	16
I.A.1. Bone tissue.....	16
I.A.1.1. Composition and properties of bone .....	16
I.A.1.2. Bone morphogenetic proteins .....	19
I.A.2. Cues for successful bone regeneration around implant material .....	21
I.A.3. Biomaterials for bone-graft substitutes or prosthetic implants.....	22
I.A.3.1. Evolution in the development of biomaterials .....	22
I.A.3.2. Polymers.....	25
I.A.3.2. Ceramics.....	26
I.A.3.3. Metals.....	29
I.A.3.4. General comparison between the types of biomaterials.....	30
I.A.4. Surface modifications of titanium implants.....	31
I.A.4.1. Mechanical, chemical and physical modifications .....	32
I.A.4.2. Coating with biomimetic hydroxyapatite (HAP) layer .....	33
I.B. BONE TISSUE ENGINEERING APPROACHES .....	35
I.B.1. Scaffold / Stem cells .....	37
I.B.2. Scaffold / Bioactive molecules .....	42
I.B.3. Summary of the remaining limitations and challenges in BTE .....	45
I.B.4. Requirements for clinical translation .....	47
I.B.5. Development of osteoinductive coatings .....	49
I.B.5.1. Grafting of BMP-2 onto a material surface.....	49
I.B.5.2. Biomimetic coatings as reservoirs for BMP-2 .....	52
I.B.5.3. Polyelectrolyte's multilayer (PEM) films .....	54
I.C. SIGNALING BY RECEPTORS: THE CASE OF BMP-2 .....	60
I.C.1. BMP receptors and signaling .....	60



I.C.2. Endocytosis and signal transduction: intertwined processes .....	64
I.C.2.1. Endocytic pathways.....	64
I.C.2.2. BMP receptors endocytosis and relation with signaling .....	66
I.C.2.3. BMP-2 endocytosis .....	68
I.D. OBJECTIVES AND STRATEGIES OF THE PHD THESIS .....	72
<b>Chapter II: Materials and Methods .....</b>	<b>75</b>
II.A. CONSTRUCTION OF PEM FILMS .....	76
II.A.1. BMP-2 and PLL labeling with fluorochrome.....	76
II.A.2. Polyelectrolyte solutions, film buildup and crosslinking .....	76
II.A.3. Loading of BMP-2 in the films .....	78
II.A.4. Film drying, long-term storage and sterilization .....	78
II.B. BMP-2 AND BMP-2-LOADED FILM CHARACTERIZATION.....	78
II.B.1. Fourier Transform Infrared (FTIR) Spectroscopy .....	78
II.B.1.1. Quantitative analysis .....	80
II.B.1.2. PLL/HA film characterization .....	81
II.B.1.3. Characterization of BMP-2 secondary structure in solution.....	82
II.B.1.4. Characterization of BMP-2 secondary structure in (PLL/HA) films.....	82
II.B.2. Fluorescent and confocal microscopy .....	83
II.B.2.1. Epifluorescence microscopy .....	83
II.B.2.2. Confocal microscopy .....	84
II.B.2.3. Fluorescence Recovery after Photobleaching (FRAP) .....	85
II.B.3. Scanning Electron Microscopy (SEM).....	86
II.B.3.1. Visualization of film cross-sections after immunogold labeling of BMP-2 ...	87
II.C. CELL CULTURE .....	87
II.C.1. C2C12 myoblasts culture.....	87
II.C.2. Evaluation of cell response.....	89
II.C.2.1. Principle of immunolabeling and protocol .....	89
II.C.2.1. Treatment with inhibitors of endocytosis .....	90
II.C.2.2. Knock-down of BMP receptors and endocytic proteins using siRNA .....	91
II.C.2.3. Imaging and quantification of internalized BMP-2 by the cells .....	92
II.C.2.4. Early osteogenic differentiation of C2C12 cells: ALP and Smad signaling...	93
II.C.2.5. Statistical analysis.....	95

<b>Chapter III:</b> .....	<b>97</b>
<b>Secondary structure of rhBMP-2 in a protective biopolymeric carrier material</b> .....	<b>97</b>
III.1. ARTICLE SUMMARY .....	98
III.2. ARTICLE 1 (PUBLISHED IN BIOMACROMOLECULES) .....	99
<b>Chapter IV:</b> .....	<b>119</b>
<b>The stability of BMP loaded polyelectrolyte multilayer coatings on titanium</b> .....	<b>119</b>
IV.1. ARTICLE SUMMARY .....	120
IV.2. ARTICLE 2 (PUBLISHED IN BIOMATERIALS).....	122
IV.2.1. Complementary data: structural stability of (PLL/HA) films up to 2.5 years ....	149
<b>Chapter V:</b> .....	<b>151</b>
<b>Matrix-bound delivery of BMP-2 to cells</b> .....	<b>151</b>
V.1. ARTICLE SUMMARY .....	152
V.2. ARTICLE (IN PREPARATION) .....	153
V.2.1. Complementary data .....	180
V.2.1.1. Bioactivity of fluorescently labeled BMP-2.....	180
V.2.1.2. Immunofluorescence labeling of BMP receptors in C2C12 cells .....	181
V.2.1.3. Immunogold labeling of BMP-2 inside cells.....	185
<b>Chapter VI:</b> .....	<b>189</b>
<b>Conclusions and directions for future research</b> .....	<b>189</b>
VI.A. CONCLUSIONS.....	190
VI.B. DIRECTIONS FOR FUTURE RESEARCH.....	193
<b>Bibliographic references</b> .....	<b>196</b>
<b>Curriculum Vitae</b> .....	<b>209</b>
<b>Abstract</b> .....	<b>211</b>
<b>Résumé</b> .....	<b>211</b>



# **Chapter I: Introduction**

## I.A. Biomaterials for bone regeneration

Understanding of bone structure, mechanics and tissue formation is crucial in the development of biomaterials for bone regeneration.

### I.A.1. Bone tissue

#### I.A.1.1. Composition and properties of bone

Bone possesses a hierarchical organization represented by several orders of magnitude (from macro- (centimeter) scale to the nanostructured (extracellular matrix or ECM)) (*Figure I- 1*).

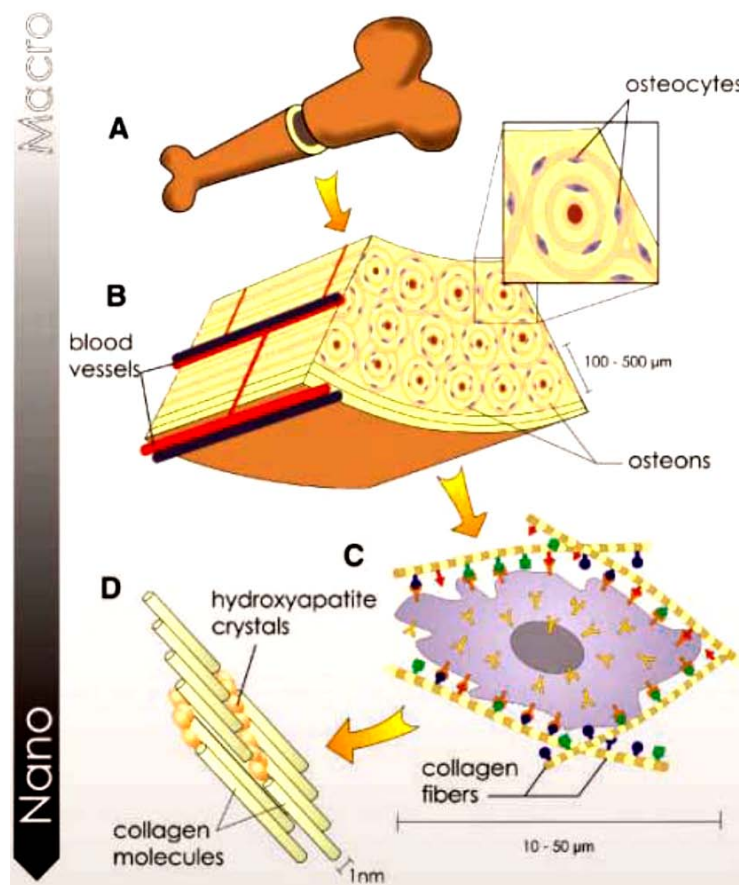


**Figure I- 1 : Hierarchical organization of bone.** Bone is covered by a strong calcified outer compact layer (a), and it is organized in osteons (b). The cell membrane receptors of the resident cells respond to specific binding sites (c) and to the well-defined nanoarchitecture of the surrounding extracellular matrix (d). From (Stevens and George, 2005).

Bone is a multiscale composite tissue that comprises a mineralized inorganic component (~ 75 wt%) and a nonmineralized organic component (~ 25 wt%) (**Figure I- 2**).

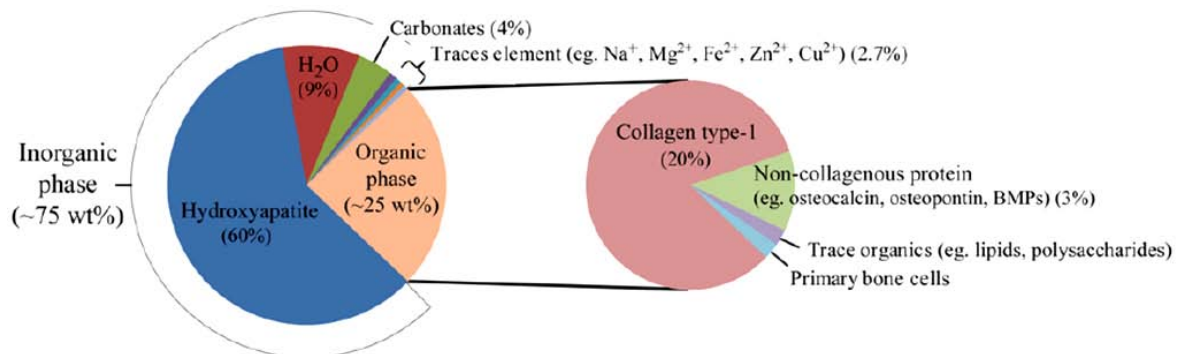


**Figure I- 2 : Composition of human bone.** Bone is made of inorganic and organic components. From (Chai et al., 2012).

The inorganic phase is mainly represented by carbonated apatite mineralites i.e. hydroxyapatite ( $\text{Ca}_{10}(\text{PO}_4)_6(\text{OH})_2$ ). Calcium carbonate and others minerals like fluoride, potassium and magnesium and others are as well components of the bone inorganic phase. Living bone in the body contains around 10% water (Weiner and Wagner, 1998).

The organic phase is predominantly composed of type-I collagen (Weiner and Wagner, 1998). Collagen molecules are secreted by osteoblasts and they self-assemble into fibrils. In addition, different types of non-collagenous matrix proteins contribute to the abundance of signals in the extracellular environment. Proteoglycans (composed of glycosaminoglycan-protein complex), sialoproteins and matrix proteins such as osteocalcin, osteonectin and osteopontin integrate the non collageneous proteins in bone. Polysaccharides such as chondroitin sulfate and keratin sulfate can also be found in bone, usually associated with protein to form proteoglycans (Rho et al., 1998).

Bone contains as well several cytokines and growth factors that aid in bone cell differentiation, activation, growth and turnover (interleukin-1 and 6 (IL-1, IL-6), insulin-like growth factor (IGF), transforming growth factors beta (TGF- $\beta$ ), bone morphogenetic proteins (BMPs)).

The mechanical properties of bone rely on its nanocomposite structure made of tough and flexible collagen fibers reinforced by hydroxyapatite crystals (Robinson, 1952). The Elastic Modulus ( $E_0$ ) of cortical bone can go from 7 to 30 GPa (Meyer and Wiesmann, 2006).

Bone extracellular matrix houses several types of bone cells that are involved in bone remodeling: osteoblasts, osteocytes, osteoclasts and osteogenic cells (stem cells) (**Figure I-3**).

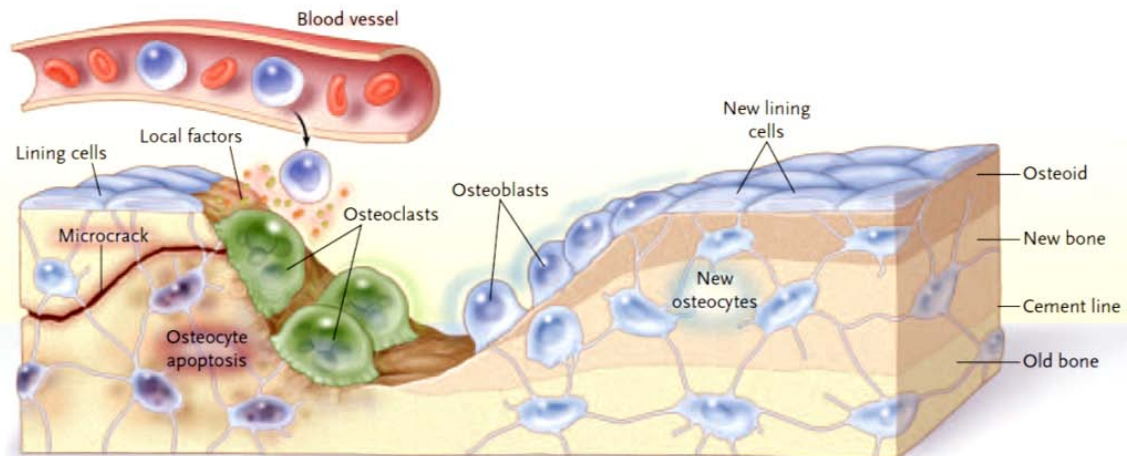


**Figure I- 3 : The remodeling cycle on a trabecula.** A microcrack which causes osteocytic apoptosis sends signals to lining cells. Lining cells and osteocytes release local factors that attract cells from blood and marrow into the remodeling compartment. Osteoclasts resorb matrix and the microcrack, and then successive teams of osteoblasts deposit new lamellar bone. Osteoblasts that are trapped in the matrix become osteocytes; others die or form new, flattened osteoblast lining cells. From (Seeman and Delmas, 2006).

During bone remodeling, resorption by osteoclasts precedes bone formation by osteoblasts. Osteoblasts produce inorganic calcium phosphates, which is converted in hydroxyapatite, and an organic matrix consisting mainly of type I collagen. Osteoclasts dissociate calcium by secreting acid and degrade organic components by releasing lysosomal enzymes. Osteocytes are the most numerous, longest-lived, and least studied cells of bone. They are osteoblasts that have become entombed in the bone matrix (osteoid) that they synthesize. Osteoblasts undergo a morphologic change and become osteocytes with cytoplasmic processes that connect them with other osteocytes and flattened lining cells. Osteocytes are part of the machinery guarding the integrity of the material and structural strength of bone (Frost, 2000; Stevens and George, 2005).

Bone continually remodels and has the capability to regenerate during life time.

### I.A.1.2. Bone morphogenetic proteins

The bone morphogenetic proteins (BMPs) are members of the transforming growth factor- $\beta$  (TGF- $\beta$ ) superfamily of multifunctional cytokines. BMPs were first reported in 1965 by Marshall R. Urist. They were isolated from demineralized bone matrix and their ability to induce ectopic bone and cartilage formation was discovered (Urist, 1965). The ability to induce osteogenesis is called osteoinduction. Known at first for their implication in bone formation, BMPs were found to play important roles in most morphogenetic processes during embryonic development, morphogenesis as well as tissue maintenance in adult individuals (**Figure I- 4**) (Hogan, 1996; Simic and Vukicevic, 2007). To date, more than 20 different BMPs have been described (Wang et al., 1988; Wozney et al., 1988; Wozney, 1992).

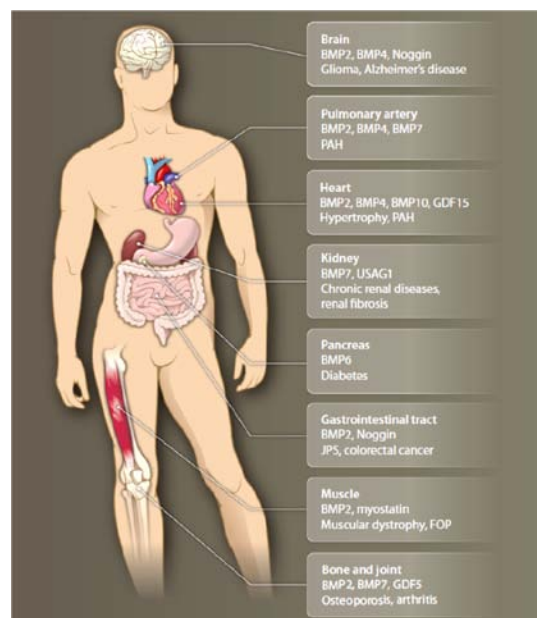


**Figure I- 4 :** BMPs functions in the different organs in the human body. From (Wagner et al., 2010).

The osteogenic activity of 14 BMPs was evaluated *in vitro* by Cheng *et al* (Cheng et al., 2003) using the alkaline phosphatase (a marker of bone differentiation) assay. Different osteoblastic precursors corresponding to the different states of differentiation were used: mesenchymal stem cells (MSCs, C3H10) or C2C12 myoblasts. Their results are illustrated in **Figure I- 5**. They have identified BMP-2, 6 and 9 as the most potent inducers of MSCs differentiation. All the others, except BMP-3, are only able to promote the terminal differentiation of committed osteoblastic precursors and osteoblasts.



## Osteogenic Hierarchy of BMPs

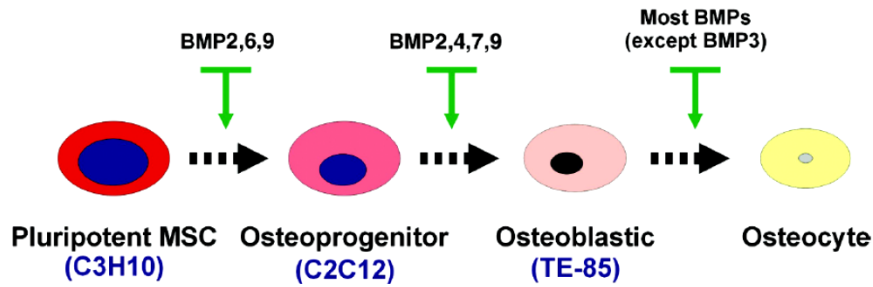


**Figure I- 5 : Distinct osteogenic activity of human BMPs.** Only BMP-2, 6, and 9 are able to induce osteoblast lineage-specific differentiation of mesenchymal progenitor cells while most BMPs can effectively promote the terminal differentiation of committed osteoblastic precursors and osteoblasts. From (Cheng et al., 2003).

In particular, BMP-2 plays an important role in the early phase of differentiation. It not only stimulates osteoprogenitor cells to differentiate into mature osteoblasts but also induces non-osteogenic cells as muscle precursors and mesenchymal stem cells to differentiate into bone cells (Katagiri et al., 1994; Rickard et al., 1994).

BMP-2 exists in a form of a dimer (**Figure I- 6**) where the two monomers are bonded by a disulfide bond. The monomer overall folding topology has been described as a hand with the  $\alpha$ -helix mimicking the wrist, the cystine-knot core the palm, and the  $\beta$ -sheets the fingers (Daopin et al., 1992; Scheufler et al., 1999).



**Figure I- 6 : Tridimensional structure of BMP-2 dimer:**  $\alpha$ -helices are indicated as spiral,  $\beta$ -strands as arrow, disulfide bridges are shown as green sticks. The subunits are color-coded blue and orange, respectively. Adapted from (Scheufler et al., 1999).

BMP-2 has an isoelectric point (pI) of  $8.2 \pm 0.4$ . Thus, the ionization and solubility of the protein is greater in acidic solutions. BMP-2 has a highly hydrophobic region at the protein surface (**Figure I- 7 A**). This hydrophobicity partially explains that BMP-2 has an unusual solubility, which is low in physiological conditions (0.15 M NaCl) (**Figure I- 7 B**) (Abbatiello and Porter, 1997; Scheufler et al., 1999). The highest solubility is in a medium without salt.

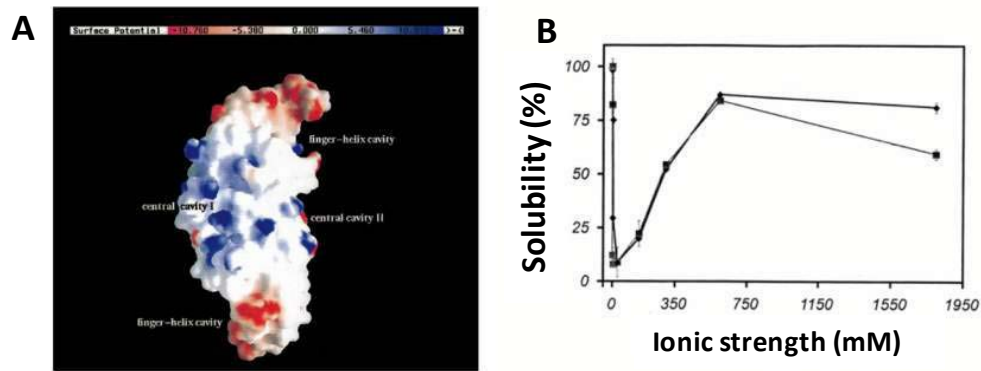


**Figure I- 7 :** Tri-dimensional representation of a BMP-2 monomer (A). White parts represent hydrophobic regions, the positively- or negatively-charged regions are colored in red and blue respectively. (B)The solubility of BMP-2 at pH 7.2 in NaCl (▲) or in Na<sub>2</sub>SO<sub>4</sub> (■). Adapted from (Abbatiello and Porter, 1997; Scheufler et al., 1999).

The discovery of bone morphogenic proteins has been fundamental in understanding the mechanisms of fracture healing and has been a source of intense clinical research as an adjunct to fracture treatment. In view of their osteoinductive properties (Urist, 1965), BMPs as BMP-2 and BMP-7 have been introduced into orthopedic clinical practice for the treatment of spinal fusion of either delayed or non-unions (Schmidmaier et al., 2008).

### I.A.2. Cues for successful bone regeneration around implant material

Bone healing is a multistage, highly regulated process involving different cells, different types of extracellular matrix and a multitude of signaling molecules (Gerstenfeld et al., 2003; Schmidt-Bleek et al., 2014).

In a material's point of view, appropriate bone regeneration around an implant relies essentially on the osteoconductive and osteoinductive properties of the material. The recruitment of osteogenic cells, angiogenesis and biomechanical stability are other crucial requirements for bone formation (Giannoudis et al., 2008; Schmidmaier et al., 2008).

Osteoconduction means that bone grows on a surface. An osteoconductive material support bone growth and encourage the ingrowth of surrounding bone. It allows bone growth not only on its surface but down into pores, channels or pipes (Albrektsson and Johansson, 2001; Stevens, 2008).

As previously mentioned, osteoinduction is the process by which osteogenesis is induced. Growth factors encourage mesenchymal stem cells or muscle precursors to differentiate into osteoblastic lineages. BMPs are well known osteoinductive growth factors that induce *de novo* bone formation (Seeherman and Wozney, 2005).

Importantly, the functional reliability a bone implant in actual operating conditions in a human body is determined by the material elastic modulus. Ideally, the  $E_0$  value of the material should be close to that of bone (~ 20 - 30 GPa). In this way, it allows to redistribute a significant part of loads on the bone and stimulate bone formation (Navarro et al., 2008).

The combination of these events results in new bone formation in a damaged site or in a stable anchorage of an implant achieved by direct bone-to-implant contact (i.e. osteointegration: integrate into surrounding bone).

### **I.A.3. Biomaterials for bone-graft substitutes or prosthetic implants**

Bone, particularly in younger people, has a high regenerative capacity. However, large bone defects, as observed after bone tumor resections and severe nonunion fractures, require a template for an orchestrated healing and need surgical intervention (Bauer and Muschler, 2000). Over a million fractures occur per year in the US and are associated with impaired healing increasing patient morbidity, stress, and economic costs (Ghodadra and Singh, 2008). Currently, the gold standard treatment is the use of autografts, harvested from a non-load-bearing site in the patient, such as like the iliac crest, followed by transplantation into the defect site (Bauer and Muschler, 2000). The use of autologous bone (i.e. bone from the patient) has a better clinical outcome than the use of allogeneic bone (i.e. bone from human cadaver) or xenogeneic bone (i.e. bone from an animal source). The use of either allogeneic or xenogeneic bone grafts can raise several immune- and disease-related complications. However, the satisfactory outcomes obtained by the use of autografts, the limited supply and the donor site morbidity associated with the harvest are severe problems (Lord et al., 1988; Silber et al., 2003). In summary, there is a clinical need for new bone regeneration strategies. The development of treatments based on biomaterials is important in the orthopedic field.

#### **I.A.3.1. Evolution in the development of biomaterials**

Over the past decades various implants and medical devices were developed to replace irreversibly damaged tissues. Biomaterials have to possess specific properties depending on the tissue or tissue function to be replaced. Thus, the constant evolution in the field has led to an increased regenerative potential of these biomaterials (*Figure I- 8*).

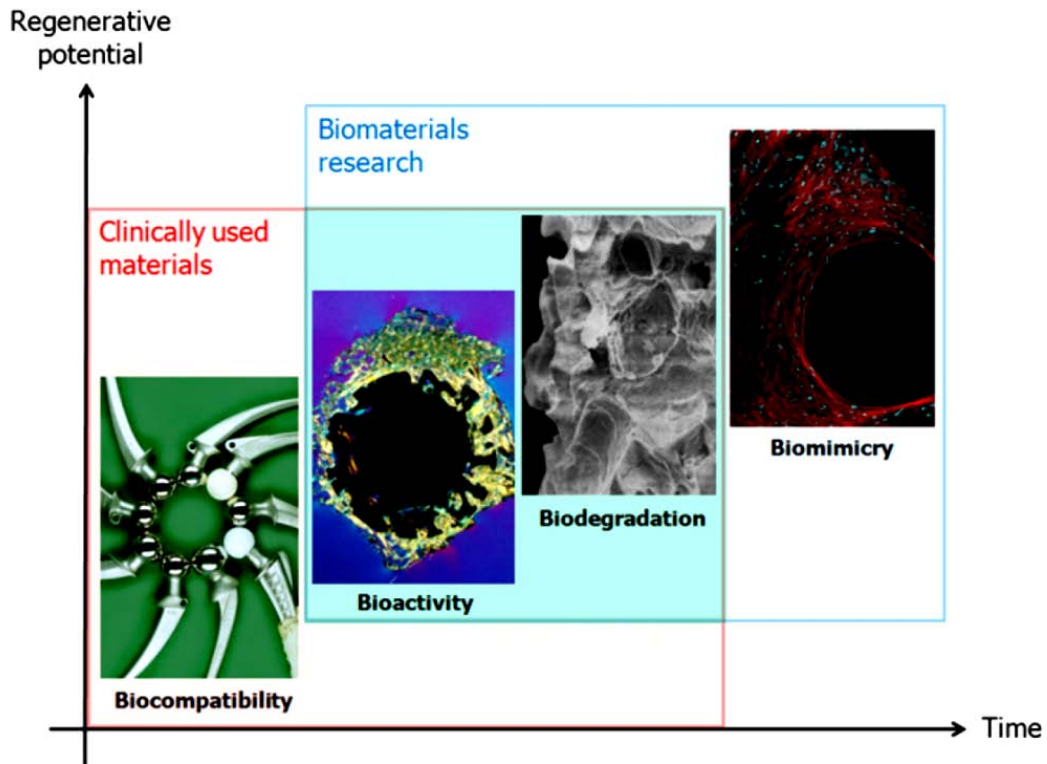


**Figure I- 8 : Time evolution of biomaterials.** Initially, classical biomaterials, such as solid metallic implants, were aimed to be biocompatible, to replace damaged tissue and to provide structural support. Then, bioactivity was introduced and in a latter step, biodegradation. More recently, biomaterials aim to fully mimic the natural tissues. From (Holzapfel et al., 2013).

The human body consists of a highly corrosive environment. During a great part of the 20<sup>th</sup> century, the materials used for the preparation of implants were the same as for other industrial applications, including car industry, aerospace, chemistry and energy. For this first generation of implantable materials, the concerns in their development were primarily driven by issues of biocompatibility and demands for enhanced mechanical performance (Geetha et al., 2009; Holzapfel et al., 2013). The outcomes of such materials in the past allowed fixing several stringent requirements that are imposed today in the production of new biomaterials. Consequently, concepts such as bioactivity, osteoconduction and osteoinduction have been gradually introduced as requirements for bone biomaterials.

Bioactive biomaterials are biocompatible and allow protein adsorption on the material surface. When implanted in the body they are immediately coated with proteins from blood and body fluids, and it is through this coated layer that cells sense and respond to the foreign implant (Wang et al., 2012; Lee et al., 2014). Bioactive materials can present active molecules to the surrounding cells, which will trigger specific cascades of events.

In the next step, the development of temporary matrices that act as guiding templates for bone growth was introduced and biodegradable materials were proposed. These provide a specific environment and architecture for bone development (Navarro et al., 2008).

In the 21<sup>st</sup> century, the introduction of new concepts in molecular biology significantly affected the biomaterials design and use. As a result, the present decade has seen the emergence of a new generation of biomaterials, the so-called smart or biomimetic materials. A key challenge in designing smart biomaterials is to capture the degree of complexity needed to mimic the extracellular matrix (ECM) of natural tissues. Such materials are able to stimulate specific cellular responses at the molecular level (Holzapfel et al., 2013).

Synthetic graft substitutes, or matrices, are formed from a variety of materials, including natural and synthetic polymers, ceramics, metals and composites. Therefore, regarding the tissue response to the material, biomaterials can be grouped into three main types: biocompatible, bioactive or biodegradable materials (*Table I- 1*).

*Table I- 1 : Classification of biomaterials for bone based on its interaction with the surrounding tissue. Adapted from (Geetha et al., 2009).*

<b>Classification</b>	<b>Response</b>	<b>Examples</b>	<b>Effect</b>
<b>Biocompatible materials</b>	Formation of thin connective tissue capsules (0.1 – 10 µm) Capsule does not adhere to the implant surface	Polytetrafluorethylene (PTFE), polymethylmethacrylate (PMMA), Metals such as Ti, Co-Cr, etc.	Possible rejection of the implant leading to failure of the implant
<b>Bioactive materials</b>	Formation of bone tissue around the implant material and strong integration with the implant surface	Bioglass, calcium phosphate including hydroxyapatite (HAP)	General acceptance of the implant leading to success of implantation
<b>Biodegradable materials</b>	Replaced by the autologous tissue	Polylactic acid (PLA) and polyglycolic acid (PGA) polymers and processed bone grafts, composites of all tissue extracts or proteins structural support system	General acceptance of the implant leading to success of implantation

### ***I.A.3.2. Polymers***

Polymers of natural or synthetic origin have been used in the orthopedic field. Two different classes of polymers have been developed depending on their application: non-degradable and degradable.

Non-degradable (or permanent) polymers are used as components of prosthesis where a stable on long-term and non-degradable material is required. For example, polyethylene (PE) with different densities was used as tibial inserts or patellar components in total knee replacement. Moreover, synthetic polymers as silicon rubber, acrylic resins, polyurethanes, and polymethyl-methacrylate (PMMA) have been used as bone cements and play a key role in the anchorage of metallic or plastic prostheses to the surrounding bone in cemented arthroplasties or dental surgery (Navarro et al., 2008). Recently, a promising polymeric material, polyetheretherketone (PEEK), has been developed as an alternative to titanium in medical devices. Implants made of PEEK are now widely accepted in spine surgery as the material of choice for fusion cages and are currently under evaluation for more demanding spine stabilization products (Kurtz and Devine, 2007; Sagomonyants et al., 2008; Zhao et al., 2013b).



***Figure I- 9 : The PEEK Prevail<sup>®</sup> Device sold by Medtronic. In cases where a diseased cervical disc is removed from the spine, this device can be used to provide stability for spinal fusion.***

Degradable polymers are used as bone-graft substitutes, developed as an alternative strategy to overcome the inherent limitation of autograft and allograft. Here, the main function is to provide a temporary matrix for bone growth, especially a specific environment and architecture for tissue development. Natural polymers as type-I collagen, fibrin, hyaluronic acid and chitosan are biodegradable and exhibit good biocompatibility. Their low mechanical stability is a problem. Biodegradable synthetic polymers, such as polyanhydrides,

polypropylene fumarate, polycaprolactones (PCL), polyphosphazenes, polylactide (PLA), polyglycolic acid (PGA), and associated copolymers poly(lactic-co-glycolic acid) (PLGA), are also used as scaffolds for tissue engineering (Burkoth et al., 2000; Lee and Mooney, 2001; Matassi et al., 2011). These polymers have different physical attributes, mechanical properties, degradation times, and modes of degradation that can be tuned on the basis of the intended application of the matrix.

Regarding applications of natural polymers in orthopedics, one can cite as the use of a resorbable type-I collagen sponge to deliver recombinant human (rh)BMP-2: the InductOs® kit is sold by Medtronic (Schmidmaier et al., 2008). This formulation includes a cross-linked collagen carrier onto which a BMP-2 solution is deposited via a syringe, just before the implantation.

### ***I.A.3.2. Ceramics***

Ceramic materials are made of inorganic material and possess a crystalline structure. Most ceramics are innately hard and brittle materials with higher elastic modulus compared to bone. They are represented by their high compressive strength and low tensile strength, providing high resistance to deformation (Ratner, 2004).

Alumina ( $\text{Al}_2\text{O}_3$ ) and zirconia ( $\text{ZrO}_2$ ) are non-bioactive ceramics being covered by a non-adherent fibrous layer at the interface after implantation. High density and highly pure alumina ( $\alpha\text{-Al}_2\text{O}_3$ ) was developed to replace traditional metallic femoral heads of hip prostheses (Boutin, 1972). Alumina is used in ceramic-on-ceramic hip replacements, as an example there is the Trident® ceramic hip replacement system by Striker where the insert and head of the system are both made of alumina ceramic, which has demonstrated significantly lower wear versus conventional plastic-on-metal or metal-on-metal joint systems. It is anticipated that the improved wear characteristics of alumina ceramic will result in a longer lasting implant. Such ceramics have demonstrated good wear rates, excellent corrosion resistance, good biocompatibility and high strength. Moreover, the modification of some parameters in the production process and the creation of ceramic composites (alumina and zirconia composites) can modulate the ceramics properties, namely their brittle nature (Ratner, 2004).

Several bioactive ceramics have been used in bone regeneration strategies. Calcium phosphates (CaP) have traditionally been used as bone fillers because of its strong resemblance to the inorganic phase of bone matrix. Ceramics such as hydroxyapatite (HAP)

and  $\beta$ -tricalciumphosphate (TCP) represent the most extensively used synthetic bone substitutes due to their osteoconductive properties (Bohner et al., 2005). They provide a surface chemistry that facilitates protein adsorption. Besides, it was shown recently that these ceramics can display an osteoinductive potential (Paul and Sharma, 2003; Boyan and Schwartz, 2011; Yuan et al., 2011).

A wide range of bioactive inorganic materials are of clinical interest. Nowadays, several CaP- or HAP-based biomaterials are produced and are used for dental and orthopaedic applications. The latest formulations include injectable pastes or granules to fill bone defects (*Figure I- 10*).



**Figure I- 10 : Macromorphology of some commercially available ceramic bone graft materials** (sold by <sup>1</sup>Curasan AG, <sup>2</sup>DePuySynthes <sup>3</sup>Geistlich). Adapted from (Stevens, 2008).

HAP and TCP have different degradation processes. HAP is almost insoluble and the slow process of *in vivo* degradation is mainly mediated by cellular resorption mechanisms. In contrary, the degradation of  $\beta$ -TCP is not only mediated by cellular mechanisms but also by chemical processes. Thus, the combination of both, namely biphasic ceramics, can match scaffold degradation kinetics with the new bone deposition and remodeling (Fleming et al., 2000). The mechanical properties of such composite can be modulated by increasing the amount of HAP and their biodegradation can be tuned by controlling the  $\beta$ -TCP content, a degradation and ion release being increased for higher  $\beta$ -TCP content (Ramay and Zhang, 2004).

As an example, a biphasic ceramic (60% HAP + 40%  $\beta$ -TCP) called TricOs® (Daculsi et al., 1989) combined with a fibrin sealant has been developed for bone reconstruction (*Figure I- 11*). A 19-years old boy suffering of fibrous dysplasia was injected with fibrin-HAP- $\beta$ -TCP in a bone lesion. After 12 months the bone substitute material was radiographically still detectable and appeared condensed indicating new bone formation



around the substitute material. At the same time, the sclerotic margin of the bone defect remained unchanged confirming no further disease progression (Reppenhagen et al., 2012). In this study, 50 of 51 patients with a mean defect size of  $\sim 12 \text{ cm}^3$  revealed complete bone defect filling in radiological controls at the time of the final follow-up ( $\sim 23$  months after surgery).

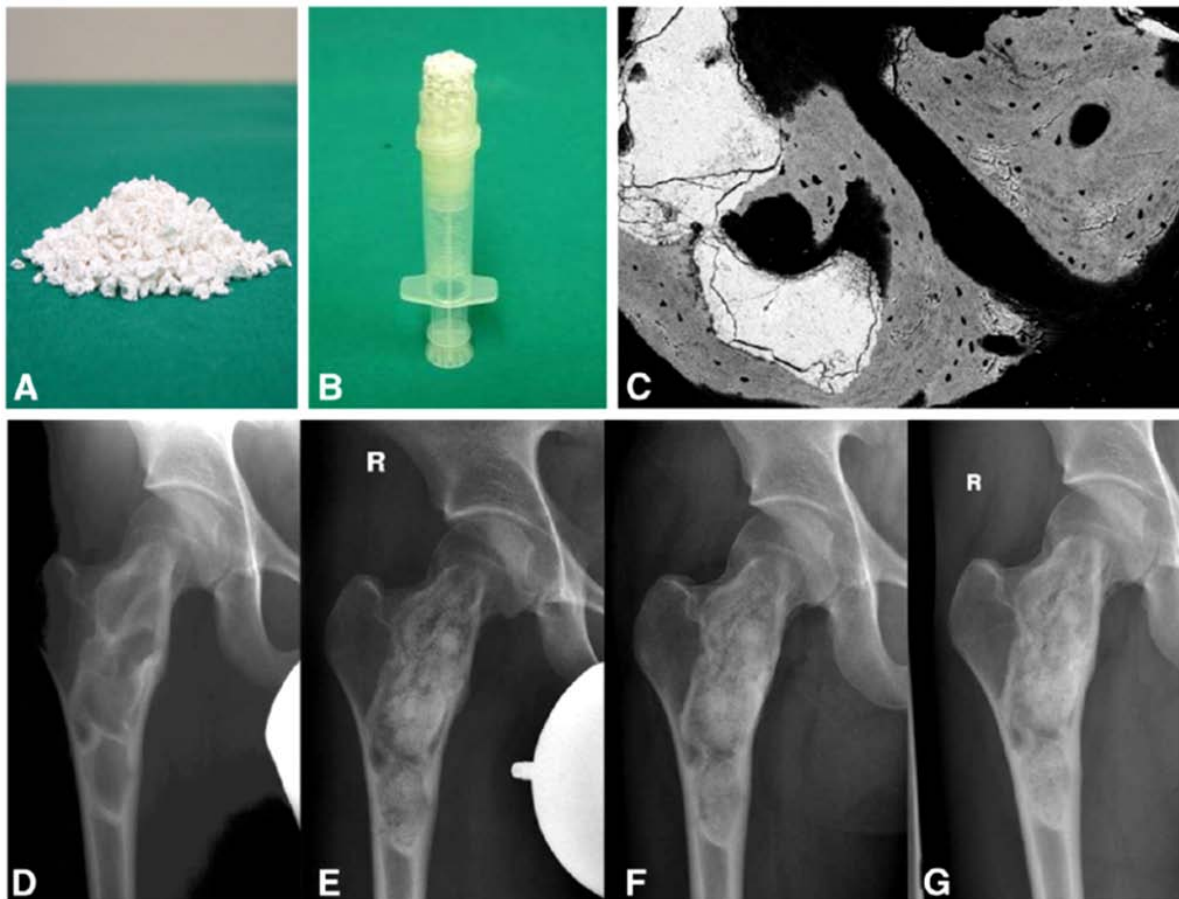


**Figure I- 11 : TricOs®: Biphasic ceramic (60% HAP and 40%  $\beta$ -TCP) combined with a fibrin sealant for bone reconstruction.** (A) Macroscopic view of granules. (B) The material was moistened with a specific solution and the diluted fibrin sealant was added to form a moldable mass, which could be easily applied to the bone lesion using a syringe. (D to G) X-ray images of a 19-year old male suffering from fibrous dysplasia of the right femur and treated with  $35 \text{ cm}^3$  of a fibrin-HAP- $\beta$ -TCP composite bone substitute (TricOs®); (D) preoperative, (E) 3 months, (F) 6 months and (G) 12 months after surgery). (C) 12 months after surgery the lesion was completely permeated with newly formed tissue as detected by Backscattered Scanning Electron Microscopy (BSEM, gray and black = new bone formation, white = remnants of the transplanted bone substitute material). Additionally, new bone formation was seen in close contact to the biomaterial indicating good osteointegration. From (Reppenhagen et al., 2012) adapted by (Holzapfel et al., 2013).

Bioactive glasses (Bioglass) are as well used as matrices for bone regeneration. They were introduced by Hench in the 1970s (Wilson et al., 1981; Hench, 1991). They can be

manufactured either by melt or sol–gel processing and have been broadly used as bone defect fillers in clinical situations. Bioglass is made of 45% silica ( $\text{SiO}_2$ ), 24.5% calcium oxide ( $\text{CaO}$ ), 24.5% sodium oxide ( $\text{Na}_2\text{O}$ ), and 6% phosphorous pentoxide ( $\text{P}_2\text{O}_5$ ) in weight percentage. The bioactivity of the Bioglass is mediated by a hydrated silicate-rich layer that is formed after contact with biological fluids. Some bioglass formulations demonstrate a higher osteogenic potential when compared to HAP alone. However, the brittleness and low fracture toughness of bioglass hampers its application for load-bearing applications (Patel et al., 2002). Calcium phosphates such as TCP and synthetic HAP are more widely used in the clinic than Bioglass. Some of the reasons are commercial, but others are due to the scientific limitations of the original Bioglass® 45S5. An example is that it is difficult to produce porous bioactive glass templates (scaffolds) for bone regeneration from Bioglass 45S5 because it crystallizes during sintering (Hench, 2006; Jones, 2013).

### ***I.A.3.3. Metals***

The first successful metallic materials used in orthopedic applications were stainless steel (SS 316L) and cobalt-chromium (Co-Cr) alloys. Titanium (Ti) and Ti alloys were introduced in 1940s. Nowadays, titanium and its alloys are being widely employed as biomaterials for dental and orthopedic implants due to their good biocompatibility, lower Young's modulus and better corrosion resistance to biological fluids than other metals (Geetha et al., 2009). It is also well known that a native titanium oxide film ( $\text{TiO}_2$ ) grows spontaneously on the titanium surface upon exposure to air. The excellent chemical inertness, corrosion resistance, repassivation ability, and even biocompatibility of titanium and most other titanium alloys are thought to result from the structure and chemical stability of the  $\text{TiO}_2$  film that is typically only a few nanometers thick. These attractive properties have been the driving force for the introduction of commercially pure titanium (CP Ti) and titanium alloys such as titanium-aluminium-vanadium (Ti6Al4V) as implantable metallic biomaterials (Liu et al., 2004; Geetha et al., 2009).

Commercially pure Ti (CP Ti), grade 4 (ASTM F67) and Ti6Al4V (ASTM F136) are the most common titanium alloys used in orthopedics. When using titanium alloys for the manufacture of implants and prostheses the extremely favorable factor is their low (approximately two times less than steel) elastic modulus. The elastic modulus of Ti can be modulated by using a correct selection of alloying elements (***Figure I- 12***).

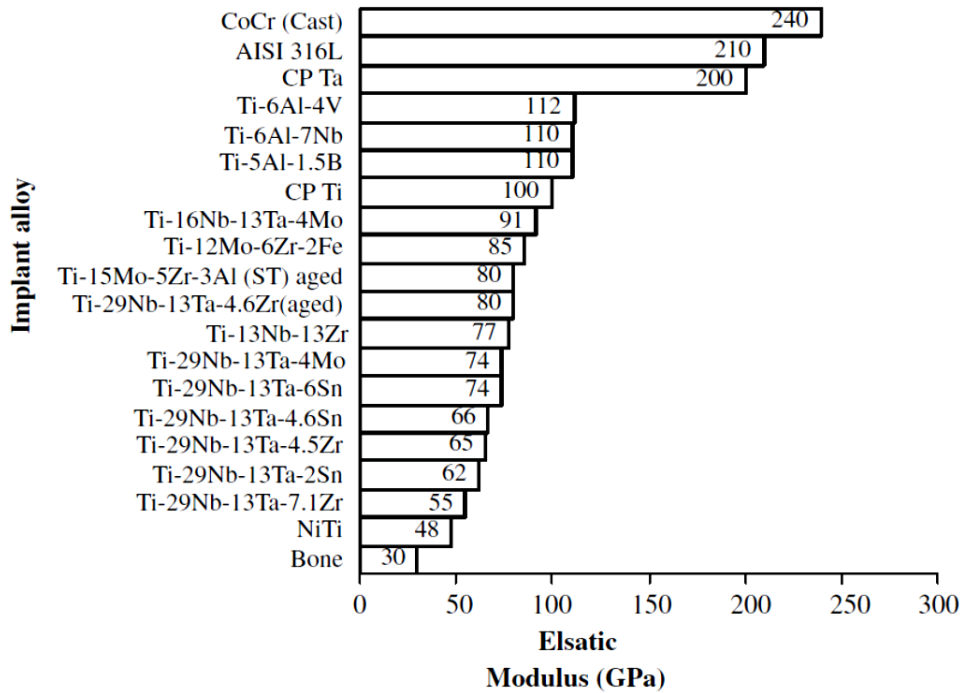


**Figure I- 12 : Elastic Modulus of titanium as compared to other metallic alloys and to bone. From (Geetha et al., 2009).**

Biocompatible metal elements such as Pt, Ta, Nb, Zr and others are being used for that purpose. Recently, Ti-alloys with niobium (Nb) have shown lower Young Modulus and superelastic properties (ductility and elasticity) than other Ti alloys (Zhao et al., 2013a).

Metals are biocompatible but not bioactive materials. Physical or chemical approaches have been used to activate those metallic surfaces and improve tissue formation and anchoring of implants (Le Guehenec et al., 2007).

#### ***I.A.3.4. General comparison between the types of biomaterials***

The four different types of biomaterials were previously described separately. They are compared in **Table I- 2** by the analysis of their typical mechanical properties, biocompatibility, biodegradability and possible applications.

**Table I- 2: The 4 groups of biomaterials in bone regeneration applications.**

<b>Materials</b>	<b>Mechanical properties</b>	<b>Biocompatibility</b>	<b>Biodegradability</b>	<b>Applications</b>
<b>Natural polymers</b>	-	+++	Degradable	Biomimetic materials (delivery of bioactive molecules, etc) Surface modification of implants
<b>Synthetic polymers</b>	+ (for degradable materials)  +++ (for new generation of polymers with mechanical properties equivalent to bone)	++ (for degradable materials)  + (for new generation of polymers with mechanical properties equivalent to bone)	Polymers as PLA, PGA, PCL are degradable  Other like PE, PEEK are non-degradable since they are used as a support component of different prosthesis	Scaffolds for bone regeneration (degradable polymers), sometimes in combination with ceramics  Surface modification of implants  Components of orthopedic implants (knee, hip, and others)
<b>Ceramics and bioglasses</b>	++ (Rigid but brittle materials)	+++ (bioactive ceramics)  + (other ceramics)	Can be degradable in applications such as filling bone defects (CaP/HAP scaffolds)  Ceramics such as alumina and zirconia are non-degradable; components of prosthesis	Surface modification of metal implants (HAP)  Components of orthopedic implants (knee, hip, and others)
<b>Metals</b>	+++	+	Non-degradable	Orthopedic implants (knee, hip, dental, and others)

#### **I.A.4. Surface modifications of titanium implants**

Nowadays, most endoprostheses used in orthopedic and maxillo-facial surgery are made of Ti or Ti alloys (Liu et al., 2004; Geetha et al., 2009). Good osteo-integration of long-term metal implants is still a clinical problem, especially in patients with poor osseous healing capabilities and impaired bone regeneration potential (Palmquist et al., 2010).

Several studies have focused on the modification of titanium surface in order to increase new bone formation around such implants, i.e., osteointegration (Le Guehennec et al., 2007). The strategies to modify the Ti surface have essentially focused on improving Ti osteoconductivity.

#### ***I.A.4.1. Mechanical, chemical and physical modifications***

At the beginning of the 1980s, the surface properties of a biomaterial were identified to be very important for the implant incorporation into bone (Albrektsson et al., 1981).

Bone tissue response to an implant surface is related to the surface topography at the nano- and micrometer level (Wennerberg and Albrektsson, 2009; Gittens et al., 2014). The engineering of a surface topography can be achieved by two methods: coating of the implant surface with an additional layer or implant surface erosion with blasting or etching protocols.

Different methods can be applied for surface modification: mechanical, chemical and/or physical methods (**Figure I- 13**). Mechanical methods include machining, grinding, polishing and blasting which involve shaping or the removal of the material from the surface. Chemical methods involve chemical and electrochemical treatment (anodic oxidation), sol-gel, chemical vapor deposition (CVD), or biochemical modification. Here, electrochemical or biochemical reactions happen at the interface between titanium and a solution. Physical methods are thermal spraying and physical vapor deposition (PVD) (Le Guehennec et al., 2007; Wennerberg and Albrektsson, 2009; Hanawa, 2010).



**Figure I- 13 : SEM images of modified titanium surfaces** (a) anodic oxidized surface (TiUnite, Nobel Biocare) showing volcanoes porous structure (b) machined surface (Fixture Original, Branemark Integration) showing ridges and valleys along the turning direction (c) laser-modified surface showing a combined surface roughness in both the micro- and nanoscale. (Scale bars, 5  $\mu\text{m}$ ). From (Palmquist et al., 2010).

The relation between surface roughness and osteointegration has been reviewed by Wennerberg et al where the *in vivo* biological outcome of several titanium modified surfaces was reported (Wennerberg and Albrektsson, 2009). They have concluded that smooth ( $S_a < 0.5 \mu\text{m}$ ) and minimally rough ( $S_a 0.5 - 1 \mu\text{m}$ ) surfaces showed less strong bone responses than rougher surfaces. Moderately rough ( $S_a > 1 - 2 \mu\text{m}$ ) surfaces showed stronger bone responses than rough ( $S_a > 2 \mu\text{m}$ ) in some studies. It has been shown that an implant surface modified on the micron-level is associated with a faster and increased osteointegration and bone-to-implant contact, when compared to polished Ti surfaces.

#### ***I.A.4.2. Coating with biomimetic hydroxyapatite (HAP) layer***

CaP has been used to coat titanium dental implants for decades. After implantation, the release of CaP into the peri-implant region increases the saturation of body fluids and results in the precipitation of a biological apatite onto the surface of the implant (de Groot et al., 1998; Daculsi et al., 2003). Such layer of biological apatite may enclose endogenous proteins and serve as a matrix for osteogenic cell attachment and growth (Davies, 2003).

HAP has been found to be an excellent coating material for enhanced osteointegration and previous studies have shown a significantly increased rate of bone formation compared to untreated surfaces (Zhang et al., 2009; Hermida et al., 2010; Yang et al., 2010). HAP coatings preceded or not by acid etching, are used to create a rough, potentially bioactive surface (Le Guehennec et al., 2007; Palmquist et al., 2010).

Different techniques can be applied to deposit HAP coatings: plasma spraying, which is based on melting the coating material and spraying it onto the material, producing rough and thick coatings. Early experience with these coatings indicated that they are prone to adhesion failure and cracking. An alternative technology is evaporation coating, such as physical vapour deposition (PVD). In PVD, the coating is evaporated by sputtering of a HAP source, and the coating is deposited atom by atom. Very thin (approx. nanometer) and up to micrometre thick coatings can be performed (Mohammadi et al., 2003; Mohammadi et al., 2004). HAP coatings can also be produced in wet chemical processes, such as sol–gel coating and biomimetic coating by immersion in simulated body fluid or phosphate buffered saline (Kokubo et al., 2001; Xia et al., 2010). By varying the solution composition, immersion time and temperature, these techniques offer multiple possibilities to vary the thickness, morphology and composition of the coatings.

Recently, *Chai et al* developed 3D functionalized porous calcium phosphate-Ti6Al4V (CaPeTi) hybrids by perfusion electrodeposition (Chai et al., 2012). In this study, various current densities at optimized deposition conditions were applied to obtain CaP coatings with sub-micrometer to nano-scale porous crystalline structures deposited on the porous Ti6Al4V scaffolds. *In vitro* and *in vivo* biological performances were evaluated using human periosteum derived cells (hPDCs). These distinctive physicochemical properties caused a significant impact on *in vitro* proliferation, osteogenic differentiation, and matrix mineralization of hPDCs. Those hybrids induced ectopic bone formation in subcutaneous implantation site (**Figure I- 14**), which was highly dependent on the physicochemical

properties of the CaP coating (including the Ca<sup>2+</sup> dissolution kinetics and coating surface topography), in a cell density-dependent manner (Chai et al., 2012).

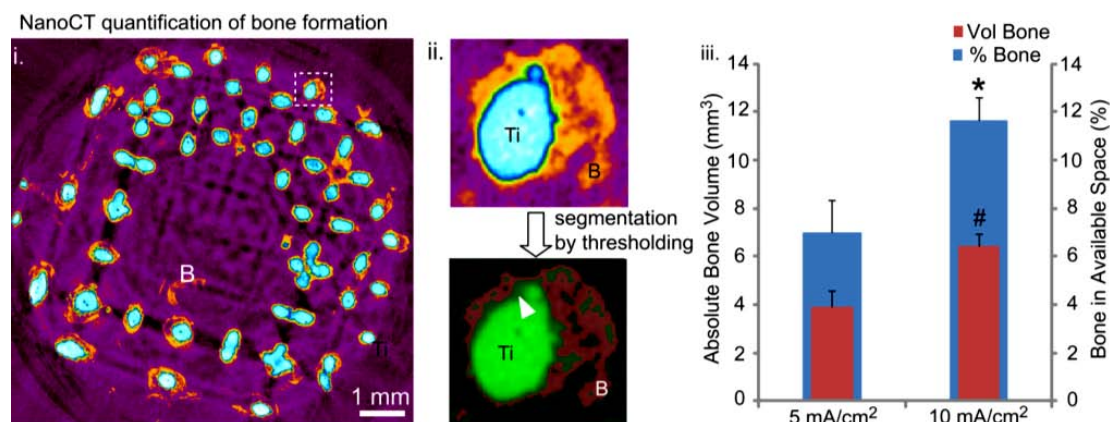


**Figure I- 14 :** Ectopic bone forming capacity of the hPDC-seeded CaPeTi hybrids. (i) representative reconstructed nanoCT image (in pseudo-colour) showing bone formation (B, in orange colour) within the hybrids produced at 10 mA/cm<sup>2</sup> (ii) By applying a global thresholding, bone (B, in brown colour) was segmented from the coating (indicated  $\Delta$  in the inset), and (iii) quantified as the absolute bone volume or percentage of bone formed in the available internal volume of a hybrid. Adapted from (Chai et al., 2012).

However, clinical long-term complications with the use of plasma-sprayed HAP have been documented (Albrektsson, 1998). Rokkum *et al* found that the use of some thick-layered apatite-coated implants resulted in severe inflammation and bone resorption due to detachment of the coating material (Rokkum et al., 2003). It was identified histologically that multinucleated giant cells were localized in the proximity of the implant, and many of the cells resided around the detached HAP particles.

The control of the HAP layer thickness is a challenge and it plays a role on the material integration. Depending on the technique used to deposit the HAP layer, thicker HAP coatings (~ 50  $\mu$ m) can be less stable than thinner films (~ 15  $\mu$ m), poor adhesion to the metallic surface and consequent delamination were observed (Chai et al., 2012).

To utilize the excellent bioactive properties of HA and to suppress the negative responses of thick HAP layers, such as the detachment of the particles and osteoclastic reactions, a thinner and rigid HAP coating may be desirable (Wennerberg and Albrektsson, 2009). The deposition of nanometer-thick HAP coating has been performed by Promimic, a spin-off from a research laboratory of Chalmers University of Technology in Gothenburg, Sweden. The company develops and commercializes a new generation of implant surface modifications and synthetic bone based on a patented method for production of nano-sized hydroxyapatite (20 nm thick) deposited by spin-coating (Johansson et al., 2014). Coating with



HA<sup>nano</sup> surface accelerates osteointegration of the coated biomaterial. The nanometer thickness of the coated layer is believed to possess higher interfacial shear strength and to minimize the risk of coating delamination. This coating can be applied onto various types of materials including metals, ceramics and polymers regardless of its dimensions and structure.

### I.B. Bone tissue engineering approaches

Back in 1993, *Langer and Vacanti* defined tissue engineering (TE) as “an interdisciplinary field that applies the principles of engineering and life sciences toward the development of biological substitutes that restore, maintain, or improve tissue function or a whole organ” (Langer and Vacanti, 1993). *Mason et al* defined regenerative medicine (RM) as “the process of replacing or regenerating human cells, tissues or organs to restore or establish normal function” (Mason and Dunnill, 2008). Since the beginning, TE relies on three pillars: scaffolds, cells, and bioactive molecules. Regenerative medicine uses strategies such as cell-based therapies, immunomodulation, gene therapy, and TE itself to stimulate organ regeneration. Thanks to their similar objectives, these two fields have merged in recent years, creating a broad field of TE and RM called TERM (Salgado et al., 2013).

Bone tissue engineering approaches can involve the single use or the combination of three factors, involved in a so-called diamond concept (*Figure I- 15*): osteoconductive scaffolds, osteoprogenitor cells and bioactive molecules. Mechanical stability is as well an essential element in bone regeneration (Giannoudis et al., 2007).

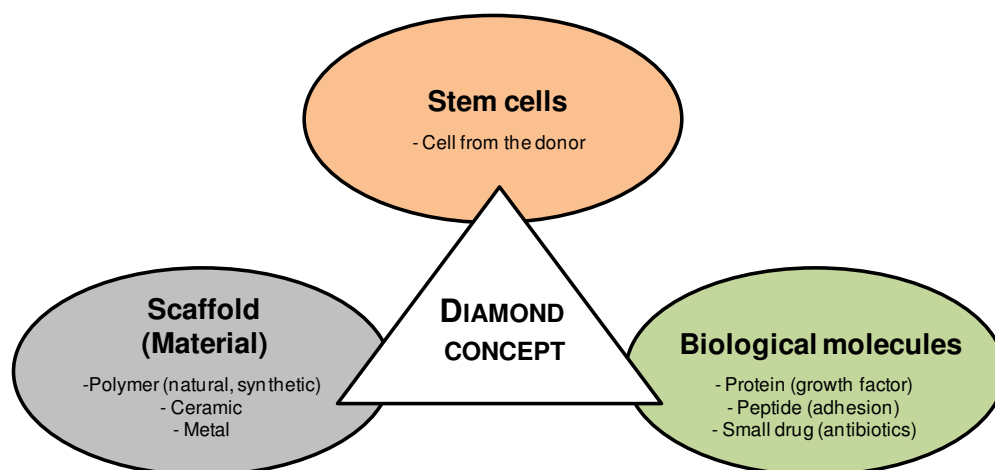


**Figure I- 15 : The diamond concept in tissue engineering.** The combination of stem cells and/or bioactive molecules with biomaterials templates has emerged as an innovative way to improve the regeneration of bone tissue. Courtesy of Catherine Picart, class of biomaterials.



Each factor provides individual and different cues in the process of bone regeneration. The scaffold biomaterial can promote bone formation by providing an osteoconductive matrix to osteogenic cells. Bioactive molecules such as osteoinductive factors or antibiotics allow the presentation of different signals to the cells to create bone.

To note, the use of one, two or three of the components of the triangle leads to products that have an increased complexity and for which the regulatory steps before approval are more numerous. Besides, the more components there are, the more safety is a concern as each of the components has to be perfectly characterized and reproducible for being used. (*Figure I- 16*).

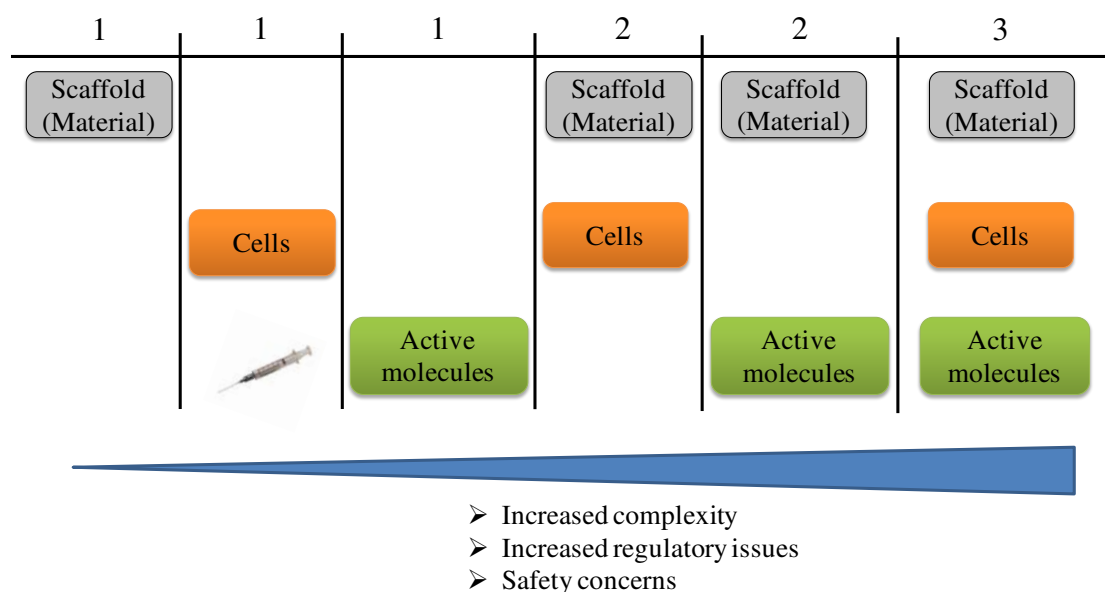


**Figure I- 16 : Increased degree of complexity in the association of the three components of the triangle: from a single component to the most complex situation with 3 components. The TE approach can use two components (scaffold/cells or scaffold/bioactive molecules) or even three components (scaffold/cells/bioactive molecules). Courtesy of Catherine Picart.**

The use in clinics of a single-component therapy, such as implantation of scaffold material, cell-based therapy or delivery of an active molecule, demands already a long development and serious proofs of concept. A product that combines two or three factors in the same TE construct increases the complexity of the product development, besides their individual effects, the combined characteristics have to be well studied. Before the creation of tissue constructs based on three-component, several research groups have been working on two-component therapies, namely, scaffold/stem cells or scaffold/bioactive molecules. In the past years, there was an increasing interest in developing three-component therapies but, for now, none is commercially available.

### I.B.1. Scaffold / Stem cells

The scaffold/stem cells approach involves first the isolation of stem cells (from the patient or from a bank), the cells are then expanded *ex vivo* before seeding on a synthetic scaffold and implantation. Cells are allowed to produce extracellular matrix and finally the construct is implanted into an osseous defect (**Figure I- 17**).

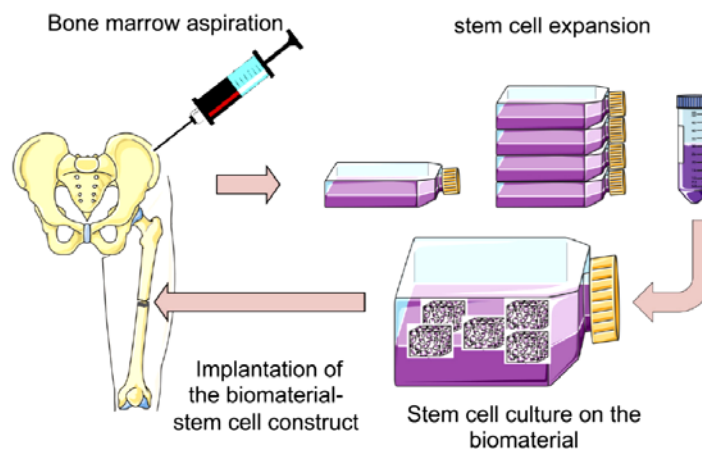


**Figure I- 17 : Bioreactor principle allowing culturing of mesenchymal stem cells on a biomaterial prior to implantation.** From (Rosset et al., 2014).

The major challenge in making these cellular therapies more efficient is the identification of the cell sources that can be implanted to bone defect site and will differentiate into osteoblasts and form neo-vasculature (Amini et al., 2012). Several cell types have been investigated to choose an effective cell type for clinical bone regeneration. Thus far, mesenchymal stem cells (MSCs), embryonic stem cells (ESCs), induced pluripotent stem cells (iPSCs), adipose derived stem cells (ADSCs) and stem cells from human exfoliated deciduous teeth (SHED) have been identified (Amini et al., 2012).

Adult stem cells such as multipotent human MSCs are a precious therapeutic tool in TE (Langer and Vacanti, 1993) as they are able to proliferate and differentiate either *in vitro* or *in vivo* into a multitude of distinct cellular phenotypes: adipogenic (fat), chondrogenic (cartilage), osteoblastic (bone), myoblastic (muscle) and fibroblastic (connective tissues) lineages (Ciapetti et al., 2006; Rice and Scolding, 2008). MSCs can be isolated from a number of adult sources including bone marrow, peripheral blood, umbilical cord blood, synovial membrane, deciduous teeth, amniotic fluid, adipose tissue, and others through a relatively simple protocol that primarily relies on their ability to adhere to plastic in tissue culture (Amini et al., 2012). Despite the several tissue options to isolate MSCs, for now only MSCs

isolated from bone marrow and adipose tissues were used in clinical studies (Amini et al., 2012). The limited number of MSCs in the bone marrow requires *ex vivo* expansion before seeding onto scaffold (Rosset et al., 2014).

*Luyten and coworkers* have demonstrated the importance of a good matching between a cell support/biological matrix and a cell type. Such relations can be used in the rational selection of biomaterials for using alternative cell types for bone engineering (Roberts et al., 2011). They evaluated *in vitro* and *in vivo* the responses of human periosteal derived cells (hPDCs) on five different commercially available orthopaedic 3D matrices composed of CaP particles in an open collagen network with different geometries and porosities. It was found that the cell-material combinations behaved quite differently *in vivo*, despite apparent *in vitro* similarities in gene expression profiles. Bone formation and quality *in vivo* was different in function of the matrix characteristics (Roberts et al., 2011).

*Layrolle and coworkers* designed an engineered construct mimicking bone components where a biocompatible hydrogel (silated hydroxypropylmethyl cellulose – Si-HPMC) was used as an extra-cellular matrix while biphasic calcium phosphate (BCP) ceramic particles were used to mimic mineralized part of the matrix (Sohier et al., 2010). The objective was to verify if such biomimetic constructs could preserve the osteogenic potential of human bone mesenchymal cells (HBMCs). HBMCs were seeded on such constructs (**Figure I- 18**) to study cell viability, proliferation, interactions within the composites, and maintenance of their osteogenic potential. This approach resulted in homogeneous structures in which cells were viable and retained their osteoblastic differentiation potential (Sohier et al., 2010).

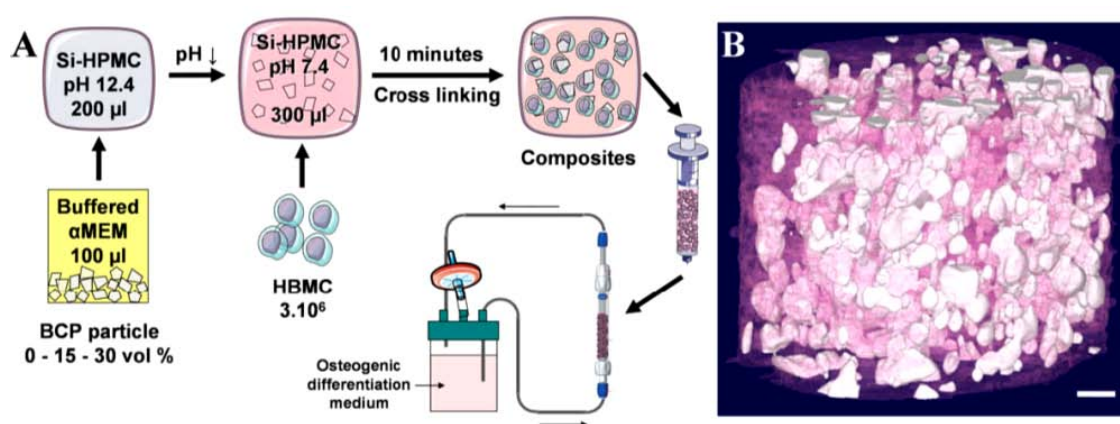


**Figure I- 18 : Different steps in the processing of biomimetic composites made of Si-HPMC hydrogel, BCP ceramic particles and human bone mesenchymal cells (A). By micro-computed tomography, Si-HPMC hydrogel appears pink and BCP ceramic particles (15 vol.%) appear white after reconstruction (B). Scale bar = 100 µm. From (Sohier et al., 2010).**

Recently, *Layrolle, Sohier and coworkers* have focused on a new way to form hybrid 3D constructs to bone engineering. They have cultured human bone marrow stromal cells (hBMSCs) on BCP (HA/ $\beta$ -TCP, 20/80) particles prior to implantation (Cordonnier et al., 2014). In this approach a higher degree of freedom is given to the cells allowing them to synthesize a three-dimensional (3D) environment. BCP particles provided a good support for high cell proliferation and extensive extracellular matrix (ECM) production resulting in the rapid formation of thick cell-synthesized 3D constructs. *In vitro*, this 3D environment can spontaneously induce osteoblastic commitment without the need for osteogenic factors. The osteoinductive potential of this 3D constructs was evaluated *in vivo* after implantation in the subcutis of nude mice. Interestingly, abundant ectopic bone formation was observed after 8 weeks.

This type of TE approach has some limitations being:

- The first one the need of two surgical approaches (one to harvest the MSCs and the second to implant the bone graft developed *in vitro*);
- MSCs extensively cultured *ex vivo* lose their phenotypic behavior such as osteodifferentiation and bone formation capacity once implanted *in vivo*;
- The low proliferative capacity of MSCs is another obstacle making difficult to obtain a sufficient cell density in a large scaffold (Lucarelli et al., 2004; Mauney et al., 2005).

To overcome those limitations some groups have been working on ways to maintain the osteodifferentiation potential of MSCs *ex vivo*.

*Reis and coworkers* have developed a nanotechnology-based strategy to enhance osteogenesis *in vitro* and *in vivo* (Oliveira et al., 2009; Oliveira et al., 2010; Oliveira et al., 2011). For example, it has been shown that dexamethasone (Dex) delivered as a medium supplement promotes the osteogenic differentiation of marrow stromal cells (Ciapetti et al., 2006; Oshina et al., 2007). They have shown that the intracellular delivery of dexamethasone using dendrimer-based nanoparticles induced osteogenic differentiation of BMSCs and enhanced de novo bone formation (**Figure I- 19**). They have also demonstrated that BMSCs *ex vivo* culturing strategies greatly influence the osteogenesis and de novo bone formation *in vivo* (Oliveira et al., 2010).

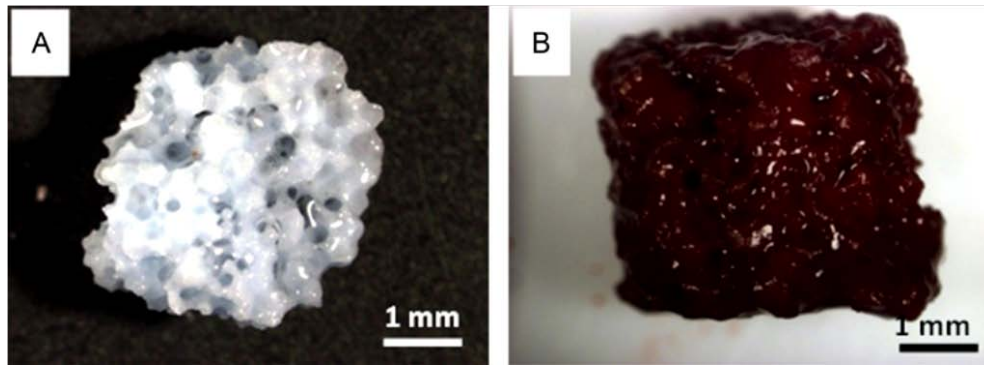


**Figure I- 19 :** *Optical microscopy images of the HAP scaffold (A) and HAP scaffold seeded with rat bone marrow stromal cells, which were stained with Alizarin red (mineralization) after culturing (14 days) in MEM medium with  $0.01 \text{ mg ml}^{-1}$  Dex-loaded CMChT/PAMAM dendrimer nanoparticles,  $0.28 \text{ mM}$  ascorbic acid, and  $10 \text{ mM}$   $\beta$ -glycerophosphate (osteogenic medium) (B). From (Salgado et al., 2013).*

On top of the previous limitations, a great challenge in the field of bone TE remains to be solved, that is, promoting vascularization in order to allow nutrients access into large TE constructs, thereby maintaining their viability at the implantation site (Brennan et al., 2013). In fact, cell death often occurs in the center of implants prior to vessel in-growth from the surrounding host tissue. Then, strategies that address the means of improving angiogenesis of bone tissue-engineered implants are vital.

Focusing on bone tissue engineering, *Amédee and coworkers* have been working on co-cultures of HBMSCs and human umbilical vein endothelial cell (HUVEC) for about ten years aiming to investigate the effects of HBMSC-HUVEC interactions on osteoblastic differentiation of HBMSC and angiogenesis of endothelial cells (Villars et al., 2002; Guillotin et al., 2004; Grellier et al., 2009; Li et al., 2010). Chemotaxis is one of the major mechanisms involved in endothelial cell angiogenesis. Typically, chemotaxis of endothelial cells is driven by growth factors such as vascular endothelial growth factor (VEGF) and basic fibroblast growth factor (bFGF) (Breier et al., 1995). VEGF is an angiogenic growth factor possessing many special properties to induce endothelial cells to proliferate, to migrate, to assemble into tubes, to survive and to increase their permeability. They have shown that the direct contact of HBMSC and HUVEC and their respective dialogue are sufficient to stimulate secretion of soluble factors (VEGF) and to activate molecules that are critical for self-assembled network formation which show a great application potential for vascularization in tissue engineering (Li et al., 2011). In addition, co-cultures of HBMSCs and HUVECs increased the expression of N-cadherin which upregulate the early osteoblastic differentiation of HBMSCs through improving cell-cell adhesion between HBMSCs and HUVECs (Li et al., 2010).

*Kirkpatrick and coworkers* have as well developed methods of co-culturing osteoblasts and endothelial cells (EC), aiming to form vascularized constructs on 3D biomaterials (Unger et al., 2007; Unger et al., 2011). Co-culturing human dermis microvascular EC (HDMEC) with primary human osteoblasts (pOB) on 3D silk fibroin scaffolds (or the same cultures plated in 2D) allowed *in vitro* formation of microcapillary-like structures containing a lumen by HDMEC (Unger et al., 2007). No exogenous angiogenic factors are required for the self-assembly of these tissue-like structures.

In summary, it would appear that the EC stimulate the osteoblasts to upregulate VEGF secretion (**Figure I- 20**). Additionally, it was evidenced that ECs can exert a pro-osteogenic stimulus on the MSCs (Rouwkema et al., 2006).

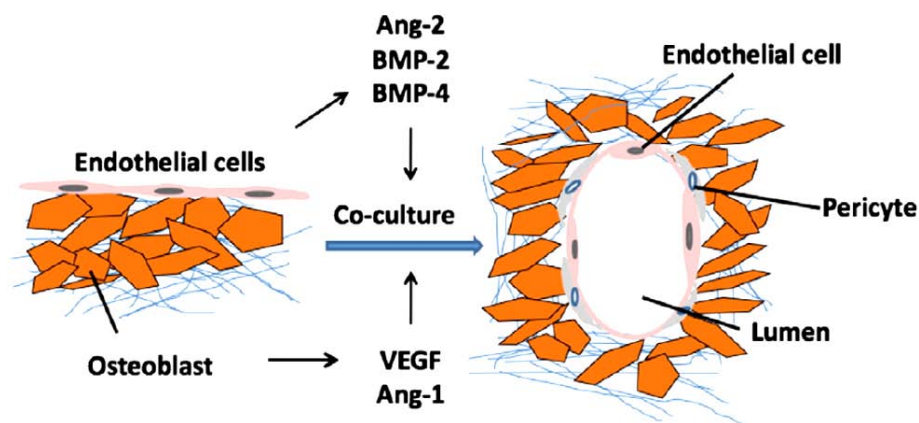


**Figure I- 20** : Schematic overview of cellular crosstalk between osteoblasts and endothelial cells leading to vascular structures in co-culture systems. In addition to mechanisms based on direct cell–cell communication (not depicted), cellular cross talk is mediated by several growth factors involving VEGF and angiopoietins (Ang-1 and -2) guiding angiogenic activity as well as vessel stabilization by pericytes. In addition, BMPs in the co-culture seem to contribute to bone formation and repair. From (*Kirkpatrick et al., 2011*).

Such results would question the rationale of incorporating pro-angiogenic drug- and gene-delivery systems into biomaterial scaffolds for bone regeneration and indicates that there is still much to learn about the biological microenvironment in the regenerative niche. The co-culture models presented before offer the experimental possibility to delineate how specific genes are regulated as a result of cell–cell interactions involving endothelial cells and osteoblasts.



## I.B.2. Scaffold / Bioactive molecules

Another approach to bone regeneration consists in the incorporation of bioactive molecules onto a material. The material acts as a reservoir and the molecules are released in a controlled manner.

The bioactive molecules that are often delivered in bone regeneration applications are:

- Osteoinductive molecules, as BMPs or growth differentiation factor-5 (GDF-5);
- Antibiotics, to fight infection after implantation;
- Angiogenic factors to promote vascularization, such as VEGF;
- Adhesion molecules (RGD).

In some cases, researchers adopt to combine such groups of molecules, for example combining BMP-2 and VEGF to stimulate both bone formation and angiogenesis (Zhang et al., 2014).

The scaffold/material can be degradable being replaced by the native tissue (in applications such as filling bone defects) or not (prosthetics). It can also be a coating to medical devices to help bone regeneration around the implantable material.

Regarding the use of osteoinductive molecules, BMPs such as BMP-2 and BMP-7 are already used in clinics. In the case of BMP-2 it is delivered from type-I collagen sponges (InductOs®, Medtronic) to promote bone repair (**Figure I- 21**).



**Figure I- 21 : InductOs® kit, Medtronic** (A) BMP-2 powder, (B) solution to dissolve powder, (C) bovine type-I collagen sponge.

The growth factor is soaked onto the collagen sponge prior to implantation, then the BMP-2 soaked matrix is transferred to the implantation site. Such kit is used in the treatment of spinal fusion and open tibial fractures (Schmidmaier et al., 2008). This formulation

presents two major problems: a supraphysiological concentration is necessary for the device to be osteoinductive (~ 12 mg) and due to the low affinity between the BMP-2 and the collagen the growth factor is completely cleared from the collagen carriers in less than 14 days *in vivo* (Kim and Valentini, 2002; Geiger et al., 2003; Carragee et al., 2011). This leads to severe side effects such as osteolysis, heterotopic ossifications and immunological reaction (Burkus et al., 2006; McClellan et al., 2006; Carragee et al., 2011).

Such results motivated researchers to continue developing more efficient materials to store and deliver BMP-2. An effective means of delivering low-dose BMP-2 is yet to be clinically validated. Emerging approaches have focused on controlling growth factor release kinetics in order to decrease the needed dose and limit side effects aiming to successfully deliver bone growth factors over longer timescales. Some selected carrier materials are not structurally optimized for bone tissue engineering applications what makes difficult to translate them to clinical applications and they should be associated with other materials that bring the appropriated mechanical properties.

*Cool and coworkers* used hyaluronan-based hydrogels made of thiol-modified hyaluronan (Glycosil™) to deliver BMP-2 (Bhakta et al., 2013). They have compared the *in vitro* and *in vivo* performances of BMP-2 loaded Glycosil™ in comparison to collagen. Glycosil™ binds electrostatically to BMP-2 and it provides a biphasic release profile: an initial burst can be attributed to the dissociation of weakly-bound BMP-2 near to or on the surface of the hydrogel, then as the ionic interactions are lost, the depolymerization of the hydrogel network allows a sustained release thereafter, a process that is enhanced *in vivo* by the actions of proteolytically active fluids and exudates from surrounding tissues. Note that collagen sponges release BMP-2 with only an initial burst phase. The *in vivo* efficacy of Glycosil™ and collagen, both loaded with BMP-2 (with 3 different doses), was assessed by their implantation in muscle pouches of a rat hind limb. Implants were retrieved after 8 weeks. Bone formation was observed in both delivery systems (**Figure I- 22**), however several results support that Glycosil™ is able to protect protein activity and release it over time up to 4 weeks (14 days for collagen). Moreover, Glycosil™ was able to form bone at low BMP-2 concentrations, 0.2 µg and 1 µg, (**Figure I- 22**), which didn't happen for collagen.





Antibiotics loaded materials are as well used in bone regeneration applications. PROSTALAC, an antibiotic-loaded acrylic cement has been used in primary reverse total arthroplasty to prevent post-operative infection (Jawa et al., 2011). Antibiotics such as tobramycin and vancomycin are impregnated in this cement. The antibiotics are release out of the hardened cement over time and kill bacteria responsible for the infection. High but safe levels of antibiotics are delivered and are very effective at curing infections (Masri et al., 1998; Nowinski et al., 2012).

*Garcia and coworkers* have shown that the presentation of VEGF and cell-adhesion motifs from degradable bioartificial hydrogel (polyethylene glycol diacrylate (PEGDA)) appears to improve vascularization after implantation (Phelps et al., 2010). In comparison with injections of VEGF these carrier material allowed 2 weeks of sustained release as the matrix degrades. When implanted subcutaneously in rats, degradable constructs containing VEGF and arginine-glycine-aspartic acid tripeptide (RGD) induced a significant number of vessels to grow into the implant at 2 weeks with increasing vessel density at 4 weeks (**Figure I- 23**).

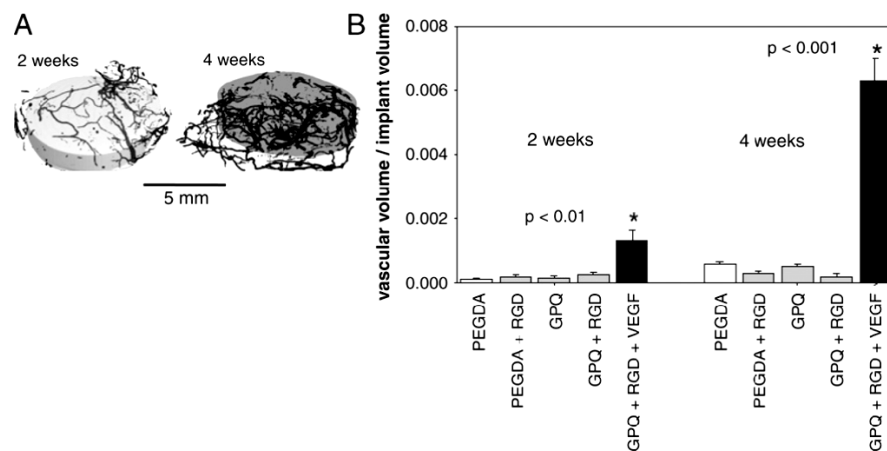


**Figure I- 23:** Analysis of vascularization of bioartificial matrices implanted subcutaneously in rats perfused with Microfil radio-opaque contrast agent. (A) Micro-CT images GPQ+RGD+VEGF implants showing vasculature in surrounding tissue growing into implant, gray volume defines hydrogel. (B) Quantification of vascular volume/total implant volume.  $\pm$ SEM. GPQ = protease degradable sites

### I.B.3. Summary of the remaining limitations and challenges in BTE

As previously mentioned, the number of elements involved in a tissue engineering approach increases the level of complexity in the product development, the regulatory issues

and the safety concerns. Namely, the use of stem cells in such “scaffold/stem cells” therapies addresses several limitations in the “scaffold/stem cells” part that are also summarized in **Table I- 3**.

In cell-free therapies, such as the “scaffold/bioactive molecules” strategy, there are advantages such as scaffolds are easier to sterilize, can have a shelf-life, and there is a lowest potential for infection or immunogenicity. It is important to mention that, in order to keep the bioactivity of the added molecules, the sterilization methods have to be adapted.

**Table I- 3 : Summary of the advantages and limitations of the different BTE approaches.**

<b>Bone tissue engineering approaches</b>	Harvest cells from donor, need two surgical procedures	Potential for infection or immunogenicity	Easy to sterilize / shelf-life	Vascularization
Scaffold	No	+	++++	No
Scaffold + cells	Yes	+++	-	Yes
Scaffold + bioactive molecules	No	+	+++	Depends on the bioactive molecule
Scaffold + cells + bioactive molecules	Yes	+++	-	Yes

The development of three-component therapies is only done at the research level. As an example, *Lee and coworkers* have combined adipose-derived stem cells (ASCs) and BMP-2 in chitosan-based 3D scaffolds (Fan et al., 2014) aiming to improve bone regeneration. Chitosan and chondroitin sulfate, natural polysaccharides, were used to fabricate the 3D porous scaffolds, which were further modified with apatite coatings for enhanced cellular responses and delivery of BMP-2. They mention that the biomimetic apatite coating allows a controlled release of BMP-2 avoiding a high initial burst release after implantation. BMP-2 adsorbs on the apatite surfaces through electrostatic forces (between the negatively charged carboxylic groups of BMP-2 and the positively charged Ca sites on hydroxyapatite) and water-bridged hydrogen bonds. Here they used ACSs cells as cellular model over the use of bone marrow-derived MSCs because of their ability to differentiate to bone in presence of BMP-2, abundant availability and easy accessibility without painful isolation procedures. The efficacy of 3D apatite-coated scaffolds supplemented with ASCs and BMP-2 were evaluated in a rat critical-sized mandibular defect model. After 8 weeks post-implantation, the scaffolds

with ASCs and BMP-2 significantly promoted rat mandibular regeneration (demonstrated by micro-computerized tomography ( $\mu$ CT), histology, and immunohistochemistry) as compared with the groups treated with ASCs or BMP-2 alone. By histology studies they have also evidenced that scaffold degradation may be accelerated by released BMP-2, and thus, provide more space for bone regeneration in the defect. They explain that BMP-2 released from the carrier may initially attract precursor cells (macrophages and monocytes), which are osteoclast precursors that may explain accelerated scaffold degradation. They conclude saying that this strategy can significantly promote mandibular regeneration, and may provide a potential tissue engineering approach to repair large bony defects.

The high complexity involved in such constructs leads to very long and expensive development and even longer testing before a possible industrialization of such products. In addition, the storage and sterilization of such constructs is difficult to imagine, since they contain live cells. One possible way is to prepare such constructs individually (using patient cells) in a completely clean environment to avoid the need for sterilization.

#### **I.B.4. Requirements for clinical translation**

From the industrial and clinical perspectives, shelf-time stability and sterilization of implantable materials are very important issues. Medical devices have to be sterilized after packaging and must maintain their functional properties upon storage for several years (Kasemo and Lausmaa, 1988), usually  $\sim 5$  years for implants and  $\sim 2$  years for bioactive products.

Nowadays the addition of bioactive molecules to several biomaterials increases the difficulty in the process of industrialization, since the storage conditions and sterilization methods should not modify the structure and activity of such molecules.

It is well known that dehydration greatly impact proteins structures (Wang, 2005). The drying process removes part of the hydration layer, which may disrupt the native state of a protein and cause protein aggregation. Protein conformation is very often lost upon storage in dry conditions, unless stabilizers like sugars, polyols or polyaminoacids are added during the freeze-drying process (Wang, 2005).

Ideally, the biomaterial carrier that delivers the bioactive molecules should preserve the protein bioactivity, which is directly related to its secondary and tertiary structure. Note that natural biopolymers are being widely used as carrier for bioactive molecules since they

provide a water-rich environment. This may be a crucial point for preserving the stability of the proteins in dry state once loaded in the biopolymeric materials or coatings.

Regarding the sterilization process, four common types of sterilization are in use today: irradiation (gamma, beta, or e-beam), gas sterilization or ethylene oxide (EtO), steam, and dry heat. Less common methods of sterilization include low-temperature hydrogen peroxide gas plasma (LTHPGP) sterilization, cold sterilization, and disinfectants (Massey, 2005). They can be divided in two main types, chemical or physical methods. Chemical methods have been avoided because of high risk of having traces of chemical residues. Autoclaving is inappropriate for sensitive materials such as natural polymers and proteins, due to the high temperatures, pressure and humidity employed. An alternative to the previous methods is the sterilization by gamma irradiation. Gamma radiation is the most widely used form of ionizing radiation sterilization; in fact, gamma has become the industry standard for high-energy sterilization due to the convenience, low cost, and good sterilization results. It involves the bombardment of photons from a 60-Cobalt ( $^{60}\text{Co}$ ) source. Because of the excellent penetrating ability of gamma rays (they have no mass and are thus able to penetrate deeper into material), a wide range of packaging materials may be gamma-sterilized. Prepackaged articles may also be gamma-sterilized since many materials such as cellophane, polyethylene, and nylon can be penetrated. Gamma is considered to have five times the penetration capability of electron beam radiation. Gamma radiation sterilization usually employs  $^{60}\text{Co}$  as the radioisotope source with a dosage of generally 2.5 megarads, although higher levels are sometimes used, and maximum temperatures usually are in the range of 30°C – 40°C (Massey, 2005). This technique has been largely used by pharmaceutical industries and for medical devices sterilization. Such sterilization method has shown to be less aggressive to sensitive materials or biological molecules and it can sterilize a significant amount of products at the same time. The ideal irradiation dose for each medical device has to be tested (Ratner, 2004).

In conclusion, the presence of biological active molecules makes medical devices more difficult to handle, store and sterilize than traditional biomaterials. Such barriers can impede clinical translation of such innovative solutions, limiting them to the research level (Ferraris et al., 2012).

### **I.B.5. Development of osteoinductive coatings**

In some clinical cases, the natural surface of bulk prostheses materials is not appropriate for successful bone regeneration and osteointegration of implants. As mentioned previously, there is a need to improve such surface properties by increasing osteoconduction and osteoinduction of surfaces.

One method to render an implant osteoinductive is by grafting or incorporating BMPs to the material surface. Such surface modification can be made by direct covalent grafting of BMP-2 onto the surface or by the use of coating in which BMP-2 will be incorporated. Local administration of BMPs onto implantable osteosynthetic materials, such as metal fixatives devices, will broaden the applications of BMPs. Thus, different strategies have been developed to efficiently deliver BMP-2 from the implant surface.

#### ***I.B.5.1. Grafting of BMP-2 onto a material surface***

One way to directly add BMP-2 to the surface of metallic implants is to chemically modify/activate their surface and further add BMP-2 that will adsorb (i.e. non covalent bond) or covalently bound to the material. The nature of the chemical bond depends on the surface treatment.

*Jennissen and coworkers* have developed a grafting technique to directly add BMP-2 to metallic implants (Jennissen, 1999). Ti implants of Ti-coated implants were treated with chromosulfuric acid (CSA) leading to a nanostructured, ultrahydrophilic, high-binding-capacity surface made of amorphous TiO<sub>2</sub> surface. To perform the covalent binding of rhBMP-2 they first activate the surface with 1,10-carbonyl diimidazole and then they add rhBMP-2. The *in vivo* performance of such modified surfaces was evaluated in comparison to untreated implants showing that the immobilized layer of rhBMP-2 retains its high osteoinductive activity (Chatzinikolaidou et al., 2010). After few weeks of implantation it led to a significant increase in bone density, a significant increase in bone-to-implant contact and the enhanced filling of a 1 mm gap with trabecular or cortical bone.

*Cavalcanti-Adam and coworkers* have immobilized BMP-2 on a surface by means of NHS-functionalized self-assembled monolayer (SAM) and then covalent immobilization of rhBMP-2 (iBMP-2) (**Figure I- 24**) (Pohl et al., 2013).

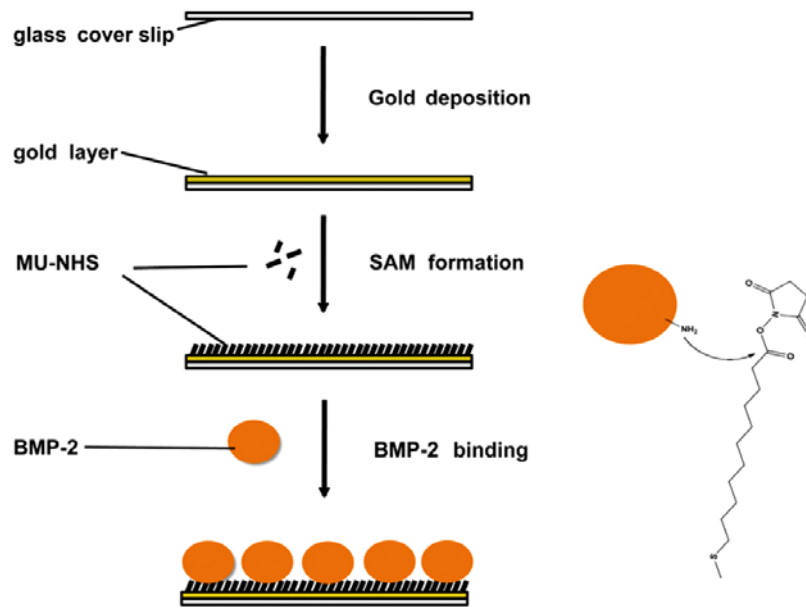


**Figure I- 24 :** *Scheme of the experimental set-up for immobilization of BMP-2 on gold layers. Preparation of iBMP-2 surfaces: A gold layer is deposited on a glass coverslip and subsequently incubated with a heterobifunctional linker that strongly binds to gold surfaces generating a self-assembled monolayer (SAM). Next rhBMP-2 is immobilized on the surface via covalent binding of its primary amines to the linker (Pohl et al., 2013).*

They were able to detect iBMP-2 with an anti-BMP-2 antibody observing the coated BMP-2 on the surface by fluorescence. Then they compared the activation of the BMP signaling in BMP responsive myoblast cells (C2C12 cells) when contacting iBMP-2 or BMP-2 in solution. Importantly, they have shown that iBMP-2 was able to activate BMP signaling pathways.

*Samitier and coworkers* have created gradients of BMP-2 by grafting biotinylated BMP-2 to a gradient of carboxylate groups created on a PMMA surface via hydrolysis. This approach for generating BMP-2 surface gradients requires a hydrolyzable substrate and the biotinylation of the growth factor.

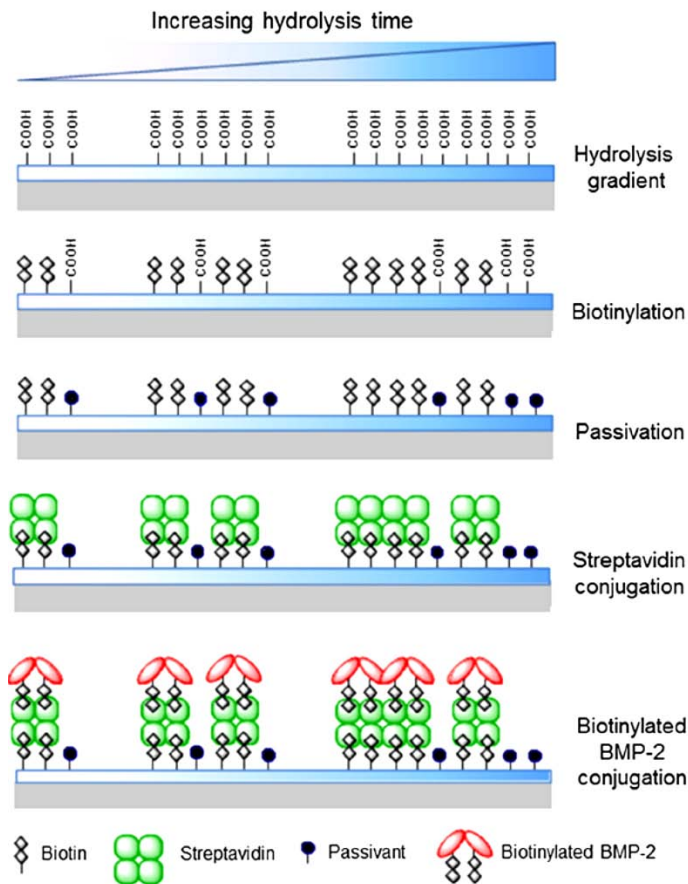


**Figure I- 25 :** Schematic representation of the functionalization steps performed on the carboxylic acid gradient initially obtained after PMMA hydrolysis. BMP-2 was immobilized on the surface by taking advantage of the well-known biotin-streptavidin complex, which ensured strong yet flexible anchoring and thus guaranteed proper ligand-receptor interactions.

They have evaluated early stages of osteogenesis in C2C12 cells after contacting the BMP-2 gradients. They have shown a dose-dependent response in the expression of two osteogenic markers, osterix (OSX) and alkaline phosphatase (ALP). In these two later examples, the BMP-2 grafted surfaces are used for *in vitro* fundamental studies aimed to understand the effect of BMP-2 presentation on the cell behavior and not for clinical applications.

In some cases, direct covalent grafting of BMP-2 onto a metal surface allows only small amounts of BMP-2 to be delivered and sometimes it is not enough to induce bone formation (Becker et al., 2006). In addition, direct adsorption of BMP-2 can lead to a rapid burst of the protein because of its low affinity with metal surfaces.



### ***I.B.5.2. Biomimetic coatings as reservoirs for BMP-2***

In order to increase the affinity between BMP-2 and the implant surfaces, biomimetic coatings as HAP or natural biopolymers have been used. These formulations are promising because of the similarity of HAP and biopolymers with bone tissue constituents. The underlying strategy is that a biomimetic matrix can trap, retain, and deliver BMP-2 locally in a more efficient manner.

To enhance peri-implant osteogenesis, the combination of an osteoconductive material such as HAP with osteoinductive molecules as BMP-2 seems ideal. HAP alone as coating is already being used to improve the osteoconductivity of implants (de Groot et al., 1987; Geesink, 1990; Freeman, 1992; Jaffe and Scott, 1996; Dumbleton and Manley, 2004).

BMP-2 incorporated in biomimetic calcium phosphate coatings were developed by *Liu et al* (Liu et al., 2005). They deposited calcium phosphates by soaking the implants under mild conditions of pH and temperature into Simulated Body Fluid (SBF), which has a similar inorganic content to human blood plasma. BMP-2 was added in the same solution to prepare BMP-2 incorporated CaP coatings (Liu et al., 2005). Two different modes of BMP-2 presentation were further studied: adsorbed BMP-2 onto the HAP coating in comparison with BMP-2 incorporated-HAP coating. Their findings indicate that the osteoinductive efficacy of BMP-2 can be influenced by its mode of delivery. Incorporation of BMP-2 in the coating augments bone formation (***Figure I- 26***) more efficaciously than when BMP-2 is adsorbed on the coating (Liu et al., 2007; Hunziker et al., 2012). BMP-2 incorporated coatings represent simple, efficacious and cost-effective tool to expedite and augment bone formation. However, the BMP-2 amount inside such coatings has to be further optimized to find the good balance between bone formation and bone resorption and the degradation rate of CaP coatings must be decreased.

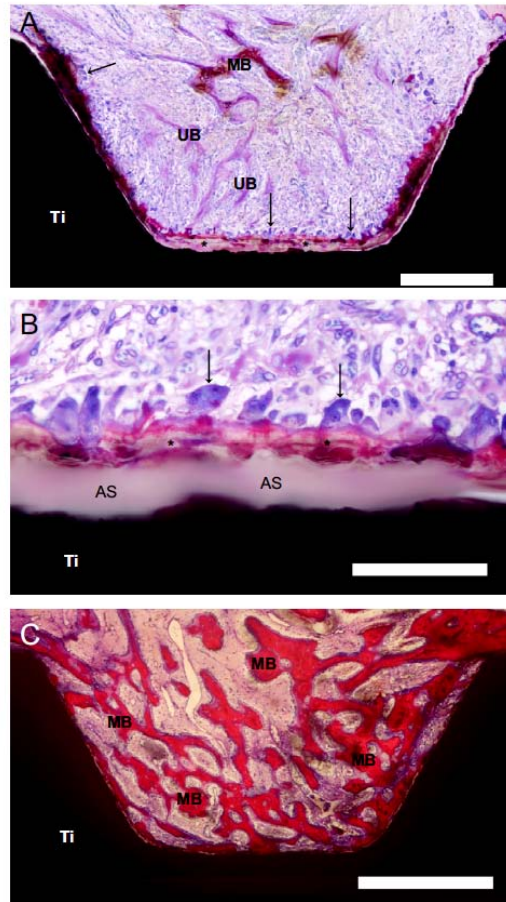


**Figure I- 26 :** Light micrographs of 100- $\mu\text{m}$ -thick sections through a bone chamber of titanium implants after surface staining with basic fuchisine, Toluidine Blue O and McNeal's Tetrachrome. (A) Titanium implant (Ti) bearing a calcium-phosphate coating into which BMP-2 was incorporated, 1 week after surgery. At this stage, the coating (\*) is being voraciously degraded by osteoclasts (arrows). Within the chamber, most of the newly formed osseous tissue is as yet unmineralized (UB). A few seams of mineralized bone (MB) are nevertheless apparent. Bar = 500  $\mu\text{m}$ . (B) High-magnification view of (A), illustrating serried osteoclasts (arrows) along the surface of the coating (\*). The space (AS) between the coating and the titanium implant (Ti) is an artefact of tissue processing. Bar = 100  $\mu\text{m}$ . (C) Titanium implant (Ti) bearing a calcium-phosphate coating into which BMP-2 was incorporated, 3 weeks after surgery. By this 3-week juncture, the coating has been completely degraded by osteoclasts. All of the newly formed osseous tissue has undergone mineralization (MB). Bar = 500  $\mu\text{m}$ . From (Liu et al., 2007).

Moreover, the addition of BMP-2 to the Ti surface was also investigated by using collagen I as carrier (Schliephake et al., 2005). It was shown that collagen alone can improve bone formation around the implant. However, the addition of BMP-2 to the collagen coating did contribute to a further increase in peri-implant bone formation. *In vivo* studies demonstrated that BMP-2 adsorbed collagen coated Ti implants allowed bone formation around the implant but no differences were observed in presence or absence of BMP-2. The bad affinity between collagen and BMP-2 may explain such results.

BMP-2 immobilization on surfaces was also performed by the grafting of chitosan (Lim et al., 2009) or heparin (Kim et al., 2011) as reservoirs for the protein. Both types of coating demonstrated satisfactory results *in vitro*, the grafting of heparin on Ti surfaces and further BMP-2 incorporation inhibited inflammation and the osteoblast function was promoted (Kim et al., 2011). Further studies are required to determine the appropriate doses of rhBMP-2 for *in vivo* application of these delivery systems and validate *in vitro* results.

### ***I.B.5.3. Polyelectrolyte's multilayer (PEM) films***

#### **I.B.5.3.1. Layer-by-layer method**

Layer-by-layer (LbL) films offer numerous possibilities for the development of substrates with well-controlled biochemical and mechanical properties and have become a highly studied class of biomaterials over the past decade. The technique was introduced in the early 1990s by Decher, Möhwald, and Lvov (Decher et al., 1992; Lvov et al., 1994; Decher, 1997) and has attracted an increasing number of researchers in recent years due to its high versatility and wide range of advantages for potential biomedical applications. PEM films are currently emerging as a new kind of biomaterials coating that can be used to guide cell fate (Leguen et al., 2007; Boudou et al., 2010; Detzel et al., 2011). They can be used either as 2D materials for investigation of cellular behavior on defined substrates, or for coating of 3D constructs such as implants or tissue engineering scaffolds.

The LbL deposition method consists in the alternate adsorption of polyelectrolytes that self-organize on the material's surface, leading to the formation of the PEM films (**Figure I-27**) (Decher et al., 1992; Lvov et al., 1994; Decher, 1997).

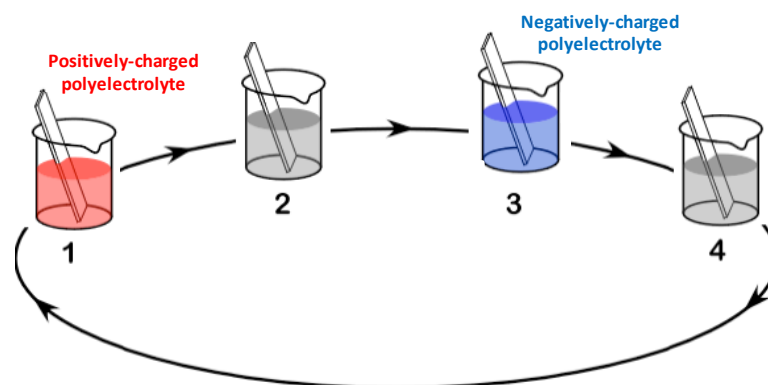


**Figure I- 27 : Schematic representation of the layer-by-layer dipping process.** Film deposition starts with a positively-charged polyelectrolyte solution onto a negatively charged substrate. Adapted from (Decher, 1997).

The procedure of LbL deposition is relatively simple and versatile as it is possible to modulate film growth and internal structure by choosing the nature of polyelectrolytes and assembly parameters such as pH and ionic strength (Shiratori and Rubner, 2000). PEM film fabrication can be performed under mild conditions in an aqueous environment, which is a great advantage when using sensitive molecules such as biopolymers and proteins that can easily lose their properties if used in harsh conditions.

The method was originally developed by dipping the substrate (e.g. glass slides or silicon wafer) in the different polyelectrolyte solutions. An analogous method consists in depositing the solutions on the substrate by spin-coating or by spray. Polyelectrolytes can also be deposited onto small particles, which can be further dissolved to give hollow microcapsules, that can be used for drug delivery and many other applications (Antipov and Sukhorukov, 2004; Becker et al., 2010), or onto viable cells (Wilson et al., 2011). Such coating helped to maintain cell viability and function upon *in vivo* transplantation.

Besides polyelectrolytes, other types of components can be assembled using LbL method, among them proteins (Johansson et al., 2005; Zhang et al., 2005), nanoparticles, nanowires and carbon nanotubes (Jan and Kotov, 2007; Srivastava and Kotov, 2008; Zhang et al., 2012), and even living cells (Matsusaki et al., 2007; Chetprayoon et al., 2013).

The mechanical properties of the films can be modulated by several techniques, including chemical cross-linking by carbodiimide (Richert et al., 2004) and photocrosslinking using photosensitive derivatives of the polyelectrolytes (Olugebefola et al., 2006; Vazquez et al., 2009).

The versatility of PEM films makes of them a valuable tool for the studies of the effects of different stimuli, physical and biochemical, on cellular processes, and for the control of cell fate.

#### **I.B.5.3.2. Incorporation of BMP-2 in PEM films**

The coating of biopolymers for retention of bioactive molecules and their delivery appears promising due to their similarity with natural tissues. Thus, PEM films made of different biopolymers can be functionalized by bioactive molecules such as adhesive peptides (Berg et al., 2004; Picart et al., 2005; Tsai et al., 2009) or charged with growth factors for local delivery (Crouzier et al., 2009; Macdonald et al., 2011; Shah et al., 2011). PEM films have already been used to trap and deliver BMP-2 (Dierich et al., 2007; Crouzier et al., 2009;

Crouzier et al., 2010; Facca et al., 2010; Macdonald et al., 2011). To this end, different strategies have been developed (**Figure I- 28**).

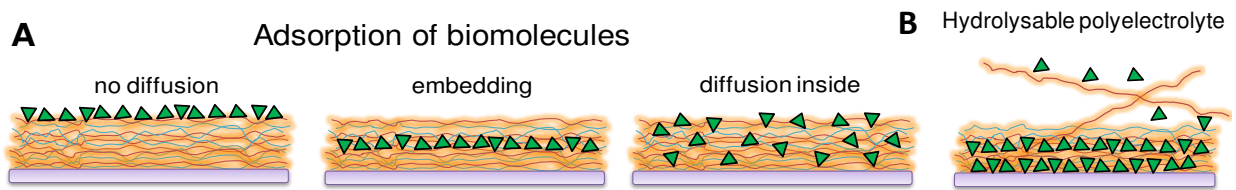


**Figure I- 28 : Schematic representation of the different possibilities of incorporating BMP-2 inside PEM films.** (A) Adsorption of the BMP-2 can be achieved after film buildup or at a certain step during buildup. In case of diffusion, the bioactive molecule can be loaded in the “bulk” of the film; (B) BMP-2 is used as a polyelectrolyte during film buildup in combination with hydrolysable polymers, which degrade and thus release BMP-2. Adapted from (Gribova et al., 2012).

BMP-2 can be adsorbed on top of PEM films, be entrapped in the film during buildup, be post-loaded into the film or directly assembled with hydrolysable polymer.

*Jansen and coworkers* have performed multilayered coatings from either poly-d-lysine (PDL) or poly(allylamine hydrochloride) (PAH) and DNA to act as carrier for BMP-2 (van den Beucken et al., 2006). BMP-2 addition to these DNA-coatings was performed using different loading modalities being one of them the presentation of adsorbed BMP-2 (superficial presentation). *In vitro* experiments using bone marrow-derived osteoblast-like cells demonstrated that BMP-2 remained biologically active and an accelerated calcium deposition was observed.

*Jessel and coworkers* developed multilayered films made of poly(L-glutamic acid) (PGA), poly(L-lysine), BMP-2 and TGFβ-1 (Dierich et al., 2007). BMP-2 and TGFβ-1 were entrapped at a certain step during film buildup to prepare these capsules. These multilayered capsules were found to be osteoinductive inducing bone formation *in vivo* (Facca et al., 2010).

In our group, the PhD thesis of Thomas Crouzier (Crouzier, 2010) was dedicated to the incorporation of BMP-2 in LbL films by post-diffusion. To this end, PLL/hyaluronan (PLL/HA) films were built, cross-linked and then loaded with BMP-2. These films were found to act as reservoir for rhBMP-2 (Crouzier et al., 2009), rhBMP-2 being trapped in the film and remaining bioactive for more than 10 days. The quantity of rhBMP-2 loaded in the film depended on the film thickness (i.e. the number of layer pairs) and on the initial BMP-2 concentration of the loading solution (**Figure I- 29**).

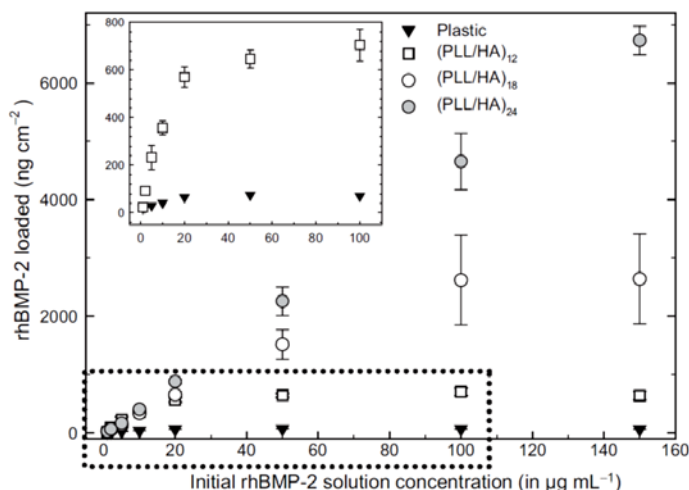


**Figure I- 29 :** *rhBMP-2 amount loaded in crosslinked (PLL/HA)<sub>i</sub> films of different thickness (i = 12, ~1 µm; i =18, ~ 1.6 µm; i =24, ~ 3.5 µm) as a function of the initial rhBMP-2 solution concentration. From (Crouzier et al., 2009).*

It is well known that C2C12 myoblasts can undergo osteogenic differentiation when treated with BMP-2 growth factor (Katagiri et al., 1994). The protein was presented to C2C12 myoblast cells in solution or trapped in the (PLL/HA) films. C2C12 culture on BMP-2 loaded (PLL/HA) films induced myoblasts differentiation into osteoblasts in a dose-dependent manner (Crouzier et al., 2009). Low doses of surface-adsorbed rhBMP-2 blocked C2C12 differentiation into myotubes, while higher doses allowed the development of an osteogenic phenotype, as measured by ALP production (**Figure I- 30**). The rhBMP-2-containing films could sustain three successive culture sequences while remaining bioactive, thus confirming the important and protective effect of rhBMP-2 immobilization. Moreover, when the protein was presented from the film in a “matrix-bound” manner, a drastic increase in cell spreading and migration was noticed (Crouzier et al., 2011a).

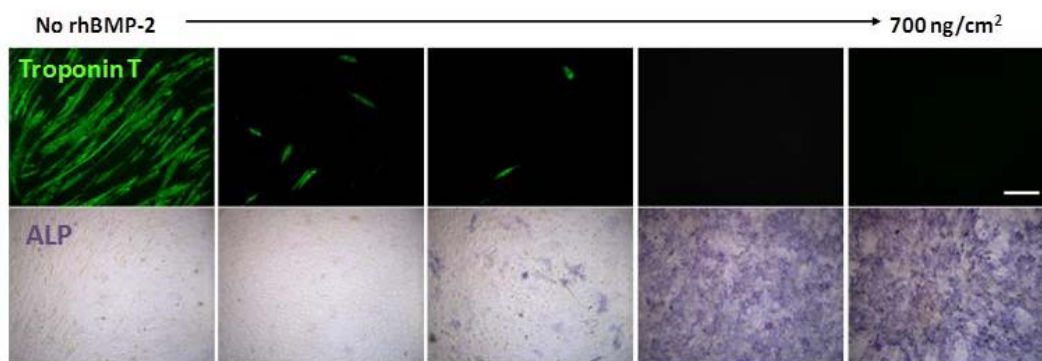


**Figure I- 30 :** *BMP-2 loaded (PLL/HA) films induce C2C12 osteogenic differentiation. Immunochemical and histochemical staining of troponin T (green) and ALP (alkaline phosphatase, violet) of C2C12 on BMP-2 loaded films for increasing BMP-2 initial concentrations. Adapted from (Crouzier et al., 2009).*



The performance of these BMP-2 loaded films as coatings for biomaterials was then assessed. The first *in vivo* study aimed to evaluate the osteoinductive properties of TCP/HA granules coated with BMP-2-loaded films (Crouzier et al., 2011b). *In vivo*, the PEM coatings loaded with rhBMP-2 exhibited rise both osteoconductive and osteoinductive capacities to the scaffold material (**Figure I- 31**), although their bone inductivity potential was not as high as TCP/HAP scaffolds with adsorbed BMP-2 used as control. Nevertheless, these polyelectrolyte multilayer films allowed achieving osteoinduction with a much lower amount of rhBMP-2 than is required for the collagen sponge. Other types of implantable materials that lack affinity for rhBMP-2, such as titanium, could greatly benefit from these surface coatings.

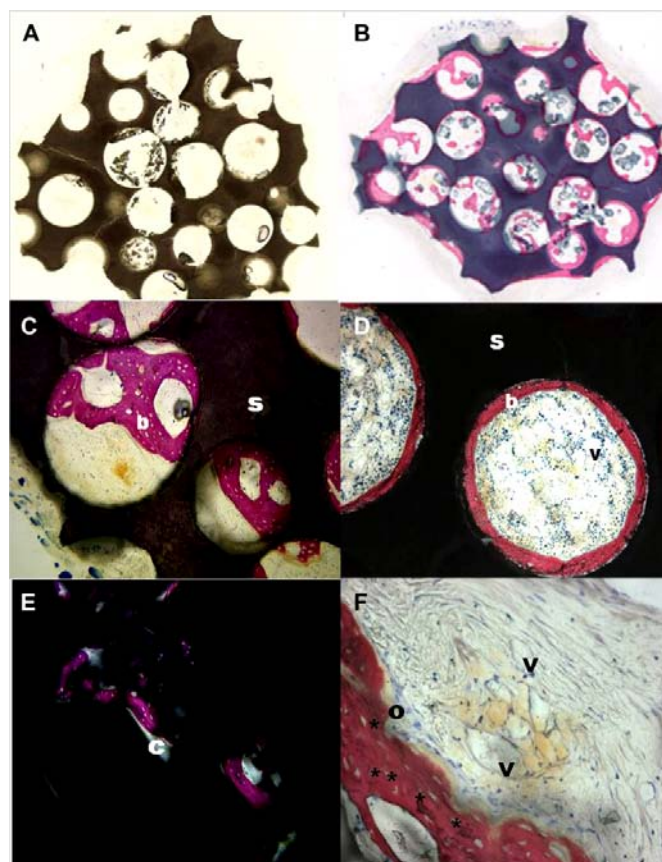


**Figure I- 31 : Histological analysis of TCP/HAP granules coated with film, with and without rhBMP-2.** Bone tissue cross sections of TCP/HAP granules coated with film@EDC50 without rhBMP-2 (A) and coated with film@EDC10 with rhBMP-2 (B) at 6 weeks post-implantation (X20). (C) Bone was found inside the pores (X100) or (D) lining around the matrix surface (X50). Section under phase contrast (C) and corresponding cross-polarized light micrographs (E) showing representative birefringence of collagen strands (X100). (F) Note the presence of embedded osteocytes and osteoblasts laying down the osteoid tissue, consistent with an active new bone formation (X200) (s, scaffold; b, mineralized bone; C, collagen birefringence; V, vessel, \* osteocytes, o, osteoid).

Due to the interesting properties of rhBMP-2 loaded (PLL/HA) films as osteo-inductive coatings, a valorization project started in 2009 at the LMGP, thanks to the help of GRAVIT (Grenoble Alpes Valorization). The aim was to coat implantable biomaterials and to investigate whether the results obtained *in vitro* can be translated *in vivo*. Ultimately, the goal is to translate the PEM technology to orthopedics and to coat bone implants with the bioactive film in order to induce and accelerate bone tissue regeneration. The requirements are that the film needs to be stored in a dry state, prior to its used in clinics and also that it should sustain a sterilization process. On a more fundamental point of view, the influence of matrix-bound BMP-2 on cell early adhesion migration was further studied in the PhD thesis of Laure Fourel (Fourel, 2012) and a crosstalk between BMP receptors and adhesion receptors was evidenced.

Finally, the last strategy for trapping BMP-2 in LbL films was proposed by *Hammond and coworkers*. It consists in using hydrolysable poly(□□ aminoesters) that are assembled with BMP-2. *Hammond and coworkers* developed a LbL coating made of a hydrolysable polymer, chondroitin sulfate and BMP-2 (**Figure I- 32**) where BMP-2 was used as a polyelectrolyte (Macdonald et al., 2011).

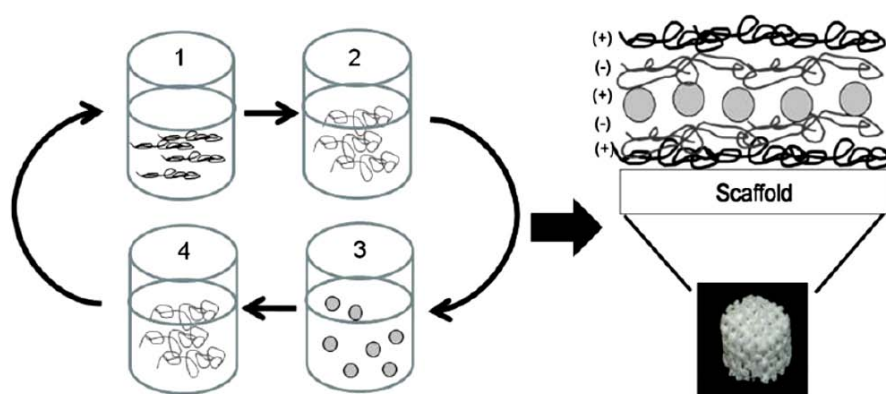


**Figure I- 32 : Schematic representation of the preparation of BMP-2-containing LbL films.** A 3-dimensionally printed  $\beta$ -tricalcium phosphate/polycaprolactone scaffold (or glass surface) is repeatedly dipped with tetralayer units consisting of (1) Poly2 (positively charged), (2) chondroitin sulfate (negatively charged), (3) BMP-2 (positively charged) and (4) chondroitin sulfate. This tetralayer structure is repeated 100 times. From (Macdonald et al., 2011).

They showed that LbL-coated polycaprolactone/ $\beta$ -tricalcium phosphate (PCL/ $\beta$ -TCP) co-polymer blend 3D-scaffolds with incorporated rhBMP-2 induced bone formation with pattern fidelity to the underlying scaffold (Macdonald et al., 2011). They evidenced that new bone formation continued at 9 weeks after *in vivo* implantation. These findings confirmed the



importance of the slow release provided by the LbL carrier and of the rhBMP-2 surface concentration to induce bone formation.

More recently, the same group used such films to coat PLGA membranes for healing of a cranial defect (Shah et al., 2011; Shah et al., 2014). In this case, they have incorporated not only BMP-2, which was enriched in bottom layers of the film, but also PDGF in the top. When the film surface degraded from the top down, the growth factors eluted, in which the PDGF eluted faster than the BMP-2. It is known that the release of specific known growth factors, BMP-2 and PDGF-BB, either individually or in combination, is critical to enhanced bone regeneration. This combination of growth factors has been reported by others to induce rapid and successful bone-tissue regeneration (Martino et al., 2014). In their study, the released growth factors directed cellular processes to induce bone repair in a critical-size rat calvaria model (Shah et al., 2014) promoting local bone formation that bridged the critical-size defect as early as 2 weeks after implantation. Mature, mechanically competent bone regenerated the native calvaria form. This approach could be clinically useful and has significant benefits as a synthetic, off-the-shelf, cell-free option for bone tissue repair and restoration. One disadvantage of these films is the high number of layers required to form the coating (100).

## **I.C. Signaling by receptors: the case of BMP-2**

### **I.C.1. BMP receptors and signaling**

BMP receptors are serine/threonine kinase receptors termed type I (BMPR-I and activin) and type II (BMPR-II) receptors. The type II receptors are constitutively active kinases, which transphosphorylate type I receptors upon ligand binding. The type I receptors activate intracellular substrates such as Smad proteins and thus determine the specificity of intracellular signals. In total, 7 different receptors have been isolated in mammals, which were originally termed activin receptor–like kinase (ALK) (*Figure I- 33*) (ten Dijke et al., 1994a; ten Dijke et al., 1994b; Massague, 1998): ALK-1, ALK-2, ALK-3, and ALK-6 are BMP type I receptors, while ActR-IIA, ActR-IIB, and BMPR-II are type II receptors.

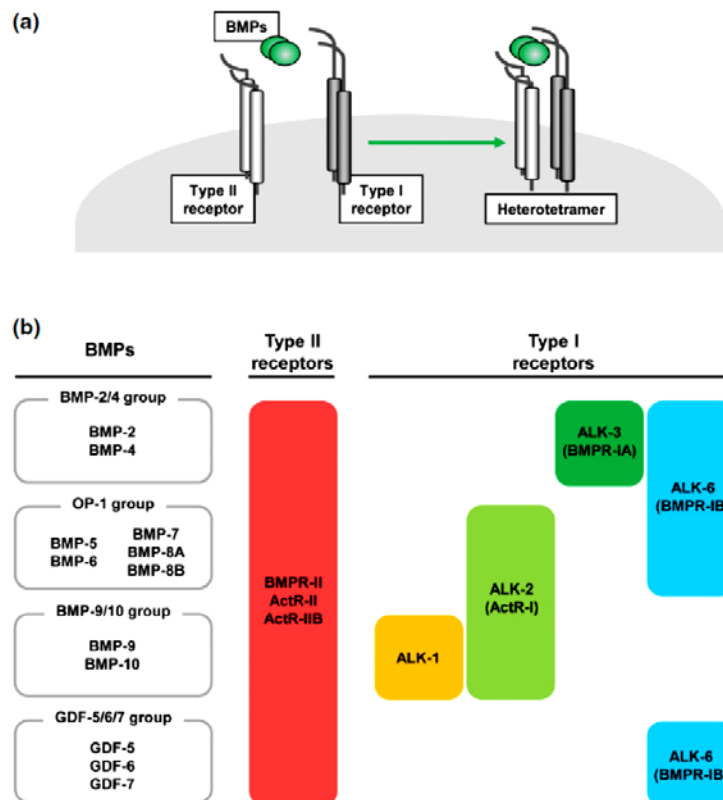


**Figure I- 33 : Binding of different BMPs to BMP type II receptors and BMP type I receptors.** (a) BMP signaling requires the formation of heterotetramers of two type II receptors and two type I receptors. Although certain BMPs bind to type I receptors in the absence of type II receptors, binding affinities to type I receptors increase in the presence of type II receptors. (b) Different BMP ligands can bind different type II and type I receptors. BMPs are divided into several subgroups, i.e., BMP-2/4 group, OP-1 group (BMP-5/6/7/8 group), GDF-5/6/7 group, and BMP-9/10 group. From (Ehata et al., 2013).

The presence of the different receptors depends on the cell type. Also, the present receptors can play a role or not in the activation of signal transduction. For instance, in C2C12 myoblasts, which will be used in this PhD thesis, the BMP receptors present are shown in **Table I- 4** (Heinecke et al., 2009). The receptors highlighted in bold are involved in the activation of BMP-2 signaling and the ones in gray are expressed at very low levels in C2C12 (Namiki et al., 1997; Heinecke et al., 2009; Mueller and Nickel, 2012).

**Table I- 4 : BMP receptors present in C2C12 cells (in bold, those that are involved in BMP-2 signaling and in gray those who are poorly expressed in C2C12).**

	<b>Type I</b>	<b>Type II</b>
<b>BMP receptors</b>	<b>BMPR-IA (ALK 3)</b>	ActR-IIA
	BMPR-IB (ALK 6)	ActR-IIB
	ActR-I (ALK 2)	<b>BMPR-II</b>

Regarding the location of BMP-2 receptors at the plasma membrane, it was shown that they are housed in caveolae and clathrin-coated pits (CCPs) regions of the plasma membrane (Nohe et al., 2005; Bonor et al., 2012; Saldanha et al., 2013). Mobility and localization of transmembrane BMP receptors was also investigated by *Guzman et al.* BMPR-IA was found exclusively in the detergent-resistant membrane (DRM) fractions and BMPR-II in both DRM and non-DRM fractions of the plasma membrane. FRAP studies on C2C12 cells containing a BMPR-IA or II receptor fused to a fluorescent protein (YFP-fused BMPR-IA or BMPR-II) revealed a greater immobile fraction for BMPR-IA than for BMPR-II (Guzman et al., 2012). BMPR-II was redistributed toward DRM fractions after BMP-2 stimulation and a reduction of BMPRII mobile fraction to BMPR-IA levels was shown, indicating that BMPR-II becomes immobilized after ligand binding. Lack of mobility of BMPR-II receptors reflects its hetero-oligomerization with BMPRI in a pre-formed heteromeric receptor complex containing Type I and type II (PFC) or its recruitment to BMPR-I in the presence of BMP-2 to form a BMP-2 induced signaling complex (called “BISC”) (Gilboa et al., 2000; Guzman et al., 2012).

Members of the TGF- $\beta$  family exert their effects via binding to the two types of receptors, both of which are essential for signal transduction (Kawabata et al., 1998; Massague, 1998; Mueller and Nickel, 2012). Similarly BMP-2 signaling involves growth factor binding to heteromeric receptor complexes composed of BMPR-I and BMPR-II receptors. These receptors are present at the plasma membrane as homomeric and heteromeric complexes, which are modulated by ligand binding (Nohe et al., 2002; Miyazono et al., 2005; Mueller and Nickel, 2012). Receptors of both types are needed to form a functional complex to initiate further signaling events. Additionally, BMP-2 binds type I and type II receptors with differing affinities showing higher affinity for the type I receptors (Ia and Ib) (Koenig et al., 1994; Knaus and Sebald, 2001; Heinecke et al., 2009).

According to *Knaus and coworkers*, binding of BMP-2 to its receptors may trigger Smad as well as non-Smad pathways (**Figure I- 34**) (Nohe et al., 2002; Hartung et al., 2006).

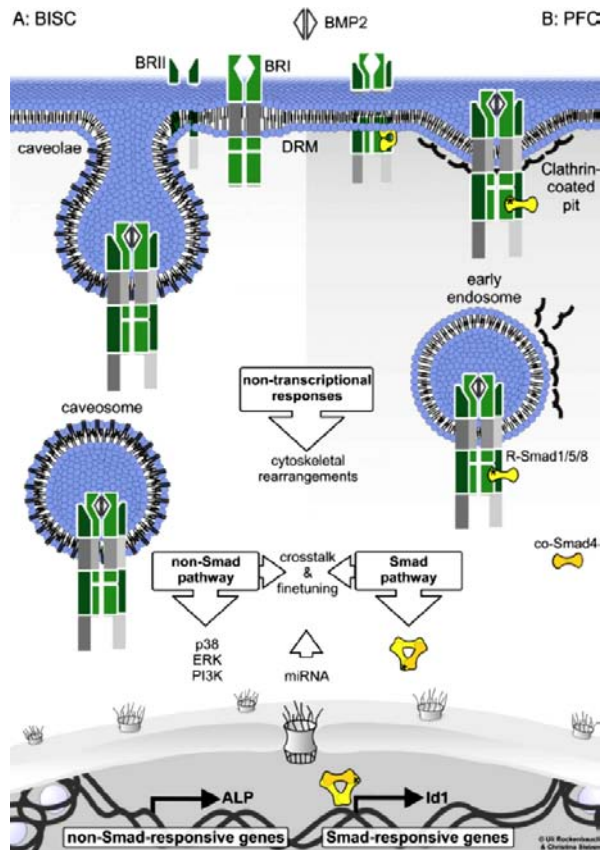


**Figure I- 34 : The BMP-2 signaling pathways.** (A) non-SMAD signaling via BMP-induced signaling complex (BISC) (B) Smad signaling via preformed complex (PFC). From (Sieber et al., 2009).

BMP-2 binds to a pre-formed complex (PFC) of BMPRIa and BMPRII on the plasma membrane resulting in the phosphorylation of the BMPRIa receptor followed by activation of Smad signaling. The complex is internalized by clathrin and the activated BMPRI receptors phosphorylate Smad1, Smad5, and Smad8 (R-Smads), which then assemble into heteromeric complexes with Smad4 (Co-Smad) and translocate into the nucleus to regulate transcription of target genes. Although activation of the Smad pathway is initiated by the binding of BMP-2 to preformed BMPRI and BMPRII complexes, a different pathway culminating in the induction of ALP through p38 MAPK is activated by the BMP-induced signaling complex formation (BISC). In this case, BMP-2 binds to its high affinity type I receptor (BMPRI) upon which the type II receptor (BMPRII) is recruited into the complex. The ligand-receptors complex is formed and internalized in caveolae creating a signaling pathway dependent of MAPK (mitogen activated protein kinase) where p38, ERK and PI3 kinases bind to BMPRI. The activation of MAPKs is followed by their translocation in the nuclei where they regulate the gene expression for osteopontin, alkaline phosphatase or collagen I. SMAD and non-SMAD are not completely independent pathways as there is cooperation and regulation

between these two routes. In addition, BMP-2 also regulates non-transcriptional signalization in the organization of the cytoskeleton (Nohe et al., 2002; Sieber et al., 2009).

### **I.C.2. Endocytosis and signal transduction: intertwined processes**

The plasma membrane of eukaryotic cells is a crucial interface that mediates communication between the cell interior and its environment. Formation and inward cytosolic movement of plasma membrane vesicles is termed *endocytosis*. Endocytosis is a basic cellular process that cells use to internalize various molecules. Any endocytic pathway that mediates transport of a specific cargo will first require mechanisms for selection at the cell surface (Ivanov, 2008; Doherty and McMahon, 2009). Endocytosis involves multiple stages. First, the cargo is engulfed in membrane invaginations that are pinched off to form membrane-bound vehicles, endosomes. Then, the endosomes deliver the cargo to various specialized vesicular structures, enabling the sorting of the cargo towards different destinations. In the end, the cargo is delivered to different intracellular compartments, recycled to the extracellular medium or delivered across the cell (process called ‘transcytosis’) (Conner and Schmid, 2003; Doherty and McMahon, 2009).

Endocytosis and signal transduction are intertwined processes and it is recognized that these processes are intimately and bidirectionally related (Chen, 2009; Sorokin and von Zastrow, 2009). The endocytosis of many signaling receptors is stimulated by ligand-induced activation. Endocytosis of cell surface receptors is an important regulatory event in signal transduction (Di Guglielmo et al., 2003).

#### **I.C.2.1. Endocytic pathways**

The endocytic pathways are defined by the protein machinery that assists the endocytic process and the cargoes they transport. They can be generally divided in two main groups: phagocytosis (uptake of large particles) or pinocytosis (uptake of fluids or solutes). The different entry pathways to the cells are illustrated in *Figure I- 35*.

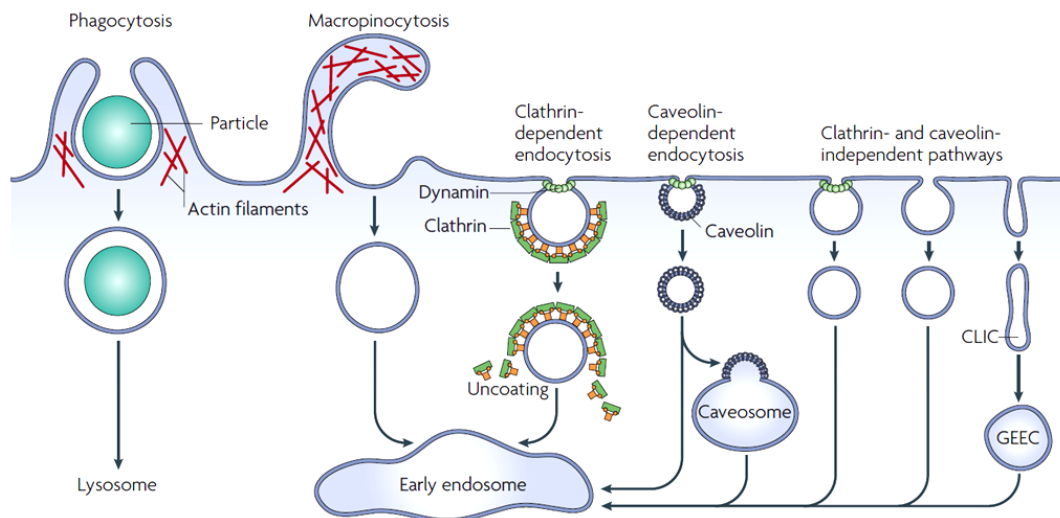


**Figure I- 35 : Pathways of entry into cells.** Large particles can be taken up by phagocytosis, whereas fluid uptake occurs by macropinocytosis. Both processes appear to be triggered by and are dependent on actin-mediated remodelling of the plasma membrane at a large scale. Compared with the other endocytic pathways, the size of the vesicles formed by phagocytosis and macropinocytosis is much larger ( $> 1 - 2 \mu\text{m}$  and can go up to  $20 \mu\text{m}$ ). Numerous cargoes can be endocytosed by mechanisms that are independent of the coat protein clathrin and the fission GTPase, dynamin. Most internalized cargoes are delivered to the early endosome via vesicular (clathrin- or caveolin-coated vesicles) or tubular intermediates (known as clathrin- and dynamin-dependent carriers (CLICs)) that are derived from the plasma membrane (typical size  $<300 \text{ nm}$ ). Some pathways may first traffic to intermediate compartments, such as the caveosome or glycosyl phosphatidylinositol-anchored protein enriched early endosomal compartments (GEEC), en route to the early endosome. From (Mayor and Pagano, 2007).

The different endocytic pathways can be described as follows:

- Phagocytosis: engulfment of a solid particle (up to  $20 \mu\text{m}$ ) forming a large F-actin-coated vacuoles known as a phagosome;
- Macropinocytosis: uptake of solute macromolecules from the extracellular space (macropinosomes) involving the formation of large F-actin-coated vacuoles;
- Clathrin-dependent endocytosis: involves the assembly of a specific coat protein, clathrin, on the intracellular face of the PM, resulting in the formation of a clathrin-coated pits (CCPs);
- Lipid rafts/Caveolae-mediated endocytosis: invaginations of cholesterol-enriched domains within the PM that may or not contain caveolin (without caveolin they are known as *lipid rafts* and in presence of caveolin, *caveolae*);
- Clathrin- and caveolin-independent endocytosis: include CDC42-, Flotilin-, RhoA- or ARF6-regulated endocytic pathways. Such pathways are a lot less described in the literature than clathrin- and caveolin-dependent routes, they are called by the name of

the GTPase involved in the internalization process (Conner and Schmid, 2003; Mayor and Pagano, 2007; Ivanov, 2008; Mayor et al., 2014).

Importantly, in **Figure I- 35** we can see that dynamin has a function in the formation of the vesicles of endocytosis. Dynamin is a GTPase involved in the scission of newly-formed vesicles from the plasma membrane (Danino and Hinshaw, 2001). CCPs, caveolae vesicles and other routes that are independent of clathrin and caveolin need the action of dynamin to finish the endocytosis process.

### **I.C.2.2. BMP receptors endocytosis and relation with signaling**

The endocytosis of transmembrane receptors by clathrin-dependent and -independent pathways plays a major role in the control of receptor density at the cell surface (Gruenberg, 2001). Internalized cell surface receptors undergo either recycling to the plasma membrane or transport to lysosomes for degradation (Katzmann et al., 2001). Moreover, endocytosis was proposed to be required for the signaling of several transmembrane receptors (Ceresa and Schmid, 2000; Di Guglielmo et al., 2003; Mitchell et al., 2004). *Di Guglielmo et al* showed that segregation of transforming growth factor  $\beta$  (TGF- $\beta$ ) receptors into distinct endocytic compartments regulates Smad activation and receptor turnover (Di Guglielmo et al., 2003).

As previously explained in section *I.C.1.*, the presence of BMP-2 receptors to bind BMP-2 ligand at the plasma membrane and further internalization is crucial in the activation of the BMP-2 signaling pathways. Until now, most studies have investigated BMP receptors endocytosis and the impact of the endocytosis inhibition on BMP-2 signaling.

By the use of several complementary approaches, *Knaus and coworkers* demonstrated that both BMPR-I and BMPR-II undergo constitutive endocytosis via clathrin-coated pits (CCPs) and that BMPR-II also undergoes caveolae-dependent internalization (Hartung et al., 2006). They evidenced several relations between receptors endocytosis and signal transduction:

- BMP-2-mediated Smad1/5 phosphorylation occurs at the plasma membrane in non-raft regions (inhibition of endocytosis did not affect Smad phosphorylation);
- Continuation of Smad signaling resulting in a transcriptional response requires endocytosis via the clathrin-mediated route;

- BMP signaling leading to alkaline phosphatase induction initiates from receptors that fractionate into cholesterol-enriched, detergent-resistant membranes (caveolin/lipid rafts endocytosis);
- BMPR-II interacts with Eps15R, a constitutive component of CCPs, and with caveolin-1, the marker protein of caveolae.

Thus, the localization of BMP receptors in distinct membrane domains is pre-requisite to their taking different endocytosis routes with specific impacts on SMAD and non-SMAD signaling cascades.

In another study they evaluated the effect of Dynasore, an inhibitor of dynamin-dependent endocytosis, which affects several routes of endocytosis that are dependent on dynamin, such as clathrin and caveolin-dependent endocytosis, on the different steps in the BMP-2 signaling (Heining et al., 2011). They observed that SMAD 1/5/8 phosphorylation was delayed and that transcriptional activity and ALP expression were significantly reduced (*Figure I- 36*).

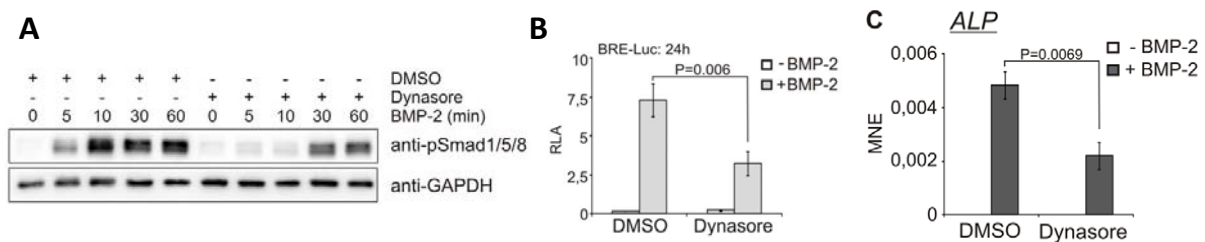


**Figure I- 36 :** Effect of the treatment with Dynasore on (A) SMAD 1/5/8 phosphorylation, (B) transcriptional activity or (C) ALP expression for C2C12 cultured on plastic in the presence or absence of BMP-2 stimulation (cells have previously been serum starved). Adapted from (Heining et al., 2011).

They also evidenced downregulation of osteoblastic markers attenuating osteoblastic differentiation after treatment with Dynasore and stimulation with BMP-2. They concluded that BMP/Smad signaling is spatially segregated into a predominant dynamin-dependent endocytosis path. Importantly, they indicated that dynasore exerts a general blockade of endocytosis. Thus, the effect in the signaling may be due to requirement for endocytosis but also to specific intracellular localization of another downstream component in the pathway. More specific ways to block endocytosis of receptors need to be used to further investigate this point.

The importance of caveolae regions where BMP receptors are housed in the BMP-2 signaling activation was also investigated by siRNA-mediated knock-down of caveolin-1



(cav-1) (Bragdon et al., 2012; Saldanha et al., 2013). In presence of soluble BMP-2 transcriptional activity was reduced for sicav-1 cells. They conclude that caveolae and CCPs regulate the Smad-dependent signaling pathway. This regulation can be related to endocytosis but also to the interactions of clathrin and caveolin with BMP receptors at the plasma membrane.

### **I.C.2.3. BMP-2 endocytosis**

BMP-2 internalization when delivered in solution to cells has already been evidenced by using different experimental approaches such as labeling the protein with radioactive or fluorescent tracer, immunofluorescence labeling of BMP-2 or by Western Blot of cell lysates.

*Jortikka et al* showed the endocytosis of radioactively-labeled BMP-2 (Jortikka et al., 1997). <sup>125</sup>I-BMP-2 was delivered to L6 myoblasts, cells were harvested, cell-surface-bound ligand removed by extensive washing and the radioactivity of internalized BMP-2 was measured.

Little literature exists on the direct visualization of internalized BMP-2 because of the difficulty on the production of a biologically active fluorescently labeled BMP-2. To our knowledge, only the group of *Alborzinia et al* has shown the endocytosis of fluorescently labeled BMP-2 by HeLa cells (Alborzinia et al., 2013). BMP-2 was delivered to spread cells in solution and the internalized amount was quantified over time up to 12h (**Figure I- 37**). The white dots represent BMP-2 vesicles inside the cell; the cell membrane is also shown.

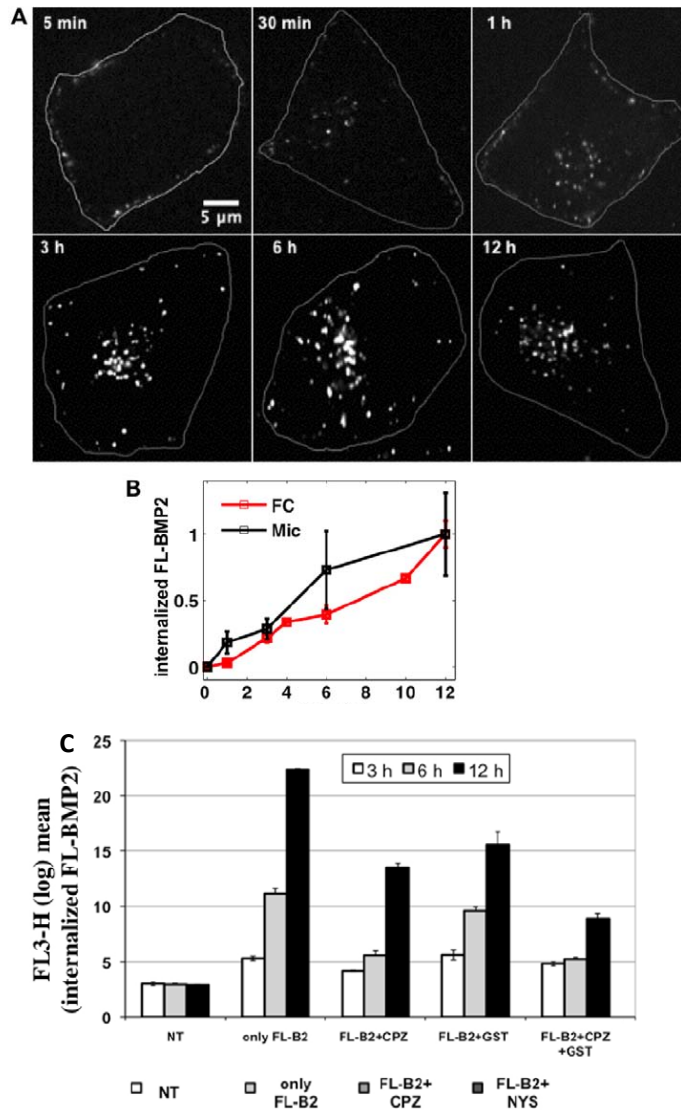


**Figure I- 37 : Analysis of labeled-BMP-2 (FL-BMP-2) uptake by HeLa cells by confocal microscopy and FACS.** (A) After incubation of cells with 400 ng/ml FL-BMP2 cells were washed, fixed and analyzed by confocal laser scanning microscopy at time points indicated; cell boundaries are highlighted. At 5 min fluorescence is visible at the plasma membrane. At later time points internalization of FL-BMP2 is visible in fluorescent endosomal vesicles. (B) Comparison of quantitative measurements of FL-BMP2 internalization, analyzed by flow cytometry (FC, red) and confocal microscopy image analysis (Mic, black). The amount of internalized FL-BMP2 was calculated from images of up to 12 hours of FL-BMP2 treatment. (C) Effect of inhibitors of endocytosis, CPZ, GST, CPZ+GST on BMP-2 uptake. From (Alborzinia et al., 2013).

The internalization route of BMP-2 was as well investigated by the use several endocytosis inhibitors (Alborzinia et al., 2013). CPZ and Genistein (GST), an inhibitor of tyrosine-specific protein kinases that depletes cholesterol (a critical lipid constituent of membrane lipid rafts and caveolae), showed to significantly reduce the BMP-2 endocytosis. A greater effect was observed when cells were pre-treated with CPZ as compared to GST,

therefore they have concluded that clathrin-dependent endocytosis is the preferential internalization route for BMP-2.

BMP-2 endocytosis was also evidenced by Western Blot analysis (von Einem et al., 2011). BMP-2 was detected in C2C12 cell lysates that contacted BMP-2. After treatment with inhibitors of endocytosis as Chlorpromazine (CP), a cationic amphiphilic drug known to block clathrin-dependent endocytosis, and Dynasore (DYN), drug that blocks dynamin-dependent pathways they have noticed a decrease in the BMP-2 uptake.

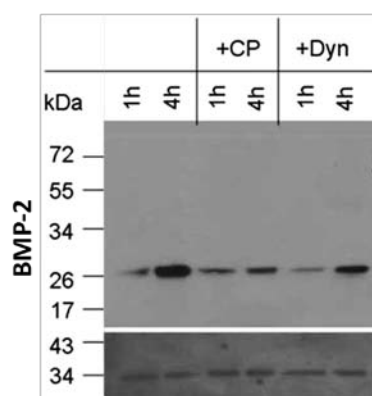


**Figure I- 38 : Inhibition of the BMP-2 internalization by C2C12 cells after treatment with inhibitors of endocytosis (CP = Chlorpromazine, Dyn: Dynasore). Adapted from (von Einem et al., 2011).**

To our knowledge, very few studies investigated the relation between BMP-2 endocytosis and the activation of BMP signaling pathways.

*Cavalcanti-Adam and coworkers* have immobilized BMP-2 on a surface by means of NHS-functionalized self-assembled monolayer (SAM) and then covalent immobilization of rhBMP-2 (iBMP-2) (Pohl et al., 2013). They have compared the activation of the SMAD and non-SMAD signaling in C2C12 cells contacting iBMP-2 or BMP-2 in solution (**Figure I- 39**).

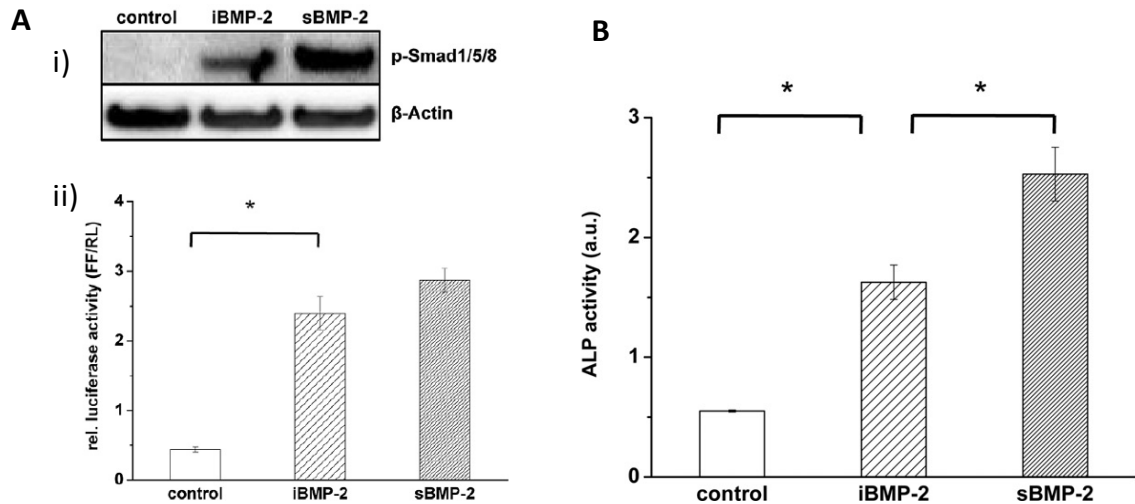


**Figure I- 39 : Immobilized BMP-2 maintains its biological activity and induces SMAD signaling and ALP expression.** C2C12 cells were stimulated with gold surfaces (control), surfaces with covalently immobilized BMP-2 (iBMP-2) and gold surfaces in the presence of soluble BMP-2 in cell culture medium (sBMP-2). (A) (i) C2C12 cells were stimulated for 30 min by exposure to surfaces approached from the top. After cell lysis the samples were immunoblotted for phospho-Smad1/5/8 and  $\beta$ -actin as a loading control. (ii) Dual luciferase reporter assay for BRE-Luc transfected C2C12 cells. The day after transfection cells were detached and seeded on the indicated surfaces for 18 h. Subsequently firefly luciferase activity was measured to determine induction of BRE-Luc reporter and is displayed relative to Renilla luciferase activity. (B) The enzymatic activity of alkaline phosphatase (ALP) indicates osteogenic differentiation of C2C12 cells. Cells were seeded and cultured for 6 days on control surfaces, on iBMP-2 surfaces or in the presence of sBMP-2 (20 nM). After cell lysis ALP activity was measured as the absorbance at 405 nm. The bar graph shows data acquired after 60 min reaction. Error bars represent standard deviations from the mean of  $n > 3$ ,  $*P < 0.001$ . Adapted from (Pohl et al., 2013).

iBMP-2 was able to activate SMAD signaling and induce ALP expression (osteogenic differentiation). However, a decreased ALP expression was observed in comparison with BMP-2 in solution. They suggested that the initial interactions and binding of iBMP-2 to its receptor at the cell surface are sufficient to trigger short-term and long-term BMP-2 signaling. In conclusion, their results indicated that BMP-2 internalization was not required to activate BMP signaling since a surface-immobilized BMP-2 was able to activate BMP-2 signaling pathways. BMP receptors internalization after contacting iBMP-2 was not explored in their study.

## I.D. Objectives and strategies of the PhD thesis

As mentioned earlier, BMPs play an essential role in several developmental processes, especially in bone formation and regeneration. In the field of orthopedics, delivery of BMPs from the surface of implantable materials would enable faster and better bone formation around the implant.

Our group has previously developed a biomimetic film made of PLL and HA, which acts as a nanoreservoir to trap BMPs and to present it to cells in a "matrix-bound" manner (Crouzier et al., 2009; Crouzier et al., 2011a). The bioactivity of BMP-2 was confirmed *in vitro* using alkaline phosphate assay and Smad signaling (Crouzier et al., 2009; Crouzier et al., 2011a) and *in vivo* in rat ectopic assays, for films deposited on TCP/HAP granules (Crouzier et al., 2011b).

In this context, the general objectives of this thesis work were to better understand the interactions between BMP-2 and the (PLL/HA) film, to investigate the biochemical stability of the film, to evaluate its ability to be sterilized, and to understand how cells interact and use the matrix-bound BMP-2.

This manuscript has thus been divided in three major parts corresponding to each subproject (**Figure I- 40**).

- In **Chapter III**, we use by Fourier Transform Infrared spectroscopy (FTIR) to investigate the secondary structure of BMP-2 trapped in the biopolymeric film (in hydrated or dry state) and compared it to the protein structure in solution, i.e. in a free environment.
- In **Chapter IV**, we focus on the possibility to store the BMP-2-loaded films over time in dry state and to sterilize them by gamma irradiation. In view of future clinical applications, it is essential to demonstrate that such coatings can be dried, stored and sterilized without damaging the film structure and bioactivity.
- In **Chapter V**, we investigate the endocytosis of matrix-bound BMP-2 (bBMP-2) by C2C12 cells. First, by the use of a fluorescent labeled BMP-2 we visualize the protein vertical diffusion inside the film and to evaluate its mobility after loading. Second, we aim to visualize the endocytosis of bBMP-2, compare the internalization when BMP-

2 is presented from films with different cross-linking degrees and evidence the players in the BMP-2 endocytosis. We aim then to explore the role of receptors, the bBMP-2 endocytic pathway(s) and to relate endocytosis with BMP signaling.

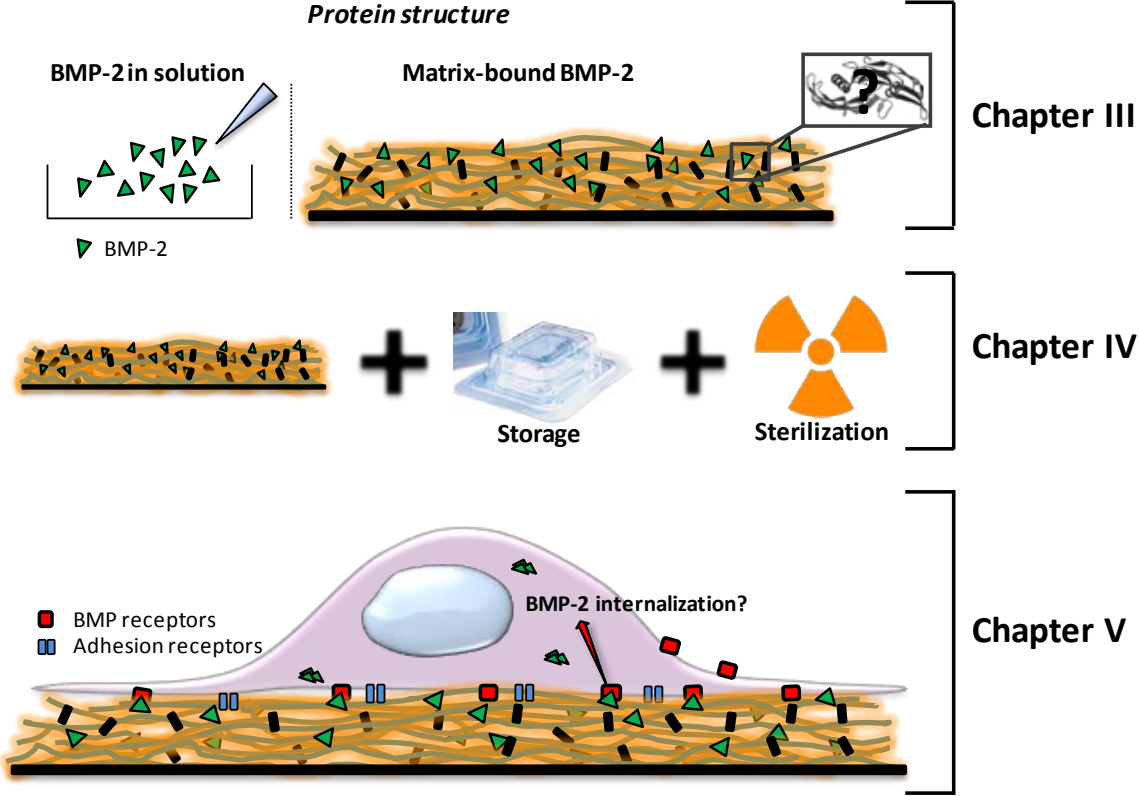


*Figure I- 40 : Schematic representation of the thesis objectives and the goal of each chapter.*



## **Chapter II: Materials and Methods**



This chapter introduces materials and techniques used during this thesis. The principles and details of different experimental methods will be described to allow the reproduction and facilitate the future research.

## **II.A. Construction of PEM films**

### **II.A.1. BMP-2 and PLL labeling with fluorochrome**

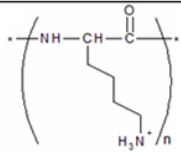
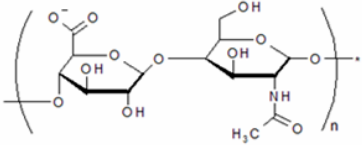
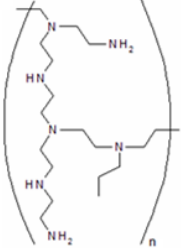
BMP-2 was labeled with 5(6)-Carboxyfluorescein N-hydroxysuccinimide ester (CF, MW 473.4 g/mol) (ref 21878, Sigma) (BMP-2<sup>CF</sup>). rhBMP-2 (0.5 mg/mL; clinical grade, Wyeth BioPharma, USA) was dissolved in 1 mM HCl and frozen at -20°C until use. For fluorescent labeling, the pH of the protein was raised to 8 with a bicarbonate buffer at 50 mM. BMP-2 reacted for 2h at room temperature with a molecular ratio of 1:20 (BMP-2/dye) before being reacidified with 0.2 M of acetate buffer at pH 3. The labeled protein (rhBMP-2<sup>CF</sup>) was separated from the reagents by using a Sephadex G25 column (GE Healthcare, France) eluted with HCl (1 mM). The molar grafting ratios were estimated by determining the respective molar concentrations of dye and protein and calculating the grafting ratio (~ 30 %).

PLL (PLL-HBr, MW 30.000 – 70.000) (P2636, Sigma) was labeled with Alexa Fluor® 568 NHS ester (A568, MW=791.8 g/mol, A20003 Life Technologies). PLL was dissolved at 5 mg/mL in a 50 mM sodium bicarbonate buffer. The dye was then added to the solution with a molecular ratio of 1/2.5 (PLL/dye). The reaction took place under slow agitation at room temperature for 2 hours. After the reaction, the free dye was removed by dialysis in 400 mL of HEPES/NaCl (4°C) using a membrane with a 6-8 kDa cut off under gentle agitation. The buffer was changed at least 4 times over 48 h. The labelled PLL was stored at -20°C.

### **II.A.2. Polyelectrolyte solutions, film buildup and crosslinking**

The polyelectrolytes used in this work are polypeptides poly(L-lysine) (PLL, P2636, 6.8 x 10<sup>4</sup> g/mol, Sigma) and hyaluronic acid (HA, 360 kDa, Lifecore, USA). Their chemical structure is shown in *Table II- 1*.

**Table II- 1 : Structure of the polyelectrolytes used in the present work for the film PEM film buildup.**

Polyelectrolyte	Charge	Structure
Poly(L-Lysine) (PLL)	+	
Hyaluronan (HA) (Hyaluronic acid)	-	
Poly(ethyleneimine) (PEI)	+	

Here, we will focus on the buildup of (PLL/HA) multilayer films. PLL was dissolved at 0.5 mg/mL, and HA at 1 mg/mL in a HEPES-NaCl buffer (20 mM HEPES at pH 7.4, 150 mM NaCl). The rinsing solution was 150 mM NaCl (pH ~6.5). The (PLL/HA)<sub>24</sub> film (PLL being the polycation, HA the polyanion and 24 the number of layer pairs of the film) were built on 14 mm glass slides (Menzel-Gläser, Allemagne) using an automatic dipping machine (Dipping Robot DR3, Kierstein GmbH, Germany). When the film had to be dried, a first layer of a positively-charged poly(ethyleneimine) (PEI) dissolved at 5 mg/mL in HEPES-NaCl buffer was deposited to improve the film anchorage to the underlying substrate. For this, dipping in the PEI solution followed by an HA layer was performed before placing the holders in the dipping machine.

Chemical cross-linking of (PLL/HA) films enables to increase their stiffness and mechanical resistance (Schneider et al., 2006). The approach is based on carbodiimide chemistry. 1-Ethyl-3-(3-dimethylaminopropyl)carbodiimide (EDC, Sigma Aldrich E7750), is used as a crosslinker and N-hydroxysulfosuccinimide (s-NHS, Chemrio), as a catalyser. During the reaction, amide bonds between amine groups of PLL (NH<sub>3</sub><sup>+</sup>) and carboxylic groups (COO<sup>-</sup>) of HA are formed. An EDC/sulfo-NHS (v/v) solution was used for the crosslinking with EDC being at 10, 30 or 70 mg/mL final concentration and s-NHS at 11 mg/mL. Both were dissolved in 150 mM NaCl at pH 5.5. The reaction occurred overnight at

4°C. Finally, the films were thoroughly washed with the HEPES-NaCl buffer. Films are then named EDC10, EDC30 or EDC70 in function of the EDC concentration.

### **II.A.3. Loading of BMP-2 in the films**

Films were first equilibrated at pH 3 (1 mM HCl) prior to protein loading (one quick rinsing and a second one during 20 min). Then, BMP-2 (clinical grade, Wyeth BioPharma, USA) dissolved at 20 µg/mL in 1 mM HCl was let in contact with the film for 1h30 at 37°C (or overnight at 4°C). Afterwards, the films were thoroughly washed to remove any loosely bound BMP-2 and to present BMP-2 in a matrix-bound manner to the cells (Crouzier et al., 2009). This mode of presentation will be named hereafter bBMP-2 in comparison to the presentation of soluble BMP-2 (sBMP-2).

### **II.A.4. Film drying, long-term storage and sterilization**

Prior to film drying, the films were rinsed with milli-Q water to remove the excess of salt. They were subsequently dried for 1 h at 37°C in an incubator. For the long-term stability experiments, the films were stored in dry state at 4°C. Before each FTIR acquisition, they were placed for 1h in an incubator at 37°C to avoid any possible effect due to variation in humidity.

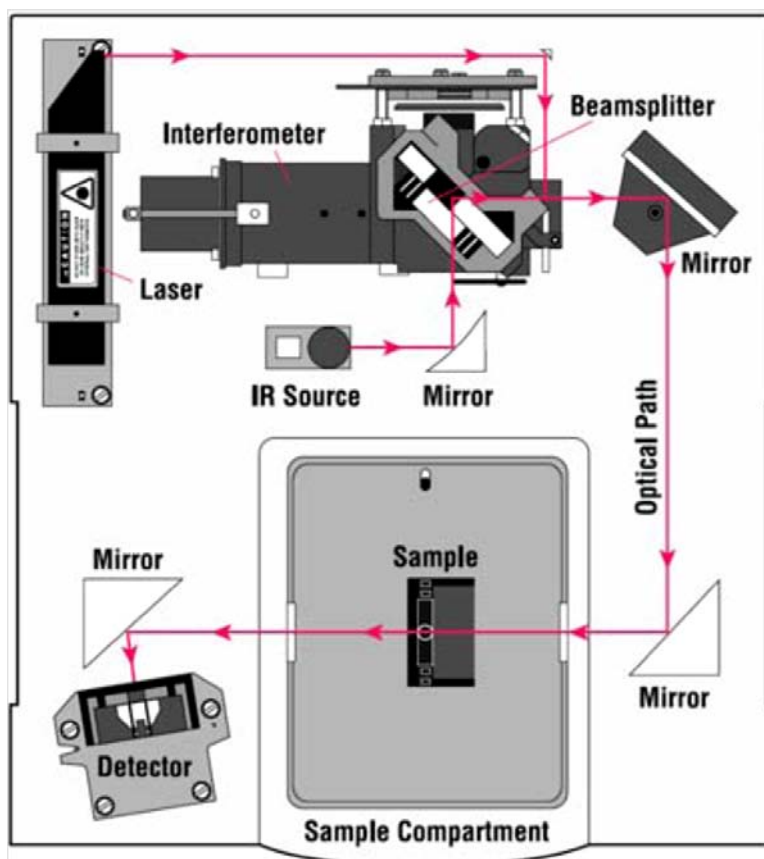
For sterilization, the films were deposited on TiO<sub>2</sub>/silicon substrates, dried and shipped to Ionisos (Lyon, France) where they were submitted to gamma irradiated sterilization according to the industrial procedure. Two doses were applied: 25 kiloGray (kGy) and 50 kGy.

## **II.B. BMP-2 and BMP-2-loaded film characterization**

### **II.B.1. Fourier Transform Infrared (FTIR) Spectroscopy**

An infrared spectrum represents a chemical fingerprint of a sample with absorption peaks that correspond to the vibration frequencies of specific chemical bonds. Therefore, infrared spectroscopy can provide a qualitative analysis of various kinds of materials. Furthermore, the intensity and width of the peaks in the spectrum are a direct indication of the amount of material present in the sample (Griffiths P R, 2007).

In Fourier Transform Infrared spectroscopy (FTIR), an infrared light is generated by an IR source. The light is sent to a Michelson interferometer, which allows the generation of an interferogram. The beam then passes through the sample, which is inserted in the sample compartment. Some of the infrared radiation is absorbed by the sample and some of it is transmitted. The transmitted light is detected by a sensitive detector (*Figure II- 1*).

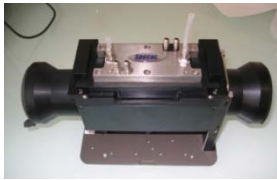






*Figure II- 1 : Top view of a FTIR apparatus.*

Afterwards, the signal is treated and a Fourier transformation is applied to it, which allows plotting the intensity of light (or absorbance) as a function of the wavenumber (in  $\text{cm}^{-1}$ , reciprocal of the wavelength) (Griffiths P R, 2007; Bruker, Booklet Bruker Optics ). The final infrared spectrum can then be manipulated using an appropriate software. FTIR is recognized as a powerful tool to quantify the secondary structure of protein in solution or on surfaces as well as, more generally, to analyze biomacromolecules (Barth and Zscherp, 2002; Crouzier and Picart, 2009).

There are several types of FTIR accessories (*Table II- 2*). They must be selected depending on the type of experiment, sample physical state, sample properties such as viscosity, hydration state, solvent, etc.

**Table II- 2 : Presentation of FTIR accessories and their use.**

NAME	REFERENCE	USE (examples)	PICTURE
<p>ATR-A537 QUICKLOCK</p> <p>Attenuated Total Internal Reflection (ATR)</p>	<p>Bruker A537</p>	<p>Films and/or proteins structures (adsorbed on the crystal):</p> <ol style="list-style-type: none"> <li>1. Follow buildup of a multilayer film, layer-by-layer</li> <li>2. Follow protein or polyelectrolyte solution adsorption on crystal</li> </ol> <p>Flushing of solutions inside the ATR cell is performed with a peristaltic pump</p>	 <p><b>Type of crystal (available):</b> ZnSe, Si</p> 
<p>Transmission</p>	<p>Bruker I18166</p>	<p>Transmission through a dry sample</p>	
<p>CaF<sub>2</sub> windows 25 mm X 4 mm</p>	<p>Eurolabo 160-1211</p>	<p>Transmission through a liquid sample (proteins, polyelectrolytes, lipids...)</p>	
<p>AQUASPEC 6 μm in width</p>	<p>Bruker A741/Q</p>	<p>Transmission in water for small protein samples</p> <p>(the introduction of the liquid sample inside the cell is done with a syringe)</p>	

### II.B.1.1. Quantitative analysis

A Vertex 70 spectrophotometer (Bruker Optics GmbH, Ettlingen, Germany) was used for the acquisition of FTIR spectra. Single-channel spectra were recorded between 400 and 4000 cm<sup>-1</sup> with a 2 cm<sup>-1</sup> resolution by means of the OPUS Software v6.5 (Bruker). A nitrogen-cooled mercury-cadmium-telluride (MCT) detector was used to improve the detection level. Such detector is known to produce a noise level 10 – 50 times lower than

other detectors (Hasegawa et al., 2009). Different accessories were used depending on the experiments: an Aquaspec transmission cell for studying BMP-2 in solution, an attenuated total reflection (ATR) liquid cell for the study of BMP-2 loaded in hydrated films, and a standard transmission accessory for the study of the BMP-2 loaded films deposited on silicon substrates and subsequently dried. All these accessories were purchased from Bruker Optics. The OPUS Software v6.5 (Bruker GmbH) was used for the treatment and deconvolution of the spectra. Residual water and CO<sub>2</sub> contributions were removed, and baseline correction was done manually, choosing always the same reference points in each group of spectra. When residual noise due to water (especially in dry conditions) was still present, the spectra were smoothed using a specific algorithm from Opus software. The frequencies of the different components forming the amide I band were first determined by calculating of the second derivative of the Fourier smoothed spectrum (Schwinte et al., 2002).

There was thus no arbitrary decomposition into a preset number of bands and on the peak position. Once the number of component bands was determined, the amide I band was fitted by using the component frequency, width, and intensity as fitting parameters. The more consistent results were obtained when all component peaks were assumed to be Gaussian. The correspondence of each component band with a given secondary structure was established by comparing the frequency of its maximum to the value given in the literature (Barth and Zscherp, 2002; Barth, 2007). We defined the relative contribution of each component (in %) by the ratio of the area of each peak over the area of the total amide I band (Schwinte et al., 2001).

### **II.B.1.2. PLL/HA film characterization**

The *in situ* buildup of PLL/HA films in HEPES-NaCl buffer was followed by FTIR spectroscopy in ATR mode as previously described (Crouzier and Picart, 2009). For studies in hydrated conditions, D<sub>2</sub>O was used as solvent instead of water in order to avoid the overlapping water band in the amide I region (O–H bending vibration at 1643 cm<sup>-1</sup> versus O–D bending vibration at 1209 cm<sup>-1</sup>). The films were built and cross-linked on a ZnSe crystal and a single-channel spectrum of 64 interferograms was recorded.

For studies in dry conditions, films were built as described previously (Shen et al., 2011) on a 1 cm<sup>2</sup> silicon substrate (Siltronix, France) using HEPES-NaCl (dissolved in H<sub>2</sub>O) followed by cross-linking. The films were then rinsed with milli-Q water to remove the salt and dried for 1 h at 37 °C. The film spectra in transmission were acquired by summing 256

interferograms. For long-term stability measurements, the films were stored in the dry state at 4 °C. Before each FTIR acquisition, they were incubated for 1 h at 37 °C.

### **II.B.1.3. Characterization of BMP-2 secondary structure in solution**

First, the BMP-2 solution was purified by precipitation using a 10% ammonium sulfate (AS) solution (Ulloa et al., 1995). The mixture was centrifuged at 13.000 rpm for 10 min after which the supernatant was removed. This procedure was repeated three times with a 2% AS solution. Finally, the protein was resuspended in the 1 mM HCl in D<sub>2</sub>O or in the HEPES-NaCl buffer in D<sub>2</sub>O (pH = 7.4). The final protein concentration was ~ 2 mg/mL for rhBMP-2 in 1 mM HCl (pH 3). At pH 7.4, the protein is known to be less soluble (Abbatiello and Porter, 1997; Hillger et al., 2005; Hauburger et al., 2009). We estimated the BMP-2 concentration of the resuspended solution to be 400 µg/mL at this pH, based on the difference of the maximum absorbance of the protein. 60 µL of BMP-2 were injected in the Aquaspec cell, and a single-channel spectrum of 64 interferograms was recorded.

### **II.B.1.4. Characterization of BMP-2 secondary structure in (PLL/HA) films**

For BMP-2 trapped in hydrated (PLL/HA)<sub>12</sub> films built in D<sub>2</sub>O, BMP-2 was loaded from a solution at 100 µg/mL in 1 mM HCl in D<sub>2</sub>O (pH = 3) following the protocol established previously (Crouzier et al., 2009). The rinsing steps were done with HEPES-NaCl buffer. The spectrum of BMP-2 was obtained by subtracting the spectrum of the film in contact with the HEPES-NaCl buffer to that of the BMP-2-loaded film (measured in the same buffer after rinsing of the film).

For the study of BMP-2 in dry films, BMP-2 in 1 mM HCl was loaded in the PLL/HA film prepared in the HEPES-NaCl buffer (in H<sub>2</sub>O) and dried as described above for the film. The spectrum of BMP-2 inside dry films was obtained by calculating the difference between the average spectrum of two independent BMP-2 loaded films and the average spectrum of two control samples (i.e., films that have followed the same procedure, except that BMP-2 was not present in the loading solution).

## II.B.2. Fluorescent and confocal microscopy

### II.B.2.1. Epifluorescence microscopy

Fluorescence is a property of a molecule to adsorb a photon and then to re-emit it at a higher wavelength (*Figure II- 2*). When it is submitted to light excitation at a given wavelength, the fluorescent molecule is brought to an excited electronic state ( $S_1'$ ). At ambient temperature, the internal conversion induces a partial loss of energy and the molecule falls down to an excited state of lower energy ( $S_1$ ). When the molecule comes back to its stable state ( $S_0$ ), the associated release of energy takes the form of light. The loss of energy corresponds to the emission of light at a higher wavelength than the initial adsorption wavelength. This phenomenon is known as Stocke's shift.

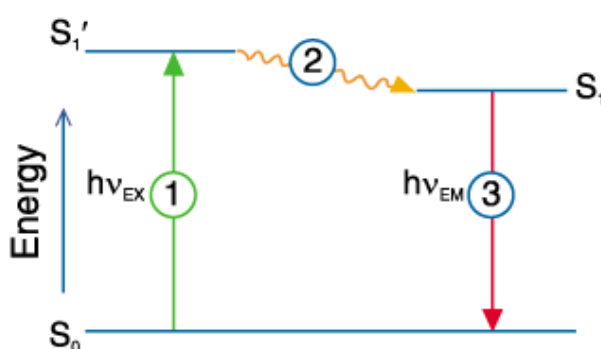


**Figure II- 2 : Jablonski diagram.** An electron from the fluorophore adsorbs light (1) and becomes excited (stage  $S_1'$ ). When it is desexcited, there is first a loss of energy by internal conversion (vibration, chock...). The molecule is then at the excitation state ( $S_1$ ) and comes back to its stable state  $S_0$ . This transition corresponds to a release of energy (light) at a higher wavelength (as the energy is lower).

In epifluorescence microscopy (*Figure II- 3A*), the light is first filtered through an excitation filter and passes through a dichroic mirror to be sent to the objective. The objective serves as a condenser of the excitation light. The objective is then used to collect the fluorescence light that is emitted by the sample. The emitted light passes through an emission filter before being detected by the camera (or observed by eye using the ocular ports). In this work, we used Zeiss Axiovert 200 inverted epifluorescence microscope equipped with a camera (*Figure II- 3B*).



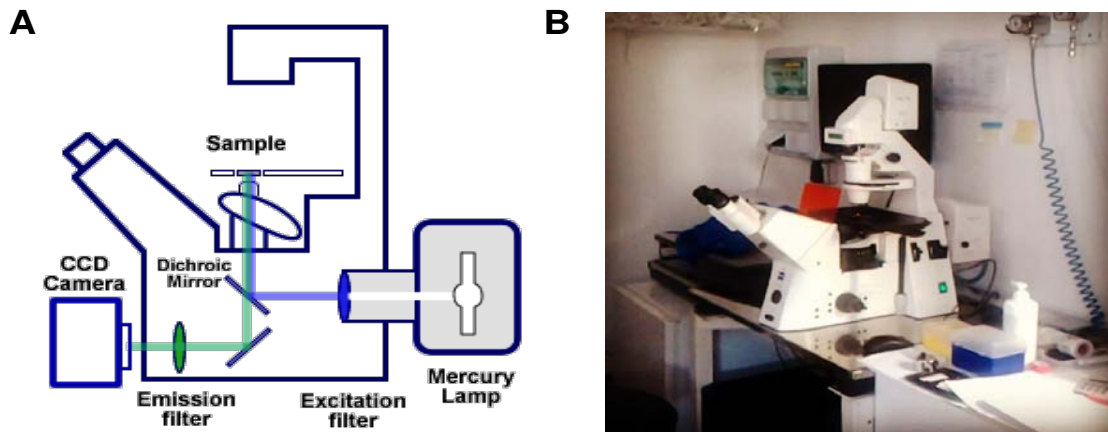


**Figure II- 3 : Epifluorescence microscopy.** (A) Schematic presentation: the light is sent to a dichroic mirror which directs it to the sample. The emitted light from the sample passes through the dichroic mirror before being collected. (B) Zeiss Axiovert 200 inverted epifluorescence microscope equipped with a camera.

### II.B.2.2. Confocal microscopy

However, the fluorescence coming from the non-focal points is also acquired and a volumetric analysis is not possible. This is the reason why confocal microscopy has been developed by Minsky in 1957. The light source has been replaced by a laser, which allows the light at a precise wavelength to be sent to the sample. However, similarly to epifluorescence microscopy, the sample generates fluorescence out of the focal plane. To avoid this unwanted fluorescence, a pinhole is placed before the detector, which only allows light from the focal plane to be detected (**Figure II- 4A**). The image obtained in these conditions has a good signal to noise ratio. The scanning of the sample in X,Y direction by the laser allows an image of the focal plane to be taken. This scanning is obtained via motorized mirrors that are disposed on the optical path of the laser. For the scanning in the Z direction, the objective is mounted on a piezo-electric mirror. It is thus possible to obtain images of different focal planes and to reconstitute a 3D structure.

The confocal microscope used is a Zeiss LSM 700, equipped with four different laser diodes, allowing the simultaneous observation of various fluorophores (**Figure II- 4B**). Thus, by the appropriate choice of the antibodies and stains, it is possible to visualize different subcellular structures at the same time. He is also equipped with an incubator that allows to maintain the cells at 37°C and 5% CO<sub>2</sub> (**Figure II- 4B**).

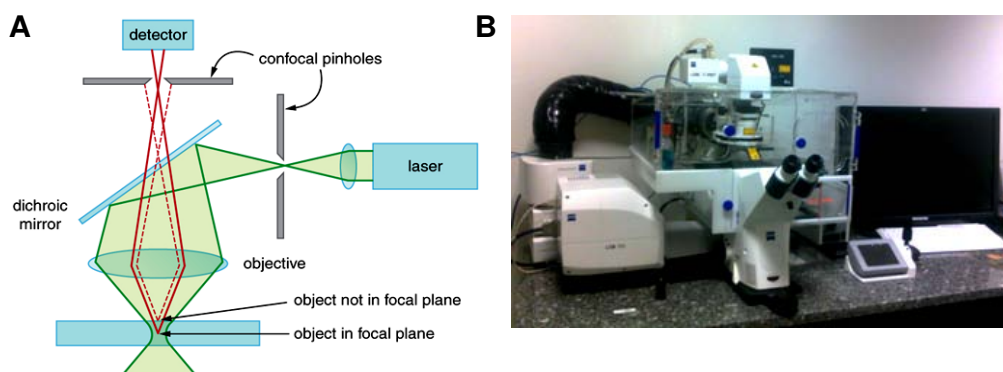


**Figure II- 4: Confocal microscopy.** (A) Schematic presentation: the laser source is condensed to a focal point being reflected by the dichroic mirror and after passing through the objective. The fluorescent light is sent collected by a detector. To avoid out of plane fluorescence, a pinhole is placed in the emitted path. (B) Zeiss LSM 700 confocal microscope equipped with an incubator. The system allows to maintain the cells at 37°C and 5% CO<sub>2</sub> during long lasting experiments.

#### II.B.2.2.1. Imaging of fluorescent BMP-2 after diffusion inside (PLL/HA) films

The fluorescence imaging of the labeled BMP-2 inside (PLL/HA) films was performed using a Zeiss LSM 700 confocal laser scanning microscope (Zeiss, Le Peck, France) equipped with a 63 x oil immersion objective and 488 nm, 555 nm laser diodes. Images were acquired with both 488 nm (BMP-2-CF) and 555 nm (PLL-A568) channels after definition of a z-stack delimitating the film thickness. To relate the vertical diffusion with the film cross-linking we performed several z-stacks for the different types of films (EDC 10, 30, 70). Using Image J software 1.44 ([imagej.nih.gov/ij/](http://imagej.nih.gov/ij/)) we extracted the fluorescence intensity profiles (green and red), which were plotted using SigmaPlot 12.0. The macro ‘Area below curve’ was used to calculate the area of each track. The intersection area between the two curves was also calculated. The overlap percentage of the two tracks was obtained by dividing the intersection area by the film area below curve. At least three images per condition were used to calculate the overlap percentage.

#### II.B.2.3. Fluorescence Recovery after Photobleaching (FRAP)

Fluorescence Recovery After Photobleaching (FRAP) enables to quantify the diffusion inside a material or living cells using fluorescence microscopy. To this end, a specific component is labeled and a small portion of the cell is photobleached (using a high power of the laser), before following the fluorescence intensity recovery in the bleached zone. The

same protocol can be used to follow the diffusion of a fluorescent molecule inside a material/hydrogel. The principle of fluorescence recovery is based on replacement of bleached molecules by the diffusion of fluorescent molecules that were located outside of the bleached region. The recovery of the fluorescence in the bleached region is observed over time.

Fluorescence recovery after photobleaching (FRAP) experiments were conducted to evaluate the carboxyfluorescein-BMP-2 diffusion inside (PLL/HA) films (in the last step of film preparation, i.e. after loading and extensive rinsing). To this end, a 20  $\mu\text{m}$  circular region of interest (ROI) was bleached using the 488 nm laser diode (100% power and the recovery after photobleaching was followed over time. The fluorescence intensity of the ROI was normalized to that of a control region.

### **II.B.3. Scanning Electron Microscopy (SEM)**

The SEM uses a focused beam of high-energy electrons to generate a variety of signals at the surface of solid specimens. The signals that derive from electron-sample interactions can provide information on the external morphology/topography, chemical composition, crystalline structure and orientation of materials making up the sample. In most applications, data are collected over a selected area of the surface of the sample, and a 2-dimensional image is generated that displays spatial variations in these properties.

The classical scanning electron microscope (SEM) operates at a high vacuum but new microscopes provide the possibility to work in pressurized chamber. The basic principle is that a beam of electrons is generated by a suitable source (typically a tungsten filament or a field emission gun) then the electron beam is accelerated through a high voltage (around 20 kV for conductive materials but lower voltages are used in biology (close to 5 kV)) and pass through a system of apertures and electromagnetic lenses to produce a thin beam of electrons. This beam scans the surface of the specimen. Electrons are emitted from the specimen by the action of the scanning beam and collected by a suitably-positioned detector. Different detectors detect different types of electrons with different energies. Typically, secondary electrons (SE), low energy electrons give information on the surface topography of the sample and back-scattered electrons (BSE), high energy electrons, give information about the chemical composition.

### **II.B.3.1. Visualization of film cross-sections after immunogold labeling of BMP-2**

Films were built on Thermanox® slides, cross-linked (EDC 30) and loaded with BMP-2 as described above. The sample was fixed with 2.5 % glutaraldehyde in 0.1M Cacodylate buffer at pH 7.2 (C0250, Sigma). Then, a post-fixation with 1% Osmium tetroxide (75632, Sigma) and 1.5% Potassium hexacyanoferrate (II) trihydrate (P9387, Sigma) was performed. The sample was then dehydrated by successive baths in ethanol mixtures and embedded in HM20 resin (14345, Electron Microscopy Sciences), known to be an uncharged resin. The resin was polymerized under indirect UV light (254 nm) for 72 h to form the resin blocks. Sections were made using an ultramicrotome (LEICA UC6). Cross-sections were placed on ~ 1 cm<sup>2</sup> silicon wafer (Siltronix, France). Immunogold labeling of BMP-2 starts with two different blocking steps: first, the silicon wafer was immersed in a 50 mM Glycine (G8898, Sigma) bath in PBS for 20 min and then blocked using a 2% BSA (900.001, Aurion) in PBS for 1h. Mouse anti-BMP-2 (B9553, Sigma) at 2.5 µg/mL was used as first antibody and goat anti-mouse IgG conjugated to 10 nm gold NPs (G7652, Sigma) diluted 1:20 was used as secondary antibody. The sample was finally rinsed with mili-Q water and air dried for few hours.

Backscattered electron (BSE) imaging at 5kV was used to image the film cross-sections by scanning electron microscopy (SEM) using a Fei-Quanta 250 SEM-FEG.

## **II.C. Cell culture**

### **II.C.1. C2C12 myoblasts culture**

Mouse myoblasts (C2C12 cells) were used as a cellular model. These cells are able to reproduce processes that take place during *in vivo* differentiation of skeletal muscle progenitors. C2C12 myoblasts are a subclone of C2 myoblasts (Yaffe and Saxel, 1977) which differentiate in culture after serum removal (Blau et al., 1983). C2C12 cells (purchased from ATCC, used at passages 4 - 15) were maintained in polystyrene dishes in an incubator at 37° C and 5% CO<sub>2</sub>. They were cultured in growth medium (GM) composed of Dulbecco's modified Eagle's medium (DMEM)/F12 medium (1:1; Gibco, Invitrogen, Cergy-Pontoise, France) supplemented with 10% fetal bovine serum (PAA Laboratories, Les Mureaux, France) containing 10 U/mL of penicillin G and 10 µg/mL of streptomycin (Gibco,

Invitrogen, Cergy-Pontoise, France). Cells were subcultured prior to reaching 60 – 70% confluence (approximately every 2 days) in GM (*Figure II- 5*).

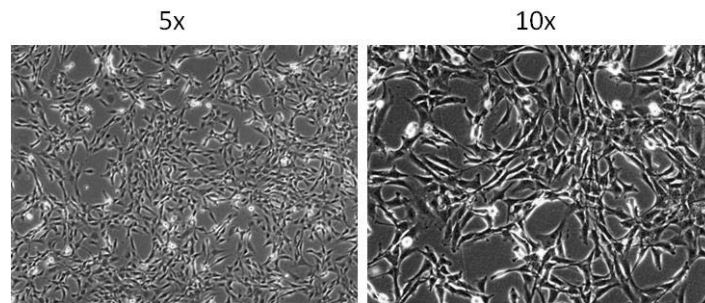


*Figure II- 5 : Phase contrast microscopy observations of C2C12 in culture.*

Cells are maintained at an appropriate temperature, humidity and gas mixture (typically, 37°C, 5% CO<sub>2</sub> for mammalian cells) in a cell incubator (*Figure II- 6*).

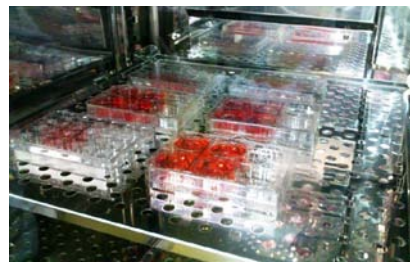


*Figure II- 6 : Cells in an incubator.*

Cell culture procedures are performed in sterile conditions. Sterile technique prevents from introducing contaminating microorganisms that can destroy the cells. All cell culture material (dishes, media, pipette tips etc.) are sterile, and all procedures are done in a laminar flow hood (or cell culture hood) that provides an aseptic work area (*Figure II- 7*).



*Figure II- 7 : Cell culture hood for the work in sterile conditions.*

## II.C.2. Evaluation of cell response

### II.C.2.1. Principle of immunolabeling and protocol

In many assays, visualization of the cells or its components was required. Immunofluorescence (IF) is a common technique that is used to fluorescently label specific components of the cell by antibodies that target specific antigens of cellular proteins. The antibody can be coupled to a fluorochrome and can thus be detected by fluorescent microscopy (direct IF, **Figure II- 8A**). However, usually a secondary antibody coupled to a fluorochrome and recognizing the primary antibody is used (indirect IF, **Figure II- 8B**). Another possibility is to use a primary antibody coupled to a biotin molecule. In this case, detection is made by a fluorochrome-conjugated streptavidin (**Figure II- 8C**).

There are also other types of direct fluorescent labeling of cellular components. For instance, phalloidin, a toxin from *Amanita phalloides*, a deadly poisonous fungus, binds F-actin and, if coupled to a fluorochrome, can be detected by fluorescent microscopy. The nuclei can be stained by DAPI or Hoechst fluorescent dyes that bind DNA.

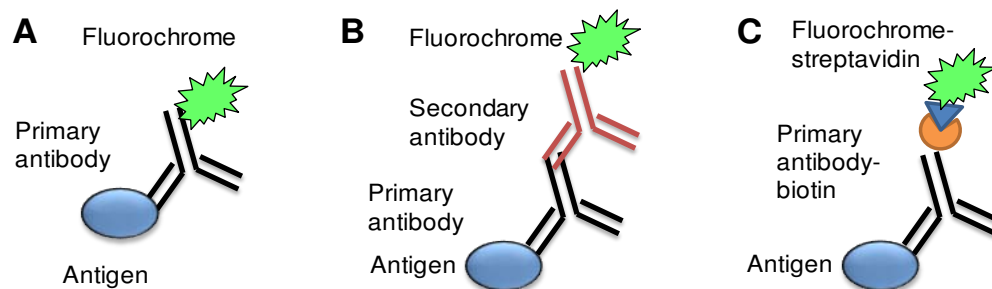


**Figure II- 8 : Different strategies for antigen detection by immunofluorescence.** (A) Direct immuno-fluorescence: a primary antibody coupled to a fluorochrome is used. (B) and (C) Indirect immuno-fluorescence. (B) A secondary antibody coupled to a fluorochrome and recognizing the primary antibody is used. (C) Fluorochrome-conjugated streptavidin binds to a primary antibody coupled to biotin molecule.

Cells were first rinsed in PBS and fixed in 3.7% formaldehyde for 20 min at RT before being permeabilized in 0.5% Triton X-100 for 4 min. After rinsing with PBS, samples were incubated for 1h in 1 - 2 % BSA (900.001, Aurion) in TRIS-buffered saline (TBS, 50 mM TRIS, 150 mM NaCl, 0.1% NaN<sub>3</sub>, pH 7.4). After the incubations with the primary antibodies (diluted in 0.2% TBS-gelatin) for 1h at RT, cells were washed 6 times in TBS and incubated for 1h with the secondary antibodies. After rinsing with TBS, actin was labeled with phalloidin-TRITC (1:800, Sigma) for 30 min. Cell nuclei were stained with Hoechst 33342

(Invitrogen) at 5 µg/mL for 10 min. A list of used antibodies and their dilutions is provided (*Table II- 3*).

**Table II- 3 : List of primary antibodies, secondary antibodies, and other products, used for fluorescent cell labeling.**

<b>Primary antibodies</b>				
<b>Antibody</b>	<b>Reference</b>	<b>Provider</b>	<b>Animal</b>	<b>Final dilution</b>
Anti-β-tubulin	T4026	Sigma	Mouse	1:200
Anti-BMP-2	B9553	Sigma	Mouse	1:250
Anti-cav-1	sc-894	Santa Cruz	Rabbit	1:200
Anti-rab7	D95F2	Abcam	Rabbit	1:50
Anti-BMPRIa	sc-20736	Santa Cruz	Rabbit	1:20
Anti-BMPRII	sc-5683	Santa Cruz	Goat	1:20
<b>Secondary antibodies</b>				
Anti-mouse Alexa Fluor 647	A-21235	Invitrogen	Goat	1:1000
Anti-rabbit Alexa Fluor 647	A-21244	Invitrogen	Goat	1:1000
Anti-goat Alexa Fluor 647	A21447	Invitrogen	Donkey	1:1000
<b>Reagents</b>				
Phalloidin	P1951	Sigma	---	1:800
DAPI	D1306	Invitrogen	---	5 µg/mL

### **II.C.2.1. Treatment with inhibitors of endocytosis**

One method to block endocytosis is to treat cells with inhibitors of endocytosis. Here we selected specific inhibitors known to disturb BMP-2 endocytosis (*Table II- 4*). Before seeding and contact with BMP-2, C2C12 cells were treated for 45 min with the different inhibitors of endocytosis at the desired concentration.



**Table II- 4 : Inhibitors of endocytosis used to block BMP-2 endocytosis.**

Inhibitor	Acronym	Pathway	Mechanism/target	Used [] (C2C12)
<b>Chlorpromazine</b> C8138 (in H <sub>2</sub> O)	<b>CPZ</b>	Clathrin-coated pits (CCPs) Receptor-mediated endocytosis	Cationic amphiphilic drug; Clathrin/AP2 depletion from plasma membrane to endosomal membranes Induces clathrin mis-assembly	5, 15, 10, 20 μM
<b>Genistein</b> G6649 (in DMSO)	<b>GST</b>	Caveolae/lipid rafts dependent endocytosis	Cholesterol depletion (a critical lipid constituent of membrane rafts and caveolae)	10, 50, 100, 150, 200 μM
<b>Nystatin</b> N6261 (in DMSO)	<b>NYS</b>	Caveolae/lipid rafts dependent endocytosis	Polyene antibiotic: Cholesterol sequestration	25 μg/mL
<b>Methyl-β-cyclodextrin</b> C4555 (in H <sub>2</sub> O)	<b>MβCD</b>	Caveolae/lipid rafts dependent (some effect on CCPs)	Cyclodextrins: Cholesterol extraction, depletion	2 mM
<b>Dynasore</b> D7693 (in DMSO)	<b>DYN</b>	Dynamine-dependent endocytosis (clathrin, caveolae-dependent and independent endocytosis)	Blocks dynamine GTPase activity (scission of newly formed vesicles from the membrane)	5, 10, 20, 40 μM

### II.C.2.2. Knock-down of BMP receptors and endocytic proteins using siRNA

Small interfering RNA (siRNA) are double-stranded RNA molecules, 20 - 25 base pairs in length. They interfere with the expression of specific genes with complementary nucleotide sequence by inducing their degradation via RNase-containing RISC (RNA-induced silencing complex) (Hamilton and Baulcombe, 1999; Elbashir et al., 2001) (**Figure II- 9**).

C2C12 cells were transfected with siRNA against BMP receptor Ia (BMPR-Ia), BMP receptor II (BMPR-II), clathrin heavy-chain (CHC), caveolin-1 (CAV-1) and dynamine-2 (DYN-2) (ON-TARGET plus SMARTpool, respectively Mouse BMPR-Ia, BMPR-II, Cltc, Cav1 and Dnm2 Thermo Scientific Dharmacon). A scrambled siRNA (all stars negative control siRNA, Qiagen) was taken as control.



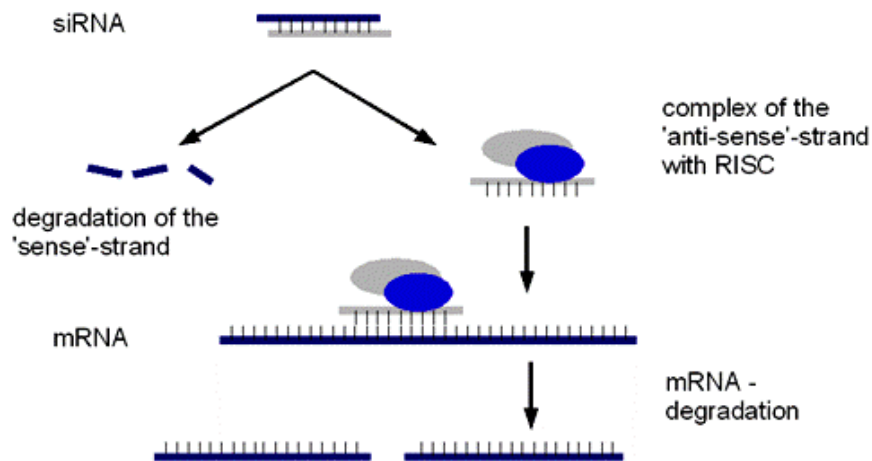


**Figure II- 9 : Mechanism of siRNA interference.**

siRNA transfection protocol: First, the cells were seeded at 30.000 cells/cm<sup>2</sup> in a 6-well plate and cultured in GM (2 mL per well) for 15 h. The transfection mix was prepared as following (volumes given for one well in a 96-well plate):

- i) 6 µL of lipofectamine RNAiMAX Reagent (Invitrogen) were added to 305 µL of Opti-MEM medium (Gibco) (= Mix 1);
- ii) 0.72 µL of 1 mM siRNA were added to another 305 µL of Opti-MEM medium (= Mix 2);
- iii) Mix 1 was gently added to Mix 2 and incubated for 20 min at room temperature.

Previously to transfection, the GM of the wells was replaced by the GM without antibiotics. Then, 610 µL of the final mix were added to each well. After 24 h of incubation at 37°C, the cells were transfected for the second time following the protocol described above and incubated for another 24 h. When working on 24-well plates the volume was adapted in function of the area of the wells. Then, the cells were detached by trypsin-EDTA, seeded on BMP-2 loaded films or on Thermanox® slides with BMP-2 in solution (at 30.000 cells/cm<sup>2</sup> in GM). They were allowed to adhere for 4h (in case of siRNA of receptors) or 8h (in case of siRNA of endocytic proteins). Then, the cells were fixed and the BMP-2 internalized amount quantified.

### **II.C.2.3. Imaging and quantification of internalized BMP-2 by the cells**

*The imaging of the internalized fluorescent BMP-2 was performed using a Zeiss LSM 700 confocal laser scanning microscope (Zeiss, Le Peck, France) equipped with a 63 x oil immersion objective and several laser diodes (488 nm was used for carboxyfluorescein-BMP-*

2). Images of isolated cells were used to quantify the total BMP-2 vesicle area per cell. The quantification of the internalized BMP-2 over time or after different treatments was performed using Image J software 1.44 ([imagej.nih.gov/ij/](http://imagej.nih.gov/ij/)). The “Analyze Particles” command was used and the total vesicle area per cell (in  $\mu\text{m}^2$ ) in one confocal plane was quantified over the 0.02 – 5  $\mu\text{m}^2$  range after image threshold. At least 50 cells were analyzed from at least two samples for each condition. The experiments were repeated at least three times.

#### II.C.2.4. Early osteogenic differentiation of C2C12 cells: ALP and Smad signaling

C2C12 myoblasts can undergo osteogenic differentiation when treated with BMP-2 growth factor (Katagiri et al., 1994). *Crouzier et al* showed that C2C12 cells cultured on top of BMP-2 loaded films express an early marker for osteogenic differentiation, the alkaline phosphatase (ALP) (Crouzier et al., 2009). After 3 days of culture, the myoblasts start to express ALP that can be dosed by ALP assay or by histochemical staining (*Figure II- 10*).

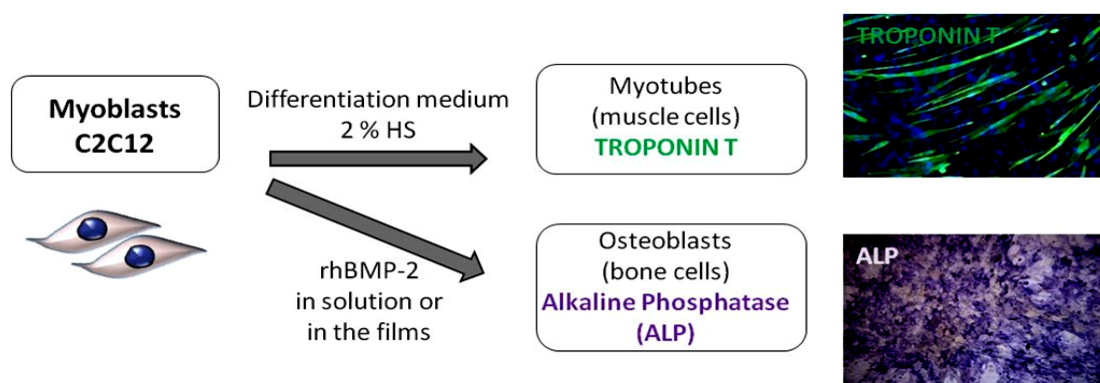


**Figure II- 10 : Differentiation potential of C2C12 myoblasts and some of the usual myogenic and osteogenic markers.**

In the present study, we used two methods for the evaluation of early osteogenic differentiation of C2C12 myoblasts in response to rhBMP-2. One method consists in following the activation of the SMAD pathway (Figure II- 11). To this end, we used C2C12-A5 myoblasts transfected with a construct containing luciferase reporter gene placed under Id1 gene promoter (Logeart-Avramoglou et al., 2006); Id1 gene is expressed in response to Smad pathway activation (*Figure II- 11*).

The second method consisted in the measurement of alkaline phosphatase (ALP) activity. ALP is a membrane bound hydrolase enzyme responsible for removing phosphate

groups, is expressed during osteogenic differentiation (**Figure II- 11**) and is often used as an early marker. The experimental plan is summarized in **Figure II- 12**.

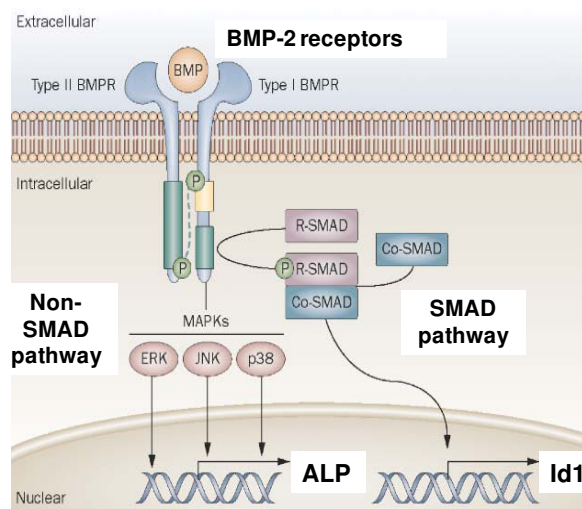


**Figure II- 11 : Early osteogenic markers ALP and Id1 induced via Smad and non-Smad pathways. Adapted from (Shore and Kaplan, 2010).**

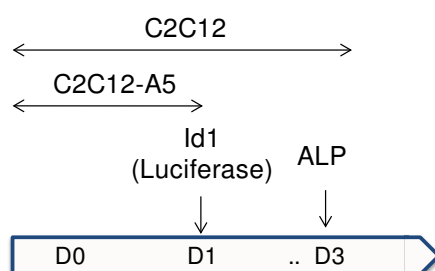


**Figure II- 12 : Time scale of the ALP and luciferase assays used to study early osteogenic differentiation.**

### **Luciferase assay**

The activation of Smad pathway was measured using the C2C12-A5 cells with the Bright-Glo™ Luciferase Assay System (E2610, Promega) after 24h of culture (**Figure II- 12**) on BMP-2 loaded films or in presence of soluble BMP-2, in 24- or 96-well plates respectively. As a positive control, cells seeded on plastic and treated with 600 ng/mL rhBMP-2 were used.

To quantify the luciferase expression, the culture medium is first replaced by 25  $\mu$ l (96-well plate) or 100  $\mu$ l (24-well plate) of PBS followed by the same volume of Luciferase Assay

Reagent. After 15 minutes at room temperature, 40  $\mu\text{l}$  of this mix are transferred into a white 96-well plate (655083, Greiner) for luminescence measurement using a plate reader.

The luminescence is finally normalized by DNA content measurement using CyQuant NF Proliferation assay kit (Molecular Probes, Invitrogen) following manufacturer's instructions. The method is based on measurement of cellular DNA content via fluorescent dye binding.

### ***ALP test***

The ALP colorimetric assay is based on monitoring the colour change, as para-nitrophenol phosphate (pNPP), which is colorless and cleaved by the ALP into phosphate and paranitrophenol (pNP), which is yellow.

For C2C12 myoblasts, the test was made after 3 days of culture on BMP-2-loaded films or in presence of soluble BMP-2.

Briefly, the cells cultured in 24-well plates were washed with PBS and lysed in 0.5 mL of 0.1% Triton X100 (Sigma) in PBS for 10 minutes at room temperature. 20  $\mu\text{L}$  of this lysate are transferred into a 96-well plate and mixed with 180  $\mu\text{L}$  of working solution prepared as following: 0.1 M 2-amino-2-methyl-1-propanol, 1 mM  $\text{MgCl}_2$  and 3.34 mg/ml (9 mM) pNPP (1026, Euromedex) in MilliQ water and adjusted to pH 10 with HCl.

The reaction kinetic is followed by the multiwell plate reader (TECAN infinite M1000) using a program that measure the absorbance at 405 nm (pNP) every 30 sec for 10 minutes. The slope (DO/min) represents the total ALP activity. It is then normalized by the amount of protein measured using a BCA protein assay kit (Interchim, France) following manufacturer's instructions. The ALP specific activity is finally expressed as micromoles of p-nitrophenol produced per min per mg of protein (using the slope obtained from the kinetics):

ALP specific activity ( $\mu\text{mol pNP} / \text{min} / \text{mg of protein}$ ) = Slope (DO/min)  $\times \epsilon(\text{pNP}) \times l \times L / [\text{prot}]$ ; where L, reaction volume = 200  $\mu\text{L}$  = 0.0002 L;  $\epsilon(\text{pNP}) = 18.75 \text{ mM}^{-1} \cdot \text{cm}^{-1} = 0.01875 \text{ M}^{-1} \cdot \text{cm}^{-1}$  and  $l = 0.2 \text{ cm}$ ;  $[\text{prot}] = \text{mg of protein in the reaction volume}$  (obtained from BCA assay).

### **II.C.2.5. Statistical analysis**

The results represent at least three independent experiments. Data were reported as means  $\pm$  standard error of the mean, or as box plots built using SigmaPlot Version 12.0 software.

Statistical comparisons were performed using SigmaPlot Version 12.0 software. Student's t-test was used for comparison of two groups of samples (sample group versus control group) ( $P < 0.001$  was considered significant). Statistically different values are reported on the figures.

**Chapter III:**  
**Secondary structure of rhBMP-2 in a protective  
biopolymeric carrier material**

### III.1. Article summary

One aim of this work was to investigate the BMP-2 structure after loading inside (PLL/HA) films (“matrix-bound” presentation) and compare it to the protein structure in solution, i.e. free environment. We have as well evaluated the impact of drying films on BMP-2 structure and *in vitro* bioactivity.

Fourier Transform InfraRed (FTIR) spectroscopy is a well-known and powerful technique to evaluate the secondary structure of proteins. By the using FTIR in different configurations, transmission and attenuated total reflection modes, we were able to characterize the structure of BMP-2 in solution and inside the films. We especially focused on the amide I band, the part of the spectrum that gives information on the secondary structure of proteins.

In the literature BMP-2 secondary structure was assessed using FTIR and Circular Dichroism spectroscopy and it was shown to be mostly represented by  $\beta$ -sheets and  $\alpha$ -helix structures (from 41 to 52 % for  $\beta$ -sheets and from 8 to 12% for  $\alpha$ -helix) (Hillger et al., 2005; Schwartz et al., 2006).

The spectrum of the BMP-2 inside a hydrated or dry film was isolated from that of the film by detailed analysis of the amide I band, including second derivative calculation and subsequent deconvolution. Here, the BMP-2 structure in solution was mainly made of  $\beta$ -sheets (~ 40 %), unordered (~ 25%) and  $\alpha$ -helix (~ 20%) structures. The trapping of BMP-2 trapping inside the hydrated films slightly impacted the protein structure and lead to a decrease in  $\beta$ -sheet content and an increase in the presence of unordered structures. A more pronounced change in structure was evidenced after drying of the films. The little changes observed in BMP-2 structure after loading inside (PLL/HA) films suggest that the possible ‘confinement’ provided by the film did not affect protein secondary structure.

In addition, we also investigated the *in vitro* bioactivity of dried BMP-2-loaded films as compared to films that were never dried. Interestingly, no change in the ALP activity was observed for films that have been dried for 2 hours and films that have been stored in dry state for 1 month. In analogy to sugars that are widely used as stabilizing agents during drying of proteins, the biopolymeric film plays the role of stabilizer, or protective carrier, for the protein.

In conclusion, natural biopolymers may not only permit the protein to be presented in a “matrix-bound” manner, but they also provide a protective structure for the protein structure. This appears as a crucial point for preserving the stability of BMP-2 molecules in dry state once they have been loaded in the biopolymeric coating.

## III.2. Article 1 (published in *Biomacromolecules*)

### Secondary structure of rhBMP-2 in a protective biopolymeric carrier material

*Flora Gilde<sup>1</sup>, Ofélia Maniti<sup>†1</sup>, Raphael Guillot<sup>1</sup>, Joao F. Mano<sup>2,3</sup>, Delphine Logeart-Avramoglou<sup>4</sup>, Frédéric Sailhan<sup>4</sup> and Catherine Picart<sup>1\*</sup>*

<sup>1</sup> CNRS UMR 5628 (LMGP), Grenoble Institute of Technology and CNRS, 3 parvis Louis Néel, F-38016 Grenoble Cedex, France

<sup>2</sup>3B's Research Group – Biomaterials, Biodegradables and Biomimetics, University of Minho, AvePark, 4806-909, Taipas, Guimarães, Portugal

<sup>3</sup> ICVS/3B's - PT Government Associate Laboratory, Braga/Guimarães, Portugal

<sup>4</sup> Laboratory of Bioengineering and Biomechanics for Bone and Articulations; UMR 7052, CNRS, University Paris Diderot, Sorbonne Paris Cité, 10 avenue de Verdun 75010 Paris, France

Corresponding Author: [catherine.picart@grenoble-inp.fr](mailto:catherine.picart@grenoble-inp.fr); phone: +33(0)4 56 52 93 11, fax: +33(0)4 56 52 93 01.

---

#### ABSTRACT

Efficient delivery of growth factors is one of the great challenges of tissue engineering. Polyelectrolyte multilayer films (PEM) made of biopolymers have recently emerged as an interesting carrier for delivering recombinant human bone morphogenetic protein 2 (rhBMP-2 noted here BMP-2) to cells in a matrix-bound manner. We recently showed that PEM made of poly(L-lysine) and hyaluronan (PLL/HA) can retain high and tunable quantities of BMP-2 and can deliver it to cells to induce their differentiation in osteoblasts. Here, we investigate quantitatively by Fourier Transform Infrared spectroscopy (FTIR) the secondary structure of BMP-2 in solution as well as trapped in a biopolymeric thin film. We reveal that the major structural elements of BMP-2 in solution are intramolecular  $\beta$ -sheets and unordered structures as well as  $\alpha$ -helices. Furthermore, we studied the secondary structure of rhBMP-2 trapped in hydrated films and in dry films since drying is an important step for future applications of these bioactive films onto orthopedic biomaterials. We demonstrate that the structural



elements were preserved when BMP-2 was trapped in the biopolymeric film in hydrated conditions and, to a lesser extent, in dry state. Importantly, its bioactivity was maintained after drying of the film. Our results appear highly promising for future applications of these films as coatings of biomedical materials, to deliver bioactive proteins while preserving their bioactivity upon storage in dry state.

**Keywords:** BMP, secondary structure, protein storage, bioactivity, polymeric film, hyaluronan

## INTRODUCTION

Efficient delivery of growth factors is one of the great challenges of tissue engineering <sup>1</sup>. It is now acknowledged that large doses of potent growth factors, delivered in solution, can lead to severe side effects <sup>2</sup>. Engineered materials that can regulate the biological presentation of growth factors represent a new class of therapeutic agents for the treatment of a wide variety of diseases <sup>3</sup>. The ideal carrier would retain and sequester the growth factor locally, thus reducing the dose needed, while enhancing its efficacy <sup>4</sup>. Importantly, the carrier should preserve the protein bioactivity, which is directly related to its secondary and tertiary structure.

The bone morphogenetic protein (BMP) family is an intensive field of research in its own for tissue engineering applications <sup>5</sup> as well as for fundamental cell biology studies <sup>6</sup> due to its physiological importance. BMPs play a crucial role in morphogenesis, tissue patterning and regeneration after tissue damage <sup>7</sup>. In particular, BMP-2 is a highly potent morphogen that induces muscle precursors and mesenchymal stem cell differentiation in bone cells <sup>8</sup>. Currently, BMP-2 is used in clinics <sup>9</sup> and the only approved formulation of BMP-2 uses an absorbable collagen sponge as a carrier agent. However, up to 12 mg (much higher dose than physiological concentrations) is used, thus raising serious concerns about its safety as reported in the recent literature <sup>10</sup>. Other carrier biomaterials have been and are currently being developed <sup>5, 11</sup>. Mimics of the natural extra cellular matrix, including fibrin films <sup>12</sup>, hyaluronan hydrogels <sup>13</sup>, polypeptide and polysaccharides-based layer-by-layer films <sup>14, 15</sup> appear particularly interesting due to their natural composition. Natural biopolymers may not only permit the protein to be presented in a “matrix-bound” manner, but they also provide a water-rich environment. This may be a crucial point for preserving the stability of the proteins in dry state once loaded in the biopolymeric coatings. In fact, dehydration is known to

possibly greatly impact proteins structures<sup>16</sup>. The drying process removes part of the hydration layer, which may disrupt the native state of a protein and cause protein aggregation<sup>16</sup>. It is known that protein conformation is very often lost upon storage in dry conditions, unless stabilizers like sugars, polyols or polyaminoacids are added during the freeze-drying process<sup>16</sup>. Very recently, atomistic molecular dynamics simulations<sup>17</sup> suggested that the environment (vacuum versus water) is a key factor in the stabilization of the secondary and tertiary structure of BMP-2. Friess and coworkers have shown that controlled precipitation of BMP-2 proteins from very high solutions of very high concentrations (20 mg/mL) of protein lead to the formation of microparticles of  $\mu\text{m}$  size (7 and 35  $\mu\text{m}$  bimodal distribution)<sup>18</sup>. They used FTIR spectroscopy to show that the structure of BMP-2 in the precipitated state and after resolubilization in an acidic buffer was similar to that of the protein in solution<sup>19</sup>. They evidenced the formation of mainly  $\beta$ -sheet structures and  $\alpha$ -helices. The formation of  $\beta$ -sheets was also observed by circular dichroism<sup>20</sup>.

However, quantitative information on BMP-2 secondary structure in solution or in a carrier material is still lacking. Here, we investigated quantitatively by FTIR the secondary structure of BMP-2 in solution as well as trapped in a nanostructured biopolymeric thin film. The film is a polyelectrolyte multilayer film made of poly(L-lysine) and hyaluronan (PLL/HA), which was recently shown to retain high and tunable quantities of rhBMP-2 and to deliver it to cells in a “matrix-bound” manner<sup>15, 21</sup>. FTIR was chosen as it is a powerful technique to qualitatively and quantitatively assess protein secondary structure<sup>22 23 24</sup> and to obtain the relative amount of different types of secondary structures based on the band areas<sup>25, 26, 27</sup>. It is a very precise ( $< 2 \text{ cm}^{-1}$ ), sensitive and reproducible technique<sup>28, 29</sup>, which is indeed routinely used to assess the secondary structure of therapeutic proteins.

## **MATERIALS AND METHODS**

### **Materials**

Poly(L-lysine) (PLL) hydrobromide (P2626,  $6.8 \times 10^4 \text{ g/mol}$ ) was purchased from Sigma (St-Quentin Fallavier, France) and hyaluronan (HA,  $3.6 \times 10^5 \text{ g/mol}$ ) was obtained from Lifecore Biomedical (USA). They were dissolved at 0.5 mg/mL and 1 mg/mL, respectively, in a buffered saline (0.15 M NaCl, 20 mM HEPES, pH 7.4, called hereafter HEPES-NaCl buffer). For film cross-linking, 1-Ethyl-3-[3-dimethylaminopropyl]carbodiimide hydrochloride (EDC, Sigma, St Quentin Fallavier, France) was mixed with a N-hydroxysulfosuccinimide (sulfo-

NHS, Chemrio, China) in 0.15 M NaCl solution (pH 5.5) at concentrations of 30 mg/mL and 11 mg/mL, respectively. BMP-2 was from Medtronic Biopharma BV.

### **Quantitative analysis by FTIR spectroscopy**

A Vertex 70 spectrophotometer (Bruker Optics GmbH, Ettlingen, Germany) was used for the acquisition of FTIR spectra. Single-channel spectra were recorded between 400 and 4000  $\text{cm}^{-1}$  with a 2  $\text{cm}^{-1}$  resolution by means of the OPUS Software v6.5 (Bruker). A nitrogen-cooled Mercury-cadmium-telluride (MCT) detector was used to improve the detection level. Such detector is known to produce a noise level 10 to 50 times lower than other detectors<sup>29</sup>. Different accessories were used depending on the experiments: an Aquaspec transmission cell for studying BMP-2 in solution, an attenuated total reflection (ATR) liquid cell for the study of BMP-2 loaded in hydrated films, and a standard transmission accessory for the study of the BMP-2 loaded films deposited on silicon substrates and subsequently dried. All these accessories were purchased from Bruker Optics.

The OPUS Software v6.5 (Bruker GmbH) was used for the treatment and deconvolution of the spectra. Residual water and  $\text{CO}_2$  contributions were removed and baseline correction was done manually, choosing always the same reference points in each group of spectra. When residual noise due to water (especially in dry conditions) was still present, the spectra were smoothed using a specific algorithm from Opus software. The frequencies of the different components forming the amide I band were first determined by calculating of the second derivative of the Fourier smoothed spectrum<sup>25, 27</sup>. There was thus no arbitrary decomposition into a preset number of bands and on the peak position. Once the number of component bands was determined, the amide I band was fitted by using the component frequency, width, and intensity as fitting parameters. The more consistent results were obtained when all component peaks were assumed to be Gaussian. The correspondence of each component band with a given secondary structure was established by comparing the frequency of its maximum to the value given in the literature<sup>30</sup>. We defined the relative contribution of each component (in %) by the ratio of the area of each peak over the area of the total amide I band<sup>27</sup>.

### **Characterization of BMP-2 secondary structure in solution**

The BMP-2 solution was first purified. To this end, it was first precipitated using a 10% Ammonium Sulfate (AS) solution<sup>31</sup>. The mixture was centrifuged at 13000 rpm for 10 min after which the supernatant was removed. This procedure was repeated three times with a 2%

AS solution. Finally, the protein was resuspended in the 1 mM HCl in D<sub>2</sub>O (pH=3) solution or in the HEPES-NaCl buffer in D<sub>2</sub>O (pH=7.4). The final protein concentration was ~ 2 mg/mL for rhBMP-2 in 1mM HCl (pH 3). At pH 7.4, the protein is known to be less soluble<sup>20, 32, 33</sup>. We estimated the BMP-2 concentration of the resuspended solution to be 400 µg/mL at this pH, based on the difference of the maximum absorbance of the protein. 60 µL of BMP-2 was injected in the Aquaspec cell and a single-channel spectrum of 64 interferograms was recorded.

### **(PLL/HA) film characterization by FTIR**

The buildup of (PLL/HA) films in HEPES-NaCl buffer was followed by FTIR spectroscopy as previously described<sup>34</sup>. For studies in hydrated conditions, D<sub>2</sub>O was used as solvent instead of water in order to avoid the overlapping water band in the amide I region (O-H bending vibration at 1643 cm<sup>-1</sup> versus O-D bending vibration at 1209 cm<sup>-1</sup>). The spectra of hydrated (PLL/HA)<sub>12</sub> films were acquired *in situ* using attenuated total reflection (ATR) mode. To this end, films were built and cross-linked on a ZnSe crystal and a single-channel spectrum of 64 interferograms was recorded. For studies in dry conditions, films were built as described previously<sup>35</sup> on a ~ 1 cm<sup>2</sup> silicon substrate (Siltronix, France) using HEPES-NaCl (dissolved in H<sub>2</sub>O) followed by cross-linking. The films were then rinsed with milli-Q water to remove the salt and dried for 1 h at 37°C. The film spectra in transmission were acquired by summing 256 interferograms. For long-term stability measurements, the films were stored in dry state at 4°C. Before each FTIR acquisition, they were incubated for 1 h at 37°C.

### **Characterization of BMP-2 secondary structure in hydrated and in dry (PLL/HA) films**

For BMP-2 trapped in hydrated (PLL/HA)<sub>12</sub> films built in D<sub>2</sub>O, BMP-2 was loaded from a solution at 100 µg/mL in 1 mM HCl in D<sub>2</sub>O (pH=3) following the protocol established previously<sup>15</sup>. The rinsing steps were done with HEPES-NaCl buffer. The spectrum of BMP-2 was obtained by subtracting the spectrum of the film in contact with the HEPES-NaCl buffer to that of the BMP-2 loaded film (measured in the same buffer after rinsing of the film).

For study of BMP-2 in dry films, BMP-2 in 1 mM HCl (in H<sub>2</sub>O) was loaded in the (PLL/HA) film prepared in the HEPES-NaCl buffer (in H<sub>2</sub>O) and dried as described above for the film. The spectrum of BMP-2 inside dry films was obtained by calculating the difference between the average spectrum of two independent BMP-2 loaded films and the average spectrum of

two control samples (i.e. films that have followed the same procedure, except that BMP-2 was not present in the loading solution).

### **C2C12 cell culture and Alkaline Phosphatase Activity test (ALP test)**

Murine C2C12 skeletal myoblasts (< 25 passages, obtained from the American Type Culture Collection, ATCC) were cultured in tissue culture Petri dishes, in a 1:1 Dulbecco's Modified Eagle Medium (DMEM)/Ham's F12 medium (Gibco, Invitrogen, France) supplemented with 10% fetal bovine serum (FBS, PAA Laboratories, France), 100 U/mL penicillin G and 100 µg/mL streptomycin (Gibco, Invitrogen, France) in a 37°C, 5% CO<sub>2</sub> incubator. Cells were subcultured prior to reaching 60-70% confluence (approximately every 2 days).

The bioactivity of BMP-2 on C2C12 cells was determined by assaying the alkaline phosphatase (ALP) activity, a marker of osteogenic differentiation, as previously described<sup>15</sup>. C2C12 cells were seeded in 24-well plates (90 000 cell per well) in 1 mL of growth medium. After 3 days of culture, the culture medium was removed and the cells were washed with PBS and lysed by sonication (5 s) in 500 µL of 0.1% Triton-X100 in PBS. 180 µL of a buffer containing 0.1 M 2-amino-2-methyl-1-propanol (Sigma, France), 1 mM MgCl<sub>2</sub>, and 9 mM p-nitrophenyl phosphate (Euromedex, France) adjusted to pH 10 was added to 20 µL of lysate. The enzymatic reaction was monitored in a 96-well plate by measuring the absorbance at 405 nm using a TECAN Infinite 1000 microplate reader (Tecan, Austria) over 10 min. The total protein content of each sample was determined using a bicinchoninic acid based protein assay kit (Interchim, France). The ALP activity was expressed as mmoles of p-nitrophenol produced per min per mg of protein (pnp/min/mg).

The bioactivity of loaded BMP-2 was also assessed after drying the film and upon storage at 4°C. To this end, the samples were loaded with BMP-2 as previously described and thoroughly washed in HEPES-NaCl buffer then in ultrapure water. They were air-dried for 2 h under a laminar flow hood and stored at 4°C. The BMP-2 activity was determined right after this drying step and after 1 month of storage. The samples were rehydrated 30 min in the HEPES-NaCl buffer and sterilized under UV irradiation before depositing cells. The ALP activity test was performed after 3 days of culture.

## **RESULTS AND DISCUSSION**

### **Secondary structure of BMP-2 in solution at acidic and at neutral pH**

The secondary structure of BMP-2 protein was first investigated by FTIR in solution (Figure 1) with a focus on the Amide I band. pH 3 was selected as it corresponds to its maximum

solubility<sup>36</sup> and to the recommended conditions of storage. Indeed, we have previously shown that loading of BMP-2 in the biopolymeric film at pH 3 was optimum in terms of homogeneity and loaded amount<sup>15</sup>. Physiological conditions (0.15 M NaCl, pH 7.4, Figure 1B), which corresponds to the conditions of film buildup and cell culture experiments, were also studied. Second derivatives of the spectra were also calculated (Figure 1A', B'). Based on these second derivatives, on FTIR data on proteins<sup>30</sup> and on a previous study on precipitated BMP-2 microparticles<sup>19</sup>, the five observed minima were attributed to four different types of secondary structures as follows:  $\sim 1630\text{ cm}^{-1}$  and  $\sim 1680\text{ cm}^{-1}$  to antiparallel  $\beta$ -sheets (two contributions at low and high wavenumbers, LW and HW, respectively),  $1645\text{ cm}^{-1}$  to unordered,  $\sim 1651\text{-}1657\text{ cm}^{-1}$  to  $\alpha$ -helix, and  $\sim 1670\text{ cm}^{-1}$  to  $\beta$ -turn structures<sup>30</sup>.

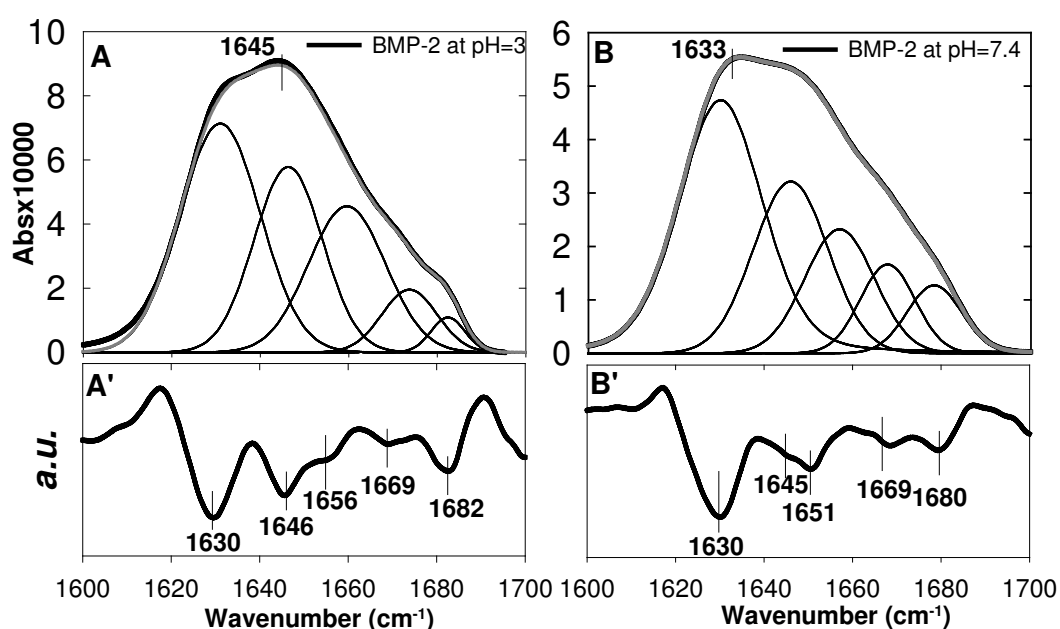


**Figure 1.** FTIR spectra and corresponding second derivatives of rhBMP-2 in solution at pH 3 (A, A') and at pH 7.4 (B, B'). (in black: experimental spectrum and in grey fitted spectrum). Measurements were performed in D<sub>2</sub>O.

At first sight, the spectra of BMP-2 at different pHs appeared to differ as its maximum was positioned at  $1645\text{ cm}^{-1}$  for BMP-2 at pH 3, whereas it was at  $1633\text{ cm}^{-1}$  for BMP-2 at pH 7.4 in the presence of salt. Decomposition of the amide I band allowed the quantification of the respective contributions of each type of secondary structure (Table 1).

Independent experiments indicated that the precision of the peak position obtained by fitting the spectra is  $< 2\text{ cm}^{-1}$ . The precision on the % of secondary structures can be estimated at  $\sim 3$  to 4% for the most prominent peaks and highest peaks and  $\sim 1\text{-}2\%$  for the smallest ones.

**Table 1.** Results of the deconvolution of the FTIR spectra of rhBMP-2 in solution at pH 3 (no salt) or at pH 7.4 (HEPES-NaCl buffer) as well as in hydrated or dry polyelectrolyte multilayer films. (LW, HW: Low, High Wavenumber). W: Wavenumber ( $\text{cm}^{-1}$ ); %: percentage relative to the total amide I band integral.

	LW Inter. $\beta$ -sheet	LW Intra. $\beta$ -sheet	Unordered	$\alpha$ -helix	$\beta$ -turn	HW Intra. $\beta$ -sheet	HW Inter. $\beta$ -sheet	
BMP-2 in solution pH 3		1631 39	1646 27	1660 24	1674 7	1683 3		W %
BMP-2 in solution Hepes-NaCl pH 7.4		1630 44	1646 24	1657 16	1668 9	1678 7		W %
BMP-2 trapped in hydrated film	1617 2	1630 28	1644 31	1658 18	1670 11	1680 8	1690 1	W %
BMP-2 trapped in dry film	1628 2	1638 21	1652 34	1664 21	1678 16	1689 5	1694 1	W %

First, one noticed that the highest contribution was that of antiparallel  $\beta$ -sheets (sum of LW and HW  $\beta$ -sheet), which accounted for 42% of the structure at pH 3 and 51% at pH 7.4 in the presence of salt. The  $\alpha$ -helix contribution represented 24% of the secondary structure at pH 3 and only 16% at pH 7.4. Of note, the % of unordered structures remained unchanged ( $\sim$  24-27%) in both conditions and the % of  $\beta$ -turn was also similar ( $\sim$  7-9%). Thus, formation of  $\beta$ -sheet structures was induced by the increase of pH closer to its isoelectric point (8.5<sup>37</sup>), where BMP-2 is less soluble<sup>32</sup>.

These experimental determinations of the % of secondary structures were indeed relatively close to the values deduced from the crystal structure of BMP-2<sup>38</sup> and from molecular dynamics simulations of BMP-2 structure in water<sup>17</sup>. These latter values range from 41 to 52 % for  $\beta$ -sheets and from 8 to 12% for  $\alpha$ -helix structures. Experimental data obtained by circular dichroism also indicated the prominence of  $\beta$ -sheets<sup>20</sup>. In addition, FTIR data on native BMP-2 at very high concentration (20 mg/mL) and on dried microparticles of BMP-2 showed that  $\beta$ -sheets represented  $\sim$ 25% of the secondary structural elements<sup>18</sup>. Thus, although performed in different experimental conditions, our data are consistent with these previous experimental and theoretical studies.

## Secondary structure of (PLL/HA) films

Next, we investigated the structure of the polyelectrolyte multilayer film that was used as reservoir for BMP-2 storage in hydrated and in dry state. This analysis was important to get information on the possible changes in the film structure. We studied the amide I region in different solvents ( $D_2O$  versus  $H_2O$ ) and in hydrated or dry conditions.

Figure 2 shows the typical infrared spectra of cross-linked  $(PLL/HA)_{12}$  films in hydrated and dry states with a focus on the amide I and amide II bands. The spectrum of the hydrated film is shown for films built in  $D_2O$  and in  $H_2O$ . The spectrum of dry film was obtained after drying a film prepared in HEPES-NaCl buffer in  $H_2O$ .

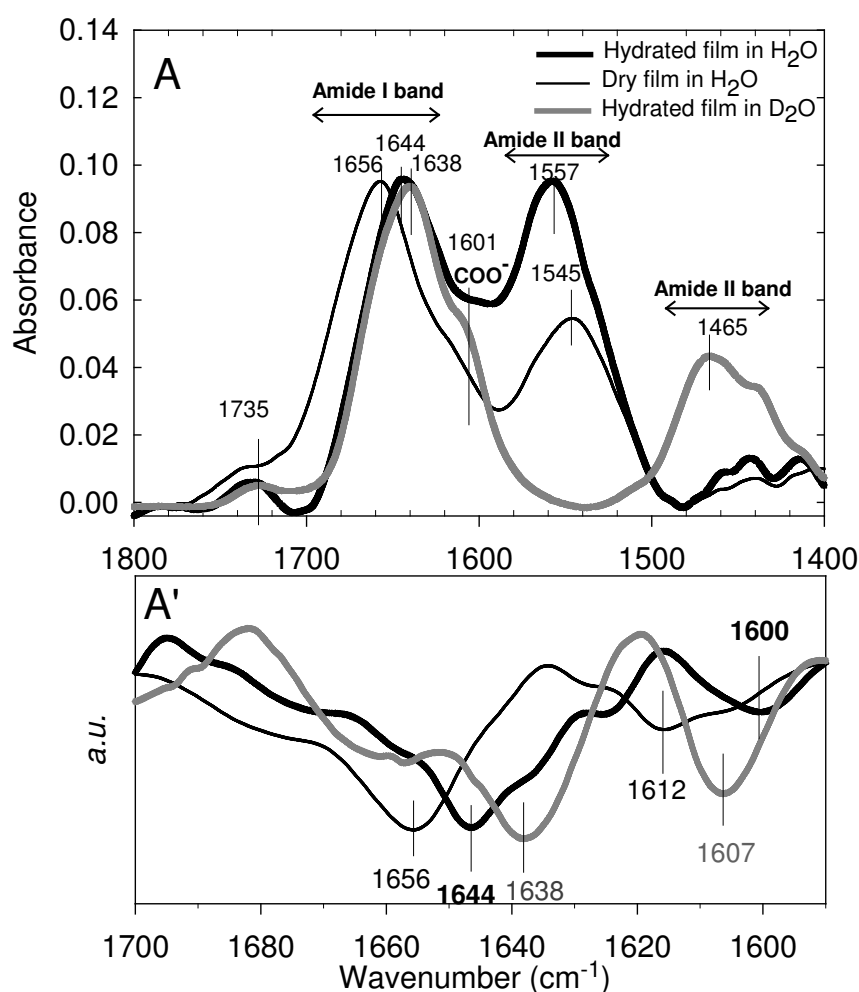


**Figure 2.** FTIR spectrum (A) and second derivative of the spectrum (A') of  $(PLL/HA)_{12}$  film in hydrated and dry state: hydrated film in  $D_2O$  (thick black line); hydrated film in  $H_2O$  (thick gray line); dry film (thin line). For the sake of comparison, the spectrum of the dry film was multiplied by 2.



**Table 2.** Position of the main peak of the amide I band for (PLL/HA) films built in Hepes-NaCl in D<sub>2</sub>O, H<sub>2</sub>O and after drying a film built in H<sub>2</sub>O.

	<b>D<sub>2</sub>O</b>	<b>H<sub>2</sub>O</b>	<b>Dry</b>
Amide I Main peak	1638	1644	1656
COO <sup>-</sup>	1607	1600	1612

The comparison between the spectra for hydrated films obtained in D<sub>2</sub>O and in H<sub>2</sub>O allowed to reveal some differences. The most significant change was the shift of the entire amide II band from 1557 cm<sup>-1</sup> (maximum of this band) to 1465 cm<sup>-1</sup> when the film was built in a D<sub>2</sub>O. This shift can be justified by the hydrogen/deuterium exchange as reported previously in the literature<sup>39</sup>. In (PLL/HA) films, the amide I band is mainly representative of PLL structure<sup>40</sup>. The second derivatives allows to determine the position of the major peak of the Amide I band (Figure 2A'). A strong minimum was visible at 1638 cm<sup>-1</sup> for the film built in D<sub>2</sub>O, at 1644 cm<sup>-1</sup> for that built in H<sub>2</sub>O, and at 1656 cm<sup>-1</sup> for the dry film, which could be attributed to unordered structures<sup>40, 41</sup>. Thus there was a significant shift toward higher wavenumbers especially for the dry film (+12 cm<sup>-1</sup> after drying the film built in water). This total shift is due to combined effect of solvent exchange and subsequent drying<sup>39</sup>, as the film was built in D<sub>2</sub>O for studies in hydrated conditions versus H<sub>2</sub>O for studies on dry and stored films. A weaker contribution, attributed to turn structures, was observed at 1663 and 1674 cm<sup>-1</sup> for hydrated films and at 1680 cm<sup>-1</sup> for dry films. The COO<sup>-</sup> contribution was also shifted from ~1600 cm<sup>-1</sup> in H<sub>2</sub>O to 1607 cm<sup>-1</sup> in D<sub>2</sub>O and ~1612 cm<sup>-1</sup> for dry films. A small contribution of COOH of HA was also visible at ~1735 cm<sup>-1</sup>.

After peak decomposition (supporting information Figure SI1), we found that ~90-95% of the structural elements in (PLL/HA) hydrated or dry films were unordered structures and that only 5-10% were turn structures. We thus conclude that the hydrated (PLL/HA) film exhibited mostly an unordered structure, which was kept after drying the film.

### **Structure of BMP-2 trapped in hydrated or dry (PLL/HA) films**

The structure of BMP-2 trapped in hydrated or dry (PLL/HA) films was subsequently investigated (Figure 3). In this case, some interactions between the protein and the film might occur, as BMP-2 has a very strong affinity with the film and remained trapped in it even after extensive washing<sup>15</sup>. In a previous study, we have quantified the amount of adsorbed BMP-2 that is trapped after thorough rinsing of the film<sup>15</sup> as a function of the concentration of the

BMP-2 solution used for the loading and as a function of film thickness. For an initial BMP-2 concentration in solution of 100  $\mu\text{g/mL}$  (used here or its loading in the film), this amount was estimated to be of  $769 \pm 69 \text{ ng/cm}^2$ <sup>15</sup>.

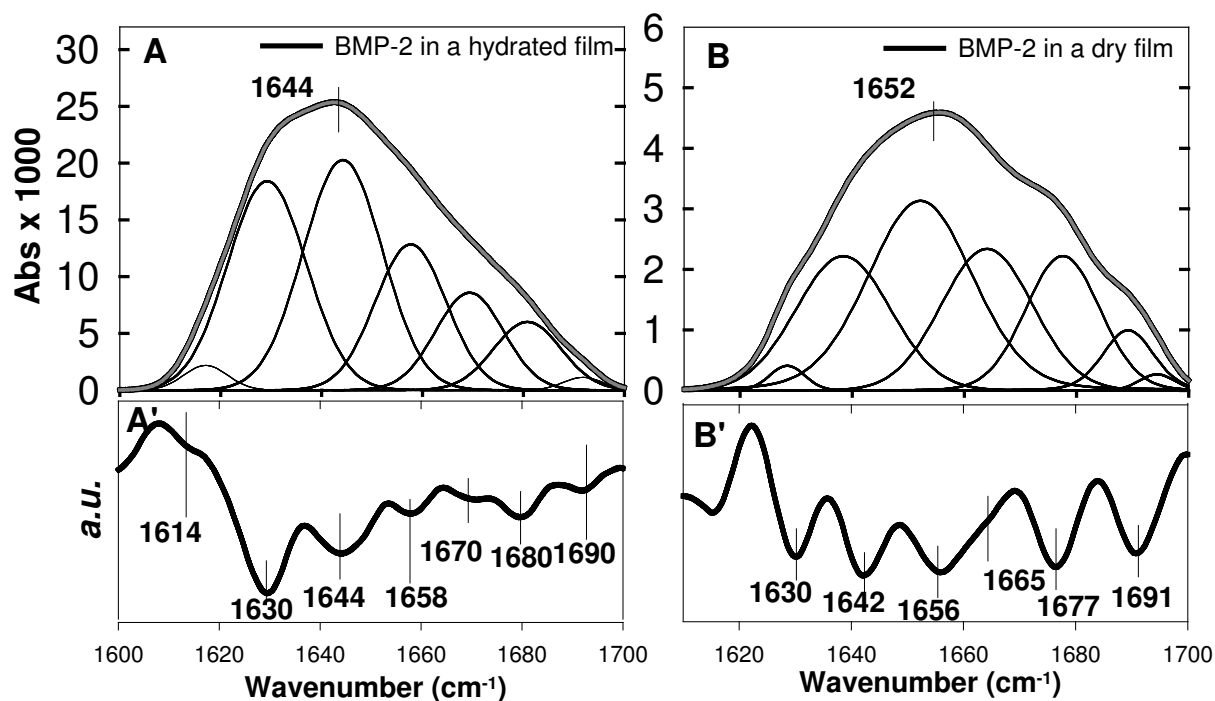


**Figure 3.** FTIR spectra and second derivative of BMP-2 trapped in cross-linked  $(\text{PLL/HA})_{12}$  films (A, A') in a HEPES-NaCl buffer at pH 7.4 (hydrated film) and (B, B') after drying the film (in black: experimental spectrum and in grey fitted spectrum).

For BMP-2 in hydrated films, we noted at first sight that the absorbance was maximal at  $\sim 1644 \text{ cm}^{-1}$ , showing similarities with that of BMP-2 in solution at pH 3 (Fig.1A). However, besides the five contributions already observed for BMP-2 in solution, two new but very small contributions appeared at low ( $\sim 1615, 1628 \text{ cm}^{-1}$ ) and high wavenumbers ( $\sim 1691 \text{ cm}^{-1}$ ) for BMP-2 in films, as compared to BMP-2 in solution (Fig. 1). They can unambiguously be attributed to intermolecular  $\beta$ -sheet structures<sup>30</sup>, which may result from either protein-protein interactions or from protein-polyelectrolyte interactions. All the other peak positions present in the second derivatives were close to those previously observed for the protein in solution. We also performed control experiments to ensure that the contribution of the film to the BMP-2 spectrum was negligible. To this end, the film was subjected to the same sequence of dipping as for BMP-2, except that BMP-2 was not added (Figure SI2). A very small decrease in the  $1600\text{-}1700 \text{ cm}^{-1}$  region of 0.001 absorbance units, which is 25 times smaller than the

BMP-2 signal measured in the amide I band region (Figure 3A). Indeed, a positive absorbance was measured for BMP-2 in the amide I band region.

The deconvolution of the spectrum (Table 1) lead to the most consistent results by now considering seven peaks. BMP-2 in hydrated films mostly formed intramolecular  $\beta$ -sheets (36 %), unordered structures (31 %),  $\alpha$ -helix (18 %),  $\beta$ -turn (11 %) and only a very minor fraction of intermolecular  $\beta$ -sheets (3 %). Indeed, the percentages of the different types of secondary structures differed by only few % from those of BMP-2 in solution at pH 3. Thus, although BMP-2 was physically confined in the film, its structure remained close to the one it had in solution at pH 3.

At first glance, the spectrum of BMP-2 trapped in a dry film (Fig. 3B) was different when compared to all other conditions (BMP-2 in hydrated film or in solution at different pHs). The maximum of the spectrum was shifted to a higher wavenumber at  $1652\text{ cm}^{-1}$ . This shift of  $\sim 8\text{ cm}^{-1}$  is reminiscent of the shift observed for (PLL/HA) films built in the Hepes-NaCl buffer (in  $\text{H}_2\text{O}$ ) and dried (Figure 2). It may thus be due to the different experimental conditions used notably i) BMP-2 loading in water and not in  $\text{D}_2\text{O}$ , which was used for the *in situ* experiments in hydrated films and ii) drying of the BMP-2 loaded film, which restricts the mobility of the polymeric and polypeptidic chains. Furthermore, the two minima previously observed at  $1670$  and  $1680\text{ cm}^{-1}$ , were replaced by a single but more pronounced minimum at  $1677\text{ cm}^{-1}$ , which renders the distinction between  $\beta$ -turn and intramolecular  $\beta$ -sheets more difficult. By considering the systematic shift in the peak positions and by still considering 7 contributions, which gave the best fits, we found that BMP-2 in dry films formed unordered structures (34 %), intramolecular  $\beta$ -sheets (26 %),  $\alpha$ -helix (21 %),  $\beta$ -turn (16 %) and intermolecular  $\beta$ -sheets (3 %). The most important differences with BMP-2 in hydrated films arose from the decrease in intramolecular  $\beta$ -sheets and the concomitant increase in unordered and  $\beta$ -turn structures.

Thus, FTIR revealed the predominance of  $\beta$ -sheets and unordered structures on BMP-2 trapped in hydrated films and in dry films as well. The fraction of intramolecular  $\beta$ -sheets decreased from 42-51% for BMP-2 in solution to 25-36 % for BMP-2 in films, the strongest decrease being observed for BMP-2 in dry films. The % of unordered structures in trapped BMP-2 was higher (31-34%) for BMP-2 in films as compared to its solution counterpart (24-27%). The presence of  $\alpha$ -helix was also confirmed, with an overall percentage of 16-24%.

### Bioactivity of “matrix-bound” BMP-2 in dry films

An important question is whether the bioactivity of “matrix-bound” BMP-2 was maintained in dry films, as we already know from our previous studies that BMP-2 loaded in hydrated films is bioactive<sup>15</sup>. In order to assess the bioactivity of BMP-2, we chose C2C12 myoblast cells as working model. These cells constitute an acknowledged *in vitro* model system to study the ability of BMPs to alter cell lineage from the myogenic to the osteogenic phenotype<sup>42</sup>; as BMP-2 induced the expression of alkaline phosphatase (ALP). In a previous study, we have already demonstrated that BMP-2 presented in a “matrix-bound” manner from hydrated (PLL/HA) films induced osteoblastic differentiation of C2C12 myoblasts<sup>15</sup>. Here, the bioactivity of the films was tested either right after their preparation, i.e. in hydrated state, or after drying of the film for a short period (2 h) or after storage of the film in dry conditions for one month. First, we verified by FTIR that the films could be stored in dry state for this time period (Supporting information Figure SI3). Only very minor changes of less than 6% were noticed in the FTIR spectra, especially in the COO<sup>-</sup> peak region and in the amide I band. The ALP test was performed on C2C12 myoblasts after 3 days of contact with the BMP-2 loaded films (Figure 4). A control value for the bioactivity of BMP-2 in solution (i.e. added to the cell culture medium for 3 days) was also obtained in conditions where the bioactivity has reached a plateau value<sup>15</sup> (ie for a BMP-2 concentration of 200 ng/mL).

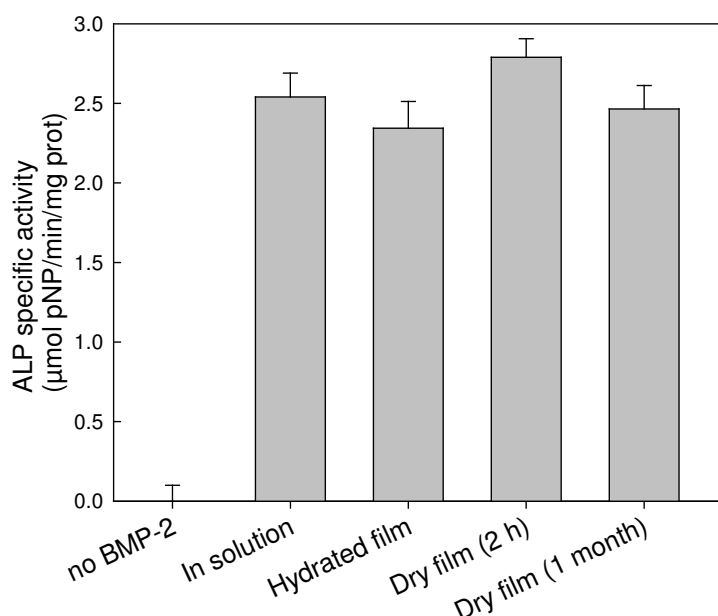


**Figure 4.** Quantification of alkaline phosphatase activity of C2C12 cells cultured for 3 days in the presence of BMP-2 in solution at 200 ng/mL (control value for BMP-2 bioactivity) or on the (PLL/HA) films loaded or not with BMP-2. Films were either hydrated or dried for 2 hrs, or dried and subsequently stored for a month. There was no statistical difference between the conditions, except for the condition without BMP-2 in the film. Error bars are SEM.

Very interestingly, the BMP-2 loaded (PLL/HA) films dried for 2 h, or dried and stored for 1 month retained a full activity, similar to that of hydrated films and to the plateau value obtained for BMP-2 in solution. It is difficult to precisely quantify the fraction of BMP-2 that is bioactive in the hydrated film, which remained bioactive after drying of the film. But a rough estimate can be made, considering the fact that the ALP response is proportional to the amount of BMP-2 loaded in the films<sup>15</sup> and that a plateau value in the ALP signal was observed for a BMP-2 concentration in film of  $\sim 400 \text{ ng/cm}^2$ <sup>15</sup>. As the effective BMP-2 loaded concentration in the film was previously determined to be of  $\sim 770 \text{ ng/cm}^2$  in our experimental conditions<sup>15</sup>, one can infer that at least 52% of BMP-2 was bioactive. Thus, although there was a slight increase in unordered structures upon drying of the BMP-2 loaded film, the overall activity of the protein was still very high after rehydration of the film. The presence of a large number of H-bond in the (PLL/HA) films<sup>40</sup> and large number of water molecules around hyaluronan, even in the dry state<sup>43</sup>, are probably playing an important role in this process. Importantly, the protein is trapped in the film but the structure of the film allowed it to retain a large fraction of intramolecular  $\beta$ -sheets and to maintain its central  $\alpha$ -helix. By analogy to sugars that are widely used as stabilizing agents during drying of proteins<sup>44</sup>, the biopolymeric film plays the role of stabilizer, or protective carrier, for the protein. In conclusion, BMP-2 trapped in hydrated and dry (PLL/HA) films retained its overall secondary structure, but an increase in unordered structures and a decrease of  $\beta$  sheets was noted as compared to BMP-2 in solution.

Importantly, the bioactivity of the dry BMP-2 loaded films remained at a similar level to that of hydrated films, which confirmed the protective role of the film in the stabilization of the BMP-2 structural elements. These results appear highly promising for future applications of these films as coatings of biomedical materials, to sequester proteins and to deliver them locally, while preserving their bioactivity and secondary structure. It would be interesting to investigate whether similar mechanisms may take place for other types of growth factors that have been successfully adsorbed on PEMs films and whose bioactivity was proved<sup>45</sup>.

## ACKNOWLEDGMENTS

This work was supported by the French Ministry of Research through an ANR-EmergenceBIO grant (ANR-09-EBIO-012-01), by the European Commission (FP7 program) via a European Research Council starting grant (BIOMIM, GA 259370) and by GRAVIT (081012\_FIBIOS). CP is grateful to IUF for financial support.

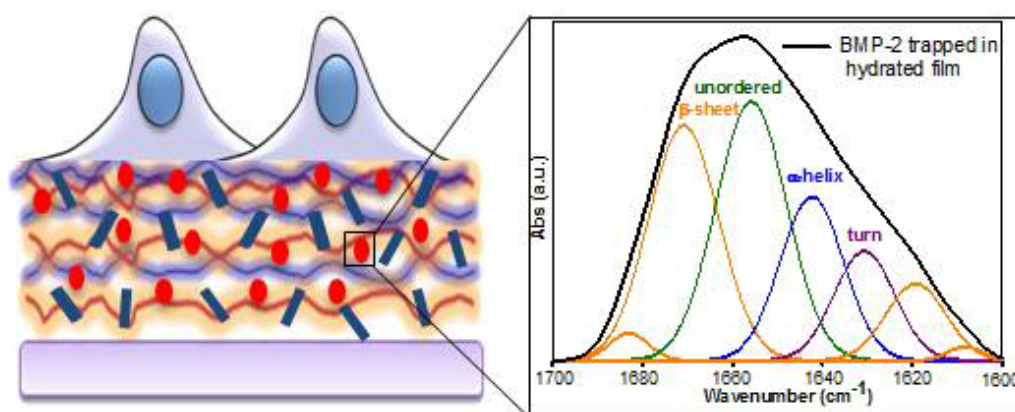
## REFERENCES

1. Lutolf, M. P.; Hubbell, J. A. *Nat. Biotech.* 2005, 23, 47-55; Hubbell, J. A. *Curr. Opin. Biotech.* 2004, 15, 381-2.
2. Shimer, A. L.; Oner, F. C.; Vaccaro, A. R. *Injury* 2009, 40 Suppl 3, S32-8.
3. Lee, K.; Silva, E. A.; Mooney, D. J. *J. R. Soc. Interface.* 2011, 8, 153-70.
4. Hynes, R. O. *Science* 2009, 326, 1216-9.
5. Haidar, Z. S.; Hamdy, R. C.; Tabrizian, M. *Biotechnol. Lett.* 2009, 31, 1817-24.
6. Obradovic Wagner, D.; Sieber, C.; Bhushan, R.; Borgermann, J. H.; Graf, D.; Knaus, P. *Sci. Signal.* 2010, 3, mr1.
7. Reddi, A. H.; Reddi, A. *Cytokine. Growth. Factor. Rev.* 2009, 20, 341-2.
8. Rickard, D. J.; Sullivan, T. A.; Shenker, B. J.; Leboy, P. S.; Kazhdan, I. *Dev. Biol.* 1994, 161, 218-28.
9. Schmidmaier, G.; Schwabe, P.; Strobel, C.; Wildemann, B. *Injury-Int. J. Care Inj.* 2008, 39 Suppl 2, S37-43.
10. Carragee, E. J.; Hurwitz, E. L.; Weiner, B. K. *Spine. J.* 2011, 11, 471-91.
11. Haidar, Z. S.; Hamdy, R. C.; Tabrizian, M. *Biotechnol Lett* 2009, 31, 1825-35.
12. Phillippi, J. A.; Miller, E.; Weiss, L.; Huard, J.; Waggoner, A.; Campbell, P. *Stem Cells* 2008, 26, 127-34.
13. Patterson, J.; Siew, R.; Herring, S. W.; Lin, A. S.; Guldberg, R.; Stayton, P. S. *Biomaterials* 2010, 31, 6772-81.
14. Dierich, A.; Le Guen, E.; Messaddeq, N.; Stoltz, S.; Netter, P.; Schaaf, P.; Voegel, J.-C.; Benkirane-Jessel, N. *Adv. Mater.* 2007, 19, 693-697.
15. Crouzier, T.; Ren, K.; Nicolas, C.; Roy, C.; Picart, C. *Small* 2009, 5, 598-608.
16. Wang, W. *Int. J. Pharm.* 2005, 289, 1-30.
17. Oliveira, A. F.; Gemming, S.; Seifert, G. *The Journal of Physical Chemistry B* 2011, 115, 1122-1130.
18. Schwartz, D.; Sofia, S.; Friess, W. *Eur. J. Pharm. Biopharm.* 2006, 63, 241-8.
19. Schwartz, D.; Sofia, S.; Friess, W. *European Journal of Pharmaceutics and Biopharmaceutics* 2006, 63, 241-248.
20. Hillger, F.; Herr, G.; Rudolph, R.; Schwarz, E. *J Biol Chem* 2005, 280, 14974-80.
21. Crouzier, T.; Fourel, L.; Boudou, T.; Albiges-Rizo, C.; Picart, C. *Adv. Mater.* 2011, 23, H111-8.
22. Izumrudov, V. A.; Kharlampieva, E.; Sukhishvili, S. A. *Biomacromolecules* 2005, 6, 1782-8.
23. Bi, X.; Taneva, S.; Keough, K. M.; Mendelsohn, R.; Flach, C. R. *Biochemistry* 2001, 40, 13659-69.
24. Zhang, X.; Ge, N.; Keiderling, T. A. *Biochemistry* 2007, 46, 5252-60; Pal, P.; Kamilya, T.; Mahato, M.; Talapatra, G. B. *Colloids Surf B Biointerfaces* 2009, 73, 122-31.
25. Dong, A.; Huang, P.; Caughey, W. S. *Biochemistry* 1990, 29, 3303-8; Schwinte, P.; Ball, V.; Szalontai, B.; Haikel, Y.; Voegel, J. C.; Schaaf, P. *Biomacromolecules* 2002, 3, 1135-43.
26. Boulmedais, F.; Schwinté, P.; Gergely, C.; Voegel, J. C.; Schaaf, P. *Langmuir* 2002, 18, 4523-4525.
27. Schwinte, P.; Voegel, J. C.; Picart, C.; Haikel, Y.; Schaaf, P.; Szalontai, B. *J. Phys. Chem. B.* 2001, 105, 11906-11916.
28. Jiang, Y.; Li, C.; Nguyen, X.; Muzammil, S.; Towers, E.; Gabrielson, J.; Narhi, L. *J. Pharm. Sci.* 2011, 100, 4631-41.
29. Hasegawa, T.; Taniguchi, K.; Sato, Y. *Vib. Spectrosc.* 2009, 51, 76-79.

30. Barth, A.; Zscherp, C. *Q.Rev. Biophys.* 2002, 35, 369-430.
31. Ulloa, R. M.; Muschietti, J. P.; Veron, M.; Torres, H. N.; Tellez-Inon, M. T. *Mol Biochem Parasitol* 1995, 70, 119-29.
32. Abbatiello, S. E.; Porter, T. J. *Prot. Sci.* 1997, poster presentation, *Protein Society Meeting Boston*, 99.
33. Hauburger, A.; von Einem, S.; Schwaerzer, G. K.; Buttstedt, A.; Zebisch, M.; Schraml, M.; Hortschansky, P.; Knaus, P.; Schwarz, E. *FEBS J* 2009, 276, 6386-98.
34. Schneider, A.; Francius, G.; Obeid, R.; Schwinte, P.; Hemmerle, J.; Frisch, B.; Schaaf, P.; Voegel, J. C.; Senger, B.; Picart, C. *Langmuir* 2006, 22, 1193-200.
35. Shen, L.; Chaudouet, P.; Ji, J.; Picart, C. *Biomacromolecules* 2011, 12, 1322-31.
36. Friess, W.; Uludag, H.; Foskett, S.; Biron, R.; Sargeant, C. *International Journal of Pharmaceutics* 1999, 187, 91-9.
37. Uludag, H.; D'Augusta, D.; Golden, J.; Li, J.; Timony, G.; Riedel, R.; Wozney, J. M. *J. Biomed. Mater. Res.* 2000, 50, 227-38.
38. Scheufler, C.; Sebald, W.; Hulsmeyer, M. *J. Mol. Biol.* 1999, 287, 103-15.
39. Flach, C. R.; Brauner, J. W.; Taylor, J. W.; Baldwin, R. C.; Mendelsohn, R. *Biophys. J.* 1994, 67, 402-10.
40. Crouzier, T.; Picart, C. *Biomacromolecules* 2009, 10, 433-42.
41. Prestrelski, S. J.; Tedeschi, N.; Arakawa, T.; Carpenter, J. F. *Biophys. J.* 1993, 65, 661-71.
42. Katagiri, T.; Yamaguchi, A.; Komaki, M.; Abe, E.; Takahashi, N.; Ikeda, T.; Rosen, V.; Wozney, J. M.; Fujisawa-Sehara, A.; Suda, T. *J. Cell. Biol.* 1994, 127, 1755-66.
43. Haxaire, K.; Marechal, Y.; Milas, M.; Rinaudo, M. *Biopolymers* 2003, 72, 10-20.
44. Wei, W. *International Journal of Pharmaceutics* 2005, 289, 1-30.
45. Muller, S.; Koenig, G.; Charpiot, A.; Debry, C.; Voegel, J.; Lavalle, P.; Vautier, D. *Adv. Funct. Mater.* 2008, 18, 1767-1775 ; Vodouhe, C.; Schmittbuhl, M.; Boulmedais, F.; Bagnard, D.; Vautier, D.; Schaaf, P.; Egles, C.; Voegel, J. C.; Ogier, J. *Biomaterials* 2005, 26, 545-554.

---

## TABLE OF CONTENT



**TOC Legend:** Quantitative analysis of the secondary structure of rhBMP-2 trapped in biopolymeric thin film was obtained by FTIR spectroscopy, revealing the preservation of the major structural elements of BMP2 ( $\beta$ -sheets and  $\alpha$ -helix).

## SUPPORTING INFORMATION

### Structure of cross-linked (PLL/HA) films in hydrated and dry state

The deconvolution of the amide I and II region for hydrated and dry films spectra in H<sub>2</sub>O is shown in Figure SI-1. The secondary structure elements of the (PLL/HA) films were found to be mostly unordered structures, which accounted for ~90-95% of the structural elements. The % of turn was always low (~5 to 10%).

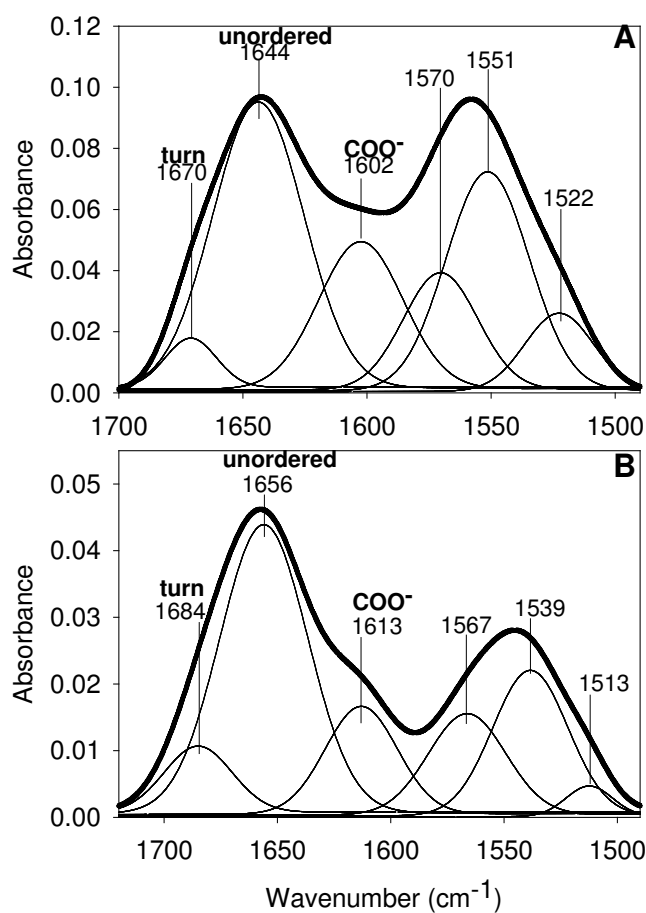


**Figure S11** – Fit of the amide I and II of the FTIR spectra of (PLL/HA)<sub>12</sub> films: hydrated (A) and dry (B) films.



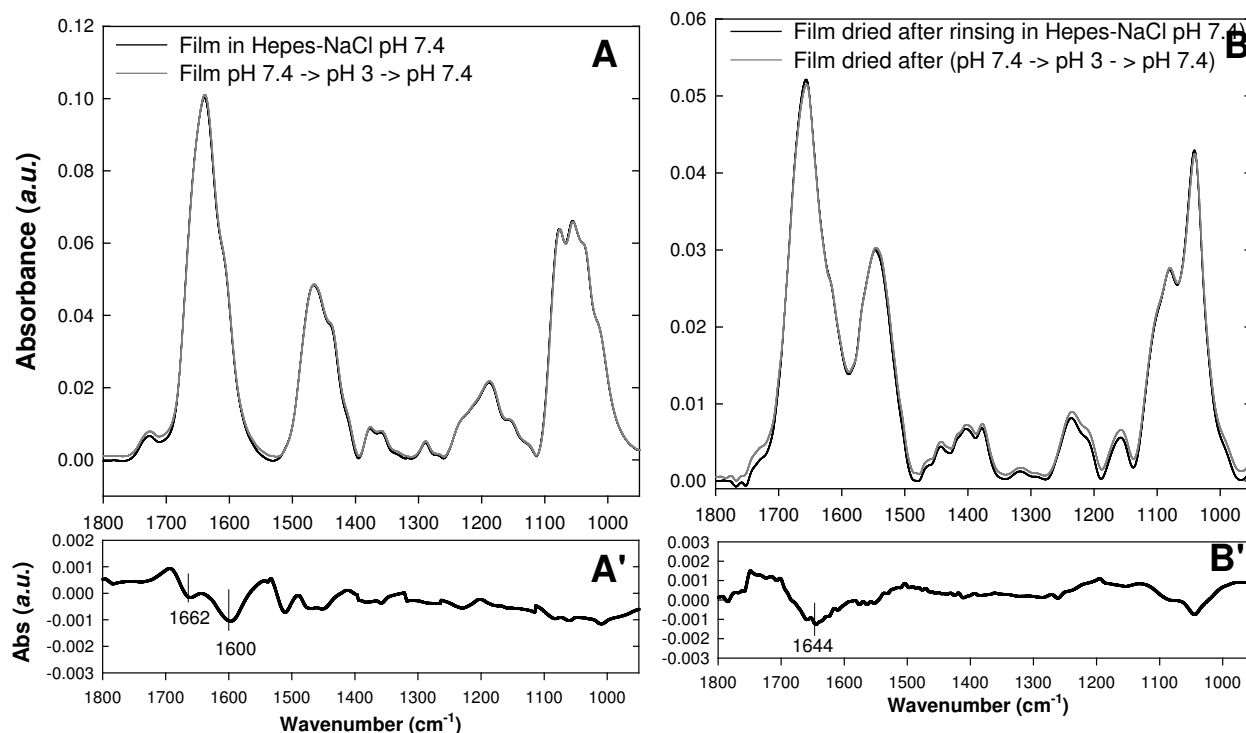


**Figure SI2** – (A) Spectrum of a (PLL/HA) film in the HEPES-NaCl buffer (in  $D_2O$ ) at pH 7.4 (black line). The film was set in contact with the solution of 1 mM HCl (in  $D_2O$ ) and was then rinsed with the HEPES-NaCl buffer (gray line). The difference between the first spectra at pH 7.4 and last spectra at pH 7.4 is shown in A'. (B) the same pH change was applied to a film that was built in the HEPES-NaCl buffer (in  $H_2O$ ) and then subsequently dried (black line). Spectrum taken after the pH change to acidic pH and back to pH 7.4 (gray line). (B') the difference between these spectra is shown.

### Stability of BMP-2 loaded (PLL/HA)<sub>12</sub> films over a 1 month period

Figure SI-3 shows the FTIR spectra of a BMP-2 loaded (PLL/HA)<sub>12</sub> film after drying and after 1 month of storage in dry state at 4°C. First, one can notice that the spectra acquired at the two time periods were very close to each other, which is a qualitative proof of the stability of (PLL/HA) films over time. Only minor changes were observed in the COO<sup>-</sup> region at 1613 cm<sup>-1</sup> and in the amide I region at 1675 cm<sup>-1</sup>. The maximum of the absorbance being ~ 0.05, a variation of ~ 0.003 corresponds to a variability of only ~ 6%. These differences may be due to slight changes in humidity.

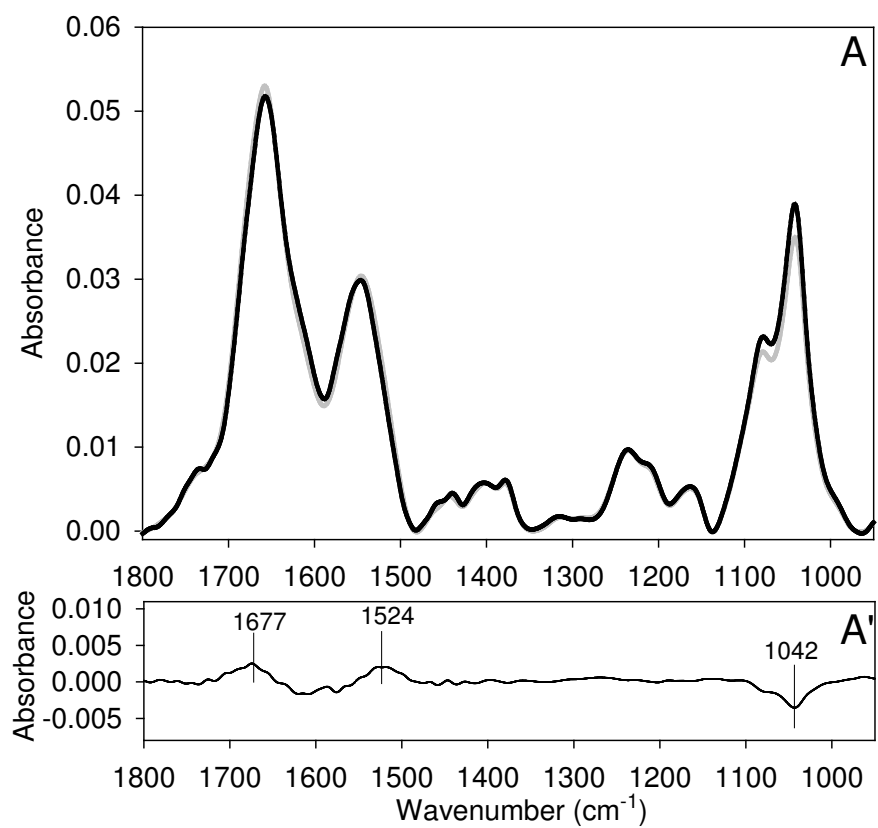


**Figure SI-3** – (A) FTIR spectra of dry BMP-2 loaded (PLL/HA)<sub>12</sub> film (black line) and the same film after 1 month of storage (gray line); (A') difference between these two spectra (A').



**Chapter IV:**  
**The stability of BMP loaded polyelectrolyte  
multilayer coatings on titanium**

## IV.1. Article summary

The aims of this work were first to characterize quantitatively the BMP-2 loading inside (PLL/HA) films and its release as a function of the initial loading concentration and film cross-linking. Secondly, we aimed to show that these films can coat titanium substrates, which are either planar or porous, 2D or 3D implants. Here, the flat titanium substrates were used to evaluate *in vitro* the bioactivity after drying, storage and sterilization of films whereas the porous implants were used to evaluate *in vivo* the osteoinductive properties of the biopolymeric coating.

The use of a fluorescently-labeled BMP-2 allowed us to quantify the initial loading amount inside the films, the release over time and the final retained amount for films cross-linked at different extents. A higher amount of BMP-2 is initially loaded inside EDC10 films as compared to more cross-linked films (EDC30 and 70) but after extensive rinsing, i.e. final step in film preparation, they retained the smaller amounts of BMP-2. Such differences may be related to the film porosity and/or to the strength of the bonds between the BMP-2 and the film. We may hypothesize that the bonds between BMP-2 and the EDC10 films are weaker as compared to EDC 30 and 70 films.

We used FTIR spectroscopy to analyze the effect of drying, long term storage and sterilization on film secondary structure. First, we investigated the structure of the films after drying. We found that HA and PLL had the same characteristic contributions in dry films as compared to hydrated films, with however shifts in the frequencies of the characteristic peaks. Then, we showed that the structure of dried films did not change over time for at least one year. The results were similar for all the films whatever their cross-linking degree. The impact of gamma sterilization on film structure was also studied. After sterilization with 25kGy or 50kGy doses no damage in the film structure was observed.

Along with pre-clinical studies to prove the osteoinduction of BMP-2-loaded films, it is important to show that the bioactivity of BMP-2 is preserved after drying, long term storage and sterilization. No impact on the bioactivity *in vitro*, as assessed by the ALP tests, was observed after drying of films. Storage up to 1 year did not significantly affect the activity of EDC10 or 30 films. However, EDC70 films were the most sensitive to storage in dry state.  $\gamma$ -sterilization induced a decrease in bioactivity by about 20% at 25kGy and 50% at 50kGy. Here again more cross-linked films were found to be more sensitive than less cross-linked films.

The *in vivo* osteoinductive properties were also assessed. BMP-2-loaded PEM films coated on 3D TA6V scaffolds were implanted in an ectopic site in rats. Similar amounts of new bone tissue were formed in the coated implants that had been dried and sterilized in comparison to those that were non-sterilized. This result suggested that, although some BMP-2 bioactivity may have been lost during the irradiation process, the remaining amount of bioactive BMP-2 was still high enough to induce *de novo* bone tissue.

Altogether, our results provided evidence of the remarkable property of PEM film coatings that both sequester BMP-2 and preserve its full *in vivo* osteoinductive potential upon both storage and  $\gamma$ -sterilization. Although not fully understood, the protective effects of PEM films on the growth factor bioactivity may be attributed to both the high water content in (PLL/HA) films (~ 90%) and to their porosity, which may provide a “protein-friendly” environment. The biopolymeric PEM film appears to mimic the natural extracellular matrix that preserves the BMP-2 bioactivity.

## IV.2. Article 2 (published in Biomaterials)

### The stability of BMP loaded polyelectrolyte multilayer coatings on titanium

by R. Guillot<sup>1#</sup>, F. Gilde<sup>1#</sup>, F. Sailhan<sup>2δ</sup>, P. Becquart<sup>2δ</sup>, A. Lapeyrere<sup>1</sup>, D. Logeart-Avramoglou<sup>2\*</sup>, C. Picart<sup>1\*</sup>

#### Affiliations:

<sup>1</sup> CNRS UMR 5628 (LMGP), Grenoble Institute of Technology and CNRS, 3 parvis Louis Néel, F-38016 Grenoble Cedex, France

<sup>2</sup> Laboratory of Bioengineering and Biomechanics for Bone and Articulations; UMR 7052, CNRS, University Paris Diderot, Sorbonne Paris Cité, 10 avenue de Verdun 75010 Paris, France

Corresponding authors: [catherine.picart@grenoble-inp.fr](mailto:catherine.picart@grenoble-inp.fr); [delphine.logeart@univ-paris-diderot.fr](mailto:delphine.logeart@univ-paris-diderot.fr)

<sup>#</sup> equal contribution (co-first author)

<sup>δ</sup> equal contribution (co-second author)

---

#### ABSTRACT

Immobilization of bone morphogenetic proteins (BMP) onto material surfaces is a promising, but still challenging, strategy for achieving dependable and consistent osseointegration of long-term metal implants. In the present study, we have developed an osteoinductive coating of a porous titanium implant using biomimetic polyelectrolyte multilayer (PEM) films loaded with BMP-2. The amount of BMP-2 loaded in these films was tuned -over a large range - depending on the cross-linking extent of the film and of the BMP-2 initial concentration. The air-dried PEM films were stable for at least one year of storage at 4°C. In addition, they

resisted exposure to  $\gamma$ -irradiation at clinically approved doses. The preservation of the growth factor bioactivity upon long-term storage and sterilization were evaluated both *in vitro* (using C2C12 cells) and *in vivo* (in a rat ectopic model) for the perspective of industrial and clinical development. BMP-2 loaded in dried PEM films exhibited shelf-life stability over one year. However, their bioactivity *in vitro* decreased from 50 to 80% after irradiation depending on the  $\gamma$ -irradiation dose. Remarkably, the *in vivo* studies showed that the osteoinductive potential of BMP-2 contained in PEM-coated Ti implants was fully preserved after air-drying of the implants and sterilization at 25 kGy. Film drying or irradiation did not affect the amount of new bone tissue formation. This “off-the-shelf” novel technology of functionalized implants opens promising applications in prosthetic and tissue engineering fields.

## 1. INTRODUCTION

Growth factor delivery is currently a great challenge in clinics [1] for both soft and hard tissue repair [2, 3]. Researchers aim at better controlling the spatial and temporal delivery of growth factors as the natural extracellular matrix (ECM) does, in order to improve clinical efficacy while limiting side effects of these potent molecules. In view of their osteoinductive potential [4], bone morphogenetic proteins (BMPs) have been introduced into orthopedic clinical practice for the treatment of spinal fusion of either delayed or non-unions [5]. Although a wide range of carrier materials have been experimentally tested in combination with BMPs, the current clinical formulation of the rhBMP-2 or rhBMP-7 (noted, hereafter, as BMP-2 and BMP-7, respectively) carrier used in practice is limited to collagen in the form of an adsorbable type I collagen sponge or paste. Currently, the growth factor is either soaked onto the collagen sponge or mixed into it; the wet matrix is then transferred to the implantation site. However, BMPs have only weak affinity for collagen, and the growth factor is completely cleared from the collagen carriers in less than 14 days *in vivo* [6, 7]. Consequently, loss of BMP-2 solution due to mechanical manipulation during implantation as well as high burst release of BMP-2 [6] *in vivo* post-implantation must be considered. For these reasons, and also because BMP-2 signaling is highly regulated *in vivo* [8], very high doses of BMPs (specifically, several mg) are needed for the device to be osteoinductive [9]. At these supraphysiological doses, pathological events (such as osteolysis, heterotopic ossifications, immunological reaction and tumorigenesis) have been reported primarily in spinal application in humans [10 - 12]. A recent review on the safety of BMP-2 in spinal



surgery concluded an incidence of 10 to 50% adverse events depending on the type of clinical application [13]. Thus, there is a strong motivation to develop delivery systems that both reduce the clinically efficient implanted BMP doses and improve safety and cost-effectiveness.

Local administration of BMPs onto implantable osteosynthetic materials, such as metal fixative devices, will broaden the clinical applications of BMPs. Most endoprostheses-used in orthopedic and maxillo-facial surgery—are manufactured from titanium (Ti) and titanium alloys. Ti alloys are widely used as implantable materials because of their excellent mechanical properties compared to other metals, their chemical inertness, corrosion resistance, bone compatibility, and ease of use during surgery [14, 15]. Dependable and consistent osteo-integration of long-term metal implants, however, is still a clinical problem, especially in patients with poor osseous healing capabilities and impaired bone regeneration potential [16]. To address this issue, several studies have focused on the modification of titanium surface in order to increase new bone formation around such implants, *i.e.*, its osteo-integration [17]. The strategies to modify the Ti surface have essentially focused on improving Ti osteo-conductivity, *i.e.*, increasing bone apposition to the implant surface. The most popular approaches have used either physical or chemical modifications such as plasma treatment, sand-blasting, and exposure to chromosulfuric acid to increase the metal surface roughness [18], as well as the coating of those surfaces with biomimetic layers such as hydroxyapatite (HAP) [17]. In addition, research endeavors aim at rendering the metal surface osteoinductive that promotes new bone formation. One method to render a metal implant osteoinductive is by incorporating or grafting BMPs at the material surface. Unfortunately, direct covalent grafting of BMP-2 onto a metal surface allows only very small amounts of BMP-2 to be delivered; whereas direct adsorption of BMP-2 leads to a rapid burst of the protein because of its low affinity with metal surfaces[19] [20]. In order to increase the affinity between BMP-2 and Ti surfaces, biomimetic coatings (for example HAP [21-23] or natural biopolymers [24-26]) have been used. These formulations are promising because of the similarity of HAP and biopolymers with bone tissue constituents. The underlying strategy is that a biomimetic matrix can trap, retain, and deliver BMPs locally in a more efficient manner.

Recently, we have developed an osteoinductive coating in the form of a polyelectrolyte multilayer (PEM) film loaded with BMP-2 [27]. The biomimetic PEM films, which are prepared by assembly of poly(L-lysine) (PLL) and hyaluronan (HA), can be used as carriers of BMP-2. Our initial studies showed that such PEM films, deposited on tricalcium

phosphate/hydroxyapatite granules, retained sufficient amounts of BMP-2 to induce bone formation *in vivo* in a rat ectopic model [28]. A major advantage of such films is that they can coat various material surfaces of either two- or three-dimensional structure [29].

From the industrial and clinical perspectives, shelf-life stability, and sterilization of BMP-2 coated on implants are important issues. To date, these issues have not yet been addressed and/or resolved [30]. Medical devices have to be sterilized after packaging and must preserve their functional properties upon storage for several years [31]. The presence of biological active molecules makes these devices more difficult to handle, store, and sterilize than traditional biomaterials. Such difficulties can hamper the clinical diffusion of these innovative solutions, limiting them to the research level [32]. Developing a device coated with BMP-2 that has shelf-life stability and sterilization resistance is of high clinical interest.

The objective of the present research project was twofold. First, we aimed to assess the osteoinductive properties of the BMP-2 loaded PEM coatings onto porous titanium scaffolds. Second, our aim was to assess its performance *in vitro* and *in vivo* pertinent to long-term storage in a dry state and to sterilization by gamma irradiation.

## **2. MATERIALS AND METHODS**

### **2.1. Materials**

Flat titanium samples (pure grade 2 titanium; 0.4 mm in thickness and 1 cm<sup>2</sup>) used for *in vitro* studies were kindly donated by TIMET Savoie S.A (Ugine, France). Titanium implants used for *in vivo* studies were TA6V ELI custom-made implants (cylinders of 3 mm height and 5 mm diameter), one of the most commonly used titanium alloy for medical applications. The implants had open, communicating pores with a diameter of 500 μm, and a porosity of 22%; the surface roughness was characterized by a  $R_a$  of 1.6 μm as measured by contact profilometry.

### **2.2. Polyelectrolyte multilayer film deposition on titanium and BMP-2 loading**

PEM deposition was performed using polyethyleneimine (PEI, Sigma) at 2 mg/mL, poly(L-lysine) hydrobromide (PLL, Sigma) at 0.5 mg/mL, and hyaluronic acid (HA, 360 kDa, Lifecore, USA) at 1 mg/mL dissolved in a buffered saline solution (0.15 M NaCl, 20 mM Hepes pH 7.4, called hereafter Hepes-NaCl buffer). The (PLL/HA)<sub>24</sub> film (PLL being the polycation, HA the polyanion and 24 the number of layer pairs of the film) buildup using an

automatic dipping machine (Dipping Robot DR3, Kierstein GmbH, Germany) and the subsequent cross-linking were done as previously described [33].

A previously established protocol for BMP-2 loading in cross-linked (PLL/HA)<sub>24</sub> films was followed [27, 28]. Briefly, each PEM coated titanium sample was deposited into a single well of 96-well plate and incubated with the BMP-2 solution (at 20 µg/mL for *in vitro* studies and 100 µg/mL for *in vivo* studies). The amounts BMP-2<sup>CF</sup> used as a tracer (2%) initially loaded into the PEM films [27] and subsequently released after several washes with HEPES-NaCl buffer were determined using a fluorescence spectrometer (TECAN Infinite 1000, Austria).

### **2.3. Film characterization by Fourier Transform Infrared spectroscopy (FTIR)**

The (PLL/HA)<sub>24</sub> films were built on a ~ 1 cm<sup>2</sup> silicon substrate (Siltronix, France) coated with a 40 nm thick TiO<sub>2</sub> layer, rinsed with milli-Q water to remove the salt and dried for 1 h at 37°C [34]. They were then analyzed by FTIR spectroscopy as previously described using a Vertex 70 spectrophotometer (Bruker Optics GmbH, Ettlingen, Germany) [34]. The film spectra in transmission were acquired by summing 256 spectra acquired between 400 and 4000 cm<sup>-1</sup> with a 2 cm<sup>-1</sup> resolution using the liquid nitrogen-cooled MCT detector. For long-term stability measurements, the films were stored in dry state at room temperature. Before each FTIR acquisition, they were incubated at 37°C for 1 h. For γ-irradiation, dried BMP-2 loaded PEM films were sterilized at two different doses (25 and 50 kGy) and then characterized by FTIR.

### **2.4. Film imaging by Scanning Electron Microscopy (SEM) and by fluorescence microscopy**

Films were imaged by scanning electron microscopy (SEM) using a Fei-Quanta 250 SEM-FEG and by a Leica Macrofluor (Z16 Apo) fluorescence system using a X0.8 objective.

### **2.5. AFM imaging**

AFM images of (PLL/HA)<sub>24</sub> films deposited on Ti substrates were obtained in tapping mode by means of a DI 3100 AFM (Veeco) with NanoScope IIIa controller using silicon cantilever (OMCL-AC240TS, Olympus). The PEM-coated titanium samples were washed in water and air-dried before observation. Substrate topographies were imaged with 512 × 512 pixels at a frequency of 1 Hz.

## **2.6. C2C12 cell culture and *in vitro* BMP-2 bioactivity assay (ALP assay)**

Murine C2C12 skeletal myoblasts (< 25 passages, obtained from the American Type Culture Collection, ATCC) were cultured in tissue culture Petri dishes, in a 1:1 Dulbecco's Modified Eagle Medium (DMEM):Ham's F12 medium (Gibco, Invitrogen, France) supplemented with 10% fetal bovine serum (FBS, PAA Laboratories, France) and 100 U/mL penicillin G and 100 µg/mL streptomycin (Gibco, Invitrogen, France) in a 37 °C, 5% CO<sub>2</sub> incubator. This medium will be named hereafter C2C12 growth medium (C2C12 GM).

The bioactivity of BMP-2 on C2C12 cells was determined by assaying the BMP-2 induced alkaline phosphatase (ALP) activity, a marker of osteogenic differentiation following a previously established protocol [27]. First, the film was thoroughly washed with the HEPES-NaCl solution for at least 2 h to discard any weakly bound or unbound BMP-2. Then, 90000 C2C12 cells were seeded on each sample in a 24-well plate. After 3 days of culture, the growth medium was removed and the cells were washed with PBS and lysed by sonication over 5 s in 500 µL of 0.1 % Triton-X100 in PBS. The ALP activity of these samples was then quantified using standard protocol [27] and normalized to the corresponding total protein content, which was determined using a bicinchoninic acid protein assay kit (Interchim, France). For bioactivity assay after film drying, the loaded titanium samples were rehydrated for 30 min in HEPES-NaCl buffer and sterilized under UV irradiation before performing the ALP test.

## **2.7. Ectopic bone formation assay**

The osteoinductive potential of BMP-2 containing TA6V scaffold was assessed *in vivo* in a rat ectopic model. Eight different groups were designed as described in Table 1. For each group, 8 implants were prepared. For experiments on dried films, PEM-coated titanium implants were washed with HEPES-NaCl buffer for 1 min and then quickly washed in ultrapure water before being dried 2 h under a laminar flow hood at room temperature. Seven week old Sprague-Dawley female rats were purchased from Janvier (Légenest-Saint-Isle, France) and handled according to the *European Guidelines for Care and Use of Laboratory Animals* (EEC Directives 86/609/CEE of 24.11.1986). The implantation protocol has been approved by the local ethics committee on animal research (Lariboisière/Villemin, Paris, France). Animals were preoperatively given analgesics, anaesthetized and then prepared as previously described [28]. Each sample was implanted aseptically in the back in space created between the muscles and the aponeurotic layer (six implants were implanted per animal). The soft tissues at the implantation sites were closed with interrupted non-resorbable sutures. Six

weeks post-implantation, the animals were sacrificed via injection of lethal doses of sodium pentobarbital (Sanofi-Aventis, Paris, France). The implants were then retrieved *en-bloc* and fixed in 10% phosphate-buffered formalin before analysis as described below.

**Table 1. Experimental design of TA6V scaffolds used per group for the *in vivo* study. The table indicates the cross-linking degree, the presence of not of BMP-2 in the coating, and whether the PEM films have been dried (D) and/or  $\gamma$ -irradiated (I).**

<b>Group (n = 8)</b>	<b>Cross-linking of PEM coating</b>	<b>Presence of BMP-2</b>	<b>PEM film dried</b>	<b>Irradiated</b>
<b>Bare Ti</b>	-	-	-	-
<b>EDC10</b>	EDC10	-	-	-
<b>Bare Ti + BMP-2</b>	-	+	-	-
<b>EDC10 + BMP-2 - UnD</b>	EDC 10	+	-	-
<b>EDC10 + BMP-2 - D</b>	EDC 10	+	+	-
<b>EDC10 + BMP-2 - D+I</b>	EDC 10	+	+	+
<b>EDC30 + BMP-2 - D</b>	EDC 30	+	+	-
<b>EDC30 + BMP-2 - D+I</b>	EDC 30	+	+	+

## 2.8. Histomorphometric analysis

Retrieved implants were processed for undecalcified histology following previously established protocols [35, 36] and as previously described for Titanium [37]. After embedding in methyl methacrylate, each sample was then cut into 6 or 7 sections (500  $\mu$ m each) using a diamond. These sections were then grounded to a thickness of 100  $\mu$ m and stained using Stevenel blue and van Gieson Picrofuschin for histological analysis [37]. Three unadjacent sections from each specimen were selected for histomorphometry analysis. Histological examination was performed under an optical microscopy (Nikon Eclipse TE2000-U, Nikon France) equipped with a numeric camera (DXM1200F, Nikon). Bone was quantified on whole sections using the NIS-Elements BR 2.30 software (Nikon). Three parameters were quantified in each section: (1) Bone area (%) which is the surface of bone (stained in red) normalized over the “available area” (calculated by subtracting the titanium scaffold surface from the whole surface delineated around each specimen); (2) Bone-scaffold contact (%) which is the available titanium scaffold perimeter in contact to bone normalized

over the titanium scaffold perimeter length and (3) Tissue-scaffold contact (%) which is the available titanium scaffold perimeter in contact to (both bony and soft) tissue normalized over the titanium scaffold perimeter length; for consistency, the percentages of both bone-scaffold contact and tissue-scaffold contact were quantified only inside the pore channels of the titanium scaffolds tested.

### **2.9. Statistical analysis**

Numerical results were reported as average  $\pm$  standard error of the mean (SEM). Data from histological findings are presented as box-and-whisker plots. When comparing data between more than two conditions, the Kruskal-Wallis one-way analysis test was used. The nonparametric Mann-Whitney U test was used to analyze data from two independent conditions. For all analyses, differences were accepted to be statistically significant at  $p < 0.05$ . Statistical analyses were conducted using the Statgraphics centurion version XV.2 (Statpoint, Inc., Herdon, VA, USA).

## **3. RESULTS**

### **3.1. PEM-film deposition on porous titanium substrates**

The principle of biofunctionalization of the titanium substrate is shown in Figure 1A. The biomimetic film deposited was formed via layer-by-layer assembly using PLL as polycation and HA as polyanion. Next, the film was covalently cross-linked using the carbodiimide chemistry to create amide bonds between the carboxylic groups of HA and the ammonium groups of PLL [38]. To modulate the crosslink extent of the films, the carbodiimide concentration was adjusted at 10, 30 and 70 mg/mL; the obtained films were noted in the following, film@EDC $_x$  ( $x = 10, 30$  and  $70$ ). Finally, the film was exposed to a solution of BMP-2. The growth factor was incorporated by passive diffusion into the film [27].

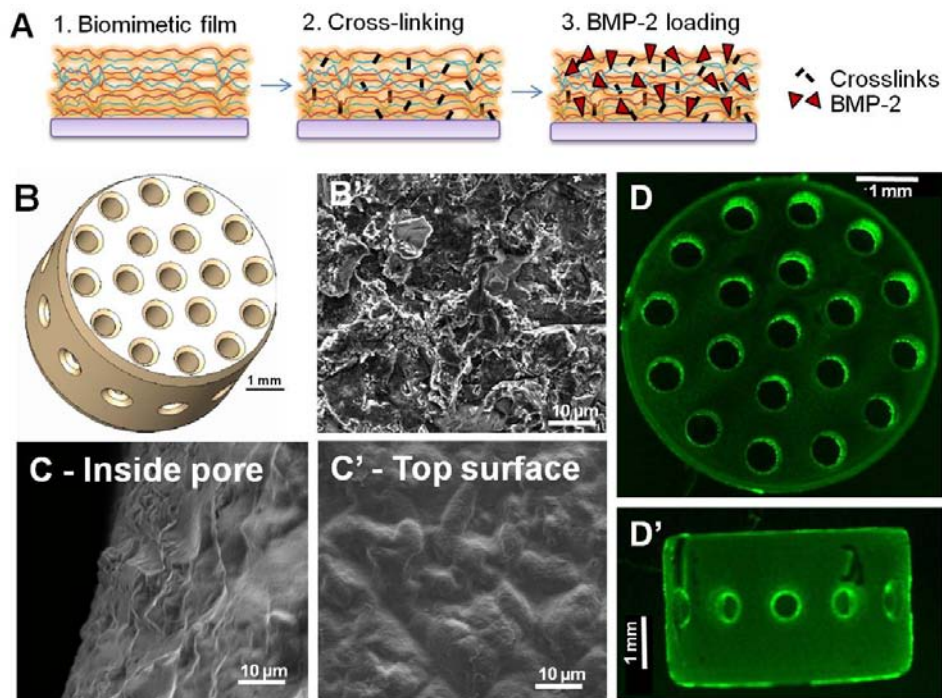


**Figure 1: Polyelectrolyte multilayer film coating of titanium substrates:** (A) Three steps of the bioactive film preparation onto a material substrate: 1) Film deposition by layer-by-layer assembly onto the substrate, 2) cross-linking, and 3) BMP-2 loading. (B) Schematic of porous TA6V scaffold with 500  $\mu\text{m}$  pore size. (B') SEM micrograph of the uncoated TA6V surface imaged at the implant surface. SEM micrographs of (PLL/HA)<sub>24</sub> film-coated surface of the TA6V scaffold either (C) inside a pore channel or (C') at the outer surface. Observation of a PEM-film deposited on the TA6V scaffold by a macroscope: (D) top view and (D') side view.

Planar titanium substrates and custom-made 3D porous substrates made of Ti-6Al-4V (TA6V) (Figure 1B and Figure S1) were coated with the biomimetic film and examined at the macro- and microscales using scanning electron microscopy (SEM) (Figure 1B', C, C') and fluorescence macroscopy, respectively (Figure 1D, D'). SEM revealed the roughness of the bare titanium substrate (Figure 1B') and the smoother surface after PEM coating (Figure 1 C, C'). The coating was visible both inside the pore channels (Figure 1C) as well as on the outer part (surface) of the implant (Figure 1C'). This observation was confirmed by atomic force microscopy (AFM) imaging (Figure S1). Indeed, film AFM measurements of film thickness on planar Ti substrates revealed that film thickness was of  $6.1 \pm 0.5 \mu\text{m}$  in wet state and  $1.1 \pm 0.2 \mu\text{m}$  in dry state. In addition, uniform fluorescence of the film ending with a final layer of PLL<sup>FITC</sup> was observed on the top of the implant and inside the channels by fluorescence macroscopy (Figure 1D, D'). Together, SEM, fluorescence macroscopy and AFM images provided evidence that the films deposited onto the porous titanium implants were homogeneous.

### 3.2. Incorporation of BMP-2 in PEM-coated TA6V substrates

To determine the BMP-2 loading capacity of PEM films cross-linked to different extents (film@EDC10, 30 and 70), we employed fluorescently-labeled BMP-2. Indeed, we showed previously that the bioactivity of carboxyfluorescein modified BMP-2 is similar to that of unlabeled BMP-2 [27]. The retention capacity of the film after loading BMP-2 at two different concentrations and its release kinetics over 7 days were investigated (Figure 2).

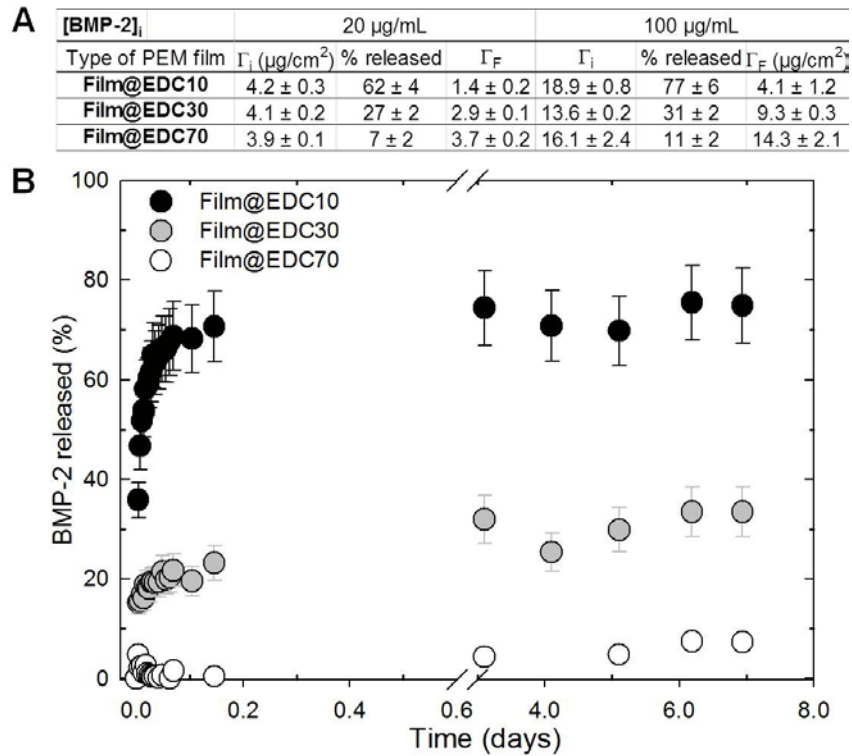


**Figure 2: Quantification of BMP-2 loaded in and released from PEM films.** The amounts of BMP-2 loaded in (PLL/HA) films made of 24 layer pairs and cross-linked@EDC10, EDC30 and EDC70 were compared. (A) Summary table of the initial ( $\Gamma_i$  in ng/cm<sup>2</sup>) and final ( $\Gamma_F$ ) BMP-2 amounts adsorbed on the three PEM films tested using initial BMP-2 concentration in solution at 20 or 100 µg/mL. (B) Release kinetics of BMP-2 from each type of PEM film tested in a Hepes-NaCl buffer as a function of time over 7 days.

The initial adsorbed amounts ( $\Gamma_i$ ) and final amounts ( $\Gamma_F$ ) of BMP-2 remaining in the films after extensive washes are given in Figure 2A. Unbound and/or loosely bound BMP-2 was mostly desorbed during the first 2 hours (corresponding to the initial burst release), after which a plateau value was observed with no significant changes over 7 days (Figure 2B). Overall, the initial amounts of BMP-2 incorporated in the film (before washing) ranged between 4.2 to 19 µg/cm<sup>2</sup>, depending on the cross-linking extent and the BMP-2 initial



concentration in solution. The film@EDC10 incorporated the highest amount of BMP-2. In this case, the percentage of weakly bound BMP-2 represented about 62-77 % of the initial amount compared to 27-31% for the film@EDC30 and 7-11 % for the film@EDC70. As a consequence, at the end of the release kinetics, the amounts of BMP-2 retained within the various films tested ranged from 1.4 to 14.3  $\mu\text{g}/\text{cm}^2$ . The sequestered amount,  $\Gamma_F$ , increased with the cross-linking extent of the film (approximately a 3-fold increase in case of film@EDC10 versus the film@EDC70). Furthermore, increasing the BMP-2 concentration from 20 to 100  $\mu\text{g}/\text{mL}$  led to a 3-4 fold increase in  $\Gamma_F$ . It should be noted that the release kinetics of BMP-2 were not affected by drying the film and subsequent rehydration (Figure S2).

Overall, these results indicated that the amount of BMP-2 incorporated in the PEM films can be tuned over a large range depending on both the extent of film cross-linking and on the initial BMP-2 concentration.

### 3.3. Shelf-life of dry PEM films containing BMP-2

In view of using PEM coatings in a clinical setting *i.e.* implants coated with BMP-2 loaded on PEM films - the option to store them in dry state while preserving the bioactivity of the protein would be advantageous. In order to assess the shelf-life of the BMP-2 coated implants, the long term stability of the PEM films and the *in vitro* bioactivity of the loaded BMP-2 were both investigated upon storage in a dry state for several months. To this end, the coated titanium implants were thoroughly washed with water, air-dried, and stored at 4°C for up to 12 months. The PEM stability was observed via infrared spectroscopy (Figure 3A). The spectra of the dry PEM films cross-linked at different extents revealed the characteristic bands of HA (polysaccharide rings and carboxylic group) and PLL (amide I, II and III bands) (Figure S3). The specific signature of the cross-linking was also visible with a decrease in the carboxylic peak and a concomitant increase of amide I, II and III bands. Interestingly, storage of the dried film@EDC30 at 4°C over 12 months did not cause noticeable changes in the infrared spectrum (Figure 3A). Only a minor change (less than 3%) was noted for the major amide I band, possibly due to the different levels of hydration of the films. Similar spectra were obtained for the film@EDC10 and EDC70 (data not shown). Overall, these data provide evidence that the PEM films were stable when stored under dry conditions for at least 12 months without noticeable chemical changes.

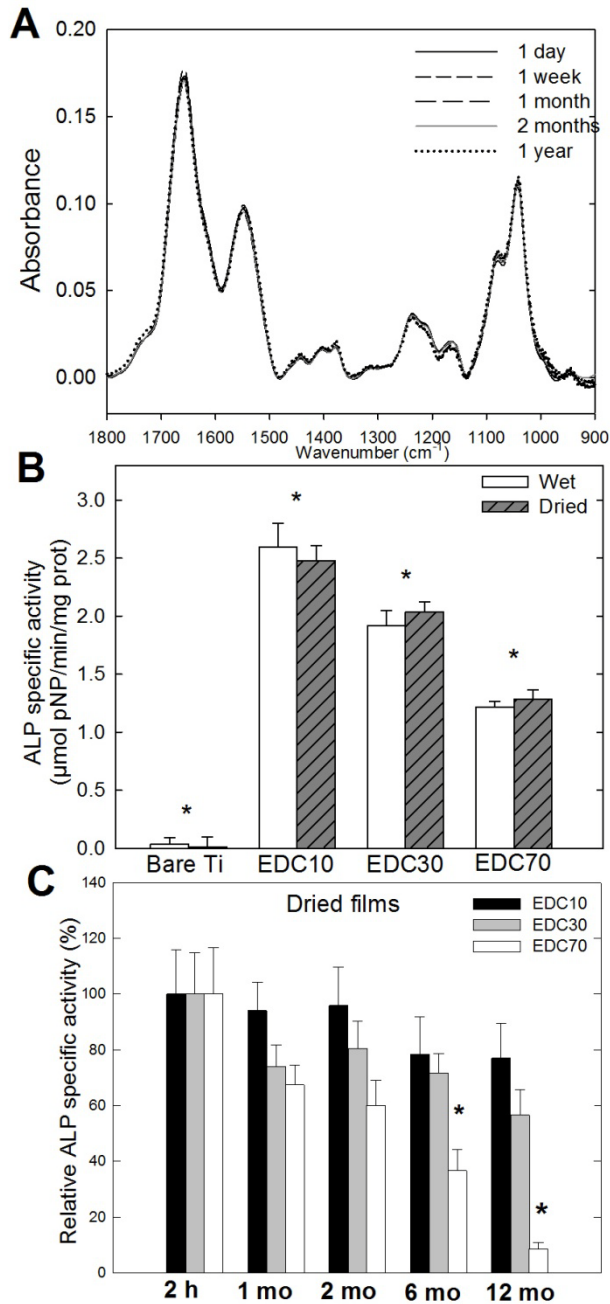


**Figure 3: Shelf-life of BMP-2 containing PEM films in dry state.** (A) Comparison of FTIR spectra of film@EDC30 in dry state obtained at different time points over one year. (B) ALP activity of C2C12 myoblasts cultured for 3 days on either bare or on a PEM film-coated Ti substrates loaded with BMP-2 at 20  $\mu\text{g}/\text{mL}$  (films@EDC10, 30 and 70). ALP activity was assessed for C2C12 cells cultured on films that were either let hydrated (wet) or air-dried for 2 h. (C) Kinetics of ALP activity of BMP-2-loaded PEM films stored in dry state for up to 6 months. Data were normalized over the values obtained with dried films stored for 2 h.

The *in vitro* bioactivity of BMP-2 was assessed using the pluripotent C2C12 myoblast cells cell model [39]. Alkaline phosphatase (ALP) activity of cells seeded on BMP-2-loaded films

cross-linked to the various extents tested in the present study was assayed after 3 days of cell culture [27]. The bioactivity of BMP-2 sequestered into either dry films or wet films (no drying step) was similar (Figure 3B). A systematic decrease of ALP activity was observed when the cross-linking extent increased, with the most cross-linked films (film@EDC70) exhibiting the lowest ALP bioactivity (Figure 3B). Of note, when bare TA6V substrates were dipped into BMP-2 loading solution (similar procedure to that of BMP-2 loading in PEM films), there was no adsorption of the growth factor and thus no ALP activity.

The BMP-2 bioactivity was then determined after storage of the PEM film-coated substrates in dry state from 2 h to 6 months at 4°C (Figure 3C). At those times, all substrates were rehydrated and the BMP-2 bioactivity was assayed. A weak, but not statistically significant, decrease in the bioactivity of BMP-2 loaded on both the film@EDC10 and film@EDC30 was noted after storage for 6 months. In contrast, a significant decrease ( $p < 0.01$ ) of ALP activity was obtained when the C2C12 cells were cultured on the film@EDC70 stored up to 6 months. In this case, only 38% of the initial ALP activity remained. Thus, the preservation of the activity of BMP-2 sequestered into PEM films that are stored in dry state depended on the film cross-linking extent. Of note, bioactivity was also preserved when films were submitted to accelerated aging for 4 days (relative humidity of 75%) at 37°C and 50° (Figure S4). All together, these findings provided evidence that implants coated with BMP-2-containing PEM films can be stored in dry state while preserving the growth factor bioactivity for at least 6 months for film@EDC10 and EDC30.

#### **3.4. Film stability and preservation of BMP-2 bioactivity upon sterilization**

The stability of both the PEM films and the sequestered BMP-2 to  $\gamma$ -irradiation at 25 and 50 kGy, typical doses used in sterilizing metallic implants [40], was assessed using AFM imaging (Figure 4A) and FTIR analysis (Figure 4 B,B'). The topographic analysis showed that the film@EDC30 at the two irradiation doses tested exhibited similar roughness as the control (*i.e.*, non-irradiated) film surface ( $2.5 \pm 1.5$  nm) (Figure 4 A, A'). The infrared spectra revealed that the films were stable after irradiation (Figure 4B). By plotting the difference between the FTIR spectra of the various cross-linked PEM films after irradiation versus that of the films prior irradiation, a small decrease of the  $\text{COO}^-$  peak at  $1611\text{ cm}^{-1}$  and a very small increase in the ester bond at  $1736\text{ cm}^{-1}$  were observed (Figure 4B'). Quantitative analysis (Figure 4C) revealed that the decrease of the  $\text{COO}^-$  peak depended both on the extent of the cross-linking and on the  $\gamma$ -irradiation dose. In fact, this decrease was more pronounced

when the extent of cross-linking was lower and when the irradiation dose was higher. These results suggested that exposure of the PEM film@EDC10 to  $\gamma$ -irradiation induced an additional cross-linking of this film. In contrast, the higher cross-linked films were barely affected.

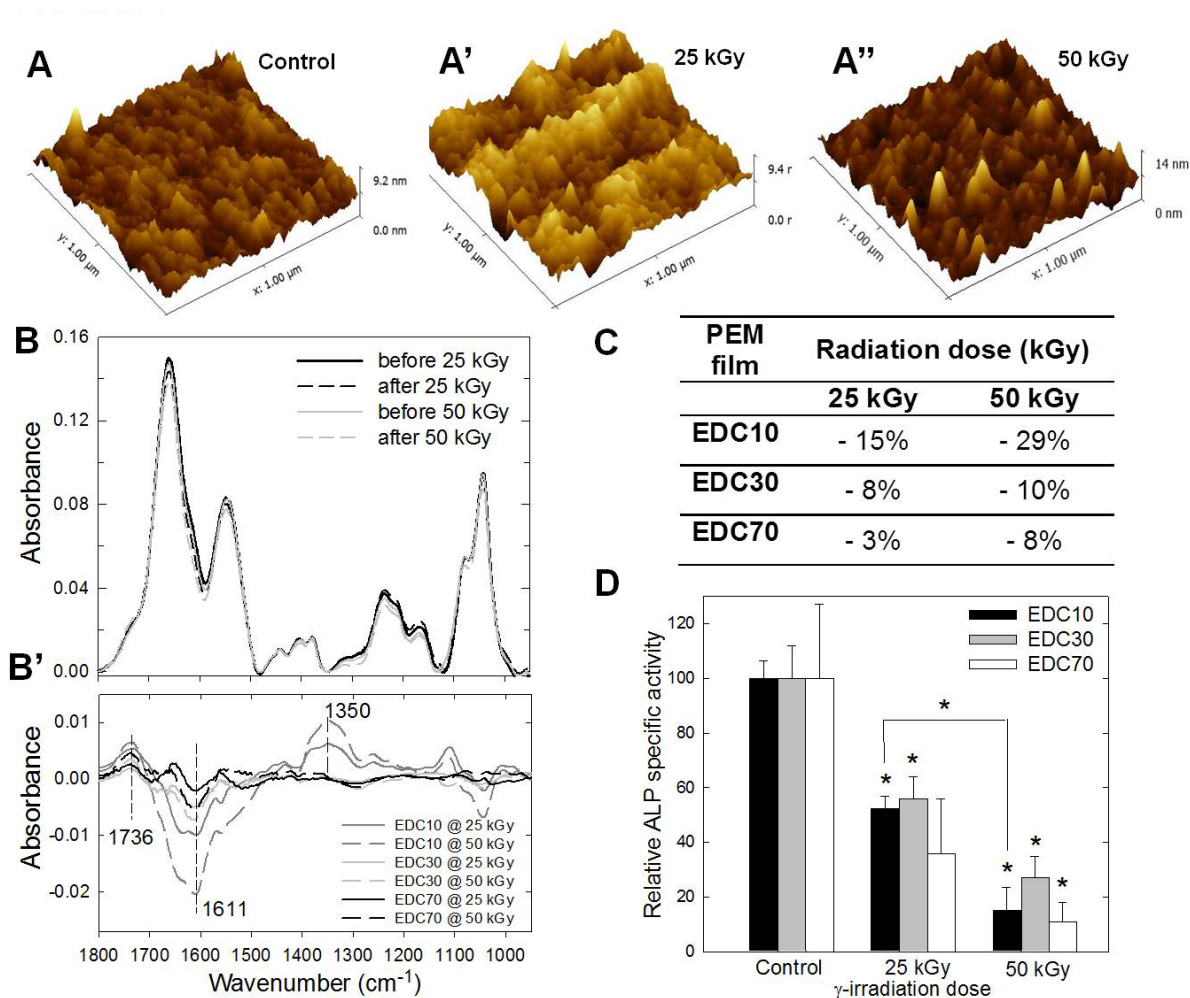


**Figure 4. Effect of  $\gamma$ -irradiation on PEM film stability and BMP-2 bioactivity.** AFM topographic images of (A) PEM film@EDC30 before and after  $\gamma$ -irradiation at either (A') 25 kGy or (A'') 50 kGy doses. (B) FTIR spectra of a PEM film@EDC30 before and after  $\gamma$ -irradiation at 25 and 50 kGy. (B') Difference in the FTIR spectra of all the PEM films (cross-linked to different extents) acquired before and after  $\gamma$ -irradiation at 25 and 50 kGy. (C) Summary of the percent of decrease of the COO<sup>-</sup> peak at 1611 cm<sup>-1</sup> measured for the three different films at two different irradiation doses. (D) ALP activity of C2C12 cells cultured on BMP-2-loaded PEM that had been air-dried and  $\gamma$ -irradiated at either 25 or 50 kGy.

We next tested the *in vitro* bioactivity of the BMP-2 loaded films after  $\gamma$ -irradiation (Figure 4D). A dose-dependent decrease of the ALP activity was noted for cells cultured on all PEM films. The ALP activity signal decreased to ~ 50% and to ~ 20% of its initial value after irradiation with the 25 and 50 kGy doses, respectively. It should be noted that, in these cases, the

ALP activity remained significantly higher than that obtained from cells cultured on bare material surfaces with adsorbed BMP-2 (control) that showed absolutely no ALP signal (Figure 3B).

All together, these data provided evidence that the chemical stability of the PEM films post-exposure to  $\gamma$ -irradiation depended on the extent of cross-linking of the film. The preservation of the bioactivity of BMP-2 sequestered in PEM films depended on the irradiation dose.

### **3.5. Osteoinductive performance of the PEM-coated TA6V scaffolds *in vivo***

In order to determine the osteoinductive potential of the porous TA6V scaffolds coated with BMP-2-containing PEM films, these materials were implanted intramuscularly in the back of rats. For these *in vivo* studies, substrates coated with the PEM film@EDC10 and film@EDC30, which exhibited the highest bioactivity upon storage and  $\gamma$ -ray irradiation *in vitro*, were used.

The eight experimental conditions, including three different controls (bare Ti, bare Ti with adsorbed BMP-2 and Ti with film@EDC10 in the absence of BMP-2) are listed in Table 1. Based on the results obtained in Figure 2, we estimated the total BMP-2 dose delivered *in vivo* to be between  $15.5 \pm 0.4 \mu\text{g}$  to  $21.5 \pm 0.9 \mu\text{g}$ , taking into account the total available surface of the Ti scaffold ( $1.14 \text{ cm}^2$ ).

The explanted specimens were examined using micro-CT. The strong scatter effects from the metallic implant (causing the so-called inherent halation artefacts), however, rendered quantitative measurements of the new bone formation invalid. For this reason, bone formation was only quantified by histology. Representative histological images from sections of both bare and of PEM-coated scaffolds loaded with BMP-2 as well as from one pore channel from each type of scaffold tested are shown in Figure 5A and A', respectively. A first global examination of the explants revealed, as expected, that in the absence of BMP-2, no bone was observed in both the bare and film@EDC10 coated substrates (0 /8 scaffolds). In addition, bare Ti with adsorbed BMP-2 did not lead to noticeable bone growth. Low and inconsistent bone deposits (3/8 scaffolds contained bone) were visible as spots inside the porous scaffold. This bone tissue was preferentially located in the junction of two orthogonally transversal pore channels (in 1 out of 4 channels). It was solely in the cases where BMP-2 was loaded in PEM films that large and consistent bone growth was observed (Figure 5A). The bone formation was found to occur inside all the 2 mm length-pore channels of these samples (Figure 5A').

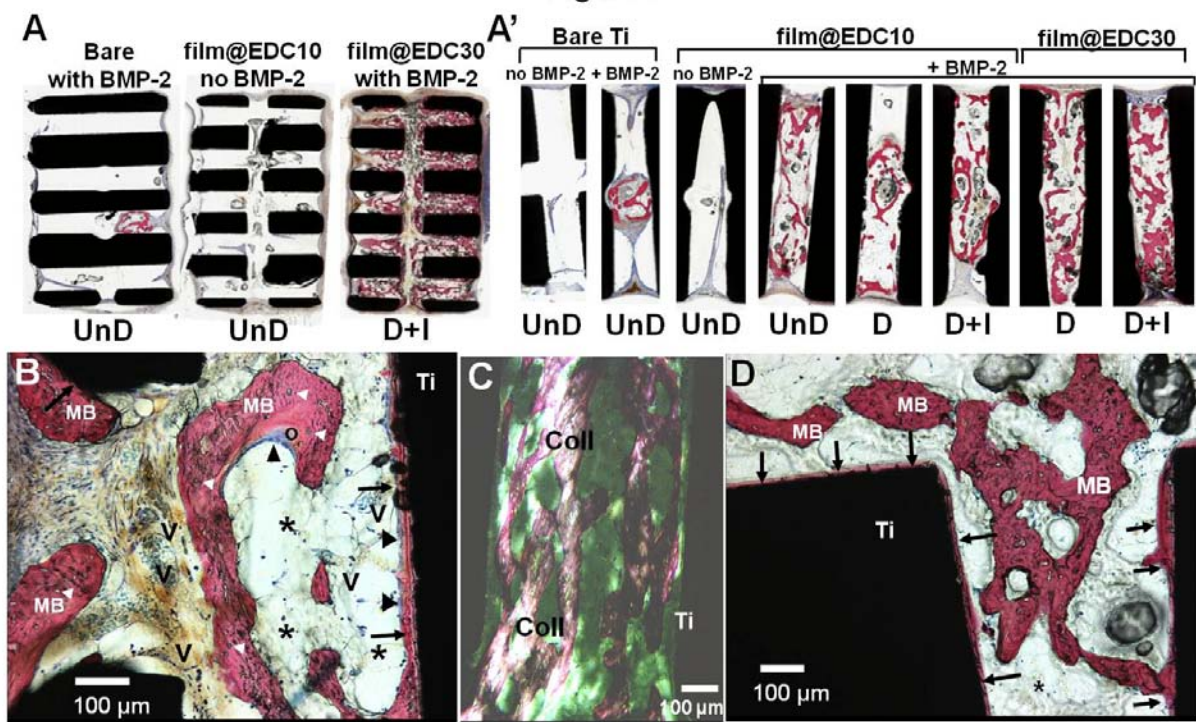


**Figure 5. Ectopic bone formation mediated by BMP-2-loaded PEM films coated on TA6V scaffolds 6 weeks post implantation.** (A) Representative histological cross-sections of the TA6V scaffolds that were either i) adsorbed with BMP-2 (left), ii) coated with film@EDC10 in (no BMP-2) (middle image) or iii) coated with film@EDC30, loaded with BMP-2, and then dried and irradiated (right image). (A') Representative histological cross-sections of one pore channel of each type of scaffold tested (see Table 1 for the detail of the 8 different experimental conditions): TA6V scaffolds were either coated with either PEM film@EDC10 or film@EDC30, then loaded with BMP-2. These scaffolds were either undried (UnD), dried (D), or both dried and  $\gamma$ -irradiated at 25 kGy (D+I) before implantation. Bare scaffolds either without or loaded with BMP-2 as well as scaffolds only coated with film@EDC10 were used as controls. Histological analysis of tissue sections of scaffolds coated with BMP-2-containing dried film@EDC30 (B and C). Woven bone was present inside the channels (B) and lined on the film-coated surface (arrows in B and C). The presence of embedded osteocytes and osteoblasts laying down osteoid tissue is consistent with active new bone formation: (Ti) TA6V scaffold; (MB) mineralized bone; (v) blood vessel; (black arrowhead) osteoblasts, (white arrowhead) osteocytes, (o) osteoid; (\*) bone marrow-like tissue; (Coll) collagen birefringence. Black arrow indicate apposition of bone at the Ti implant surface. (C) Corresponding cross-polarized light micrograph showing representative birefringence of collagen strands. (D) Histological analysis for film@EDC30 that have been dried and irradiated (same symbols as for (B)).

We noted that the quality of the formed bone in BMP-2 loaded scaffolds was similar, whatever the cross-linking extent of the PEM film and the treatment (drying and  $\gamma$ -irradiation). Predominance of woven bone with areas of some lamellar bone, proven by the presence of collagen strands, was observed (Figure 5B and 5C). Both types of bone tissue contained embedded osteocytes and osteoblasts laying down osteoid tissue. Such observations



were consistent with active new bone formation (Figure 5C-D). Notably, the bone tissue was surrounded by vascularized marrow spaces containing adipose tissue (Figure 5B). In addition, there was no inflammation in any section examined. Neither giant cells nor osteoclasts were observed indicating absence of bone tissue remodelling. Interestingly, bone tissue lined along the surfaces of PEM-coated Ti scaffolds regardless of both the type of PEM film tested and their pre-implantation treatment (air-drying and/or  $\gamma$ -irradiation) (arrows in Figure 5B and 5D).

Histomorphometric analysis (Figure 6) confirmed these observations. The bone formation areas were similar in all PEM-coated scaffolds that contained BMP-2. They were of the order of 10 to 30 % as compared to 0.7% for BMP-2-adsorbed bare scaffolds ( $p < 0.001$ ) (Figure 6A). In addition, the bone-implant contact was similar in all BMP-2/PEM-coated scaffolds and varied between 7 and 27 % (Figure 6B). Similarly, the surface of TA6V scaffold in contact with the embedding host tissue did not also statistically varied between the different BMP-2/PEM groups. However, all the BMP-2 PEM films were significantly different from the control groups. Indeed, a very high tissue-implant contact (mean between 55 and 73%) was noted (Figure 6C).

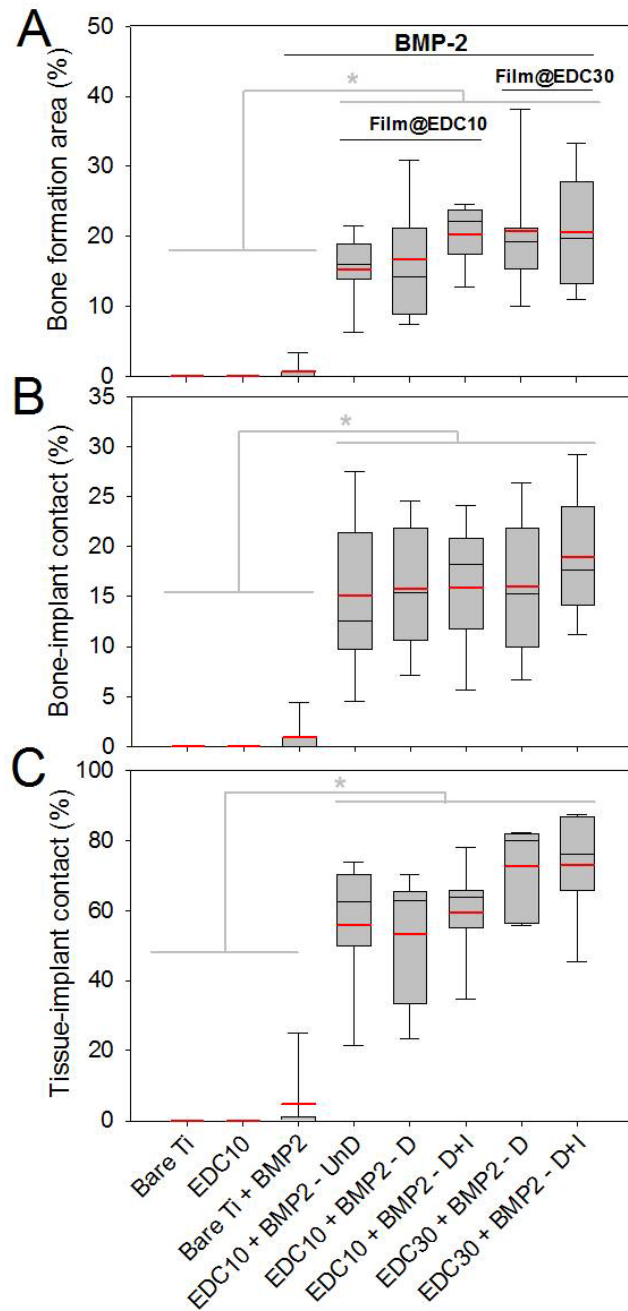


**Figure 6. Osteoinductive performance of the PEM-coated TA6V scaffolds.** Box-and-whisker plots of (A) bone formation area given as a % of the “available area” (by subtracting the titanium scaffold surface from the whole surface) (B) bone-implant contact, given as the % of Ti scaffold perimeter in contact to bone normalized over the Ti scaffold perimeter length and (C) tissue-implant contact in each group of TA6V scaffolds tested determined by histomorphometric analysis. \*:  $p < 0.05$ .

All together, these results provided evidence of the following: (i) the BMP-2 containing-PEM films coated onto TA6V scaffolds promoted new bone formation; (ii) the degree of PEM film cross-linking did not affect the BMP-2 mediated bone induction; and, more importantly that



(iii) drying and  $\gamma$ -sterilization treatments did not affect the osteoinductive potential of BMP-2 loaded within the PEM films as well as the osteo-conductive property of the PEM-coated scaffolds.

#### 4. DISCUSSION

Although BMP-2 is recognized as an important molecule for bone regeneration, its supraphysiological doses currently used in clinical practice has raised serious concerns about cost-effectiveness and safety issues [13, 41]. Thus, there is a strong motivation to engineer new delivery systems or to provide already approved materials with new functionalities. Immobilizing the growth factor onto the surface of implants would reduce protein diffusion and increase residence time at the implantation site. To date, modifying the surfaces of metal materials, such as titanium or titanium alloys, at the nanometer scale to render them osteoinductive remains a challenging approach [16].

In the present study, our results provided evidence that the coating of titanium implants with BMP-2-loaded polyelectrolyte multilayer films conferred the implant surface with osteoinductive properties, promoting local bone formation activity. In addition, bone formation was also found to occur inside the 500  $\mu\text{m}$  wide pore channels. Several strategies have already been attempted by other research groups to either graft or adsorb BMP-2 on the titanium surface using inorganic, organic, or hybrid organic/inorganic coatings [14, 16, 17]. Large amounts of BMP-2 (specifically, 5-8  $\mu\text{g}/\text{cm}^2$ ) can be adsorbed or grafted onto roughened Ti surfaces treated with chromosulfuric acid [42]. Proof of successful subsequent osteo-induction of such treated implants was obtained in a gap-healing model in the trabecular bone of the distal femur condyle in sheep. Inorganic coatings based on HAP are also very popular because of the high affinity of BMP-2 for HAP. In this case, the growth factor was either directly adsorbed onto or incorporated into the crystal latticework and is delivered as the inorganic layer undergoes degradation [21, 23, 43]. Biomimetic coatings based on biopolymers are also currently developed in view of their similarities with natural tissues. For example, collagen coatings of dental screws enhanced the bone-implant contact and peri-implant bone formation in dogs 3 months post-implantation [24].

Addition of BMP-2, however, did not increase peri-implant bone formation in implants [24]. Other studies used BMP-2 immobilized on chitosan- [25] and on heparin-grafted titanium [26]. So far, effective osteoinduction in these cases was only shown *in vitro*. Due to the variation of findings between different studies, there is still a need for an optimal and stable

carrier on the implant surface to provide sufficient retention of BMPs at the repair site. In addition, none of the above mentioned studies investigated the shelf-life duration and sterilization of the coating.

The results of the present study using cross-linked PEM films loaded with BMP-2 showed that various amounts of BMP-2 can be loaded in such films depending on the cross-linking extent and initial BMP-2 concentration (Figure 2). An advantage of the process tested is that film deposition, and then BMP-2 loading, were both performed in mild conditions (only salt solutions, no solvent) using an automated dipping machine. The BMP-2 amounts loaded varied between 4 and 19  $\mu\text{g}/\text{cm}^2$  before rinsing of the films, and between 1.5 to 15  $\mu\text{g}/\text{cm}^2$  after the first release phase. The highly cross-linked PEM film (film@EDC70) trapped and retained more protein. BMP-2 bioactivity *in vitro*, however, was higher on less cross-linked PEM films (film@EDC10 and EDC30). This result may be explained by the different levels of hydration and/or smaller pore size in highly cross-linked films, causing either reduced accessibility to the BMP-2 molecules or partial denaturation of part of BMP-2 molecules.

In addition to the amount of growth factor loaded and sequestered, packaging, and storage of the devices are important issues that may limit a wide application of biologically functionalized materials [32]. Growth factors present low stability under environmental conditions since they are heat sensitive and tend to be rapidly denatured. For these reasons, growth factors often have to be freeze-dried and stored in solid forms to achieve an acceptable shelf-life [44]. Currently, the shelf-life of BMPs is 2 years for BMP-7 (Osigraft®) and 3 years for BMP-2 (Inductos®) (data from EMEA). Nevertheless, their bioactivity after immobilization onto a substrate may be reduced. Information from literature reports regarding the effects of storage conditions and extent on the bioactivity of growth factors contained in coatings of implants is scarce. Immobilized transforming growth factor beta 1 (TGF- $\beta$ 1) on titanium alloys was shown to remain biologically active for at least 3 weeks upon storage at 4°C [45]. Insulin growth factor I and TGF- $\beta$ 1 deposited on poly(D,L)lactide materials remained bioactive when stored dry at -20°C for 5 to 14 months [46].

To date, there are no data available regarding the shelf-life of BMP-2 immobilized onto implant material surfaces. In the present study, we evaluated *in vitro* the bioactivity of retained BMP-2 by quantification of the alkaline phosphatase activity induction on C2C12 cells and showed that BMP-2 contained in PEM-coated Ti implants remained bioactive *in vitro* for at least 6 months once coated implants had been air-dried and stored at 4°C. No significant loss of BMP-2 bioactivity was observed for the films cross-linked@EDC10 and EDC30 upon storage while there was a significant decrease for the most cross-linked

films@EDC70. This result may be explained by smaller pore size in highly cross-linked film and lower residual water content, thus leading to a lower protection of BMP-2 molecules or to conformational changes leading to protein denaturation. Indeed, we recently showed that BMP-2 secondary structure may be slightly changed upon drying of the PEM-loaded film [34]. Importantly, our *in vivo* results from the rat ectopic model provided evidence that BMP-2 loaded on both weakly cross-linked PEM films (film@EDC10 and EDC30) coated onto Ti implants that had been air-dried prior to implantation remained as osteoinductive as the undried implants.

Finally, prior to their clinical use as implants, medical devices have to be sterilized after packaging and must maintain their functional characteristics as well as their sterility after storage [31, 47]. Among the different procedures available to sterilize medical devices, ethylene oxide is not recommended for natural materials. Indeed, sterilization of Ti implants coated with TGF- $\beta$ 1 by ethylene oxide at 42°C for 12 h resulted in complete inactivation of TGF- $\beta$ 1 [45]. In addition, the doses of ethylene oxide required for sterilization purposes affect adversely the BMP-2 osteo-inductivity [48]. Because steam autoclaving and  $\gamma$ -irradiation are both sterilization processes considered to be safe with respect to chemical contamination, they are commonly used for metal implant materials. However, heat autoclaving is not recommended for heat-sensitive compounds, such as polymers and proteins. In contrast,  $\gamma$ -irradiation is the appropriate sterilization method for heat sensitive materials [40] because the temperature does not noticeably increased during or after the process [49]. For instance, conventional 25 kGy  $\gamma$ -sterilization procedure can be applied to ALP enzyme-grafted biomaterials without noticeable loss of ALP activity [32]. Several other literature reports suggested that  $\gamma$ -irradiation is less detrimental for growth factor stability and, therefore, this method has already been applied to BMP-2 using an irradiation dose of 25 kGy [50 - 53]. Indeed, this dose is recommended by the European Medicines Agency [40]. For the sterilization of orthopedic Ti implants, a higher dose at ~50 kGy is usually used. However, no study has attempted to sterilize BMP-coated implants.

In the present study, we assessed the osteoinductive performance properties of the BMP-2 contained in PEM-coated Ti implants *in vitro* and *in vivo* upon sterilization by gamma irradiation. Our data showed that sterilization had a little effect on the structure of PEM film itself, depending on the film cross-linking extent. Film@EDC10 had an infrared signature after  $\gamma$ -irradiation, which was similar to that of a slight additional cross-linking (Figure 4). Such findings are consistent with literature reports of cross-linking of polymers upon  $\gamma$ -irradiation [50]. Furthermore, we showed that  $\gamma$ -irradiation had a dose-dependent effect on the

expression of ALP by C2C12 cells *in vitro*. Regardless of the cross-linking extent, the BMP-2 sequestered in PEM films maintained 50% of its initial bioactivity after  $\gamma$ -irradiation at 25 kGy, while it preserved only 20% of its initial value at 50 kGy. Interestingly, the *in vivo* studies showed that the osteoinductive potential of BMP-2 contained in PEM coated Ti implants was fully preserved after implant sterilization at 25 kGy. Similar amounts of new bone tissue were formed in both non-irradiated and irradiated implants. This result suggested that, although some BMP-2 bioactivity may have been lost during the irradiation process, the remaining amount of bioactive BMP-2 was still high enough to induce *de novo* bone tissue. Altogether, our results provided evidence of the remarkable property of PEM film coatings that both sequester BMP-2 and preserve its full *in vivo* osteoinductive potential upon both storage and  $\gamma$ -sterilization. Although not fully understood, the protective effects of PEM films on the growth factor bioactivity may be attributed to both the high water content in (PLL/HA) films (~90%) and to their porosity, which may provide a “protein-friendly” environment. The biopolymeric PEM film appears to mimic the natural extracellular matrix that preserves the BMP-2 bioactivity.

## 5. CONCLUSION

Our results showed that the (PLL/HA) PEM film coating can both sequester BMP-2 and preserve its full *in vivo* osteoinductive potential upon both storage and  $\gamma$ -sterilization. This “off-the-shelf” technology of functionalized implants by layer-by-layer films loaded with BMP-2 open promising applications in prosthetic and tissue engineering fields. The potential applications of such PEM-coated Ti materials featuring enhanced and/or accelerated osseointegration are numerous in orthopedics, dentistry, and maxillo-facial surgery. In addition, such coatings may be coated on other materials used in bone-related clinical applications, including synthetic polymers. The coating may be translated to use in human since its components, *i.e.* hyaluronan, poly-L-lysine, and BMP-2, are already approved by regulatory agencies for various biomedical applications.

## ACKNOWLEDGMENTS

The authors are grateful to Jean Luc Coll and Veronique Josserand for providing access to the Imaging facilities at IAB Grenoble and to Gerard Puyoulet for technical assistance. We also thank Jorge Almodovar for careful reading of the manuscript. The present study was supported by Gravit (FIBIOS project), by the French Ministry of Research (Agence Nationale

pour la Recherche) through an ANR-EmergenceBIO (ANR-09-EBIO-012-01 to CP and DLA) and by the European Commission (FP7 program) via a European Research Council starting grant (FP7, ERC BIOMIM to CP, GA 259370). C.P. is indebted to the Institut Universitaire de France for financial support.

## REFERENCES

- [1] Lee K, Silva EA, Mooney DJ. Growth factor delivery-based tissue engineering: general approaches and a review of recent developments. *J R Soc Interface*. 2011;8:153–70.
- [2] Hubbell JA. Tissue and cell engineering. *Curr. Opin. Biotechnol*. 2004;15:381–2.
- [3] Martino MM, Tortelli F, Mochizuki M, Traub S, Ben-David D, Kuhn GA, et al. Engineering the growth factor microenvironment with fibronectin domains to promote wound and bone tissue healing. *Sci Transl Med*. 2011;3:100ra89.
- [4] Urist MR. Bone - formation by autoinduction. *Science*. 1965;150:893.
- [5] Schmidmaier G, Schwabe P, Strobel C, Wildemann B. Carrier systems and application of growth factors in orthopaedics. *Injury*. 2008;39(Suppl 2):S37–43.
- [6] Kim HD, Valentini RF. Retention and activity of BMP-2 in hyaluronic acid-based scaffolds in vitro. *J. Biomed. Mater. Res*. 2002;59:573–84.
- [7] Geiger M, Li RH, Friess W. Collagen sponges for bone regeneration with rhBMP-2. *Adv Drug Deliv Rev*. 2003;55:1613–29.
- [8] Bessa PC, Casal M, Reis RL. Bone morphogenetic proteins in tissue engineering: the road from the laboratory to the clinic, part I (basic concepts) *J Tissue Eng Regen Med*. 2008;2:1–13.
- [9] Hollinger JO, Uludag H, Winn SR. Sustained release emphasizing recombinant human bone morphogenetic protein-2. *Adv Drug Deliv Rev*. 1998;31:303–318.
- [10] Burkus JK, Sandhu HS, Gornet MF. Influence of rhBMP-2 on the healing patterns associated with allograft interbody constructs in comparison with autograft. *Spine*. 2006;31:775–81.
- [11] McClellan JW, Mulconrey DS, Forbes RJ, Fullmer N. Vertebral bone resorption after transforaminal lumbar interbody fusion with bone morphogenetic protein (rhBMP-2) *J Spinal Disord Tech*. 2006;19:483–6.
- [12] Axelrad TW, Kakar S, Einhorn TA. New technologies for the enhancement of skeletal repair. *Injury*. 2007;38:S49–S62.
- [13] Carragee EJ, Hurwitz EL, Weiner BK. A critical review of recombinant human bone morphogenetic protein-2 trials in spinal surgery: emerging safety concerns and lessons learned. *Spine J*. 2011;11:471–91.
- [14] Liu XY, Chu PK, Ding CX. Surface modification of titanium, titanium alloys, and related materials for biomedical applications. *Mater. Sci. Eng. R-Rep*. 2004;47:49–121.
- [15] Geetha M, Singh AK, Asokamani R, Gogia AK. Ti based biomaterials, the ultimate choice for orthopaedic implants: A review. *Prog. Mater. Sci*. 2009;54:397–425.
- [16] Palmquist A, Omar OM, Esposito M, Lausmaa J, Thomsen P. Titanium oral implants: surface characteristics, interface biology and clinical outcome. *J R Soc Interface*. 2010;7(Suppl 5):S515–27.
- [17] Le Guehennec L, Soueidan A, Layrolle P, Amouriq Y. Surface treatments of titanium dental implants for rapid osseointegration. *Dent Mater*. 2007;23:844–54.
- [18] Wennerberg A, Albrektsson T. Effects of titanium surface topography on bone integration: a systematic review. *Clin Oral Implants Res*. 2009;20(Suppl 4):172–84.

- [19] Becker J, Kirsch A, Schwarz F, Chatzinikolaidou M, Rothamel D, Lekovic V, et al. Bone apposition to titanium implants biocoated with recombinant human bone morphogenetic protein-2 (rhBMP-2). A pilot study in dogs. *Clin Oral Investig*. 2006;10:217–24.
- [20] Wikesjo UM, Huang YH, Xiropaidis AV, Sorensen RG, Rohrer MD, Prasad HS, et al. Bone formation at recombinant human bone morphogenetic protein-2-coated titanium implants in the posterior maxilla (Type IV bone) in non-human primates. *J Clin Periodontol*. 2008;35:992–1000.
- [21] Liu Y, de Groot K, Hunziker EB. BMP-2 liberated from biomimetic implant coatings induces and sustains direct ossification in an ectopic rat model. *Bone*. 2005;36:745–57.
- [22] Liu Y, Enggist L, Kuffer AF, Buser D, Hunziker EB. The influence of BMP-2 and its mode of delivery on the osteoconductivity of implant surfaces during the early phase of osseointegration. *Biomaterials*. 2007;28:2677–86.
- [23] Hunziker EB, Enggist L, Kuffer A, Buser D, Liu Y. Osseointegration: the slow delivery of BMP-2 enhances osteoinductivity. *Bone*. 2012;51:98–106.
- [24] Schliephake H, Aref A, Scharnweber D, Bierbaum S, Roessler S, Sewing A. Effect of immobilized bone morphogenetic protein 2 coating of titanium implants on peri-implant bone formation. *Clin Oral Implants Res*. 2005;16:563–9.
- [25] Lim TY, Wang W, Shi Z, Poh CK, Neoh KG. Human bone marrow-derived mesenchymal stem cells and osteoblast differentiation on titanium with surface-grafted chitosan and immobilized bone morphogenetic protein-2. *J Mater Sci Mater Med*. 2009;20:1–10.
- [26] Kim SE, Song SH, Yun YP, Choi BJ, Kwon IK, Bae MS, et al. The effect of immobilization of heparin and bone morphogenetic protein-2 (BMP-2) to titanium surfaces on inflammation and osteoblast function. *Biomaterials*. 2011;32:366–73.
- [27] Crouzier T, Ren K, Nicolas C, Roy C, Picart C. Layer-by-Layer films as a biomimetic reservoir for rhBMP-2 delivery: controlled differentiation of myoblasts to osteoblasts. *Small*. 2009;5:598–608.
- [28] Crouzier T, Sailhan F, Becquart P, Guillot R, Logeart-Avramoglou D, Picart C. The performance of BMP-2 loaded TCP/HAP porous ceramics with a polyelectrolyte multilayer film coating. *Biomaterials*. 2011;32:7543–54.
- [29] Boudou T, Crouzier T, Ren K, Blin G, Picart C. Multiple functionalities of polyelectrolyte multilayer films: new biomedical applications. *Adv Mater*. 2010;22:441–67.
- [30] Neoh KG, Hu X, Zheng D, Kang ET. Balancing osteoblast functions and bacterial adhesion on functionalized titanium surfaces. *Biomaterials*. 2012;33:2813–22.
- [31] Kasemo B, Lausmaa J. Biomaterial and implant surfaces: on the role of cleanliness, contamination, and preparation procedures. *J. Biomed. Mater. Res*. 1988;22:145–158.
- [32] Ferraris S, Pan G, Cassinelli C, Mazzucco L, Verne E, Spriano S. Effects of sterilization and storage on the properties of ALP-grafted biomaterials for prosthetic and bone tissue engineering applications. *Biomed Mater*. 2012;7:054102.
- [33] Ren K, Crouzier T, Roy C, Picart C. Polyelectrolyte multilayer films of controlled stiffness modulate myoblast differentiation. *Adv. Funct. Mater*. 2008;18:1378–1389.
- [34] Gilde F, Maniti O, Guillot R, Mano JF, Logeart-Avramoglou D, Sailhan F, et al. Secondary structure of rhBMP-2 in a protective biopolymeric carrier material. *Biomacromolecules*. 2012
- [35] Kihara A, Morimoto K, Suetsugu T. Improved method using a bubble-free adhesion technique for the preparation of semi-serial undecalcified histologic sections containing dental implants. *J Oral Implantol*. 1989;15:87–94.
- [36] Murice-Lambert E, Banford AB, Folger RL. Histological preparation of implanted biomaterials for light microscopic evaluation of the implant-tissue interaction. *Stain Technol*. 1989;64:19–24.

- [37] Guillemain G, Meunier A, Dallant P, Christel P, Pouliquen JC, Sedel L. Comparison of coral resorption and bone apposition with two natural corals of different porosities. *J Biomed Mater Res.* 1989;23:765–79.
- [38] Richert L, Boulmedais F, Lavallo P, Mutterer J, Ferreux E, Decher G, et al. Improvement of stability and cell adhesion properties of polyelectrolyte multilayer films by chemical cross-linking. *Biomacromolecules.* 2004;5:284–294.
- [39] Katagiri T, Yamaguchi A, Komaki M, Abe E, Takahashi N, Ikeda T, et al. Bone morphogenetic protein-2 converts the differentiation pathway of C2C12 myoblasts into the osteoblast lineage. *J. Cell Biol.* 1994;127:1755–66.
- [40] EMEA The use of ionising radiation in the manufacture of medicinal products (3AQ4a) 1991 <http://www.gmpcompliance.info/euguide.htm>.
- [41] Garrison KR, Donell S, Ryder J, Shemilt I, Mugford M, Harvey I, et al. Clinical effectiveness and cost-effectiveness of bone morphogenetic proteins in the non-healing of fractures and spinal fusion: a systematic review. *Health Technol Assess.* 2007;11:1–150. iii–iv.
- [42] Chatzinikolaidou M, Lichtinger TK, Muller RT, Jennissen HP. Peri-implant reactivity and osteoinductive potential of immobilized rhBMP-2 on titanium carriers. *Acta Biomater.* 2010;6:4405–21.
- [43] Liu Y, Li JP, Hunziker EB, de Groot K. Incorporation of growth factors into medical devices via biomimetic coatings. *Philos Trans A Math Phys Eng Sci.* 2006;364:233–48.
- [44] Wang W. Lyophilization and development of solid protein pharmaceuticals. *Int J Pharm.* 2000;203:1–60.
- [45] Fischer U, Hempel U, Becker D, Bierbaum S, Scharnweber D, Worch H, et al. Transforming growth factor beta1 immobilized adsorptively on Ti6Al4V and collagen type I coated Ti6Al4V maintains its biological activity. *Biomaterials.* 2003;24:2631–41.
- [46] Wildemann B, Lubberstedt M, Haas NP, Raschke M, Schmidmaier G. IGF-I and TGF-beta 1 incorporated in a poly(D,L-lactide) implant coating maintain their activity over long-term storage-cell culture studies on primary human osteoblast-like cells. *Biomaterials.* 2004;25:3639–44.
- [47] Ratner BD, Hoffman AS, Schoen FJ, Lemons JE. *Biomaterials science : an introduction to materials in medicine.* Academic Press; 1996.
- [48] Pekkarinen T, Hietalal O, Jamsa T, Jalovaara P. Gamma irradiation and ethylene oxide in the sterilization of native reindeer bone morphogenetic protein extract. *Scand J Surg.* 2005;94:67–70.
- [49] Park JH, Olivares-Navarrete R, Baier RE, Meyer AE, Tannenbaum R, Boyan BD, et al. Effect of cleaning and sterilization on titanium implant surface properties and cellular response. *Acta Biomater.* 2012;8:1966–1975.
- [50] Razem D, Katusin-Razem B. The effects of irradiation on controlled drug delivery/controlled drug release systems. *Radiat. Phys. Chem.* 2008;77:288–344.
- [51] Ripamonti U, Van Den Heever B, Crooks J, Tucker MM, Sampath TK, Rueger DC, et al. Long-term evaluation of bone formation by osteogenic protein 1 in the baboon and relative efficacy of bone-derived bone morphogenetic proteins delivered by irradiated xenogeneic collagenous matrices. *J. Bone Miner. Res.* 2000;15:1798–1809.
- [52] Wientroub S, Reddi AH. Influence of irradiation on the osteoinductive potential of demineralized bone-matrix. *Calcif. Tissue Int.* 1988;42:255–260.
- [53] Pekkarinen T, Jamsa T, Maatta M, Hietala O, Jalovaara P. Reindeer BMP extract in the healing of critical-size bone defects in the radius of the rabbit. *Acta Orthop.* 2006;77:952–959.

## SUPPLEMENTARY MATERIALS

**Figure S1.** SEM and AFM images of bare titanium substrates and of PEM-coated Ti substrates

**Figure S2.** Comparison of loading of BMP-2 in (PLL/HA) films and subsequent release from the films for hydrated films and for films that have been dried prior to rehydration.

**Figure S3.** FTIR spectra of dry PEM films cross-linked at different extents.

**Figure S4.** ALP activity after accelerated aging of PEM films at 37°C and 50°C

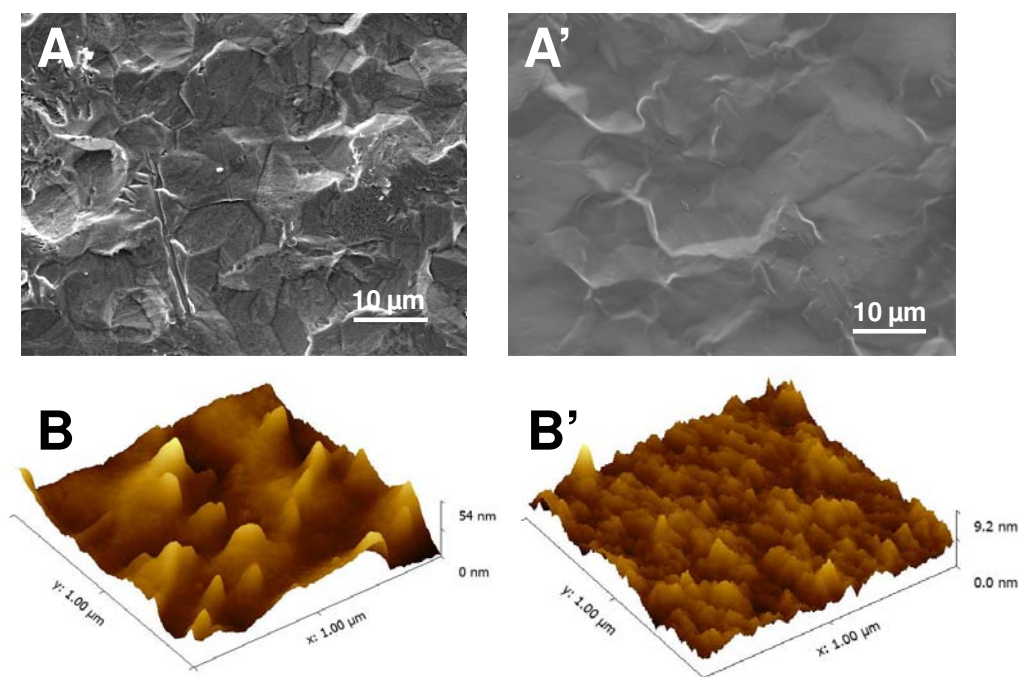


**Figure S1:** SEM images (A, A') and AFM images of bare titanium substrates (A, B) and of PEM-film coated Ti substrates (A', B'). The (PLL/HA) film was made of 24 pairs of layers. The corresponding roughness are 8.1 nm and 1.2 nm for B and B', respectively, indicating that the film coating is smoothing the Ti surface.



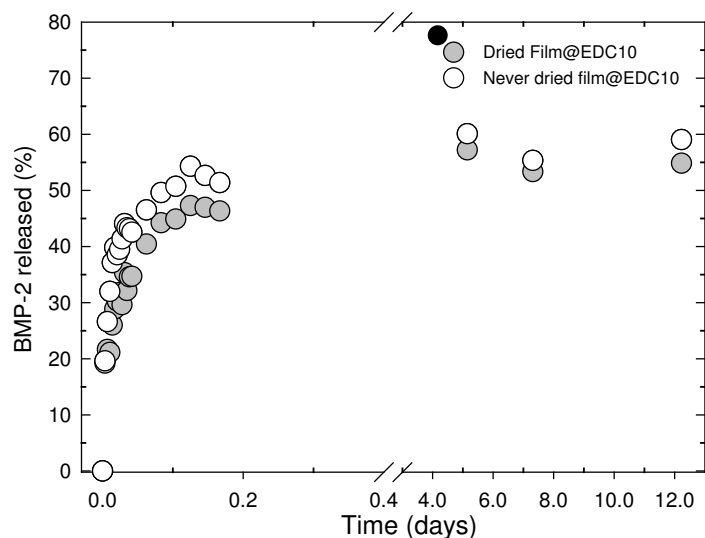


**Figure S2:** Comparison of loading of BMP-2 in  $(PLL/HA)_{24}$  films crosslinked at EDC10 and subsequent release from the films for hydrated films (never dried films) and for films that have been dried prior to rehydration (dried film).

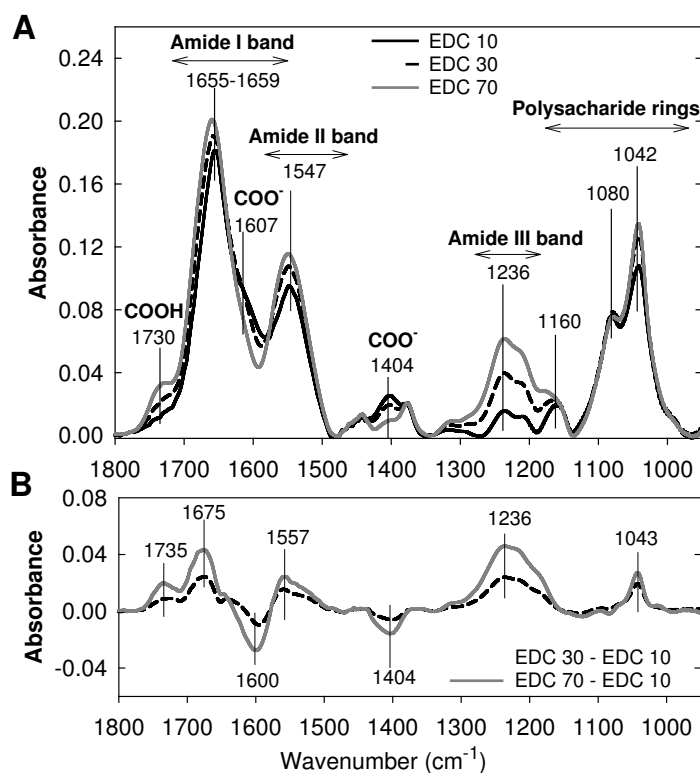


**Figure S3:** FTIR spectra of dry PEM films crosslinked at EDC10, 30 and 70. (A) Comparison between the FTIR spectra and (A') difference between the FTIR spectra of the film@EDC30 and 70 to that obtained for film@EDC10.

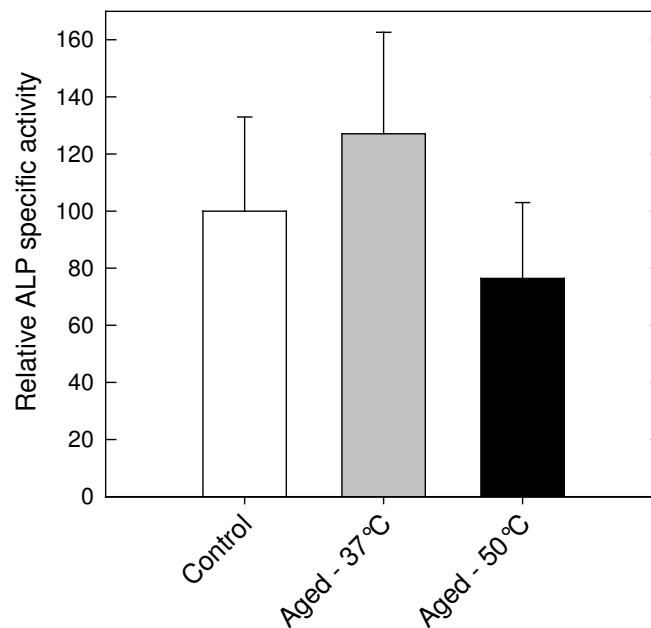


**Figure S4: ALP bioactivity of films after ageing.** ALP activity of C2C12 cells cultured on films that were either let dry for 1 month on the shelf and then submitted to accelerated ageing (relative humidity of 75%) for 4 days at 37°C (gray bar) or 50°C (black bar) as compared to the control samples (no ageing). For accelerated ageing, BMP-2 loaded film coated Ti substrates were placed in a climatic chamber (Ineltec)

#### IV.2.1. Complementary data: structural stability of (PLL/HA) films up to 2.5 years

(PLL/HA) films structural stability in dry state was evaluated by FTIR as previously reported in our recent paper in *Biomaterials* (Guillot et al., 2013). We showed that the film structure do not change after storage for one year in dry state.

We continued to investigate the structure of those films and even after 2.5 years of storage the film structure didn't suffer visible degradation as can be observed in **Figure IV- 1**.

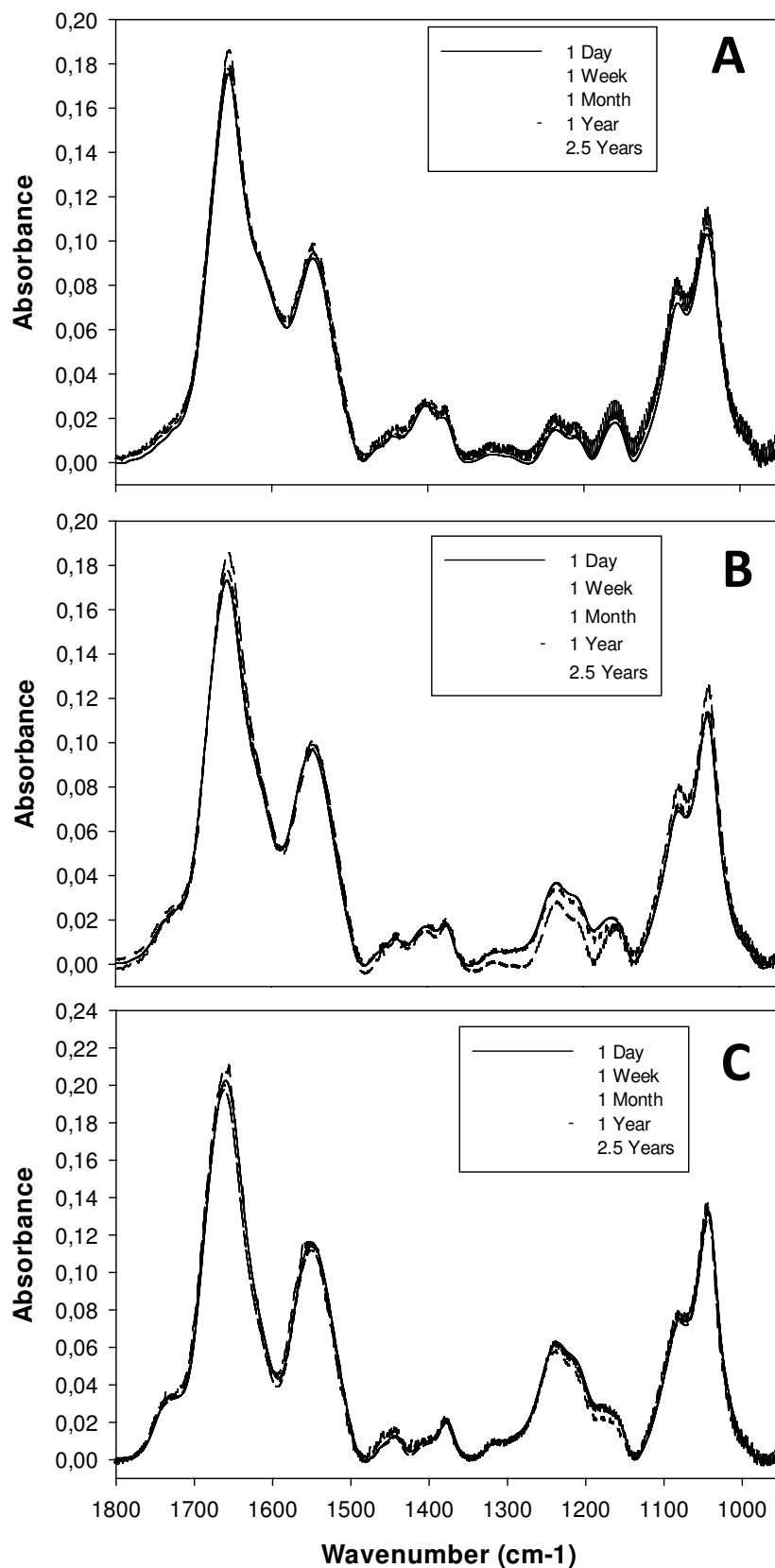


**Figure IV- 1:** FTIR spectra of  $(PLL/HA)_{24}$  films showing the structural stability of films up to 2.5 years (A) EDC 10, (B) EDC 30 and (C) EDC 70.

**Chapter V:**  
**Matrix-bound delivery of BMP-2 to cells**

## V.1. Article summary

A close insight into how BMP-2 interacts with a biomaterial carrier is essential to further understand how the BMP molecules are effectively processed by the cells. In this study, we aimed to understand how BMP-2 presented in a “matrix-bound” manner by a biopolymeric thin film is delivered to BMP-2 responsive cells. Using fluorescently-labeled BMP-2, we showed that BMP-2 partially diffused inside the film and is then trapped in it, a process which depends on the film cross-linking. The vertical diffusion inside films was higher for less cross-linked films than for more cross-linked films, EDC30 and 70. Note that a deeper penetration inside the films does not indicate a greater amount of loaded BMP-2. It was previously shown that the initial adsorbed amount of BMP-2 is higher for EDC10 films but that BMP-2 is washed during the thorough rinsing phase. Thus, the final adsorbed amounts are higher for the EDC30 and 70 films (Chapter IV). The fact that BMP-2 can penetrate more deeply into EDC10 films but then be released quickly may be due to the higher porosity of such films. Next, we showed that matrix-bound BMP-2 is internalized by the cells in the form of vesicles of endocytosis. The quantification of the internalized amount allowed us to follow uptake over time and compare the uptake when cells are seed on top of films cross-linked at different extents. Despite the higher BMP-2 quantity inside EDC30 and 70 films the cells internalized less BMP-2 than on top of EDC10 films, where smaller amounts of BMP-2 were shown to remain inside the film. As previously mentioned such differences may be related to the film porosity and/or to the strength of the bonds between the BMP-2 and the film. After, the use of inhibitors of endocytosis, siRNA-mediated knock-down of endocytic proteins and immunostaining of endocytic markers showed that matrix-bound BMP-2 is internalized through clathrin- and caveolin-dependent endocytosis. The same analysis was performed when BMP-2 is delivered in solution to cells and similar results were obtained. So, the fact that BMP-2 is presented to cells from the film do not change selected the endocytic pathway(s). The importance of BMP receptors in BMP-2 internalization was evidenced using siRNA-mediated knock-down of BMP receptors Ia and II. Internalized amount was reduced to ~ 50% after receptors knock-down. Finally, using the same methods as to discover the BMP-2 internalization pathways we showed that clathrin and caveolin-1 are important in the regulation of both Smad and non Smad-dependent pathway whereas dynamin-2 was only required for the Smad pathway.

## V.2. Article (in preparation)

### Matrix-bound delivery of BMP-2 to cells: internalization

*By Flora Gilde<sup>1,2</sup>, Laure Fourel<sup>3</sup>, Raphael Guillot<sup>1,2</sup>, Isabelle Paintrand<sup>1,2</sup>, Takaharu Okada<sup>4</sup>,  
Thomas Boudou<sup>1,2</sup>, Corinne Albiges-Rizo<sup>3</sup> and Catherine Picart<sup>1,2</sup>*

#### Affiliations:

<sup>1</sup> CNRS UMR 5628 (LMGP), MINATEC, 3 parvis Louis Néel, 38016, Grenoble, France

<sup>2</sup> Université de Grenoble, Grenoble Institute of Technology, 3 parvis Louis Néel, 38016, Grenoble, France

<sup>3</sup> INSERM U823, ERL CNRS3148, Université Joseph Fourier, Institut Albert Bonniot, Site Santé, BP170, 38042 Grenoble cedex 9, France

<sup>4</sup> Biomaterials Unit, International Center for Materials Nanoarchitectonics (WPI-MANA), National Institute for Materials Science (NIMS), 1-1 Namiki, Tsukuba, Ibaraki 305-0044, Japan

Corresponding authors: [catherine.picart@grenoble-inp.fr](mailto:catherine.picart@grenoble-inp.fr)

---

#### ABSTRACT

Biomaterial carriers of bone morphogenetic proteins (BMPs) are currently being developed in order to improve and control the local delivery of these osteoinductive proteins. Further understanding of how BMP molecules interact with the carrier material and how the BMP molecules are effectively processed by the cells is needed. In this study, we aimed to understand how BMP presented in a “matrix-bound” manner by a biopolymeric thin film is delivered to BMP responsive cells. Using fluorescently-labeled BMP-2, we showed that

BMP-2 partially diffused inside the film and is then trapped in it, a process which depends on the film crosslinking. We showed that matrix-bound BMP-2 is internalized by the cells, a stronger internalization being observed for low crosslinked films. The use of inhibitors of endocytosis, siRNA-mediated knock-down of endocytic proteins and immunostaining of endocytic proteins showed that matrix-bound BMP-2 is internalized through clathrin- and caveolin-dependent pathways, which is qualitatively similar to the internalization of soluble BMP-2. Besides, we revealed the importance of the BMP receptors IA and II in the internalization process. Finally, we showed that inhibitors of endocytosis also affected the BMP signaling pathways, clathrin and caveolin-1 being important in the regulation of both Smad and non Smad-dependent pathway whereas dynamin-2 was only required for the Smad pathway.

## **INTRODUCTION**

The bone morphogenetic proteins (BMPs) are members of the transforming growth factor- $\beta$  (TGF- $\beta$ ) family of multifunctional cytokines, which are able to induce ectopic bone (Urist, 1965). BMPs play important roles in a large number of physiological and pathological processes, from morphogenesis in embryo to tissue maintenance in adults (Hogan, 1996; Simic and Vukicevic, 2007). In particular, BMP-2 is a highly potent morphogen that not only stimulates osteoprogenitor cells to differentiate into mature osteoblasts but also induces non-osteogenic cells as muscle precursors and mesenchymal stem cells to differentiate into bone cells (Katagiri et al., 1994; Rickard et al., 1994). In view of its osteoinductive properties, BMP-2 has been introduced into orthopedic clinical practice for the treatment of spinal fusion and non-unions (Schmidmaier et al., 2008), but its use is restricted to an approved formulation using an adsorbable type I collagen sponge onto which a BMP-2 solution is injected. However, the low affinity of BMP-2 for collagen leads a complete clearance from the collagen carrier in less than 14 days *in vivo* (Kim and Valentini, 2002; Geiger et al., 2003) and a very high dose of ~ 12 mg is required for the protein to be osteoinductive. Furthermore, this inappropriate delivery may lead to severe side effects such as osteolysis, heterotopic ossifications and immunological reactions (Burkus et al., 2006; McClellan et al., 2006; Carragee et al., 2011).

Spatially controlled administration of lower doses of BMP-2 from implantable materials could broaden their clinical use. In body BMPs exist in both matrix-bound and soluble forms (Reddi and Reddi, 2009). Mimics of the natural extracellular matrix, including fibrin films (Phillippi et al., 2008), hyaluronan hydrogels (Patterson et al., 2010) and

polypeptide and polysaccharide-based layer-by-layer films (Dierich et al., 2007; Crouzier et al., 2009) appear particularly interesting as carrier for BMP-2 in view of their affinity for BMP-2, which enables an enhanced retention and localized delivery. We recently showed that poly(L-lysine) (PLL) and hyaluronan (HA) (PLL/HA) multilayer films can be used as an efficient carrier of BMP-2 (Crouzier et al., 2009) and are osteoinductive *in vivo* when deposited on ceramic (Crouzier et al., 2011b) or titanium implants (Guillot et al., 2013). Besides, the BMP-2 loaded films can be dried and sterilized. They were found to preserve BMP-2 secondary structure in comparison to its conformation in solution at acidic pH (Gilde et al., 2012). Additionally, these BMP-2 loaded films have been used for studying *in vitro* early cellular events related to the presentation of BMP-2 to the cells by the matrix (Crouzier et al., 2011a). However, how do the cells respond to BMP-2 presented from carrier materials is still poorly known, especially whether BMP-2 is internalized and how signaling pathways are engaged.

On the biological side, understanding BMP-2 signaling is an important topic of research (Hartung et al., 2006b; Bandyopadhyay et al., 2013). Until now, biologists have always studied the response of cells to soluble BMP-2, BMP-2 being added in solution to serum-starved cells that are plated on polystyrene dishes or glass slides. The activation of the BMP-2 signaling cascades involves growth factor binding to heteromeric receptor complexes composed of two types of BMP receptors, named type I and type II (Kawabata et al., 1998; Massague, 1998; Nohe et al., 2002). According to *Knaus and coworkers* (Nohe et al., 2002) the BMP-2 ligand may bind directly to preformed receptor complexes or to signaling complexes composed of BMPR-I and II, which may activate either Smad or Smad-independent pathways (leading to the induction of alkaline phosphatase (ALP)). The mechanism of ligand binding to the receptors, subsequent internalization of the ligand–receptor complex, and initiation of signaling pathways, is a highly complex process that is not still not fully understood (Sieber et al., 2009).

Signal transduction and endocytosis are bi-directionally related (Di Guglielmo et al., 2003; Chen, 2009; Sorkin and von Zastrow, 2009). Several studies used chemical inhibitors and showed that both clathrin-coated pits and caveolin/lipid raft are involved in the endocytosis of BMP receptors (Hartung et al., 2006a) and that inhibition of endocytosis may disturb both Smad and Smad-independent pathways. However, some controversy exists regarding the exact roles of specific membrane proteins, such as caveolin-1, in receptor endocytosis and BMP-2 signaling (Saldanha et al., 2013). To date, little information is available on the possible internalization of the BMP-2 ligand. Recently, Alborzinia *et al.* showed, using



fluorescently labeled BMP-2, that soluble BMP-2 could be internalized by HeLa cells (Alborzinia et al., 2013) and that the clathrin pathway was involved in this process. No relation between BMP-2 endocytosis and BMP-2 signaling was demonstrated.

In this context, our goal was to investigate how matrix-bound BMP-2 is delivered to the cells, whether the underlying matrix plays a role and how the bioactive signal is transduced. To this end, we used fluorescently labeled BMP-2 to study matrix-bound delivery from films cross-linked to different degrees. We compared matrix-bound delivery to the conventional delivery of BMP-2 in solution. In addition, we studied how BMP receptors are involved in this process and the effect of blocking endocytosis in BMP-2 signaling.

## **EXPERIMENTAL SECTION**

### **Polyelectrolyte multilayer (PEM) film buildup and BMP-2 loading**

PEM deposition was performed using poly(L-lysine) hydrobromide (PLL, P2626,  $6.8 \times 10^4$  g/mol, Sigma) at 0.5 mg/mL, and hyaluronic acid (HA, 360 kDa, Lifecore, USA) at 1 mg/mL dissolved in a HEPES-NaCl buffer (0.15 M NaCl, 20 mM HEPES pH 7.4). The (PLL/HA)<sub>24</sub> film (i.e. film made of 24 layer pairs) buildup using an automatic dipping machine (Dipping Robot DR3, Kierstein GmbH, Germany) and the subsequent cross-linking were done as previously described (Crouzier et al., 2009). BMP-2 was loaded at 20 µg/mL in the cross-linked (PLL/HA)<sub>24</sub> films by post-diffusion of the protein in 1 mM HCl (Crouzier et al., 2009). Three concentrations of the 1-Ethyl-3-(3-Dimethylamino-propyl) carbodiimide (EDC) crosslinker, namely EDC10, 30 and 70 were used (corresponding to 10, 30 and 70 mg/mL of EDC). The BMP-2 loaded films were thoroughly washed in the HEPES-NaCl buffer to remove any loosely bound BMP-2 and to present BMP-2 in a matrix-bound manner to the cells. This mode of presentation will be named hereafter bBMP-2 in comparison to the presentation of soluble BMP-2 (sBMP-2). For confocal observation, BMP-2 labeled with carboxyfluorescein (BMP-2<sup>CF</sup>, 21878, Sigma) was used (Crouzier et al., 2009) as well as PLL labeled with Alexa Fluor® 568 (A568, A20003 Life Technologies).

### **Immunogold labeling of BMP-2**

Films were built on Thermanox® slides, cross-linked and loaded with BMP-2 as described above. The sample was fixed with 2.5 % glutaraldehyde in 0.1 M cacodylate (C0250, Sigma) buffer, pH 7.2). Then, a post-fixation with 1% osmium tetroxide (ref 75632, Sigma) and 1.5% potassium hexacyanoferrate (II) trihydrate (P9387, Sigma) was performed. The sample was then dehydrated with ethanol dilution series and embedded in HM20 resin (14345, Electron

Microscopy Sciences), known to be an uncharged resin. The resin was polymerized under indirect UV light at 254 nm for 72 h. Sections were made using an ultramicrotome (LEICA UC6). Cross-sections were placed on ~ 1 cm<sup>2</sup> silicon wafer (Siltronix, France). Immunogold labeling of BMP-2 starts with two different blocking steps: first, the silicon wafer was immersed in a 50 mM Glycine (G8898, Sigma) bath in PBS for 20 min and then blocked using a 2% BSA (900.001, Aurion) in PBS for 1h. Mouse anti-BMP-2 (B9553, Sigma) at 2.5 µg/mL was used as first antibody and goat anti-mouse IgG conjugated to 10 nm gold NPs (G7652, Sigma) diluted 1:20 was used as secondary antibody. The sample was finally rinsed with milli-Q water and air dried for few hours. Backscattered electron (BSE) imaging at 5kV was used to image the film cross-sections by scanning electron microscopy (SEM) using a Fei-Quanta 250 SEM-FEG.

### **Cell culture and reagents**

Murine C2C12 skeletal myoblasts (< 15 passages, obtained from the American Type Culture Collection, ATCC) were cultured in tissue culture Petri dishes, in a 1:1 Dulbecco's Modified Eagle Medium (DMEM):Ham's F12 medium (Gibco, Invitrogen, France) supplemented with 10% fetal bovine serum (FBS, PAA Laboratories, France) and 100 U/mL penicillin G and 100 µg/mL streptomycin (Gibco, Invitrogen, France) in a 37 °C, 5% CO<sub>2</sub> incubator.

For BMP-2 internalization studies, 3x10<sup>4</sup> cells/cm<sup>2</sup> were seeded on top of the films or on Thermanox® slides. After different contact times with bBMP-2 or sBMP-2 (5 min, 30 min, 1, 4, 8, 12, 24, 48 or 72 h), the cells were fixed with 3.7% formaldehyde in PBS for 20 min.

To evaluate the impact of inhibitors of endocytosis on BMP-2 internalization, C2C12 cells were pre-incubated for 45 min with several chemical inhibitors of the endocytic pathways, including 5 – 20 µM of chlorpromazine (CPZ, Sigma), 5 - 200 µM of genistein (GST, Sigma), 25 µg/mL of nystatin (NYS, Sigma), 2 mM of methyl-β-cyclodextrin (MβCD, Sigma), or 5 - 40 µM of dynasore (DYN, Sigma). Pre-treated cells were seeded at 3x10<sup>4</sup> cells/cm<sup>2</sup> on top of the films or on Thermanox® slides and fixed after 8h contacting bBMP-2 or sBMP-2.

### **Immunofluorescence**

Fixed cells were permeabilized for 4 min in TBS (50 mM Tris-HCl, 0.15 M NaCl, pH 7.4) containing 0.2% Triton X-100. After rinsing with TBS, the cell samples were blocked for 1h at room temperature with 2% BSA (900.001, Aurion) in TBS. The samples were incubated for 1h at room temperature with the primary antibodies against BMP-2 (mouse anti-BMP-2, B9553 Sigma, at 2.5 µg/mL), rab7 (rabbit anti-rab7, D95F2 Abcam, dilution 1:50), cav-1

(rabbit anti-cav-1, sc 894, Santa Cruz at 2  $\mu\text{g/mL}$ ), or mouse anti- $\beta$ -tubulin (T4026, Sigma 1:200). A 0.2% gelatin (G7765, Sigma) in TBS was used as incubation buffer. After extensive washing with TBS, the cells were further incubated with goat anti-mouse A647 (A21335, Invitrogen) or goat anti-rabbit A647 (A21244, Invitrogen) secondary antibodies diluted to 1:200 in 0.2% gelatin in TBS for 1h at room temperature. The actin was labeled with phalloidin-TRITC (1:800, Sigma) for 30 min. The cell nuclei were stained with 5  $\mu\text{g/mL}$  of DAPI (Life Technologies) for 10 min.

### **Transfection by siRNA**

C2C12 cells were transfected with siRNA against BMP receptor Ia (BMPR-Ia), BMP receptor II (BMPR-II), clathrin heavy-chain (CHC), caveolin-1 (CAV-1) and dynamin-2 (DYN-2) (ON-TARGET plus SMARTpool, respectively Mouse BMPR-Ia, BMPR-II, Cltc, Cav1 and Dnm2 Thermo Scientific Dharmacon). A scrambled siRNA (all stars negative control siRNA, Qiagen) was taken as control. Cells were seeded at  $3 \times 10^4$  cells/ $\text{cm}^2$  in 6-well plates and cultured in 2 mL of GM for 15h. The transfection protocol was followed as previously described (Gribova et al., 2013). After transfection the cells were detached by trypsin-EDTA, seeded in GM at  $3 \times 10^4$  cells/ $\text{cm}^2$  on the films and allowed to adhere for 4h (in case of siRNA against receptors) or 8h (for siRNA against endocytic proteins).

### **Confocal microscopy observations**

Confocal images were acquired with a Zeiss LSM 700 confocal laser scanning microscope (Zeiss, Le Peck, France) equipped with a 63x oil immersion objective and several laser diodes (405, 488, 555 and 639 nm). Fluorescence recovery after photobleaching (FRAP) experiments were conducted to evaluate the BMP-2<sup>CF</sup> diffusion inside (PLL/HA) films. To this end, a 20  $\mu\text{m}$  circular region of interest (ROI) was bleached using the 488 nm laser diode and the recovery after photobleaching was followed over time. The fluorescence intensity of the ROI was normalized to that of a control region.

### **Quantification of BMP-2 internalized amount**

Images of the isolated cells (taken with a 63x objective) were used to quantify the total BMP-2 vesicle area per cell. The quantification of the internalized BMP-2 by the cells over time and after different chemical treatments was performed using Image J software 1.44 ([imagej.nih.gov/ij/](http://imagej.nih.gov/ij/)). The total vesicle area per cell (in  $\mu\text{m}^2$ ) in one confocal plane was quantified over the 0.02 – 5  $\mu\text{m}^2$  range after image threshold using the “Analyze Particles”

function. At least 50 cells were analyzed from at least two samples for each condition. The experiments were repeated at least three times with at least two samples per condition in each experiment.

### **Smad assay using Luciferase reporter gene**

The impact of inhibitors of endocytosis and siRNA-mediated knocking-down of endocytic proteins on SMAD BMP-2 signaling pathway was determined by using C2C12 stably transfected with an expression construct (BRE-Luc) containing a BMP-responsive element fused to the firefly luciferase reporter gene (Logeart-Avraroglou et al., 2006) (generous gift from D. Logeart-Avraroglou (Univ Paris Diderot)). These cells were treated with inhibitors of endocytosis at increasing concentrations (CPZ 5 - 20  $\mu$ M, GST 5 - 200  $\mu$ M; DYN 5 - 40  $\mu$ M) or transfected with siRNA against endocytic proteins. They were cultured under the same conditions as untransfected C2C12 cells. After the two different treatments, cells were cultured on the BMP-2 loaded films (bBMP-2) for 15 h. Cell lysis and luciferase measurements were carried out according to the manufacturer's instructions (Bright-Glo<sup>TM</sup> luciferase assay system, Promega). Measurements were normalized to the DNA content of each sample as measured by the cyQUANT assay (CyQUANT, Molecular Probes, Invitrogen, France). For bBMP-2, the effect of inhibitors or knockdowns of endocytic proteins on BMP pathway was assessed on film coated glass slides introduced in 24-well plates. For sBMP-2, experiments were done in 96-well plates using  $1.5 \times 10^4$  cells/cm<sup>2</sup> and BMP-2 at 100 ng/mL.

### **Alkaline Phosphatase Activity (ALP) test**

The impact of inhibitors of endocytosis and siRNA-mediated knocking-down of endocytic proteins on non-SMAD BMP-2 signaling pathway was determined by assaying the BMP-2 induced alkaline phosphatase (ALP) activity, a marker of osteogenic differentiation following a previously established protocol (Crouzier et al., 2009). First, the film was thoroughly washed with the HEPES-NaCl solution for at least 2 h to discard any weakly bound or unbound BMP-2. Then, C2C12 cells were pre-treated with different concentrations of CPZ, GST and DYN before contacting BMP-2. Then, after treatment with inhibitors or after transfection by siRNA,  $9 \times 10^4$  C2C12 cells were seeded on each film coated glass slide in a 24-well plate. After 3 days of culture, the growth medium was removed and the cells were washed with PBS and lysed by sonication for 5 s in 500  $\mu$ L of 0.1 % Triton-X100 in PBS. The ALP activity of these samples was then quantified using standard protocol and normalized to the corresponding total protein content, which was determined using a bicinchoninic acid protein

assay kit (Interchim, France). Same experiments were conducted for sBMP-2: for the experiment with the inhibitors, the medium was refreshed every 12 h for 3 days, so a BMP-2 concentration was adapted to 100 ng/mL; for the transfected cells a concentration of 600 ng/mL was added in the media.

### **Statistical analysis**

Numerical results on BMP-2 internalized amount are mainly presented in box-and-whisker plots. If not they were reported as average  $\pm$  standard error of the mean. Data comparison was performed by *t-test* analysis test by comparing each experimental data group to the control one. Statistical analyses were conducted using SigmaPlot software. Statistically significant differences between the groups were identified in the images with \* representing a *p* value < 0.001.

## **RESULTS**

### **BMP-2 diffusion inside (PLL/HA) films**

The vertical diffusion of fluorescently labeled BMP-2 (BMP-2<sup>CF</sup>) inside the (PLL/HA) film labeled with A568 is shown in Figure 1. Films made of 24 layer pairs have typical thicknesses of the order of 5  $\mu$ m, as observed by confocal microscopy. A confocal section of the film and the corresponding fluorescence intensity profiles (Figure 1 A, A') showed the partial diffusion of BMP-2 inside the film. Note that the imaging was performed several hours after extensive rinsing of BMP-2 loaded films so that only loaded BMP-2 is visible. The percentage of overlap between the BMP-2 and the film fluorescence was calculated for films cross-linked to different degrees, i.e. EDC10, 30 and 70 (Figure 1A''). The overlap was  $42 \pm 7\%$  for the EDC10 and decreased to  $\sim 26\%$  for the two other films (EDC30 and EDC70). The BMP-2 adsorbed amounts, which have been calculated as a function of the cross-linking degree (Guillot et al., 2013) are also given. The EDC70 films retained a higher concentration of BMP-2 than the EDC30 and 10, respectively. The partial diffusion of BMP-2 inside the film during the loading phase at pH 3 was also confirmed by immunogold labeling of BMP-2 on film cross-sections (Figure 1B), the gold nanoparticles being essentially visible on the upper part of the film. Then, the potential diffusion of the loaded BMP-2 was quantified by FRAP for EDC10) films (Figure 1C). No recovery of fluorescence was observed after the bleaching of BMP-2<sup>CF</sup> indicating the absence of diffusion of bBMP-2, once trapped in the film. Together, fluorescence and SEM images showed that BMP-2 has penetrated inside the (PLL/HA) film during the loading phase at pH 3, a process that depends on the film cross-

linking degree, and that it is trapped in it after thorough rinsing at physiological pH. BMP-2 is thus presented to the cells in a matrix-bound manner (bBMP-2).

### **Internalization of matrix-bound BMP-2 by cells**

Next, BMP-2<sup>CF</sup> was used to investigate internalization of bBMP-2 by C2C12 cells. Of note, the BMP-2<sup>CF</sup> was already shown to remain bioactive and to behave similarly to unlabeled BMP-2 (Crouzier et al., 2009). bBMP-2 is internalized in the form of endocytic vesicles (Figure 2A). For more clarity, the confocal microscopy images were split, in order to represent the vesicles containing BMP-2 as dark spot on one side (upper row) and the cell cytoskeleton and nucleus on the other side (lower row). At early times, cell spreading on film and bBMP-2 internalization occurred simultaneously. We previously showed that C2C12 cells need typically 4h to adhere and spread on BMP-2 loaded films (Crouzier et al., 2011a). After 4h in contact with BMP-2 loaded films, several BMP-2 vesicles can be observed inside adherent cells (Figure 2B), both at the cell film interface but also above the nucleus (Figure 2C). The immunolabeling of BMP-2<sup>CF</sup> with an anti-BMP-2 antibody confirmed the presence of BMP-2 inside the fluorescent vesicles (Figure 2D). Indeed, a colocalization was observed between the green (BMP-2<sup>CF</sup>) and violet (detection by BMP-2 antibody) channels. Moreover, the specificity of the BMP-2 uptake by C2C12 cells was confirmed by loading BSA-FITC in the films and by following cellular uptake. After 4h in contact with BSA-FITC loaded films, no uptake was observed (Figure SI-1).

### **Kinetics and comparison between different substrates and presentation mode**

We then studied the influence of film cross-linking on bBMP-2 internalization as well as the influence of the presentation mode, i.e. bBMP-2 delivery in comparison to delivery of BMP-2 in solution (sBMP-2). A representative image of a cell after 3 days in contact with BMP-2 is given for all the conditions (Figure 3A). First, we observed a clear decrease in the number of BMP-2 containing vesicles as a function of the film cross-linking. This was confirmed by the quantitative analysis over time of the internalized amount of bBMP-2 per cell (Figure 3A'). Indeed, internalization was significantly higher for EDC10 films, reaching a value of  $\sim 21 \mu\text{m}^2/\text{cell}$  as compared to  $\sim 9 \mu\text{m}^2/\text{cell}$  and  $\sim 2.5 \mu\text{m}^2/\text{cell}$  for EDC30 and 70, respectively, after 3 days. To note, no direct relation between the cell spreading area and the amount of internalized BMP-2 could be evidenced, when pulling all data together (Figure SI-2).

When sBMP-2 was added to the cells cultured on Thermanox® or on EDC10 films, the internalized amounts at day 3 were similar in both conditions (Figure 3A''), reaching  $\sim 11$

$\mu\text{m}^2/\text{cell}$  but the kinetics were different. To note, the maximum internalized amounts for sBMP-2 were lower than those internalized on bBMP-2 films from EDC10 films but of the order of magnitude than those on EDC30 films.

In addition, analysis of the size of BMP-2 vesicles at 4h revealed that, for all the conditions, 80 % of the vesicles were below  $0.5 \mu\text{m}^2$ . This corresponds to a diameter of  $\sim 400 \text{ nm}$  if we consider perfectly round vesicles (Figure SI 3).

All together, these data showed that the internalization kinetics and the maximum amount of bBMP-2 internalized depended on the film cross-linking. In addition, we showed that the internalization kinetics of sBMP-2 was faster, but that the internalized amount did not reach the highest values observed for bBMP-2.

In the following experiments, we focused on the bBMP-2 delivered from EDC10 films, for which the strongest internalization was observed.

### **Role of BMP receptors in BMP-2 internalization**

Initiation of BMP-2 signaling involves growth factor binding to heteromeric receptor complexes composed of two types of transmembrane serine/threonine kinases, named type I and type II receptors (Liu et al., 1995; Nohno et al., 1995). Little information exists on the role of the BMP receptors in the BMP-2 endocytosis process. In C2C12 cells, the presence and functional importance of BMPR-Ia and BMPR-II in signal transduction (Nickel et al., 2009), especially Smad signaling (Nohe et al., 2002) and ALP activation (Heinecke et al., 2009; Ono et al., 2011) has already been demonstrated. Therefore, we investigated whether knock-down of BMPR-Ia and of BMPR-II could impact BMP-2 internalization by C2C12 cells. A representative image of transfected cells cultured on the BMP-2 loaded films is shown in Figure 4A. The transfection with siRNA against BMPR-Ia, against BMPR-II and the double transfection with both siRNA significantly decreased the BMP-2 internalized amount to half (Figure 4B). The efficacy of the siRNA against BMPR-Ia and BMPR-II was confirmed by quantitative PCR (Figure 4C). These results showed that both BMPR-Ia and BMPR-II are important receptors in mediating BMP-2 internalization.

### **Internalization pathways of matrix-bound BMP-2**

In order to determine the endocytic pathway(s) for bBMP-2 in comparison to sBMP-2, we studied the effect of several inhibitors of endocytosis on BMP-2 internalization by C2C12 cells (Figure 5A, A') as well as the effect of specific knock-down of endocytic proteins (Figure 5B, B'). We selected specific concentrations of a series of inhibitors that have been

shown to interfere with soluble BMP-2 endocytosis by C2C12 cells (Rauch et al., 2002; von Einem et al., 2011; Alborzinia et al., 2013). Chlorpromazine (CPZ) is known to disturb clathrin-dependent endocytosis (Wang et al., 1993), Genistein (GST) and Nystatin (NYS) perturb the lipid rafts/caveolin-dependent endocytosis (Rothberg et al., 1992; Aoki et al., 1999). Methyl- $\beta$ -cyclodextrin (M $\beta$ CD) interferes with lipid rafts and has also been shown to inhibit clathrin-dependent endocytosis (Rodal et al., 1999). Finally, we studied the effect of dynasore, (DYN), known to affect both clathrin and lipid rafts/caveolin-dependent endocytosis by blocking the GTPase activity of dynamin and impeding the scission of newly formed vesicles from the membrane (Macia et al., 2006). No effect was observed with CPZ (Figure 5A, A' and Figure SI 4) but a strong decrease in internalization (up to 50-60%) was observed when these cells were treated with GST, NYS or M $\beta$ CD. DYN, which affects both routes of internalization, had the highest effect and blocked  $\sim$  70% of the BMP-2 internalization. To note, the results obtained for bBMP-2 and sBMP-2 were qualitatively similar, but the inhibition was stronger for bBMP-2 as compared to sBMP-2, except for DYN. In order to further study the specific roles of clathrin, caveolin and dynamin in BMP-2 endocytosis, we quantified the effect of siRNA against clathrin heavy-chain (CHC), caveolin-1 (Cav-1) and dynamin-2 (Dyn-2) on BMP-2 endocytosis (Figure 5B, B'). CHC, Cav-1 and Dyn-2 were selected since they were shown to interfere with the endocytosis of BMP receptors endocytosis, which itself impacts BMP signaling (Nohe et al., 2005; Hartung et al., 2006a; Bragdon et al., 2012). The efficacy of the siRNA against CHC, Cav-1 and Dyn-2 was confirmed by Western Blot. A decrease of  $\sim$  70% in the internalized amount was observed for siCHC, siCav-1 and siDyn-2 cells. The effects of the siRNA on BMP-2 endocytosis were systematically stronger than that of the inhibitors and were more pronounced for bBMP-2 in comparison to sBMP-2. Furthermore, colocalization studies with caveolin-1, a marker for caveolae internalization (Di Guglielmo et al., 2003; Kelley et al., 2009; Du et al., 2011), and rab7, a later marker for clathrin-dependent internalization (Bucci et al., 2000; Kelley et al., 2009) revealed a good colocalization with BMP-2 vesicles (Figure 5C). All together, these results indicated that both clathrin- and caveolin-dependent endocytosis are involved in BMP-2 uptake and that the internalization pathways for bBMP-2 was very similar to those of sBMP-2.

### **BMP signaling pathways after inhibition of endocytosis**

Endocytosis and signal transduction are intertwined processes (Chen, 2009; Sorkin and von Zastrow, 2009). The endocytosis of many signaling receptors is stimulated by the presence of



the ligand. In the case of BMP-2, the importance of BMP receptors on the BMP-2 signaling pathways has been described (Hartung et al., 2006a; Marom et al., 2011; Saldanha et al., 2013). However, to date, little is known on the relation between the internalization of the BMP-2 ligand and BMP signaling.

We thus studied the effect of the endocytosis inhibitors CPZ, GST and DYN (Figure 6A) and of the siRNA-mediated knock-down of specific proteins (Figure 6B) on BMP-2 signaling pathways for sBMP-2. BMP-2 signaling has been reported to be both Smad-dependent and Smad-independent (Nohe et al., 2002). Expression of a BRE-luc in C2C12 cells is an acknowledged model to study Smad pathway whereas ALP expression is used as a hallmark of the Smad-independent pathway (Nohe et al., 2002; Hartung et al., 2006a).

A dose-dependent decrease in the luciferase signal was observed after treatment with CPZ and DYN. In contrary, GST strongly increased the luciferase signal, which may be explained by the fact that GST alone promotes osteogenic differentiation (Pan et al., 2005; Dai et al., 2013). In addition, siRNA knock-down of CHC, Cav-1 and Dyn-2 strongly affected luciferase signal with a decrease of respectively ~ 70 % for siCHC, ~ 100 % for siCav-1, and ~ 80 % for siDyn-2 (Figure 6A'). With respect to the non-Smad signaling pathway, the inhibitors decreased the ALP expression in a dose-dependent manner, with a full inhibition at the highest concentrations (Figure 6B). To note, DYN had the greatest impact on the ALP signal and was already very efficient when added at the lowest concentration of 5  $\mu$ M. siCHC and siCav-1 confirmed that a 80 % decrease of ALP when the proteins were knocked-down (Figure 6B'). In contrary, there was no effect of siDyn-2 on the ALP activity.

All together, these results showed that the presence of clathrin and caveolin at the plasma membrane is crucial both for Smad and non-Smad pathway activation. However, whereas Dyn-2 played an important role in the Smad response, it did not affect the ALP expression.

## **DISCUSSION**

A close insight into how bioactive molecules interact with a biomaterial carrier is essential to further understand how cells sense molecules presented by the matrix. In addition, such information is useful for the development of biomaterials aimed to delivery drugs locally. Here, we explored the process of BMP-2 trapping in a biopolymeric thin film and studied how cells interact and use the BMP-2 presented from the film.

Although BMP-2 vertical penetration was evidenced for all the films, the penetration was never over the full thickness of the film. BMP-2 penetrated deeper in EDC10 films as compared to EDC30 and EDC70 (Figure 1). Note that a deeper penetration inside the films

does not indicate a greater amount of loaded BMP-2. It was previously shown that the initial adsorbed amount of BMP-2 is higher for EDC10 films but that BMP-2 is washed during the thorough rinsing phase (Guillot et al., 2013). Thus, the final adsorbed amounts are higher for the EDC30 and 70 films (Figure 1 and (Guillot et al., 2013)). The fact that BMP-2 can penetrate more deeply into EDC10 films but then be released quickly may be due to the higher porosity of such films. Unfortunately, the resolution of AFM images in liquid did not allow us to confirm this point (data not shown) whereas SEM imaging required drying of the films, thus changing their structure. Note that a higher porosity of low cross-linked films would be associated with weaker interactions with BMP-2. Importantly, after loading at pH 3 in conditions where HA is protonated and BMP-2 at the maximum of its solubility (Abbatiello and Porter, 1997), extensive rinsing at pH 7.4, BMP-2 remained trapped in the film at pH 7.4 without further diffusion. This lack of diffusion may be due to the combined effect of a high local concentration of BMP-2 in the film and of its poor solubility at pH 7.4 (Abbatiello and Porter, 1997) (Figure 1C).

It has already been evidenced by radioactive measurement on BMP-2 (Jortikka et al., 1997) and by Western blots using an anti-BMP2 antibody (von Einem et al., 2011) that cells can internalize sBMP-2. Furthermore, uptake of fluorescently labeled sBMP-2 by HeLa cells was recently demonstrated by *Alborzinia et al* (Alborzinia et al., 2013) using confocal microscopy and FACS. To our knowledge, the internalization of a BMP-2 presented from a carrier material has never been shown before. Here, we showed using BMP-2<sup>CF</sup> and confocal microscopy (Figure 2) that matrix-bound BMP-2 can be uptaken by C2C12 cells and that the amount of BMP-2 containing vesicles was increasing or stable over at least 3 days. Our data for matrix-bound BMP-2 are thus consistent with previous data showing a continuous increase in the internalized amount of BMP-2 over at 3 days (von Einem et al., 2011) and the visualization of endocytic vesicles after 12 hours (Alborzinia et al., 2013). To note, no decrease of the amount of BMP-2 internalized was evidenced over this time period.

The amount of BMP-2 internalized depended on the film crosslinking extent and presentation mode, the higher internalized amount being observed for cells on EDC 10 films (Figure 3). This stronger internalization may be related to weaker interactions of BMP-2 with the EDC10 films, as a higher amount of BMP-2 was washed away during the initial thorough rinsing phase (Figure 1 and Guillot, 2013), prior to the cell culture. Also, as cells are able to sense physically and exert forces on their underlying matrix (Lo et al., 2000), cell traction forces may further contribute to the bBMP-2 uptake. Furthermore, the superior internalization of BMP-2 by the EDC10 in comparison to soluble BMP-2 may be due to the “reservoir effect”

of the film, which provides an almost unlimited source of BMP-2. In comparison, the life time of BMP-2 in solution is known to be ~ 13 h (Zhao et al., 2006).

BMP-2 is known to bind to BMP receptor complexes and to activate BMP-2 signaling cascades (Kawabata et al., 1998; Massague, 1998; Nohe et al., 2002). It is already known that BMP receptors, especially BMPR-Ia and BMPR-II play a key role in BMP-2 induced signaling (Nickel et al., 2009) and that they can be internalized via different endocytic pathways, especially clathrin-coated pits and caveolae (Nohe et al., 2005; Hartung et al., 2006a; Bragdon et al., 2012). Furthermore, biochemical and AFM studies have shown that BMP-2 exhibits a higher affinity for BMPR-Ia (Nickel et al., 2009; Bonor et al., 2012). Here, using siRNA-mediated knock-down of BMPR-Ia and BMPR-II receptors, we showed that both receptors played a role in the internalization process (Figure 4). These results are consistent with the previous data of *Alborzinia et al.*, who observed an increase in the amount of BMP-2 internalized after overexpression of BMPR-Ia (Alborzinia et al., 2013) and with those of *Kelley et al.*, who showed that internalization of BMP-4 decreased for cells expressing a mutant BMPR-II with no cytoplasmic extension downstream of the kinase domain (Lee-Hoeflich et al., 2004; Kelley et al., 2009).

Using complementary experimental approaches with inhibitors of endocytosis and siRNA mediated knock-down of selected endocytic proteins, we showed that bBMP-2, similarly to sBMP-2, is internalized both through clathrin- and caveolin pathways (Figure 5), although with some quantitative differences. Our results are globally in agreement with previous studies using chemical inhibitors such as DYN, CPZ, GST and NYS, where they showed that sBMP-2 was internalized through clathrin- and caveolin-dependent pathways in C2C12 cells (Rauch et al., 2002; Heining et al., 2011; von Einem et al., 2011). We found that DYN exhibited the strongest effect, which was confirmed by the specific effects of the siRNA of CHC, Cav-1 and Dyn-2 (Figure 5B', B'') as well as by the colocalization with rab7 (a later marker of endocytosis by clathrin route) (Figure 5D). However, in contrary to previous studies (von Einem et al., 2011; Alborzinia et al., 2013), we did not observe any effect CPZ. These may be due to the strong and peculiar effect of this drug on the shape of the endocytic vesicles (Figure SI 4) or by an alternative internalization route taken in the presence of this drug.

Whether and how endocytosis of specific components of clathrin-coated pits and caveolae are related to BMP-2 signaling, especially Smad and non-Smad pathways, is a key question. Here, we showed that CHC and Cav-1 strongly impacted Smad as well as non-Smad signaling, the effects obtained by the siRNA approach being stronger than those obtained

using the chemical inhibitors CPZ, GST and DYN. Indeed, CPZ exhibited only little effect on the Smad pathway and GST a peculiar and reverse effect (Figure 6A). Our data are in agreement with the previous data showing that DYN at 40  $\mu$ M inhibited both Smad and ALP signaling (Hartung et al., 2006a; Heining et al., 2011). Interestingly, dynamin-2 influenced the Smad signaling pathway but not the ALP (non-Smad) pathway. All together, our results on BMP-2 endocytosis and Smad/non smad signaling suggest that both CHC and Cav-1 are key in BMP-2 endocytosis, whereas dynamin-2 is important for Smad mediated signaling but is dispensable for ALP expression. To our knowledge, this is the first time that a relationship between BMP-2 endocytosis and BMP-induced signaling is established using complementary approaches (inhibitors and knock-down of selected proteins).

To note, previous studies have rather focused on the role of BMP receptors in BMP-induced signaling. BMP receptors have been shown to be localized in caveolae and CCPs regions of the plasma membrane (Nohe et al., 2005; Bonor et al., 2012; Saldanha et al., 2013), where Smad phosphorylation was found to occur in caveolae (Saldanha et al., 2013). Thus, the stability of caveolae and CCPs regions was shown to be essential for activation of BMP-2 signaling cascades. siRNA against CHC and Cav-1 were shown to disturb the location of BMP receptors and Smad signaling (Bragdon et al., 2012). Thus, it may well be that the knock-down of CHC and Cav-1 also perturbs the location of the receptors and, as a consequence, impedes the endocytosis of BMP receptors, which is required for the endocytosis of BMP-2.

## **CONCLUSIONS**

We showed that the penetration of BMP-2 inside the polyelectrolyte multilayer films depends on the cross-linking degree of the film, and that the trapped BMP-2 did not freely diffuse after immobilization. We showed that matrix-bound BMP-2 can be internalized by C2C12 cells and that the internalized amount is dependent on the film cross-linking. The major pathways of internalization of bBMP-2 were found to be clathrin and caveolin, which is similar to that of sBMP-2. We showed that BMPR-Ia and BMPR-II are important in the process of BMP-2 endocytosis. Finally, we showed that clathrin heavy chain and Cav-1 strongly impacted Smad as well as non-Smad signaling, while dynamin-2 was important for Smad mediated signaling but dispensable for ALP expression.

## **ACKNOWLEDGEMENTS**

The authors thank D. Logeart-Avramoglou for providing the C2C12-A5 transfected cells. We are grateful to O. Destaing and F. Bruckert for the fruitful discussions. We thank Prof Takao Aoyagi for supporting T Okada's stay in the Picart group. This work was supported by the European Commission, FP7 via an ERC Starting grant to CP (BIOMIM, GA 239370), by the FRM (CAR) and by the Ligue Nationale contre le Cancer for Equipe labellisée Ligue 2010 (CAR). The groups of C.P. and C.A.R. belong to the CNRS consortium CellTiss.

## FIGURES

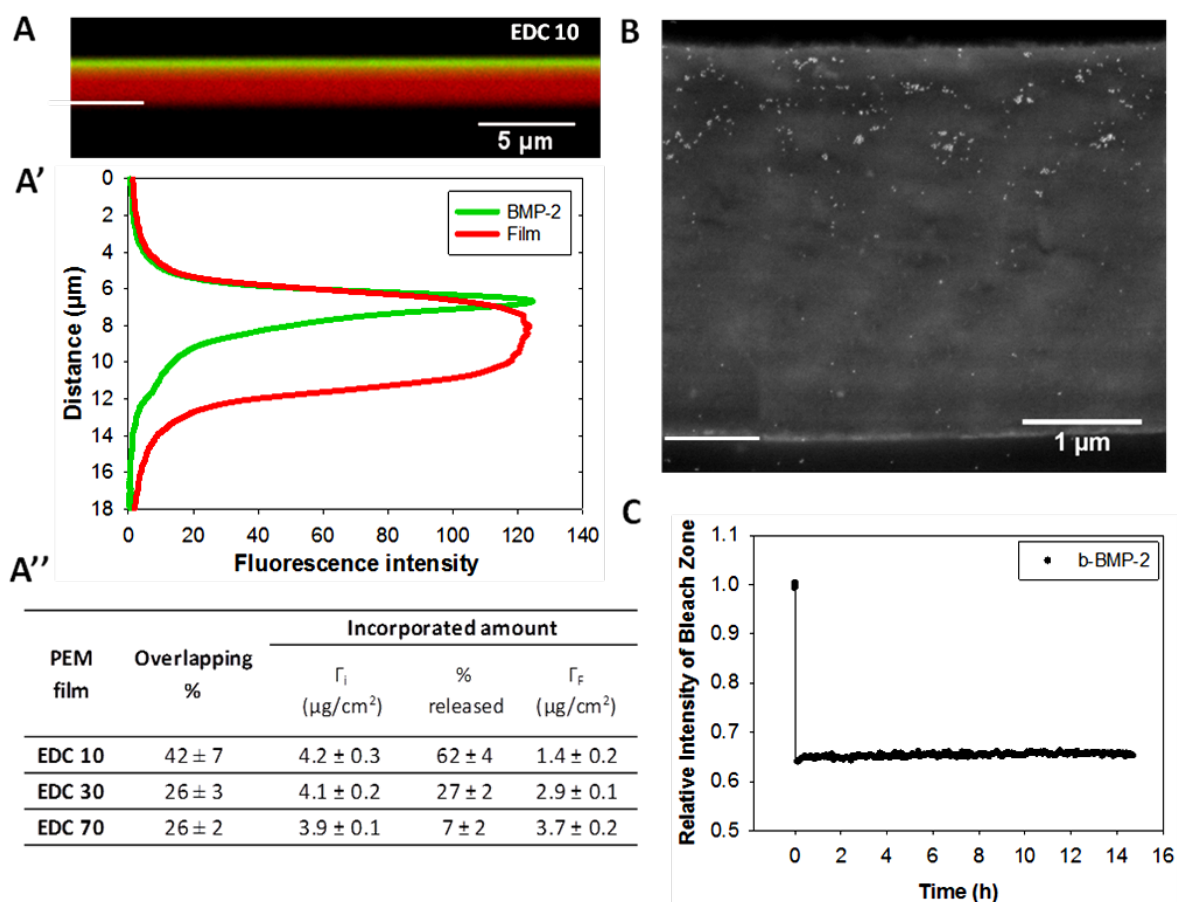


**FIGURE 1.** Spatial distribution of  $\text{BMP-2}^{\text{CF}}$  inside a  $(\text{PLL}/\text{HA})_{24}$  film. (A) Confocal image in XZ section of  $\text{BMP-2}^{\text{CF}}$  loaded inside a PLL-A568 labeled film (EDC10 film), (A') Fluorescence profiles along the film thickness, (A'') Percentage of overlap between the two channels in the XZ section; initial and final BMP-2 adsorbed amounts ( $\Gamma_i$ , and  $\Gamma_f$  in  $\mu\text{g}/\text{cm}^2$ ) incorporated in the different cross-linked films, (B) SEM image of a film cross-section after immunogold labeling of BMP-2 (white dots: 10 nm Au nanoparticles), (C) Fluorescence recovery after photobleaching of  $\text{BMP-2}^{\text{CF}}$  inside a film cross-linked at EDC 10.

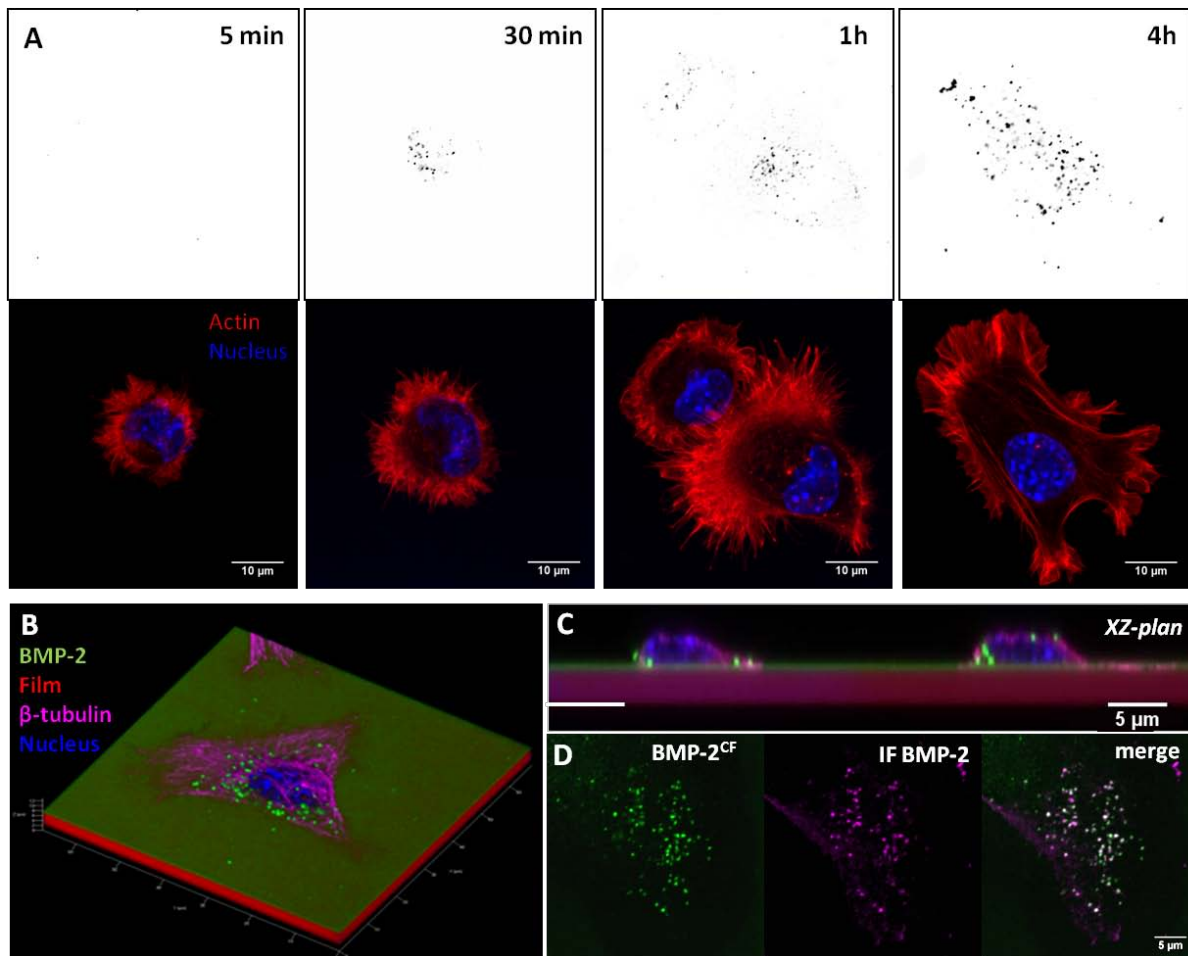


**FIGURE 2. Imaging of BMP-2 uptake by C2C12 cells using confocal microscopy.** (A) confocal images of internalized bBMP-2 after 5 min, 30 min, 1h or 4h of cell contact with EDC 10 film; (B) 3D representation of a C2C12 cell on top of a BMP-2<sup>CF</sup> loaded film after 4 h of culture (image size is 80 x 80 x 12  $\mu\text{m}$ ); (C) XZ section of C2C12 cells after internalization of BMP-2<sup>CF</sup>; (D) co-staining of BMP-2<sup>CF</sup> (green) inside vesicles with an anti-BMP-2 antibody (violet).

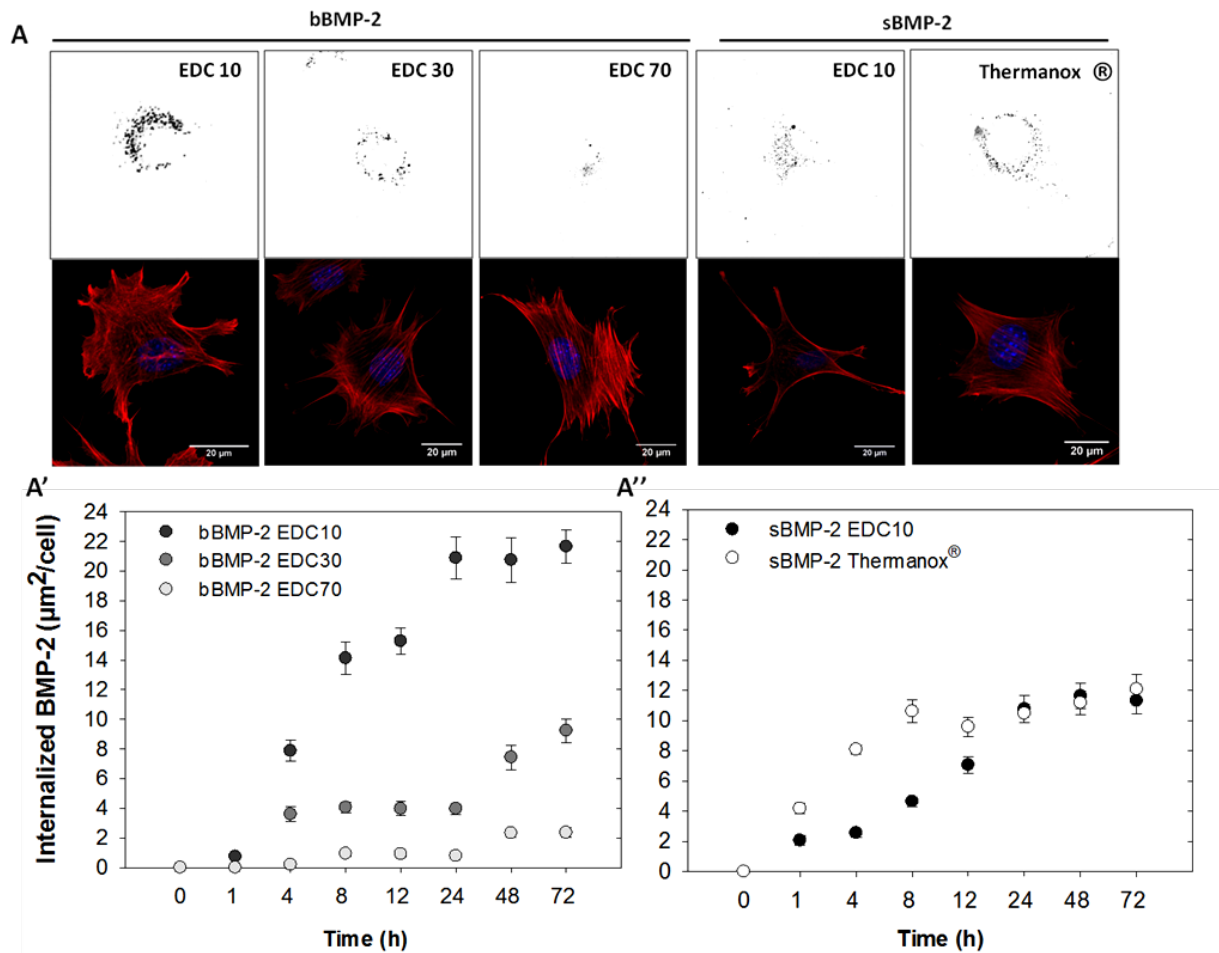


**FIGURE 3.** *BMP-2 internalized amount over time and in function of the BMP-2 presentation mode (matrix-bound versus soluble). (A) Confocal images of internalized bBMP-2 when presented from the cross-linked films (EDC10, 30 and 70) and when sBMP-2 is presented to cells on film or Thermanox® slides (72h). Quantification of the internalized amounts over time, from 1h up to 3 days for (A') bBMP-2 and (A'') sBMP-2 on the different substrates.*



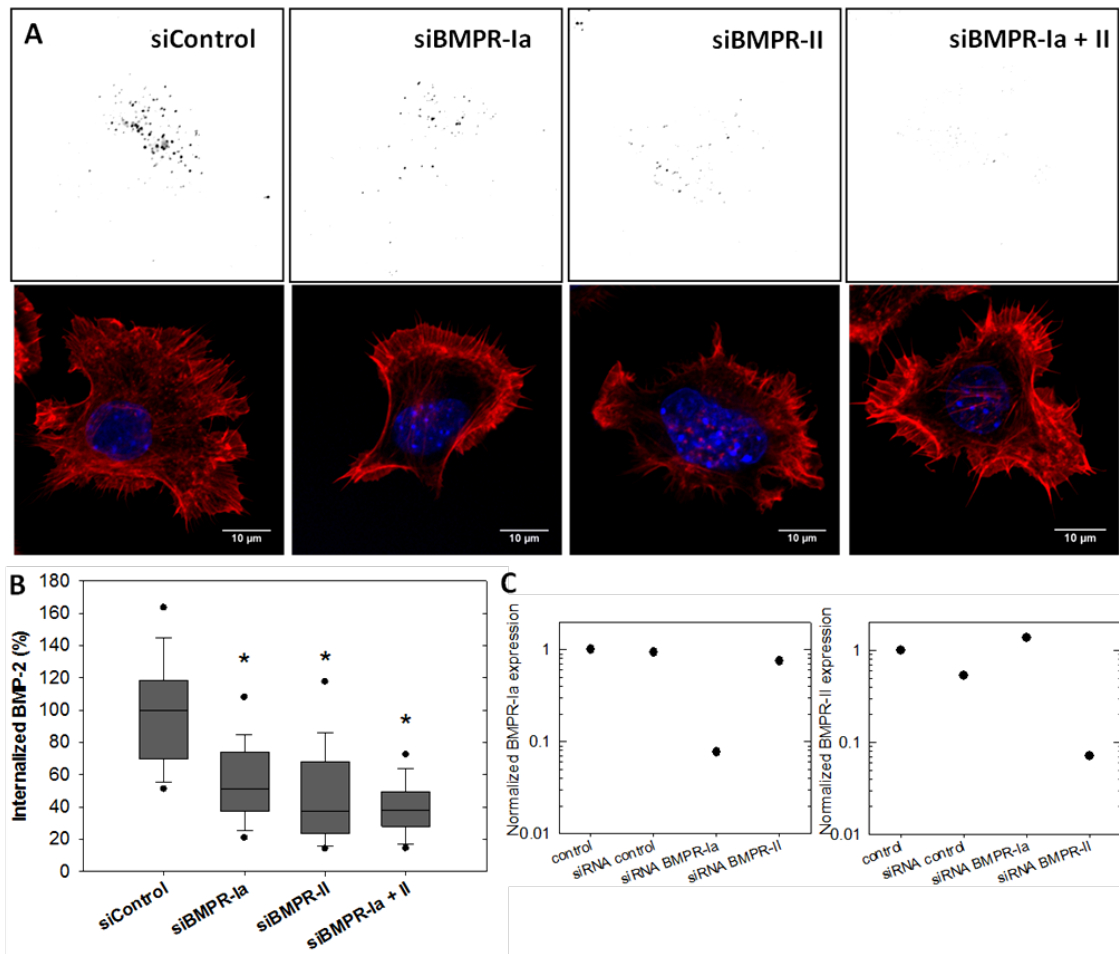


**FIGURE 4. Role of BMP receptors on bBMP-2 internalization.** (A) Typical shape and internalized amount after 4h for transfected cells with siRNA for BMPR-Ia and/or BMPR-II receptors; (B) Quantification of the internalized amount after transfection; (C) The efficacy of the siRNA against receptors was confirmed by qPCR. \* $p < 0.001$

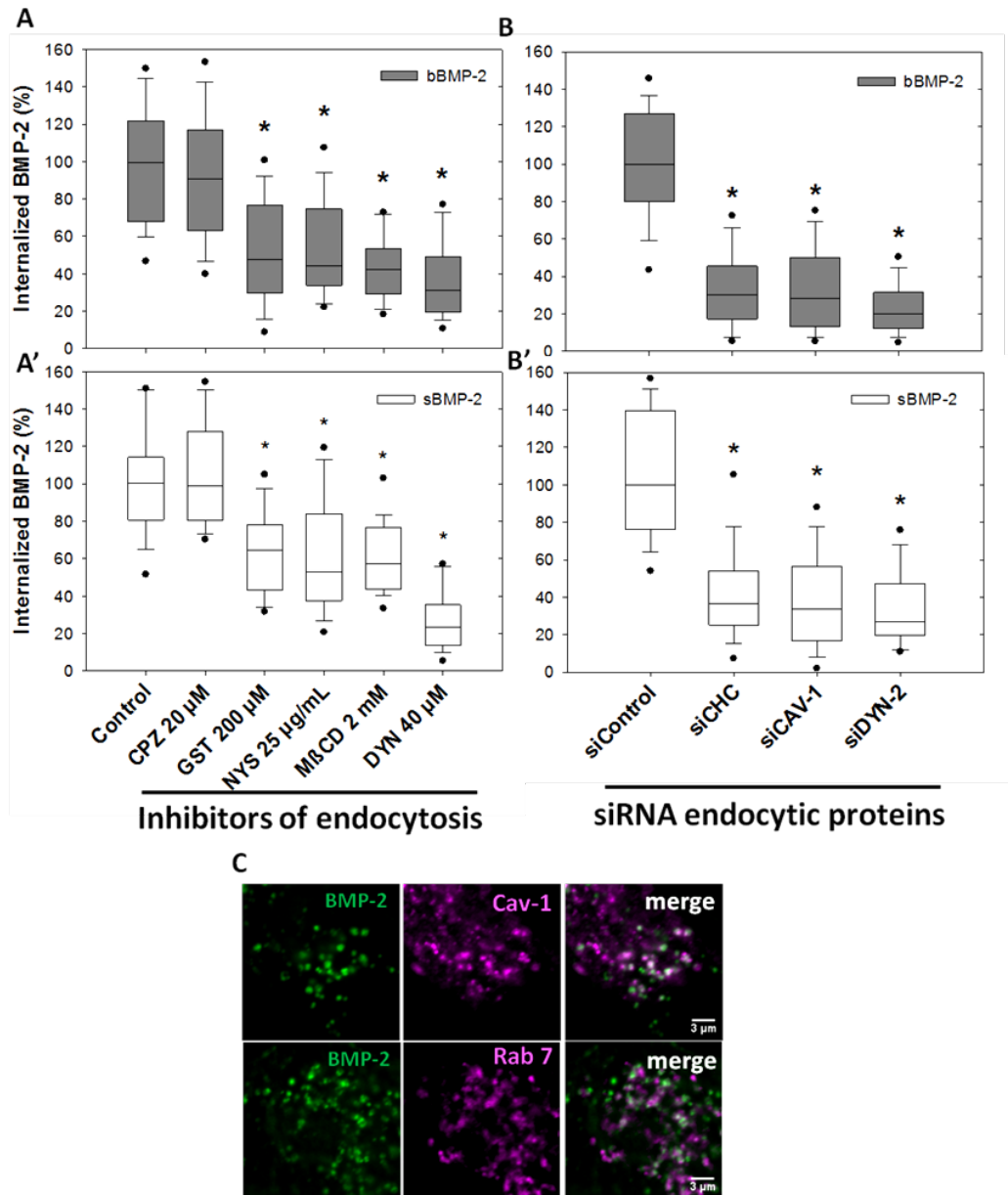


**FIGURE 5. *bBMP-2* and *sBMP-2* internalization routes.** (A, A') Effect of different inhibitors, CPZ, GST, NYS, M $\square$ CD and DYN on *bBMP2* and *sBMP-2* internalization; (B, B') Effect of siRNA-mediated knock-down of endocytic proteins on *bBMP-2* and *sBMP-2* internalization; (C) Confocal images showing colocalization of *BMP-2* vesicles with the endocytic markers *cav-1* and *rab7*. \* $p < 0.001$

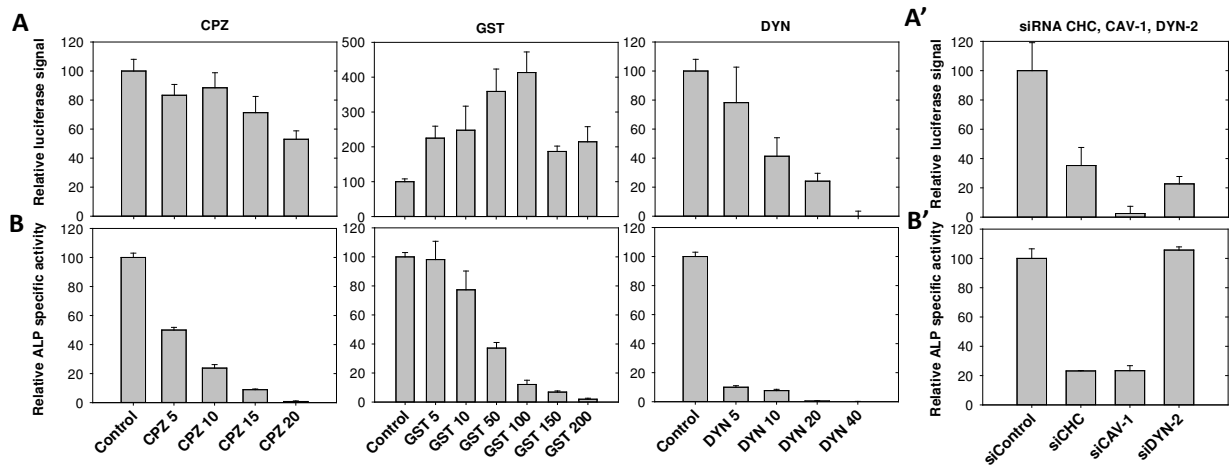


**FIGURE 6. Endocytosis and BMP signaling pathways.** The luminescence of C2C12 cells transfected with *p(BRE)4-luciferase* and the ALP activity were assessed for cells contacting *sBMP-2* after treatment with inhibitors of endocytosis in a dose-dependent manner (A, A') or after transfection with siRNA against CHC, Cav-1 and Dyn-2 (B, B').

## SUPPORTING INFORMATION

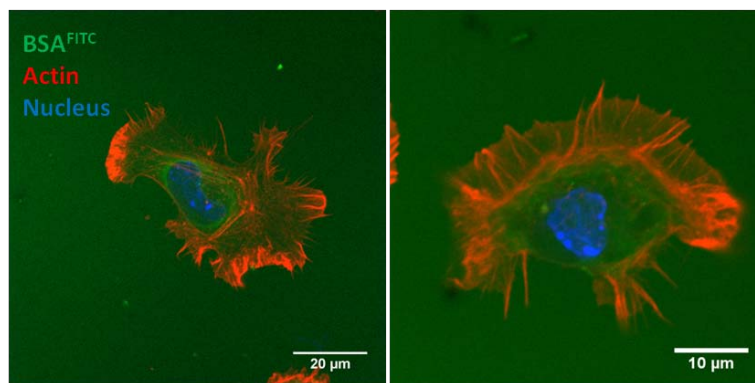


**FIGURE SI 1. Matrix bound BSA-FITC is not internalized by C2C12 cells.** Confocal images of C2C12 cells on top of BSA-FITC loaded films after 4h contacting the film (EDC 10).

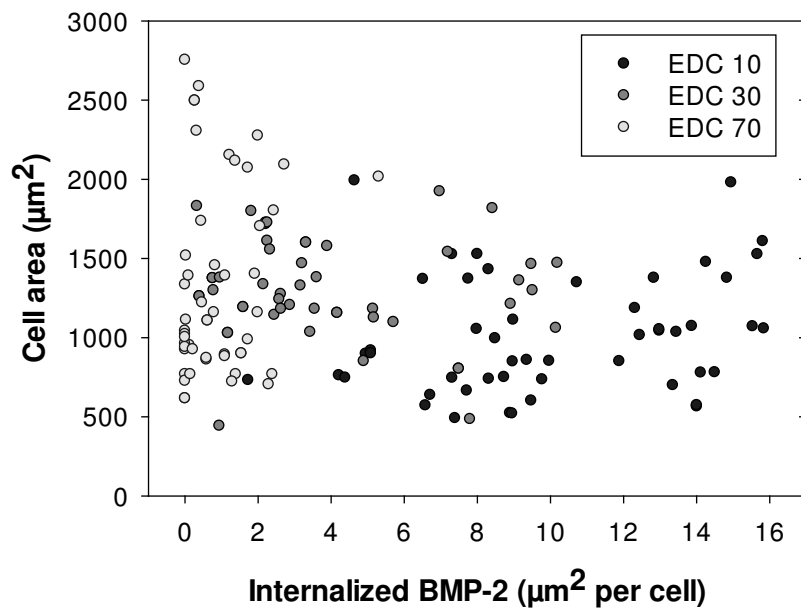


**FIGURE SI 2. Relation between cell area and sBMP-2 internalized amount.** Cells were seeded on top of films with different cross-linking degrees (EDC 10, 30, 70) for 4h with sBMP-2. No relation between cell area (in  $\mu\text{m}^2$ ) and internalized amount ( $\mu\text{m}^2/\text{cell}$ ) was observed.

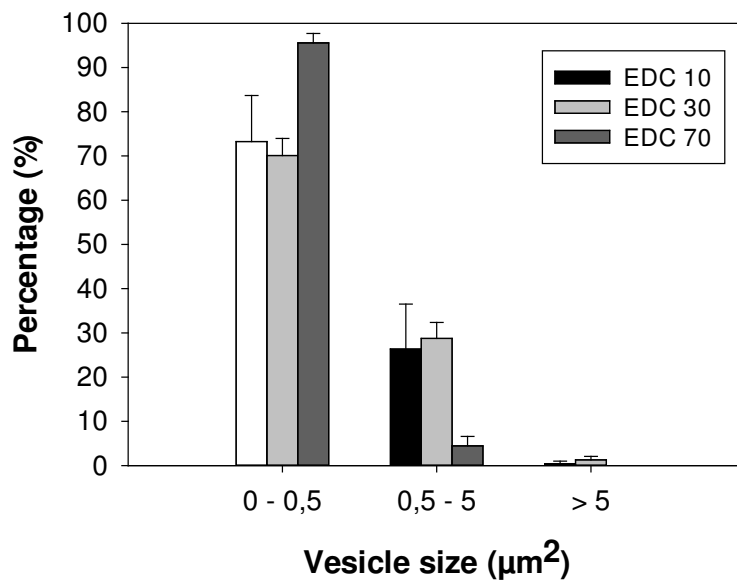


**FIGURE SI 3. Vesicle size distribution in C2C12 cells after internalization of bBMP-2.** Cells contacted bBMP-2 for 4h on EDC10, 30 or 70 films.

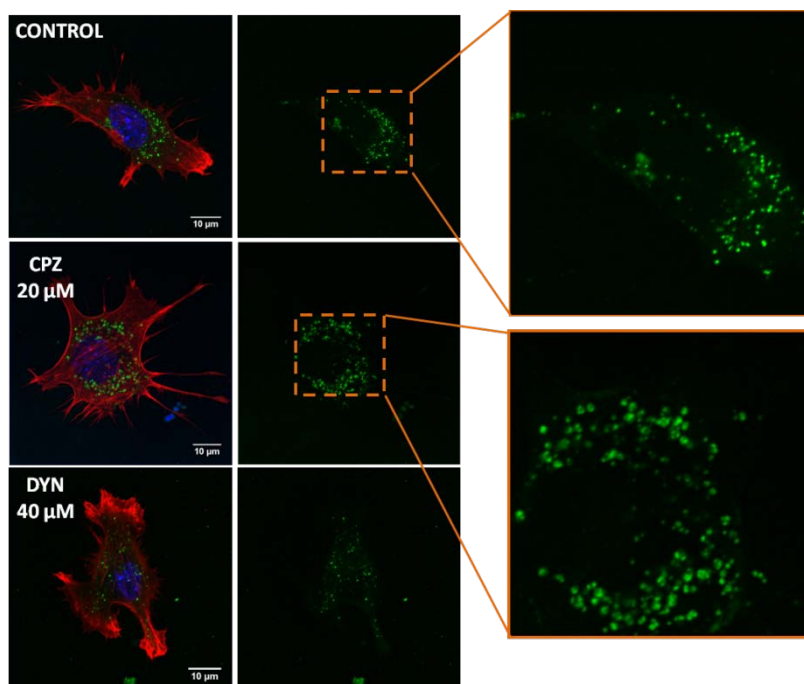


**FIGURE SI 4.** Typical confocal images of C2C12 cells treated with CPZ or DYN after contacting bBMP-2 for 8h (EDC10 film). The shape of the vesicles of endocytosis when cells were treated with CPZ was distinct from the ones of the control or when treated with DYN. When zooming in ring-shaped vesicles were often observed after treatment with CPZ.

## REFERENCES

- Abbatiello, S.E., and T.J. Porter. 1997. Anion-mediated precipitation of human recombinant protein 2 (Rh-BMP2) is dependent upon the heparin binding N-terminal region. *Protein Science*. poster presentation, Protein Society Meeting Boston:99.
- Alborzina, H., H. Schmidt-Glenewinkel, I. Ilkavets, K. Breitkopf-Heinlein, X. Cheng, P. Hortschansky, S. Dooley, and S. Wolf. 2013. Quantitative kinetics analysis of BMP2 uptake into cells and its modulation by BMP antagonists. *J Cell Sci*. 126:117-127.
- Aoki, T., R. Nomura, and T. Fujimoto. 1999. Tyrosine phosphorylation of caveolin-1 in the endothelium. *Exp Cell Res*. 253:629-636.
- Bandyopadhyay, A., P.S. Yadav, and P. Prashar. 2013. BMP signaling in development and diseases: a pharmacological perspective. *Biochem Pharmacol*. 85:857-864.
- Bonor, J., E.L. Adams, B. Bragdon, O. Moseychuk, K.J. Czymmek, and A. Nohe. 2012. Initiation of BMP2 signaling in domains on the plasma membrane. *J Cell Physiol*. 227:2880-2888.
- Bragdon, B., A. D'Angelo, L. Gurski, J. Bonor, K.L. Schultz, W.G. Beamer, C.J. Rosen, and A. Nohe. 2012. Altered plasma membrane dynamics of bone morphogenetic protein receptor type Ia in a low bone mass mouse model. *Bone*. 50:189-199.
- Bucci, C., P. Thomsen, P. Nicoziani, J. McCarthy, and B. van Deurs. 2000. Rab7: a key to lysosome biogenesis. *Mol Biol Cell*. 11:467-480.
- Burkus, J.K., H.S. Sandhu, and M.F. Gornet. 2006. Influence of rhBMP-2 on the healing patterns associated with allograft interbody constructs in comparison with autograft. *Spine J*. 31:775-781.

- Carragee, E.J., E.L. Hurwitz, and B.K. Weiner. 2011. A critical review of recombinant human bone morphogenetic protein-2 trials in spinal surgery: emerging safety concerns and lessons learned. *Spine J.* 11:471-491.
- Chen, Y.G. 2009. Endocytic regulation of TGF-beta signaling. *Cell Res.* 19:58-70.
- Crouzier, T., L. Fourel, T. Boudou, C. Albiges-Rizo, and C. Picart. 2011a. Presentation of BMP-2 from a soft biopolymeric film unveils its activity on cell adhesion and migration. *Adv Mater.* 23:H111-118.
- Crouzier, T., K. Ren, C. Nicolas, C. Roy, and C. Picart. 2009. Layer-by-Layer films as a biomimetic reservoir for rhBMP-2 delivery: controlled differentiation of myoblasts to osteoblasts. *Small.* 5:598-608.
- Crouzier, T., F. Sailhan, P. Becquart, R. Guillot, D. Logeart-Avramoglou, and C. Picart. 2011b. The performance of BMP-2 loaded TCP/HAP porous ceramics with a polyelectrolyte multilayer film coating. *Biomaterials.* 32:7543-7554.
- Dai, J., Y. Li, H. Zhou, J. Chen, M. Chen, and Z. Xiao. 2013. Genistein promotion of osteogenic differentiation through BMP2/SMAD5/RUNX2 signaling. *Int J Biol Sci.* 9:1089-1098.
- Di Guglielmo, G.M., C. Le Roy, A.F. Goodfellow, and J.L. Wrana. 2003. Distinct endocytic pathways regulate TGF-beta receptor signalling and turnover. *Nat Cell Biol.* 5:410-421.
- Dierich, A., E. Le Guen, N. Messaddeq, S. Stoltz, P. Netter, P. Schaaf, J.-C. Voegel, and N. Benkirane-Jessel. 2007. Bone formation mediated by synergy-acting growth factors embedded in a polyelectrolyte multilayer film. *Adv Mater.* 19:693-697.
- Du, J., X. Chen, X. Liang, G. Zhang, J. Xu, L. He, Q. Zhan, X.Q. Feng, S. Chien, and C. Yang. 2011. Integrin activation and internalization on soft ECM as a mechanism of induction of stem cell differentiation by ECM elasticity. *Proc Natl Acad Sci U S A.* 108:9466-9471.
- Geiger, M., R.H. Li, and W. Friess. 2003. Collagen sponges for bone regeneration with rhBMP-2. *Adv Drug Deliv Rev.* 55:1613-1629.
- Gilde, F., O. Maniti, R. Guillot, J.F. Mano, D. Logeart-Avramoglou, F. Sailhan, and C. Picart. 2012. Secondary structure of rhBMP-2 in a protective biopolymeric carrier material. *Biomacromolecules.* 13:3620-3626.
- Gribova, V., C. Gauthier-Rouviere, C. Albiges-Rizo, R. Auzely-Velty, and C. Picart. 2013. Effect of RGD functionalization and stiffness modulation of polyelectrolyte multilayer films on muscle cell differentiation. *Acta Biomater.* 9:6468-6480.
- Guillot, R., F. Gilde, P. Becquart, F. Sailhan, A. Lapeyrere, D. Logeart-Avramoglou, and C. Picart. 2013. The stability of BMP loaded polyelectrolyte multilayer coatings on titanium. *Biomaterials.* 34:5737-5746.
- Hartung, A., K. Bitton-Worms, M.M. Rechtman, V. Wenzel, J.H. Boergemann, S. Hassel, Y.I. Henis, and P. Knaus. 2006a. Different routes of bone morphogenetic protein (BMP) receptor endocytosis influence BMP signaling. *Mol Cell Biol.* 26:7791-7805.
- Hartung, A., C. Sieber, and P. Knaus. 2006b. Yin and Yang in BMP signaling: Impact on the pathology of diseases and potential for tissue regeneration. *Signal Transduction.* 6:314-328.
- Heinecke, K., A. Seher, W. Schmitz, T.D. Mueller, W. Sebald, and J. Nickel. 2009. Receptor oligomerization and beyond: a case study in bone morphogenetic proteins. *BMC Biol.* 7:59.
- Heining, E., R. Bhushan, P. Paarmann, Y.I. Henis, and P. Knaus. 2011. Spatial segregation of BMP/Smad signaling affects osteoblast differentiation in C2C12 cells. *PLoS One.* 6:e25163.

- Hogan, B.L. 1996. Bone morphogenetic proteins: multifunctional regulators of vertebrate development. *Genes Dev.* 10:1580-1594.
- Jortikka, L., M. Laitinen, T.S. Lindholm, and A. Marttinen. 1997. Internalization and intracellular processing of bone morphogenetic protein (BMP) in rat skeletal muscle myoblasts (L6). *Cell Signal.* 9:47-51.
- Katagiri, T., A. Yamaguchi, M. Komaki, E. Abe, N. Takahashi, T. Ikeda, V. Rosen, J.M. Wozney, A. Fujisawa-Sehara, and T. Suda. 1994. Bone morphogenetic protein-2 converts the differentiation pathway of C2C12 myoblasts into the osteoblast lineage. *J Cell Biol.* 127:1755-1766.
- Kawabata, M., H. Inoue, A. Hanyu, T. Imamura, and K. Miyazono. 1998. Smad proteins exist as monomers in vivo and undergo homo- and hetero-oligomerization upon activation by serine/threonine kinase receptors. *EMBO J.* 17:4056-4065.
- Kelley, R., R. Ren, X. Pi, Y. Wu, I. Moreno, M. Willis, M. Moser, M. Ross, M. Podkova, L. Attisano, and C. Patterson. 2009. A concentration-dependent endocytic trap and sink mechanism converts Bmper from an activator to an inhibitor of Bmp signaling. *J Cell Biol.* 184:597-609.
- Kim, H.D., and R.F. Valentini. 2002. Retention and activity of BMP-2 in hyaluronic acid-based scaffolds in vitro. *J Biomed Mater Res.* 59:573-584.
- Lee-Hoeflich, S.T., C.G. Causing, M. Podkova, X. Zhao, J.L. Wrana, and L. Attisano. 2004. Activation of LIMK1 by binding to the BMP receptor, BMPRII, regulates BMP-dependent dendritogenesis. *EMBO J.* 23:4792-4801.
- Liu, F., F. Ventura, J. Doody, and J. Massague. 1995. Human type II receptor for bone morphogenetic proteins (BMPs): extension of the two-kinase receptor model to the BMPs. *Mol Cell Biol.* 15:3479-3486.
- Lo, C.M., H.B. Wang, M. Dembo, and Y.L. Wang. 2000. Cell movement is guided by the rigidity of the substrate. *Biophys J.* 79:144-152.
- Logeart-Avramoglou, D., M. Bourguignon, K. Oudina, P. Ten Dijke, and H. Petite. 2006. An assay for the determination of biologically active bone morphogenetic proteins using cells transfected with an inhibitor of differentiation promoter-luciferase construct. *Anal Biochem.* 349:78-86.
- Macia, E., M. Ehrlich, R. Massol, E. Boucrot, C. Brunner, and T. Kirchhausen. 2006. Dynasore, a cell-permeable inhibitor of dynamin. *Dev Cell.* 10:839-850.
- Marom, B., E. Heining, P. Knaus, and Y.I. Henis. 2011. Formation of stable homomeric and transient heteromeric bone morphogenetic protein (BMP) receptor complexes regulates Smad protein signaling. *J Biol Chem.* 286:19287-19296.
- Massague, J. 1998. TGF-beta signal transduction. *Annu Rev Biochem.* 67:753-791.
- McClellan, J.W., D.S. Mulconrey, R.J. Forbes, and N. Fullmer. 2006. Vertebral bone resorption after transforaminal lumbar interbody fusion with bone morphogenetic protein (rhBMP-2). *J Spinal Disord Tech.* 19:483-486.
- Nickel, J., W. Sebald, J.C. Groppe, and T.D. Mueller. 2009. Intricacies of BMP receptor assembly. *Cytokine Growth Factor Rev.* 20:367-377.
- Nohe, A., S. Hassel, M. Ehrlich, F. Neubauer, W. Sebald, Y.I. Henis, and P. Knaus. 2002. The mode of bone morphogenetic protein (BMP) receptor oligomerization determines different BMP-2 signaling pathways. *J Biol Chem.* 277:5330-5338.
- Nohe, A., E. Keating, T.M. Underhill, P. Knaus, and N.O. Petersen. 2005. Dynamics and interaction of caveolin-1 isoforms with BMP-receptors. *J Cell Sci.* 118:643-650.
- Nohno, T., T. Ishikawa, T. Saito, K. Hosokawa, S. Noji, D.H. Wolsing, and J.S. Rosenbaum. 1995. Identification of a human type II receptor for bone morphogenetic protein-4 that forms differential heteromeric complexes with bone morphogenetic protein type I receptors. *J Biol Chem.* 270:22522-22526.

- Ono, Y., F. Calhabeu, J.E. Morgan, T. Katagiri, H. Amthor, and P.S. Zammit. 2011. BMP signalling permits population expansion by preventing premature myogenic differentiation in muscle satellite cells. *Cell Death Differ.* 18:222-234.
- Pan, W., L.D. Quarles, L.H. Song, Y.H. Yu, C. Jiao, H.B. Tang, C.H. Jiang, H.W. Deng, Y.J. Li, H.H. Zhou, and Z.S. Xiao. 2005. Genistein stimulates the osteoblastic differentiation via NO/cGMP in bone marrow culture. *J Cell Biochem.* 94:307-316.
- Patterson, J., R. Siew, S.W. Herring, A.S. Lin, R. Guldborg, and P.S. Stayton. 2010. Hyaluronic acid hydrogels with controlled degradation properties for oriented bone regeneration. *Biomaterials.* 31:6772-6781.
- Phillippi, J.A., E. Miller, L. Weiss, J. Huard, A. Waggoner, and P. Campbell. 2008. Microenvironments engineered by inkjet bioprinting spatially direct adult stem cells toward muscle- and bone-like subpopulations. *Stem Cells.* 26:127-134.
- Rauch, C., A.C. Brunet, J. Deleule, and E. Farge. 2002. C2C12 myoblast/osteoblast transdifferentiation steps enhanced by epigenetic inhibition of BMP2 endocytosis. *Am J Physiol Cell Physiol.* 283:C235-243.
- Reddi, A.H., and A. Reddi. 2009. Bone morphogenetic proteins (BMPs): from morphogens to metabologens. *Cytokine Growth Factor Rev.* 20:341-342.
- Rickard, D.J., T.A. Sullivan, B.J. Shenker, P.S. Leboy, and I. Kazhdan. 1994. Induction of rapid osteoblast differentiation in rat bone marrow stromal cell cultures by dexamethasone and BMP-2. *Dev Biol.* 161:218-228.
- Rodal, S.K., G. Skretting, O. Garred, F. Vilhardt, B. van Deurs, and K. Sandvig. 1999. Extraction of cholesterol with methyl-beta-cyclodextrin perturbs formation of clathrin-coated endocytic vesicles. *Mol Biol Cell.* 10:961-974.
- Rothberg, K.G., J.E. Heuser, W.C. Donzell, Y.S. Ying, J.R. Glenney, and R.G. Anderson. 1992. Caveolin, a protein component of caveolae membrane coats. *Cell.* 68:673-682.
- Saldanha, S., B. Bragdon, O. Moseychuk, J. Bonor, P. Dhurjati, and A. Nohe. 2013. Caveolae regulate Smad signaling as verified by novel imaging and system biology approaches. *J Cell Physiol.* 228:1060-1069.
- Schmidmaier, G., P. Schwabe, C. Strobel, and B. Wildemann. 2008. Carrier systems and application of growth factors in orthopaedics. *Injury.* 39 Suppl 2:S37-43.
- Sieber, C., J. Kopf, C. Hiepen, and P. Knaus. 2009. Recent advances in BMP receptor signaling. *Cytokine Growth Factor Rev.* 20:343-355.
- Simic, P., and S. Vukicevic. 2007. Bone morphogenetic proteins: from developmental signals to tissue regeneration. Conference on bone morphogenetic proteins. *EMBO Rep.* 8:327-331.
- Sorkin, A., and M. von Zastrow. 2009. Endocytosis and signalling: intertwining molecular networks. *Nat Rev Mol Cell Biol.* 10:609-622.
- Urist, M.R. 1965. Bone: formation by autoinduction. *Science.* 150:893-899.
- von Einem, S., S. Erler, K. Bigl, B. Frerich, and E. Schwarz. 2011. The pro-form of BMP-2 exhibits a delayed and reduced activity when compared to mature BMP-2. *Growth Factors.* 29:63-71.
- Wang, L.H., K.G. Rothberg, and R.G. Anderson. 1993. Mis-assembly of clathrin lattices on endosomes reveals a regulatory switch for coated pit formation. *J Cell Biol.* 123:1107-1117.
- Zhao, B., T. Katagiri, H. Toyoda, T. Takada, T. Yanai, T. Fukuda, U.I. Chung, T. Koike, K. Takaoka, and R. Kamijo. 2006. Heparin potentiates the in vivo ectopic bone formation induced by bone morphogenetic protein-2. *J Biol Chem.* 281:23246-23253.



## V.2.1. Complementary data

### V.2.1.1. Bioactivity of fluorescently labeled BMP-2

The bioactivity of BMP-2<sup>CF</sup> was previously confirmed by *Thomas Crouzier* (Crouzier et al., 2009). We showed here that labeled BMP-2 used in this thesis experiments was bioactive as observed by ALP expression *Figure V- 1*.

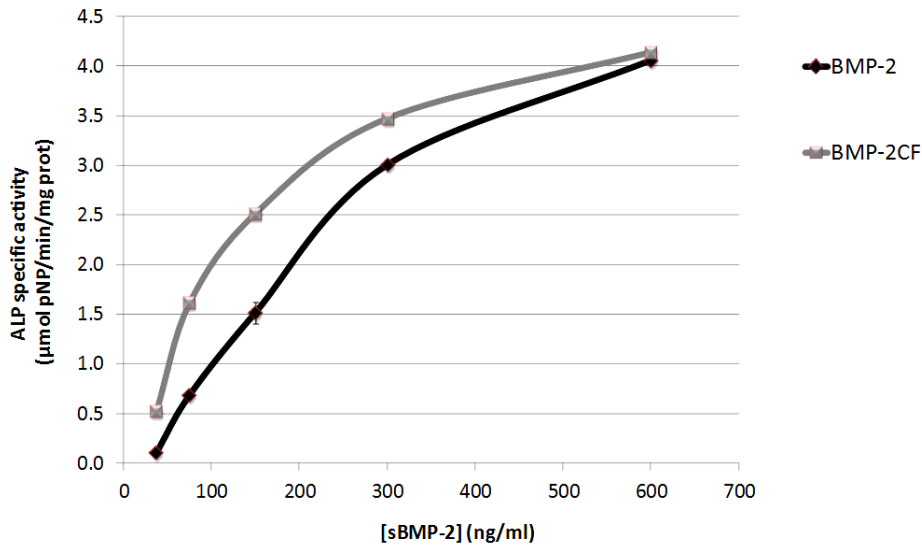


*Figure V- 1 : ALP activity after C2C12 cells stimulation with different concentrations of sBMP-2 (3 days).*

The labeling did not affect BMP bioactivity. ALP expression was dependent of BMP concentration for BMP-2<sup>CF</sup> and BMP-2.

### V.2.1.2. Immunofluorescence labeling of BMP receptors in C2C12 cells

After visualization of the BMP-2 internalization we wonder if BMP receptors were as well internalized along with BMP-2. To answer this question we attempted to label BMPR-Ia and BMPR-II by immunofluorescence and look for a possible colocalization with fluorescently-labeled BMP-2 inside the endocytic vesicles.

Two controls were defined to test the specificity of the BMP receptors labeling (for primary and secondary antibodies). The first control was to skip the incubation with 1<sup>st</sup> antibody (*Figure V- 2, Figure V- 3*) as a control for the secondary antibody and the other control was the use of transfected C2C12 cells with siRNA against BMPR-Ia and BMPR-II as a control for primary antibody detection (*Figure V- 4, Figure V- 5*, respectively).

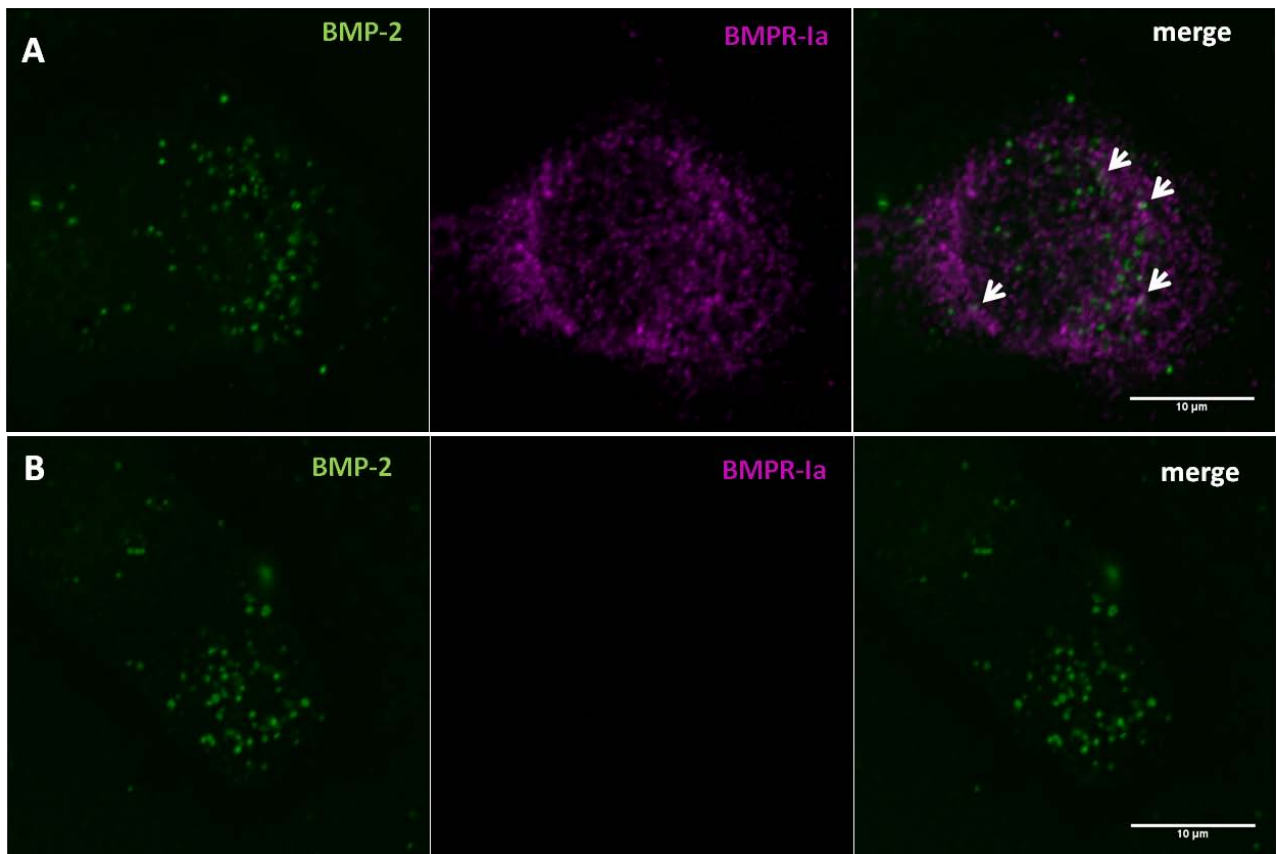


*Figure V- 2 : Immunolabeling of BMPR-Ia in C2C12 cells after 4h contacting bBMP-2, EDC 10 (A) positive sample. White arrows show colocalization areas in the images between BMP-2 and BMPR-Ia (B) control, no incubation with 1<sup>st</sup> antibody.*

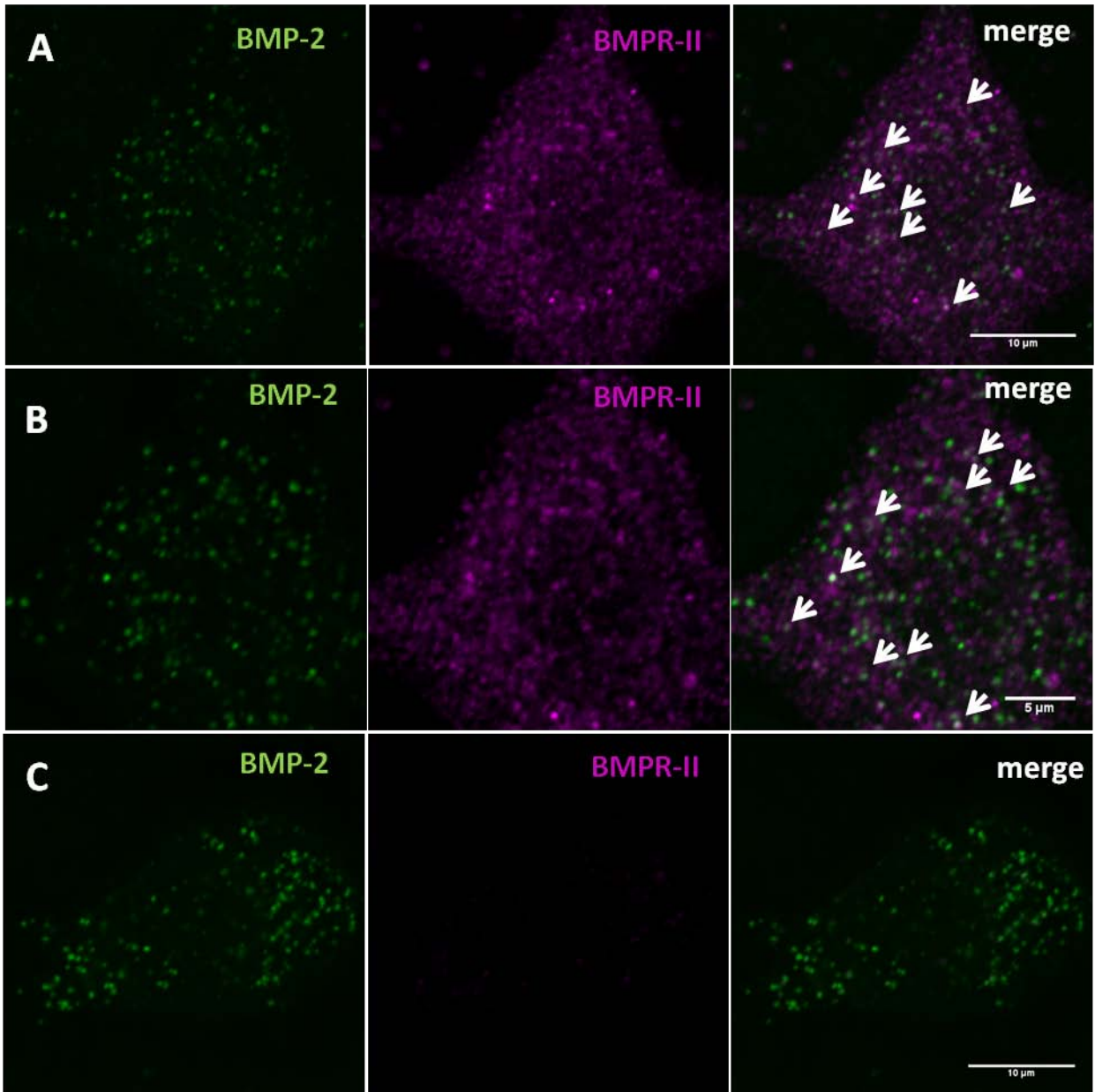


**Figure V- 3 : Immunolabeling of BMPR-II in C2C12 cells after 4h contacting bBMP-2, EDC 10 (A) positive sample (B) zoomed image of the region shown in (A). White arrows show colocalization areas in the images between BMP-2 and BMPR-II (C) control, no incubation with 1<sup>st</sup> antibody.**

After labeling of BMPR-Ia and BMPR-II we observed fluorescent dots inside the cells which correspond to what was previously observed by others using the same antibody, namely the anti-BMPR-Ia from Santa Cruz (Du et al., 2011). Regarding the control the absence of labeling in absence of primary antibody evidences the specificity of the secondary antibodies.

We showed in *Figure V- 2* and *Figure V- 3* some evidence of colocalization between BMP-2 and the BMP receptors. In this preliminary experiment, the colocalization between BMPR-II and BMP-2 inside vesicles was clearer than for BMPR-Ia.

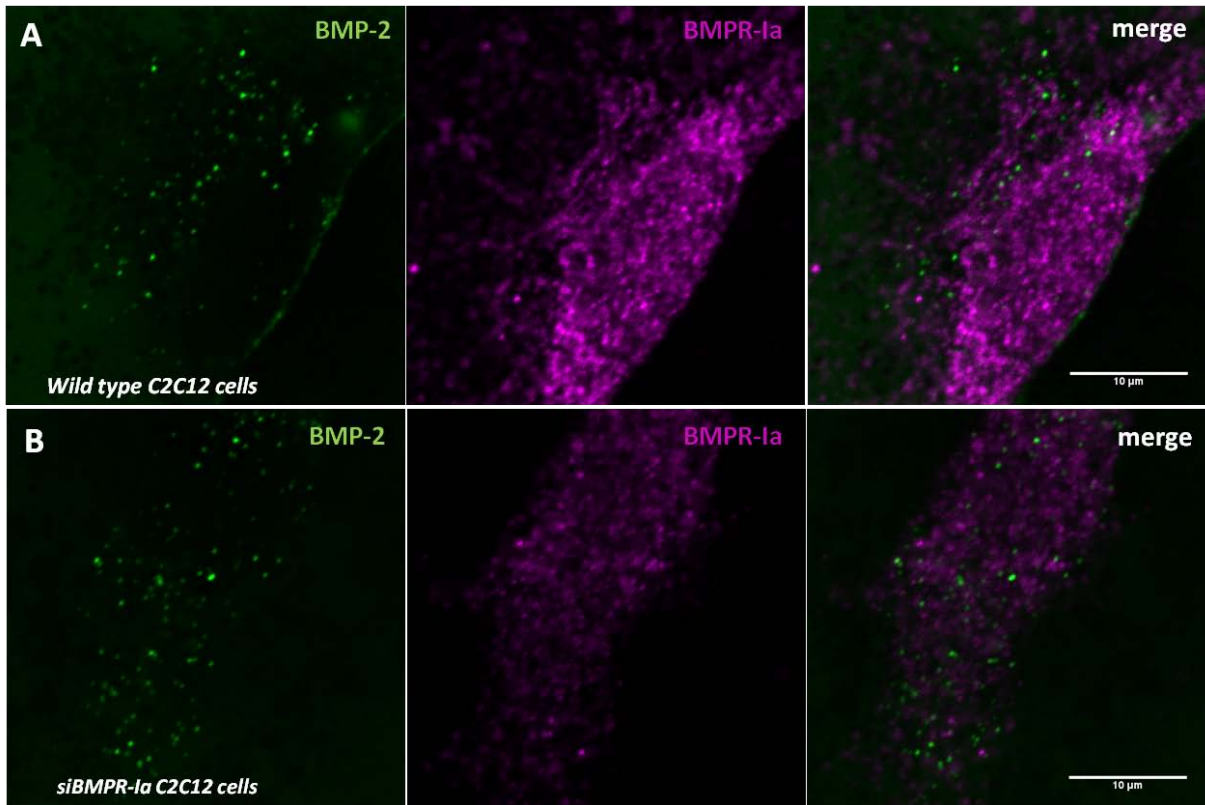


*Figure V- 4 : Immunolabeling of BMPR-Ia in C2C12 cells after 4h contacting sBMP-2 (A) wild type (B) cells transfected with siRNA against BMPR-Ia. Scale bar = 10 $\mu$ m.*

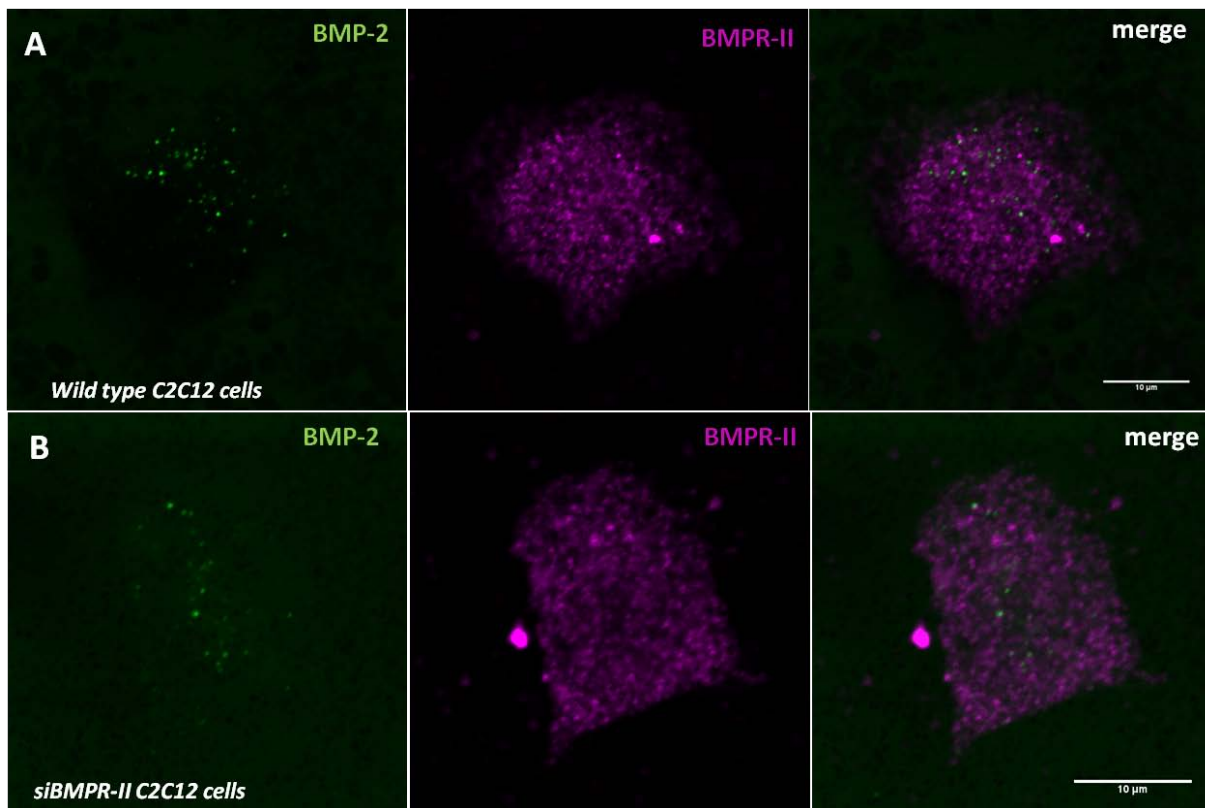


**Figure V- 5 : Immunolabeling of BMPR-II in C2C12 cells after 4h contacting sBMP-2 (A) cells transfected with siRNA against BMPR-II (B) wild type. Scale bar = 10 $\mu$ m.**

In this preliminary test, the labeling of receptors in transfected cells appeared to be weaker but several labeled ‘points’ were still present (*Figure V- 4 B, Figure V- 5 B*). We wonder about the specificity of the labeling of both receptors.

In a next step, we could test other antibodies against BMPR-Ia and BMPR-II to see if we can increase the specificity of the labeling. However, in the literature there are very few successful results where antibodies were capable to detect receptors by immunofluorescence labeling. The optimization of the labeling protocol including the blocking steps can be also an option to obtain a clearer staining.

### V.2.1.3. Immunogold labeling of BMP-2 inside cells

By the immunogold labeling (IGL) of BMP-2 inside film cross-sections we were able to observe BMP-2 diffusion inside films in SEM images where BMP-2 location was shown by the presence of gold nanoparticles in the upper parts of the film cross-section (V.2. subchapter; Article 3 – in preparation).

We next performed the same labeling on cross-sections of C2C12 cells seeded on top of films to detect the presence of BMP-2 inside the cell / in vesicles of endocytosis. We started developing this tool to have another method to study the BMP-2 internalization with increased image resolution. We wanted not only to confirm the results obtained in fluorescence images but also to identify other proteins involved in the endocytosis process by a dual labeling. In this last case, we could perform IGL of two proteins at the same time by using secondary antibodies conjugated with gold nanoparticles of different sizes. In addition to the labeling in these SEM images we can also visualize other structures of the cell thanks to contrast agents used in the preparation of samples for SEM. For example, the post-fixation with osmium tetroxide which is a lipid stain allows the visualization of all the cell organelles with membrane-like structures such as vesicles of endocytosis.

Using the same protocol as described in V.2. subchapter we performed IGL on cells seeded on top of films. The obtained results are shown in *Figure V- 6* and *Figure V- 7*.

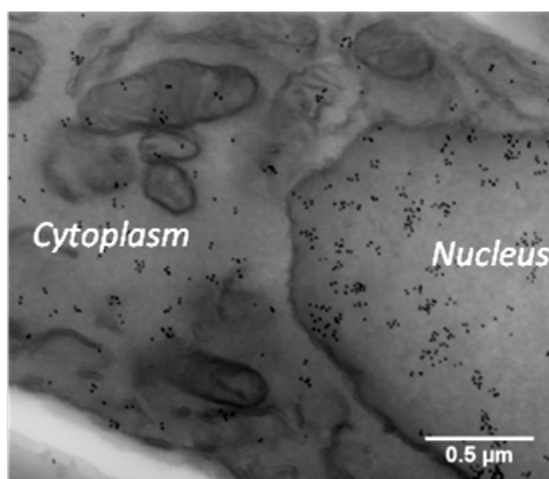


*Figure V- 6 : SEM images of cross-sections of C2C12 cells on top of films without BMP-2. Dark spots in the images are gold nanoparticles. An example of non-specific labeling inside the nucleus is shown. This is an image of a control sample where cells did not contact BMP-2.*



In the first experiments we have observed labeling inside the nuclei of cells, in absence of presence of BMP-2, which indicated non-specific labeling (**Figure V- 6**). We solved this problem by improving the blocking steps in the IGL protocol. By performing this type of labeling inside cells increases the changes of non-specific labeling since the cell body is a highly charged environment.

Then, after optimization of the IGL protocol some preliminary but encouraging results were obtained (**Figure V- 7**) where an initial proof of successful IGL of BMP-2 inside C2C12 cells is evidenced.

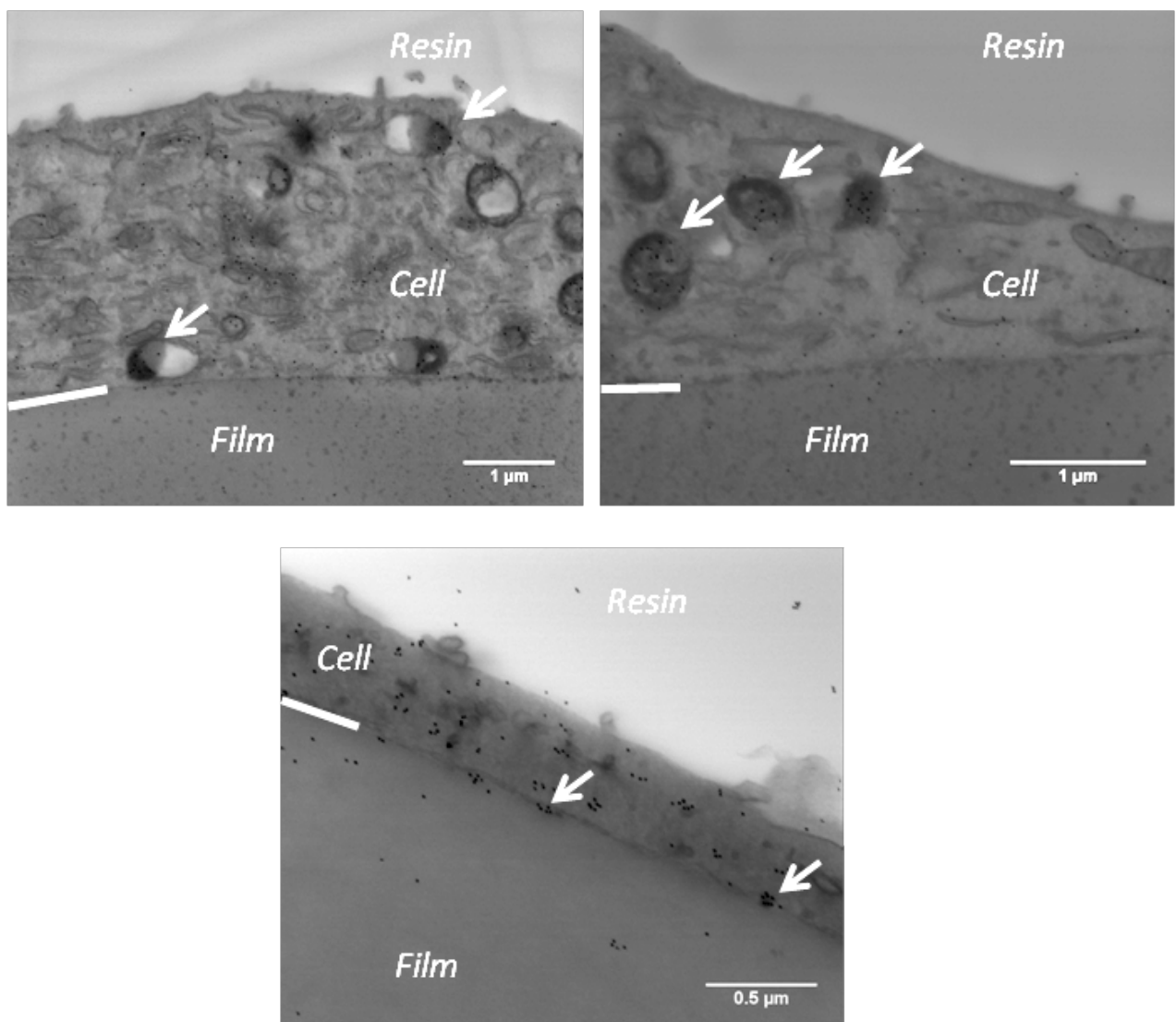


**Figure V- 7 : SEM images of cross-sections of C2C12 cells on top of BMP-2 loaded films.** Dark spots in the images are gold nanoparticles detecting BMP-2 after immunogold labeling protocol. In the upper images we can observe the detection of BMP-2 inside vesicles (white arrows). In the lower image we observe agglomerates of gold nanoparticles in the cell-film interface which could represent the formation of vesicles of endocytosis.

Unfortunately, we were not able to get as many images as we needed. The lack of reproducibility between experiments make us think that the adopted method by post-embedding labeling (labeling directly after cross-section preparation) is maybe not appropriated and that we should perform a pre-embedding IGL of BMP-2 (labeling after cell fixation, before resin embedding and cross-section preparation). Indeed, the sample preparation before cross-section could damage the structure of the proteins inside the cell/sample. Along with the problem of possible denaturation of proteins during the cross-sections preparation comes also the non-specificity of the labeling mostly due to the highly charged environment inside a cell. It is important to mention that such experiments involve several meticulous steps which results in a long experiment time. These preliminary results will help continuing the development of this tool to observe the presence of proteins inside cells by a high resolution technique.





**Chapter VI:**  
**Conclusions and directions for future research**

## VI.A. Conclusions

In this work, we used a biopolymeric coating made of hyaluronan and poly(L-Lysine) prepared using the layer-by-layer technique, which is able to trap and release BMP-2. This reservoir presents BMP-2 to cells in a "matrix-bound" manner. The *in vitro* bioactivity and *in vivo* osteoinductive properties of BMP-2-loaded films have previously been proved by the group.

First, we aimed to better characterize the trapping of BMP-2 inside the biomimetic films. The following aspects were investigated: quantification of the incorporated amount and release as well as the protein vertical diffusion inside films in function of film cross-linking extent; evaluation of BMP-2 secondary structure when trapped inside the film as compared to BMP-2 in solution, i.e. free environment. Secondly, we explored the potential of such films to preserve the bioactivity of BMP-2 after drying, long-term storage and sterilization. Finally, we investigated the BMP-2 uptake by cells when BMP-2 is presented in a "matrix-bound" manner.

### ***BMP-2 loading amount, release and vertical diffusion inside films***

The use of a fluorescently-labeled BMP-2 allowed us to quantify the initial loading amount inside the films, the release over time and the final retained amount for films cross-linked at different extents. A higher amount of BMP-2 is initially loaded inside EDC10 films as compared to more cross-linked films (EDC30 and 70) but after extensive rinsing, i.e. final step in film preparation, they retained the smaller amounts of BMP-2. The analysis of the vertical diffusion of fluorescently-labeled BMP-2 inside films showed that the BMP-2 really diffuses inside the films (it is not adsorbed on top of films) and that the penetration inside the film depends on film cross-linking. Vertical diffusion was higher for EDC10 films (~ 42 %) as compared to EDC30 and 70 films (~ 26 %). Such differences may be related to the film porosity and/or to the strength of the bonds between the BMP-2 and the film. We may hypothesize that the bonds between BMP-2 and the EDC10 films are weaker as compared to the ones of EDC30 and 70 films.

### ***BMP-2 secondary structure inside films in hydrated or dry conditions***

It is well-known that FTIR spectroscopy is a powerful technique to evaluate the secondary structure of proteins. Using this technique we were able to characterize the BMP-2 structure inside films and in solution. The trapping of BMP-2 trapping inside the hydrated

films slightly impacted the protein structure leading to a decrease in  $\beta$ -sheet content and an increase in the presence of unordered structures. A more pronounced change in structure was evidenced after drying of the films. The little changes observed in BMP-2 structure after loading inside (PLL/HA) films suggest that the possible ‘confinement’ provided by the film did not affect protein secondary structure.

These results suggest that the possible ‘confinement’ after BMP-2 loading inside (PLL/HA) films do not affect its structure. Also, in analogy to sugars that are widely used as stabilizing agents during drying of proteins, the biopolymeric film plays the role of stabilizer, or protective carrier, for the protein.

### ***Structure and bioactivity of BMP-2-loaded films after drying, long term storage and sterilization***

In view of the clinical translation of this BMP-2 loaded coating it is important to show that their osteoinductive properties are preserved after drying, long term storage and sterilization. Film structure, *in vitro* bioactivity and *in vivo* osteoinduction properties after such processes were then evaluated.

In what concerns the structural analysis of films we were able to show by FTIR spectroscopy that they can be dried, stored up to 2.5 years and  $\gamma$ -sterilized without damaging film structure.

The impact on the *in vitro* bioactivity was evaluated by the ALP activity test. The bioactivity of films dried for 2 hours was the same as hydrated films. In addition, a weak but not statistically significant decrease on the activity of the films was noticed after 1 year of storage in dry state. Only the bioactivity of more cross-linked films (EDC 70) was shown to be affected by storage in dry state. Concerning sterilization effect on films bioactivity we demonstrated that it affects the bioactivity decreasing the initial ALP activity to 50% when sterilized using 25kGy and to 20% when using 50kGy. Here again more cross-linked films were shown to be more sensitive than less cross-linked films.

Osteoinduction properties *in vivo* of such films were also assessed. BMP-2-loaded PEM films coated on TA6V scaffolds were implanted in ectopic site in rats. Similar amounts of new bone tissue were formed in both non-sterilized and sterilized implants. This result suggested that, although some BMP-2 bioactivity may have been lost during the irradiation process, the remaining amount of bioactive BMP-2 was still high enough to induce *de novo* bone tissue.

### ***Cellular uptake of matrix-bound BMP-2 by C2C12 cells***

Using a fluorescently-labeled BMP-2 we showed that matrix-bound BMP-2 is internalized by C2C12 cells forming vesicles of endocytosis. The bioactivity of the labeled BMP-2 was proved by ALP activity test. The quantification of the internalized amount allowed us to follow uptake over time and compare the uptake when cells are seed on top of films cross-linked at different extents. Despite the higher BMP-2 quantity inside EDC30 and 70 films the cells internalized less BMP-2 than on top of EDC10 films, where smaller amounts of BMP-2 were shown to remain inside the film. These results may be related to the film porosity and/or to the strength of the bonds between the BMP-2 and the film. We may hypothesize that the bonds between BMP-2 and the EDC 10 films are weaker and this is why the cell is able get more BMP-2. The use of inhibitors of endocytosis, siRNA-mediated knock-down of endocytic proteins and immunostaining of endocytic markers showed that matrix-bound BMP-2 is internalized through clathrin- and caveolin-dependent endocytosis. Similar results were obtained when BMP-2 is delivered in solution to cells. The type of presentation does not change the selected endocytic pathway(s). The importance of BMP receptors in BMP-2 internalization was evidenced using siRNA-mediated knock-down of BMP receptors Ia and II. Internalized amount was reduced to ~ 50% after receptors knock-down. Finally, using the same methods as to discover the BMP-2 internalization pathways we showed that clathrin and caveolin-1 are important in the regulation of both Smad and non Smad-dependent pathway whereas dynamin-2 was only required for the Smad pathway.

Altogether, our results highlighted the peculiar properties of the PEM films for BMP-2 sequestration and for preservation of its osteoinductive potential after storage in dry state and sterilization by  $\gamma$ -irradiation. Although not fully understood, the protective effects of PEM films on the growth factor bioactivity may be attributed to both the high water content in (PLL/HA) films (~ 90%) and to their porosity, which may provide a “protein-friendly” environment. The biopolymeric PEM film appears to mimic the natural extracellular matrix that preserves the BMP-2 bioactivity.

## **VI.B. Directions for future research**

Development of the materials with controlled properties is a crucial aspect in the development of implantable materials and drug delivery systems. PEM films appear as a new type of biomaterial with controlled physical and chemical properties, being able to trigger specific cellular responses.

### ***Characterization of film porosity in function of cross-linking degree***

The (PLL/HA) films developed in our group can be used for the controlled presentation of bioactive molecules to cells. The interaction of bioactive molecules with these films would be better understood if we were able to know more about the internal structure of films. In contrary to metals or ceramics, polymeric materials can hardly be characterized by high resolution techniques such as electron microscopy and tomography because of their poor conductive properties.

Information about the porosity (pore size) of (PLL/HA) films would allow us to clarify the different loading profiles of BMP-2 inside films cross-linked at different extents. In addition, it would also elucidate why cells internalize higher amounts of BMP-2 when on top of films that contain an inferior quantity of BMP-2 (EDC10). At last it could also give information on the porosity variation along the film thickness: is it homogeneous? The investigation of film porosity could be performed by making uncharged fluorescent beads or particles of different diameter from several nanometers to micrometer size diffuse inside films. The film should be labeled with another color, by using a labeled-PLL. By the analysis of z-stack confocal images, we would be able to visualize the diffusion of the different size beads or particles and then conclude on the film pore size. To be sure that the film porosity is homogeneous over the thickness, beads of different size labeled with different dyes (a three or four color experiment) could be conducted.

### ***Film resistance to implantation and adhesion of film onto different biomaterials***

We recently showed the high stability of (PLL/HA) films after drying, long-term storage and sterilization. This was a good starting point but more studies are required in view of a possible clinical application of these films as carriers for BMP-2. Importantly we didn't explore yet if the films/coatings remain at the surface of a material after implantation. It would be of high importance to show that for example a (PLL/HA)-coated screw could be inserted in bone without removing the coating from the surface of the implant. The film

resistance to wear (by abrasion or friction) and the adhesion of film onto different materials could be qualified by tribological methods. A scratch tester or a nanotribometer could be used to evaluate the film wear under different loading conditions. Of note, such techniques are not always easily applied to soft and thin polymeric coatings.

### ***In vivo experiments in bone critical defects***

The osteoinductive properties in ectopic site of BMP-2 loaded films on ceramics (Crouzier et al., 2011b) and on Ti6AV scaffolds (Chapter IV of this thesis, (Guillot et al., 2013)) was evidenced by the group. It remains to investigate whether the BMP-2 loaded films are able to induce bone in a bone site. The induction of bone formation in a critical sized defect by the presentation of BMP-2 from the films would be a very important proof of concept. To do so, the group has recently started a collaboration with the team of Georges Bettega who is the head of maxillofacial surgery department in Grenoble hospital. Thanks to Michael Bouyer, a master student working with Professor Bettega, experiments in a critical sized rat femoral defect model are ongoing (Brown et al., 2011; Sato et al., 2014). The selected biomaterial to support the film is a synthetic membrane made of the poly(lactic-co-glycolic acid) (PLGA), already widely used in maxillofacial surgery (Potter et al., 2012). In a next step, another important investigation would be to work on a larger animal model in critical size defect on minipig, goat or sheep for example. Finally, if the osteoinductive properties of the films are proved, a long term perspective could be to launch clinical trials on humans.

### ***Relation between BMP-2/BMP receptors endocytosis and BMP signaling***

In this PhD thesis we started to answer to some questions regarding the importance of BMP-2 endocytosis and proteins such as clathrin, caveolin-1 and dynamin-2 on the activation of BMP signaling in presence of matrix-bound BMP-2. It is unclear if BMP-2 endocytosis is required to activate BMP-2 signaling or if only the BMP receptors are needed in the process. It is difficult to fully separate their respective roles in the BMP-2 signaling since it is difficult to block endocytosis of BMP-2 without disturbing BMP receptors location and uptake since they are internalized by the same endocytic pathways. We were able to visualize the internalization of fluorescently-labeled BMP-2 by C2C12 cells but unfortunately we did not achieve to visualize BMP receptors internalization. To visualize BMP receptors inside the cells we tried to perform immunofluorescence labeling of receptors. We have tried antibodies against BMPR-Ia and BMPR-II from Santa Cruz Biotechnology but preliminary results

showed that the specificity of the antibodies to receptors was low. Thus, we could not show if BMP receptors are internalized with BMP-2.

This remains an important question since it is unclear if BMP-2 and/or BMP receptors endocytosis is required to activate BMP-2 signaling. To our knowledge, there are no studies where they investigate both BMP-2 and BMP receptors internalization. Importantly, in the literature we perceive that the labeling of receptors is very often performed in an ‘indirect’ form. As an example, *Knaus and coworkers* have transfected cells with tagged BMP receptors thus visualizing the BMP receptors by the labeling of the tag (Nohe et al., 2002). This method could also be adopted in the future by the group to visualize BMP receptors in fluorescence and explore their presence inside BMP-2 vesicles.

#### ***(PLL/HA) films as reservoir for other bioactive molecules***

(PLL/HA) films were shown to be a protective carrier and to present BMP-2 to cells inducing bone formation. These films could be used as reservoir for other types of active molecules which would broaden their applications. We observed for BMP-2 that the loading inside the films does not change protein structure neither bioactivity even after drying of films. We think that the hyaluronan in the film provides a water-rich environment which is essential to maintain the activity of proteins. We can imagine that other BMPs could be loaded and presented from these films for bone or other tissues regeneration. Some preliminary studies aiming to load BMP-7 inside (PLL/HA) films are being performed by the group. Another possibility would be to load BMP-2 and other active molecule both in the same film. Angiogenic factors and/or antibacterial drugs appear as interesting candidates. The addition of angiogenic factors to the film would improve vascularization which a challenge in 3D scaffold structures and the antibacterial drugs would limit the biomaterial-associated bacterial infections that are common and challenging complications in the field.



## Bibliographic references

- Abbatiello, S.E., and T.J. Porter. 1997. Anion-mediated precipitation of human recombinant protein 2 (Rh-BMP2) is dependent upon the heparin binding N-terminal region. *Protein Science*. poster presentation, Protein Society Meeting Boston:99.
- Alborzinia, H., H. Schmidt-Glenewinkel, I. Ilkavets, K. Breilkopf-Heinlein, X. Cheng, P. Hortschansky, S. Dooley, and S. Wolf. 2013. Quantitative kinetics analysis of BMP2 uptake into cells and its modulation by BMP antagonists. *J Cell Sci*. 126:117-127.
- Albrektsson, T. 1998. Hydroxyapatite-coated implants: a case against their use. *J Oral Maxillofac Surg*. 56:1312-1326.
- Albrektsson, T., P.I. Branemark, H.A. Hansson, and J. Lindstrom. 1981. Osseointegrated titanium implants. Requirements for ensuring a long-lasting, direct bone-to-implant anchorage in man. *Acta Orthop Scand*. 52:155-170.
- Albrektsson, T., and C. Johansson. 2001. Osteoinduction, osteoconduction and osseointegration. *Eur Spine J*. 10 Suppl 2:S96-101.
- Amini, A.R., C.T. Laurencin, and S.P. Nukavarapu. 2012. Bone tissue engineering: recent advances and challenges. *Crit Rev Biomed Eng*. 40:363-408.
- Antipov, A.A., and G.B. Sukhorukov. 2004. Polyelectrolyte multilayer capsules as vehicles with tunable permeability. *Adv Colloid Interface Sci*. 111:49-61.
- Barth, A. 2007. Infrared spectroscopy of proteins. *Biochim Biophys Acta*. 1767:1073-1101.
- Barth, A., and C. Zscherp. 2002. What vibrations tell us about proteins. *Q Rev Biophys*. 35:369-430.
- Bauer, T.W., and G.F. Muschler. 2000. Bone graft materials. An overview of the basic science. *Clin Orthop Relat Res*:10-27.
- Becker, A.L., A.P. Johnston, and F. Caruso. 2010. Layer-by-layer-assembled capsules and films for therapeutic delivery. *Small*. 6:1836-1852.
- Becker, J., A. Kirsch, F. Schwarz, M. Chatzinikolaidou, D. Rothamel, V. Lekovic, M. Laub, and H.P. Jennissen. 2006. Bone apposition to titanium implants biocoated with recombinant human bone morphogenetic protein-2 (rhBMP-2). A pilot study in dogs. *Clin Oral Investig*. 10:217-224.
- Berg, M.C., S.Y. Yang, P.T. Hammond, and M.F. Rubner. 2004. Controlling mammalian cell interactions on patterned polyelectrolyte multilayer surfaces. *Langmuir*. 20:1362-1368.
- Bhakta, G., Z.X. Lim, B. Rai, T. Lin, J.H. Hui, G.D. Prestwich, A.J. van Wijnen, V. Nurcombe, and S.M. Cool. 2013. The influence of collagen and hyaluronan matrices on the delivery and bioactivity of bone morphogenetic protein-2 and ectopic bone formation. *Acta Biomater*. 9:9098-9106.
- Blau, H.M., C.P. Chiu, and C. Webster. 1983. Cytoplasmic activation of human nuclear genes in stable heterocaryons. *Cell*. 32:1171-1180.
- Bohner, M., U. Gbureck, and J.E. Barralet. 2005. Technological issues for the development of more efficient calcium phosphate bone cements: A critical assessment. *Biomaterials*. 26:6423-6429.
- Bonor, J., E.L. Adams, B. Bragdon, O. Moseychuk, K.J. Czymmek, and A. Nohe. 2012. Initiation of BMP2 signaling in domains on the plasma membrane. *J Cell Physiol*. 227:2880-2888.
- Boudou, T., T. Crouzier, K. Ren, G. Blin, and C. Picart. 2010. Multiple functionalities of polyelectrolyte multilayer films: new biomedical applications. *Adv Mater*. 22:441-467.
- Boutin, P. 1972. Total arthroplasty of the hip by fritted alumina prosthesis. Experimental study and 1st clinical applications. *Orthop Traumatol Surg Res*. 100:15-21.

- Boyan, B.D., and Z. Schwartz. 2011. Regenerative medicine: Are calcium phosphate ceramics 'smart' biomaterials? *Nat Rev Rheumatol*. 7:8-9.
- Bragdon, B., A. D'Angelo, L. Gurski, J. Bonor, K.L. Schultz, W.G. Beamer, C.J. Rosen, and A. Nohe. 2012. Altered plasma membrane dynamics of bone morphogenetic protein receptor type Ia in a low bone mass mouse model. *Bone*. 50:189-199.
- Breier, G., M. Clauss, and W. Risau. 1995. Coordinate expression of vascular endothelial growth factor receptor-1 (flt-1) and its ligand suggests a paracrine regulation of murine vascular development. *Dev Dyn*. 204:228-239.
- Brennan, M., J.M. Davaine, and P. Layrolle. 2013. Pre-vascularization of bone tissue-engineered constructs. *Stem Cell Res Ther*. 4:96.
- Brown, K.V., B. Li, T. Guda, D.S. Perrien, S.A. Guelcher, and J.C. Wenke. 2011. Improving bone formation in a rat femur segmental defect by controlling bone morphogenetic protein-2 release. *Tissue Eng Part A*. 17:1735-1746.
- Bruker. Booklet Bruker Optics Booklet Bruker Optics
- Burkoth, A.K., J. Burdick, and K.S. Anseth. 2000. Surface and bulk modifications to photocrosslinked polyanhydrides to control degradation behavior. *J Biomed Mater Res*. 51:352-359.
- Burkus, J.K., H.S. Sandhu, and M.F. Gornet. 2006. Influence of rhBMP-2 on the healing patterns associated with allograft interbody constructs in comparison with autograft. *Spine J*. 31:775-781.
- Carragee, E.J., E.L. Hurwitz, and B.K. Weiner. 2011. A critical review of recombinant human bone morphogenetic protein-2 trials in spinal surgery: emerging safety concerns and lessons learned. *Spine J*. 11:471-491.
- Ceresa, B.P., and S.L. Schmid. 2000. Regulation of signal transduction by endocytosis. *Curr Opin Cell Biol*. 12:204-210.
- Chai, Y.C., A. Carlier, J. Bolander, S.J. Roberts, L. Geris, J. Schrooten, H. Van Oosterwyck, and F.P. Luyten. 2012. Current views on calcium phosphate osteogenicity and the translation into effective bone regeneration strategies. *Acta Biomater*. 8:3876-3887.
- Chatzinikolaïdou, M., T.K. Lichtinger, R.T. Muller, and H.P. Jennissen. 2010. Peri-implant reactivity and osteoinductive potential of immobilized rhBMP-2 on titanium carriers. *Acta Biomater*. 6:4405-4421.
- Chen, Y.G. 2009. Endocytic regulation of TGF-beta signaling. *Cell Res*. 19:58-70.
- Cheng, H., W. Jiang, F.M. Phillips, R.C. Haydon, Y. Peng, L. Zhou, H.H. Luu, N. An, B. Breyer, P. Vanichakarn, J.P. Szatkowski, J.Y. Park, and T.C. He. 2003. Osteogenic activity of the fourteen types of human bone morphogenetic proteins (BMPs). *J Bone Joint Surg Am*. 85-A:1544-1552.
- Chetprayoon, P., K. Kadowaki, M. Matsusaki, and M. Akashi. 2013. Survival and structural evaluations of three-dimensional tissues fabricated by the hierarchical cell manipulation technique. *Acta Biomater*. 9:4698-4706.
- Ciapetti, G., L. Ambrosio, G. Marletta, N. Baldini, and A. Giunti. 2006. Human bone marrow stromal cells: In vitro expansion and differentiation for bone engineering. *Biomaterials*. 27:6150-6160.
- Conner, S.D., and S.L. Schmid. 2003. Regulated portals of entry into the cell. *Nature*. 422:37-44.
- Cordonnier, T., A. Langonne, P. Corre, A. Renaud, L. Sensebe, P. Rosset, P. Layrolle, and J. Sohier. 2014. Osteoblastic differentiation and potent osteogenicity of three-dimensional hBMSC-BCP particle constructs. *J Tissue Eng Regen Med*. 8:364-376.
- Crouzier, T. 2010. Films Multicouches à base de polysaccharides: étude de la composition interne et délivrance du facteur de croissance BMP-2. Vol. PhD. Université de Montpellier II.

- Crouzier, T., L. Fourel, T. Boudou, C. Albiges-Rizo, and C. Picart. 2011a. Presentation of BMP-2 from a soft biopolymeric film unveils its activity on cell adhesion and migration. *Adv Mater.* 23:H111-118.
- Crouzier, T., and C. Picart. 2009. Ion pairing and hydration in polyelectrolyte multilayer films containing polysaccharides. *Biomacromolecules.* 10:433-442.
- Crouzier, T., K. Ren, C. Nicolas, C. Roy, and C. Picart. 2009. Layer-by-Layer films as a biomimetic reservoir for rhBMP-2 delivery: controlled differentiation of myoblasts to osteoblasts. *Small.* 5:598-608.
- Crouzier, T., F. Sailhan, P. Becquart, R. Guillot, D. Logeart-Avramoglou, and C. Picart. 2011b. The performance of BMP-2 loaded TCP/HAP porous ceramics with a polyelectrolyte multilayer film coating. *Biomaterials.* 32:7543-7554.
- Crouzier, T., A. Szarpak, T. Boudou, R. Auzely-Velty, and C. Picart. 2010. Polysaccharide-blend multilayers containing hyaluronan and heparin as a delivery system for rhBMP-2. *Small.* 6:651-662.
- Daculsi, G., O. Laboux, O. Malard, and P. Weiss. 2003. Current state of the art of biphasic calcium phosphate bioceramics. *J Mater Sci Mater Med.* 14:195-200.
- Daculsi, G., R.Z. LeGeros, E. Nery, K. Lynch, and B. Kerebel. 1989. Transformation of biphasic calcium phosphate ceramics in vivo: ultrastructural and physicochemical characterization. *J Biomed Mater Res.* 23:883-894.
- Danino, D., and J.E. Hinshaw. 2001. Dynamin family of mechanoenzymes. *Curr Opin Cell Biol.* 13:454-460.
- Daopin, S., K.A. Piez, Y. Ogawa, and D.R. Davies. 1992. Crystal structure of transforming growth factor-beta 2: an unusual fold for the superfamily. *Science.* 257:369-373.
- Davies, J.E. 2003. Understanding peri-implant endosseous healing. *J Dent Educ.* 67:932-949.
- de Groot, K., R. Geesink, C.P. Klein, and P. Serekian. 1987. Plasma sprayed coatings of hydroxylapatite. *J Biomed Mater Res.* 21:1375-1381.
- de Groot, K., J.G. Wolke, and J.A. Jansen. 1998. Calcium phosphate coatings for medical implants. *Proc Inst Mech Eng H.* 212:137-147.
- Decher, G. 1997. Fuzzy Nanoassemblies: Toward Layered Polymeric Multicomposites. *Science.* 277:1232-1237.
- Decher, G., J.D. Hong, and J. Schmitt. 1992. Buildup of ultrathin multilayer films by a self-assembly process: III. Consecutively alternating adsorption of anionic and cationic polyelectrolytes on charged surfaces. *Thin Solid Films.* 210-211, Part 2:831-835.
- Detzel, C.J., A.L. Larkin, and P. Rajagopalan. 2011. Polyelectrolyte multilayers in tissue engineering. *Tissue Eng Part B Rev.* 17:101-113.
- Di Guglielmo, G.M., C. Le Roy, A.F. Goodfellow, and J.L. Wrana. 2003. Distinct endocytic pathways regulate TGF-beta receptor signalling and turnover. *Nat Cell Biol.* 5:410-421.
- Dierich, A., E. Le Guen, N. Messaddeq, S. Stoltz, P. Netter, P. Schaaf, J.-C. Voegel, and N. Benkirane-Jessel. 2007. Bone formation mediated by synergy-acting growth factors embedded in a polyelectrolyte multilayer film. *Adv Mater.* 19:693-697.
- Doherty, G.J., and H.T. McMahon. 2009. Mechanisms of endocytosis. *Annu Rev Biochem.* 78:857-902.
- Du, J., X. Chen, X. Liang, G. Zhang, J. Xu, L. He, Q. Zhan, X.Q. Feng, S. Chien, and C. Yang. 2011. Integrin activation and internalization on soft ECM as a mechanism of induction of stem cell differentiation by ECM elasticity. *Proc Natl Acad Sci U S A.* 108:9466-9471.
- Dumbleton, J., and M.T. Manley. 2004. Hydroxyapatite-coated prostheses in total hip and knee arthroplasty. *J Bone Joint Surg Am.* 86-A:2526-2540.

- Ehata, S., Y. Yokoyama, K. Takahashi, and K. Miyazono. 2013. Bi-directional roles of bone morphogenetic proteins in cancer: another molecular Jekyll and Hyde? *Pathol Int.* 63:287-296.
- Elbashir, S.M., J. Harborth, W. Lendeckel, A. Yalcin, K. Weber, and T. Tuschl. 2001. Duplexes of 21-nucleotide RNAs mediate RNA interference in cultured mammalian cells. *Nature.* 411:494-498.
- Facca, S., C. Cortez, C. Mendoza-Palomares, N. Messadeq, A. Dierich, A.P. Johnston, D. Mainard, J.C. Voegel, F. Caruso, and N. Benkirane-Jessel. 2010. Active multilayered capsules for in vivo bone formation. *Proc Natl Acad Sci U S A.* 107:3406-3411.
- Fan, J., H. Park, M.K. Lee, O. Bezouglaia, A. Fartash, J. Kim, T. Aghaloo, and M. Lee. 2014. Adipose-Derived Stem Cells and BMP-2 Delivery in Chitosan-Based 3D Constructs to Enhance Bone Regeneration in a Rat Mandibular Defect Model. *Tissue Eng Part A.* 20:2169-2179.
- Ferraris, S., G. Pan, C. Cassinelli, L. Mazzucco, E. Verne, and S. Spriano. 2012. Effects of sterilization and storage on the properties of ALP-grafted biomaterials for prosthetic and bone tissue engineering applications. *Biomed Mater.* 7:054102.
- Fleming, J.E., Jr., C.N. Cornell, and G.F. Muschler. 2000. Bone cells and matrices in orthopedic tissue engineering. *Orthop Clin North Am.* 31:357-374.
- Fourel, L. 2012. Synergic action between BMP receptors and integrins on SMAD signaling and mechanotransduction Université de Grenoble.
- Freeman, M.A. 1992. Hydroxyapatite coating of prostheses. *J Bone Joint Surg Br.* 74:933-934.
- Frost, H.M. 2000. The Utah paradigm of skeletal physiology: an overview of its insights for bone, cartilage and collagenous tissue organs. *J Bone Miner Metab.* 18:305-316.
- Geesink, R.G. 1990. Hydroxyapatite-coated total hip prostheses. Two-year clinical and roentgenographic results of 100 cases. *Clin Orthop Relat Res:*39-58.
- Geetha, M., A.K. Singh, R. Asokamani, and A.K. Gogia. 2009. Ti based biomaterials, the ultimate choice for orthopaedic implants – A review. *Prog Mater Sci.* 54:397-425.
- Geiger, M., R.H. Li, and W. Friess. 2003. Collagen sponges for bone regeneration with rhBMP-2. *Adv Drug Deliv Rev.* 55:1613-1629.
- Gerstenfeld, L.C., D.M. Cullinane, G.L. Barnes, D.T. Graves, and T.A. Einhorn. 2003. Fracture healing as a post-natal developmental process: Molecular, spatial, and temporal aspects of its regulation. *J Cell Biochem.* 88:873-884.
- Ghodadra, N., and K. Singh. 2008. Recombinant human bone morphogenetic protein-2 in the treatment of bone fractures. *Biologics.* 2:345-354.
- Giannoudis, P.V., T.A. Einhorn, and D. Marsh. 2007. Fracture healing: the diamond concept. *Injury.* 38 Suppl 4:S3-6.
- Giannoudis, P.V., T.A. Einhorn, G. Schmidmaier, and D. Marsh. 2008. The diamond concept – open questions. *Injury.* 39 Suppl 2:S5-8.
- Gilboa, L., A. Nohe, T. Geissendorfer, W. Sebald, Y.I. Henis, and P. Knaus. 2000. Bone morphogenetic protein receptor complexes on the surface of live cells: a new oligomerization mode for serine/threonine kinase receptors. *Mol Biol Cell.* 11:1023-1035.
- Gittens, R.A., R. Olivares-Navarrete, Z. Schwartz, and B.D. Boyan. 2014. Implant osseointegration and the role of microroughness and nanostructures: lessons for spine implants. *Acta Biomater.* 10:3363-3371.
- Grellier, M., N. Ferreira-Tojais, C. Bourget, R. Bareille, F. Guillemot, and J. Amedee. 2009. Role of vascular endothelial growth factor in the communication between human osteoprogenitors and endothelial cells. *J Cell Biochem.* 106:390-398.

- Gribova, V., R. Auzely-Velty, and C. Picart. 2012. Polyelectrolyte Multilayer Assemblies on Materials Surfaces: From Cell Adhesion to Tissue Engineering. *Chem Mater.* 24:854-869.
- Griffiths P R, D.H.J.A. 2007. Fourier Transform Infrared Spectrometry. Wiley.
- Gruenberg, J. 2001. The endocytic pathway: a mosaic of domains. *Nat Rev Mol Cell Biol.* 2:721-730.
- Guillot, R., F. Gilde, P. Becquart, F. Sailhan, A. Lapeyrere, D. Logeart-Avramoglou, and C. Picart. 2013. The stability of BMP loaded polyelectrolyte multilayer coatings on titanium. *Biomaterials.* 34:5737-5746.
- Guillot, B., C. Bourget, M. Remy-Zolgadri, R. Bareille, P. Fernandez, V. Conrad, and J. Amedee-Vilamitjana. 2004. Human primary endothelial cells stimulate human osteoprogenitor cell differentiation. *Cell Physiol Biochem.* 14:325-332.
- Guzman, A., M. Zelman-Femiak, J.H. Boergermann, S. Paschkowsky, P.A. Kreuzaler, P. Fratzl, G.S. Harms, and P. Knaus. 2012. SMAD versus non-SMAD signaling is determined by lateral mobility of bone morphogenetic protein (BMP) receptors. *J Biol Chem.* 287:39492-39504.
- Hamilton, A.J., and D.C. Baulcombe. 1999. A species of small antisense RNA in posttranscriptional gene silencing in plants. *Science.* 286:950-952.
- Hanawa, T. 2010. Biofunctionalization of titanium for dental implant. *Jpn Dent Sci Rev.* 46:93-101.
- Hartung, A., K. Bitton-Worms, M.M. Rechtman, V. Wenzel, J.H. Boergermann, S. Hassel, Y.I. Henis, and P. Knaus. 2006. Different routes of bone morphogenic protein (BMP) receptor endocytosis influence BMP signaling. *Mol Cell Biol.* 26:7791-7805.
- Hasegawa, T., K. Taniguchi, and Y. Sato. 2009. Selection of modulation frequency of FT-IR equipped with an MCT detector for thin-film analysis. *Vibrat Spec.* 51:76-79.
- Hauburger, A., S. von Einem, G.K. Schwaerzer, A. Buttstedt, M. Zebisch, M. Schräml, P. Hortschansky, P. Knaus, and E. Schwarz. 2009. The pro-form of BMP-2 interferes with BMP-2 signalling by competing with BMP-2 for IA receptor binding. *FEBS J.* 276:6386-6398.
- Heinecke, K., A. Seher, W. Schmitz, T.D. Mueller, W. Sebald, and J. Nickel. 2009. Receptor oligomerization and beyond: a case study in bone morphogenetic proteins. *BMC Biol.* 7:59.
- Heining, E., R. Bhushan, P. Paarmann, Y.I. Henis, and P. Knaus. 2011. Spatial segregation of BMP/Smad signaling affects osteoblast differentiation in C2C12 cells. *PLoS One.* 6:e25163.
- Hench, L.L. 1991. Bioceramics: From Concept to Clinic. *J Am Ceram Soc.* 74:1487-1510.
- Hench, L.L. 2006. The story of Bioglass. *J Mater Sci Mater Med.* 17:967-978.
- Hermida, J.C., A. Bergula, F. Dimaano, M. Hawkins, C.W. Colwell, Jr., and D.D. D'Lima. 2010. An in vivo evaluation of bone response to three implant surfaces using a rabbit intramedullary rod model. *J Orthop Surg Res.* 5:57.
- Hillger, F., G. Herr, R. Rudolph, and E. Schwarz. 2005. Biophysical comparison of BMP-2, ProBMP-2, and the free pro-peptide reveals stabilization of the pro-peptide by the mature growth factor. *J Biol Chem.* 280:14974-14980.
- Hogan, B.L. 1996. Bone morphogenetic proteins: multifunctional regulators of vertebrate development. *Genes Dev.* 10:1580-1594.
- Holzappel, B.M., J.C. Reichert, J.T. Schantz, U. Gbureck, L. Rackwitz, U. Noth, F. Jakob, M. Rudert, J. Groll, and D.W. Hutmacher. 2013. How smart do biomaterials need to be? A translational science and clinical point of view. *Adv Drug Deliv Rev.* 65:581-603.
- Hunziker, E.B., L. Enggist, A. Kuffer, D. Buser, and Y. Liu. 2012. Osseointegration: the slow delivery of BMP-2 enhances osteoinductivity. *Bone.* 51:98-106.

- Ivanov, A.I. 2008. Exocytosis and endocytosis. Preface. *Methods Mol Biol.* 440:v-vi.
- Jaffe, W.L., and D.F. Scott. 1996. Total hip arthroplasty with hydroxyapatite-coated prostheses. *J Bone Joint Surg Am.* 78:1918-1934.
- Jan, E., and N.A. Kotov. 2007. Successful differentiation of mouse neural stem cells on layer-by-layer assembled single-walled carbon nanotube composite. *Nano Lett.* 7:1123-1128.
- Jawa, A., L. Shi, T. O'Brien, J. Wells, L. Higgins, J. Macy, and J.J. Warner. 2011. Prosthesis of antibiotic-loaded acrylic cement (PROSTALAC) use for the treatment of infection after shoulder arthroplasty. *J Bone Joint Surg Am.* 93:2001-2009.
- Jennissen, H.P. 1999. Method for immobilizing mediator molecules on inorganic and metal implant materials. Vol. WO9926674A2. E.P. Office, editor, Germany.
- Johansson, J.A., T. Halthur, M. Herranen, L. Soderberg, U. Elofsson, and J. Hilborn. 2005. Build-up of collagen and hyaluronic acid polyelectrolyte multilayers. *Biomacromolecules.* 6:1353-1359.
- Johansson, P., R. Jimbo, P. Kjellin, F. Currie, B.R. Chrcanovic, and A. Wennerberg. 2014. Biomechanical evaluation and surface characterization of a nano-modified surface on PEEK implants: a study in the rabbit tibia. *Int J Nanomedicine.* 9:3903-3911.
- Jones, J.R. 2013. Review of bioactive glass: from Hench to hybrids. *Acta Biomater.* 9:4457-4486.
- Jortikka, L., M. Laitinen, T.S. Lindholm, and A. Marttinen. 1997. Internalization and intracellular processing of bone morphogenetic protein (BMP) in rat skeletal muscle myoblasts (L6). *Cell Signal.* 9:47-51.
- Kasemo, B., and J. Lausmaa. 1988. Biomaterial and implant surfaces: on the role of cleanliness, contamination, and preparation procedures. *J Biomed Mater Res.* 22:145-158.
- Katagiri, T., A. Yamaguchi, M. Komaki, E. Abe, N. Takahashi, T. Ikeda, V. Rosen, J.M. Wozney, A. Fujisawa-Sehara, and T. Suda. 1994. Bone morphogenetic protein-2 converts the differentiation pathway of C2C12 myoblasts into the osteoblast lineage. *J Cell Biol.* 127:1755-1766.
- Katzmann, D.J., M. Babst, and S.D. Emr. 2001. Ubiquitin-Dependent Sorting into the Multivesicular Body Pathway Requires the Function of a Conserved Endosomal Protein Sorting Complex, ESCRT-I. *Cell.* 106:145-155.
- Kawabata, M., H. Inoue, A. Hanyu, T. Imamura, and K. Miyazono. 1998. Smad proteins exist as monomers in vivo and undergo homo- and hetero-oligomerization upon activation by serine/threonine kinase receptors. *EMBO J.* 17:4056-4065.
- Kim, H.D., and R.F. Valentini. 2002. Retention and activity of BMP-2 in hyaluronic acid-based scaffolds in vitro. *J Biomed Mater Res.* 59:573-584.
- Kim, S.E., S.H. Song, Y.P. Yun, B.J. Choi, I.K. Kwon, M.S. Bae, H.J. Moon, and Y.D. Kwon. 2011. The effect of immobilization of heparin and bone morphogenetic protein-2 (BMP-2) to titanium surfaces on inflammation and osteoblast function. *Biomaterials.* 32:366-373.
- Kirkpatrick, C.J., S. Fuchs, and R.E. Unger. 2011. Co-culture systems for vascularization--learning from nature. *Adv Drug Deliv Rev.* 63:291-299.
- Kisiel, M., M. Ventura, O.P. Oommen, A. George, X.F. Walboomers, J. Hilborn, and O.P. Varghese. 2012. Critical assessment of rhBMP-2 mediated bone induction: an in vitro and in vivo evaluation. *J Control Release.* 162:646-653.
- Knaus, P., and W. Sebald. 2001. Cooperativity of binding epitopes and receptor chains in the BMP/TGFbeta superfamily. *Biol Chem.* 382:1189-1195.

- Koenig, B.B., J.S. Cook, D.H. Wolsing, J. Ting, J.P. Tiesman, P.E. Correa, C.A. Olson, A.L. Pecquet, F. Ventura, R.A. Grant, and et al. 1994. Characterization and cloning of a receptor for BMP-2 and BMP-4 from NIH 3T3 cells. *Mol Cell Biol.* 14:5961-5974.
- Kokubo, T., H.M. Kim, M. Kawashita, and T. Nakamura. 2001. Process of calcification on artificial materials. *Z Kardiol.* 90 Suppl 3:86-91.
- Kurtz, S.M., and J.N. Devine. 2007. PEEK biomaterials in trauma, orthopedic, and spinal implants. *Biomaterials.* 28:4845-4869.
- Langer, R., and J.P. Vacanti. 1993. Tissue engineering. *Science.* 260:920-926.
- Le Guehennec, L., A. Soueidan, P. Layrolle, and Y. Amouriq. 2007. Surface treatments of titanium dental implants for rapid osseointegration. *Dent Mater.* 23:844-854.
- Lee, K.Y., and D.J. Mooney. 2001. Hydrogels for tissue engineering. *Chem Rev.* 101:1869-1879.
- Lee, W.H., C.Y. Loo, and R. Rohanzadeh. 2014. A review of chemical surface modification of bioceramics: Effects on protein adsorption and cellular response. *Colloids Surf B Biointerfaces.*
- Leguen, E., A. Chassepot, G. Decher, P. Schaaf, J.C. Voegel, and N. Jessel. 2007. Bioactive coatings based on polyelectrolyte multilayer architectures functionalized by embedded proteins, peptides or drugs. *Biomol Eng.* 24:33-41.
- Li, H., R. Daculsi, M. Grellier, R. Bareille, C. Bourget, and J. Amedee. 2010. Role of neural-cadherin in early osteoblastic differentiation of human bone marrow stromal cells cocultured with human umbilical vein endothelial cells. *Am J Physiol Cell Physiol.* 299:C422-430.
- Li, H., R. Daculsi, M. Grellier, R. Bareille, C. Bourget, M. Remy, and J. Amedee. 2011. The role of vascular actors in two dimensional dialogue of human bone marrow stromal cell and endothelial cell for inducing self-assembled network. *PLoS One.* 6:e16767.
- Lim, T.Y., W. Wang, Z. Shi, C.K. Poh, and K.G. Neoh. 2009. Human bone marrow-derived mesenchymal stem cells and osteoblast differentiation on titanium with surface-grafted chitosan and immobilized bone morphogenetic protein-2. *J Mater Sci Mater Med.* 20:1-10.
- Liu, X., Y. Guan, Z. Ma, and H. Liu. 2004. Surface modification and characterization of magnetic polymer nanospheres prepared by miniemulsion polymerization. *Langmuir.* 20:10278-10282.
- Liu, Y., K. de Groot, and E.B. Hunziker. 2005. BMP-2 liberated from biomimetic implant coatings induces and sustains direct ossification in an ectopic rat model. *Bone.* 36:745-757.
- Liu, Y., L. Enggist, A.F. Kuffer, D. Buser, and E.B. Hunziker. 2007. The influence of BMP-2 and its mode of delivery on the osteoconductivity of implant surfaces during the early phase of osseointegration. *Biomaterials.* 28:2677-2686.
- Logeart-Avramoglou, D., M. Bourguignon, K. Oudina, P. Ten Dijke, and H. Petite. 2006. An assay for the determination of biologically active bone morphogenetic proteins using cells transfected with an inhibitor of differentiation promoter-luciferase construct. *Anal Biochem.* 349:78-86.
- Lord, C.F., M.C. Gebhardt, W.W. Tomford, and H.J. Mankin. 1988. Infection in bone allografts. Incidence, nature, and treatment. *J Bone Joint Surg Am.* 70:369-376.
- Lucarelli, E., D. Donati, A. Cenacchi, and P.M. Fornasari. 2004. Bone reconstruction of large defects using bone marrow derived autologous stem cells. *Transfus Apher Sci.* 30:169-174.
- Lvov, Y., G. Decher, H. Haas, H. Möhwald, and A. Kalachev. 1994. X-ray analysis of ultrathin polymer films self-assembled onto substrates. *Physica B.* 198:89-91.

- Macdonald, M.L., R.E. Samuel, N.J. Shah, R.F. Padera, Y.M. Beben, and P.T. Hammond. 2011. Tissue integration of growth factor-eluting layer-by-layer polyelectrolyte multilayer coated implants. *Biomaterials*. 32:1446-1453.
- Martinez-Sanz, E., D.A. Ossipov, J. Hilborn, S. Larsson, K.B. Jonsson, and O.P. Varghese. 2011. Bone reservoir: Injectable hyaluronic acid hydrogel for minimal invasive bone augmentation. *J Control Release*. 152:232-240.
- Martino, M.M., P.S. Briquez, E. Guc, F. Tortelli, W.W. Kilarski, S. Metzger, J.J. Rice, G.A. Kuhn, R. Muller, M.A. Swartz, and J.A. Hubbell. 2014. Growth factors engineered for super-affinity to the extracellular matrix enhance tissue healing. *Science*. 343:885-888.
- Mason, C., and P. Dunnill. 2008. A brief definition of regenerative medicine. *Regen Med*. 3:1-5.
- Masri, B.A., C.P. Duncan, and C.P. Beauchamp. 1998. Long-term elution of antibiotics from bone-cement: an in vivo study using the prosthesis of antibiotic-loaded acrylic cement (PROSTALAC) system. *J Arthroplasty*. 13:331-338.
- Massague, J. 1998. TGF-beta signal transduction. *Annu Rev Biochem*. 67:753-791.
- Massey, L. 2005. The Effect of Sterilization Methods on Plastics and Elastomers. William Andrew, Inc.
- Matassi, F., L. Nistri, D. Chicon Paez, and M. Innocenti. 2011. New biomaterials for bone regeneration. *Clin Cases Miner Bone Metab*. 8:21-24.
- Matsusaki, M., K. Kadowaki, Y. Nakahara, and M. Akashi. 2007. Fabrication of cellular multilayers with nanometer-sized extracellular matrix films. *Angew Chem Int Ed Engl*. 46:4689-4692.
- Mauney, J.R., V. Volloch, and D.L. Kaplan. 2005. Role of adult mesenchymal stem cells in bone tissue engineering applications: current status and future prospects. *Tissue Eng*. 11:787-802.
- Mayor, S., and R.E. Pagano. 2007. Pathways of clathrin-independent endocytosis. *Nat Rev Mol Cell Biol*. 8:603-612.
- Mayor, S., R.G. Parton, and J.G. Donaldson. 2014. Clathrin-Independent Pathways of Endocytosis. *Cold Spring Harb Perspect Biol*. 6.
- McClellan, J.W., D.S. Mulconrey, R.J. Forbes, and N. Fullmer. 2006. Vertebral bone resorption after transforaminal lumbar interbody fusion with bone morphogenetic protein (rhBMP-2). *J Spinal Disord Tech*. 19:483-486.
- Meyer, U., and H.P. Wiesmann. 2006. Bone and Cartilage Engineering. Springer.
- Mitchell, H., A. Choudhury, R.E. Pagano, and E.B. Leof. 2004. Ligand-dependent and -independent transforming growth factor-beta receptor recycling regulated by clathrin-mediated endocytosis and Rab11. *Mol Biol Cell*. 15:4166-4178.
- Miyazono, K., S. Maeda, and T. Imamura. 2005. BMP receptor signaling: transcriptional targets, regulation of signals, and signaling cross-talk. *Cytokine Growth Factor Rev*. 16:251-263.
- Mohammadi, S., M. Esposito, J. Hall, L. Emanuelsson, A. Krozer, and P. Thomsen. 2003. Short-term bone response to titanium implants coated with thin radiofrequency magnetron-sputtered hydroxyapatite in rabbits. *Clin Implant Dent Relat Res*. 5:241-253.
- Mohammadi, S., M. Esposito, J. Hall, L. Emanuelsson, A. Krozer, and P. Thomsen. 2004. Long-term bone response to titanium implants coated with thin radiofrequency magnetron-sputtered hydroxyapatite in rabbits. *Int J Oral Maxillofac Implants*. 19:498-509.
- Mueller, T.D., and J. Nickel. 2012. Promiscuity and specificity in BMP receptor activation. *FEBS Lett*. 586:1846-1859.



- Namiki, M., S. Akiyama, T. Katagiri, A. Suzuki, N. Ueno, N. Yamaji, V. Rosen, J.M. Wozney, and T. Suda. 1997. A kinase domain-truncated type I receptor blocks bone morphogenetic protein-2-induced signal transduction in C2C12 myoblasts. *J Biol Chem.* 272:22046-22052.
- Navarro, M., A. Michiardi, O. Castano, and J.A. Planell. 2008. Biomaterials in orthopaedics. *J R Soc Interface.* 5:1137-1158.
- Nohe, A., S. Hassel, M. Ehrlich, F. Neubauer, W. Sebald, Y.I. Henis, and P. Knaus. 2002. The mode of bone morphogenetic protein (BMP) receptor oligomerization determines different BMP-2 signaling pathways. *J Biol Chem.* 277:5330-5338.
- Nohe, A., E. Keating, T.M. Underhill, P. Knaus, and N.O. Petersen. 2005. Dynamics and interaction of caveolin-1 isoforms with BMP-receptors. *J Cell Sci.* 118:643-650.
- Nowinski, R.J., R.J. Gillespie, Y. Shishani, B. Cohen, G. Walch, and R. Gobezie. 2012. Antibiotic-loaded bone cement reduces deep infection rates for primary reverse total shoulder arthroplasty: a retrospective, cohort study of 501 shoulders. *J Shoulder Elbow Surg.* 21:324-328.
- Oliveira, J.M., N. Kotobuki, M. Tadokoro, M. Hirose, J.F. Mano, R.L. Reis, and H. Ohgushi. 2010. Ex vivo culturing of stromal cells with dexamethasone-loaded carboxymethylchitosan/poly(amidoamine) dendrimer nanoparticles promotes ectopic bone formation. *Bone.* 46:1424-1435.
- Oliveira, J.M., R.A. Sousa, N. Kotobuki, M. Tadokoro, M. Hirose, J.F. Mano, R.L. Reis, and H. Ohgushi. 2009. The osteogenic differentiation of rat bone marrow stromal cells cultured with dexamethasone-loaded carboxymethylchitosan/poly(amidoamine) dendrimer nanoparticles. *Biomaterials.* 30:804-813.
- Oliveira, J.M., R.A. Sousa, P.B. Malafaya, S.S. Silva, N. Kotobuki, M. Hirose, H. Ohgushi, J.F. Mano, and R.L. Reis. 2011. In vivo study of dendronlike nanoparticles for stem cells "tune-up": from nano to tissues. *Nanomedicine.* 7:914-924.
- Olugebefola, S.C., S.W. Ryu, A.J. Nolte, M.F. Rubner, and A.M. Mayes. 2006. Photo-cross-linkable polyelectrolyte multilayers for 2-D and 3-D patterning. *Langmuir.* 22:5958-5962.
- Oshina, H., S. Sotome, T. Yoshii, I. Torigoe, Y. Sugata, H. Maehara, E. Marukawa, K. Omura, and K. Shinomiya. 2007. Effects of continuous dexamethasone treatment on differentiation capabilities of bone marrow-derived mesenchymal cells. *Bone.* 41:575-583.
- Palmquist, A., O.M. Omar, M. Esposito, J. Lausmaa, and P. Thomsen. 2010. Titanium oral implants: surface characteristics, interface biology and clinical outcome. *J R Soc Interface.* 7 Suppl 5:S515-527.
- Patel, N., S.M. Best, W. Bonfield, I.R. Gibson, K.A. Hing, E. Damien, and P.A. Revell. 2002. A comparative study on the in vivo behavior of hydroxyapatite and silicon substituted hydroxyapatite granules. *J Mater Sci Mater Med.* 13:1199-1206.
- Paul, W., and C.P. Sharma. 2003. Ceramic drug delivery: a perspective. *J Biomater Appl.* 17:253-264.
- Phelps, E.A., N. Landazuri, P.M. Thule, W.R. Taylor, and A.J. Garcia. 2010. Bioartificial matrices for therapeutic vascularization. *Proc Natl Acad Sci U S A.* 107:3323-3328.
- Picart, C., A. Schneider, O. Etienne, J. Mutterer, P. Schaaf, C. Egles, N. Jessel, and J.C. Voegel. 2005. Controlled Degradability of Polysaccharide Multilayer Films In Vitro and In Vivo. *Adv Funct Mater.* 15:1771-1780.
- Pohl, T.L., E.H. Schwab, and E.A. Cavalcanti-Adam. 2013. Covalent binding of BMP-2 on surfaces using a self-assembled monolayer approach. *J Vis Exp.*
- Potter, J.K., M. Malmquist, and E. Ellis, 3rd. 2012. Biomaterials for reconstruction of the internal orbit. *Oral Maxillofac Surg Clin North Am.* 24:609-627.

- Ramay, H.R., and M. Zhang. 2004. Biphasic calcium phosphate nanocomposite porous scaffolds for load-bearing bone tissue engineering. *Biomaterials*. 25:5171-5180.
- Ratner, B.D. 2004. Biomaterials science : an introduction to materials in medicine. Elsevier Academic Press, Amsterdam; Boston.
- Reppenhagen, S., J.C. Reichert, L. Rackwitz, M. Rudert, P. Raab, G. Daculsi, and U. Noth. 2012. Biphasic bone substitute and fibrin sealant for treatment of benign bone tumours and tumour-like lesions. *Int Orthop*. 36:139-148.
- Rho, J.Y., L. Kuhn-Spearing, and P. Zioupos. 1998. Mechanical properties and the hierarchical structure of bone. *Med Eng Phys*. 20:92-102.
- Rice, C.M., and N.J. Scolding. 2008. Autologous bone marrow stem cells--properties and advantages. *J Neurol Sci*. 265:59-62.
- Richert, L., F. Boulmedais, P. Lavalle, J. Mutterer, E. Ferreux, G. Decher, P. Schaaf, J.C. Voegel, and C. Picart. 2004. Improvement of stability and cell adhesion properties of polyelectrolyte multilayer films by chemical cross-linking. *Biomacromolecules*. 5:284-294.
- Rickard, D.J., T.A. Sullivan, B.J. Shenker, P.S. Leboy, and I. Kazhdan. 1994. Induction of rapid osteoblast differentiation in rat bone marrow stromal cell cultures by dexamethasone and BMP-2. *Dev Biol*. 161:218-228.
- Roberts, S.J., L. Geris, G. Kerckhofs, E. Desmet, J. Schrooten, and F.P. Luyten. 2011. The combined bone forming capacity of human periosteal derived cells and calcium phosphates. *Biomaterials*. 32:4393-4405.
- Robinson, R.A. 1952. An electron-microscopic study of the crystalline inorganic component of bone and its relationship to the organic matrix. *J Bone Joint Surg Am*. 34-A:389-435; passim.
- Rokkum, M., A. Reigstad, C.B. Johansson, and T. Albrektsson. 2003. Tissue reactions adjacent to well-fixed hydroxyapatite-coated acetabular cups. Histopathology of ten specimens retrieved at reoperation after 0.3 to 5.8 years. *J Bone Joint Surg Br*. 85:440-447.
- Rosset, P., F. Deschaseaux, and P. Layrolle. 2014. Cell therapy for bone repair. *Orthop Traumatol Surg Res*. 100:S107-112.
- Rouwkema, J., J. de Boer, and C.A. Van Blitterswijk. 2006. Endothelial cells assemble into a 3-dimensional prevascular network in a bone tissue engineering construct. *Tissue Eng*. 12:2685-2693.
- Sagomonyants, K.B., M.L. Jarman-Smith, J.N. Devine, M.S. Aronow, and G.A. Gronowicz. 2008. The in vitro response of human osteoblasts to polyetheretherketone (PEEK) substrates compared to commercially pure titanium. *Biomaterials*. 29:1563-1572.
- Saldanha, S., B. Bragdon, O. Moseychuk, J. Bonor, P. Dhurjati, and A. Nohe. 2013. Caveolae regulate Smad signaling as verified by novel imaging and system biology approaches. *J Cell Physiol*. 228:1060-1069.
- Salgado, A.J., J.M. Oliveira, A. Martins, F.G. Teixeira, N.A. Silva, N.M. Neves, N. Sousa, and R.L. Reis. 2013. Tissue engineering and regenerative medicine: past, present, and future. *Int Rev Neurobiol*. 108:1-33.
- Sato, K., Y. Watanabe, N. Harada, S. Abe, T. Matsushita, K. Yamanaka, T. Kaneko, and Y. Sakai. 2014. Establishment of Reproducible, Critical-Sized, Femoral Segmental Bone Defects in Rats. *Tissue Eng Part C Methods*.
- Scheufler, C., W. Sebald, and M. Hulsmeyer. 1999. Crystal structure of human bone morphogenetic protein-2 at 2.7 Å resolution. *J Mol Biol*. 287:103-115.
- Schliephake, H., A. Aref, D. Scharnweber, S. Bierbaum, S. Roessler, and A. Sewing. 2005. Effect of immobilized bone morphogenetic protein 2 coating of titanium implants on peri-implant bone formation. *Clin Oral Implants Res*. 16:563-569.

- Schmidmaier, G., P. Schwabe, C. Strobel, and B. Wildemann. 2008. Carrier systems and application of growth factors in orthopaedics. *Injury*. 39 Suppl 2:S37-43.
- Schmidt-Bleek, K., A. Petersen, A. Dienelt, C. Schwarz, and G.N. Duda. 2014. Initiation and early control of tissue regeneration - bone healing as a model system for tissue regeneration. *Expert Opin Biol Ther*. 14:247-259.
- Schneider, A., G. Francius, R. Obeid, P. Schwinte, J. Hemmerle, B. Frisch, P. Schaaf, J.C. Voegel, B. Senger, and C. Picart. 2006. Polyelectrolyte multilayers with a tunable Young's modulus: influence of film stiffness on cell adhesion. *Langmuir*. 22:1193-1200.
- Schwartz, D., S. Sofia, and W. Friess. 2006. Integrity and stability studies of precipitated rhBMP-2 microparticles with a focus on ATR-FTIR measurements. *Eur J Pharm Biopharm*. 63:241-248.
- Schwinte, P., V. Ball, B. Szalontai, Y. Haikel, J.C. Voegel, and P. Schaaf. 2002. Secondary structure of proteins adsorbed onto or embedded in polyelectrolyte multilayers. *Biomacromolecules*. 3:1135-1143.
- Schwinte, P., J.C. Voegel, C. Picart, Y. Haikel, P. Schaaf, and B. Szalontai. 2001. Stabilizing effects of various polyelectrolyte multilayer films on the structure of adsorbed/embedded fibrinogen molecules: An ATR-FTIR study. *J Phys Chem B*. 105:11906-11916.
- Seeherman, H., and J.M. Wozney. 2005. Delivery of bone morphogenetic proteins for orthopedic tissue regeneration. *Cytokine Growth Factor Rev*. 16:329-345.
- Seeman, E., and P.D. Delmas. 2006. Bone quality--the material and structural basis of bone strength and fragility. *N Engl J Med*. 354:2250-2261.
- Shah, N.J., M.N. Hyder, M.A. Quadir, N.M. Dorval Courchesne, H.J. Seeherman, M. Nevins, M. Spector, and P.T. Hammond. 2014. Adaptive growth factor delivery from a polyelectrolyte coating promotes synergistic bone tissue repair and reconstruction. *Proc Natl Acad Sci U S A*. 111:12847-12852.
- Shah, N.J., M.L. Macdonald, Y.M. Beben, R.F. Padera, R.E. Samuel, and P.T. Hammond. 2011. Tunable dual growth factor delivery from polyelectrolyte multilayer films. *Biomaterials*. 32:6183-6193.
- Shen, L., P. Chaudouet, J. Ji, and C. Picart. 2011. pH-Amplified multilayer films based on hyaluronan: influence of HA molecular weight and concentration on film growth and stability. *Biomacromolecules*. 12:1322-1331.
- Shiratori, S.S., and M.F. Rubner. 2000. pH-Dependent Thickness Behavior of Sequentially Adsorbed Layers of Weak Polyelectrolytes. *Macromolecules*. 33:4213-4219.
- Shore, E.M., and F.S. Kaplan. 2010. Inherited human diseases of heterotopic bone formation. *Nat Rev Rheumatol*. 6:518-527.
- Sieber, C., J. Kopf, C. Hiepen, and P. Knaus. 2009. Recent advances in BMP receptor signaling. *Cytokine Growth Factor Rev*. 20:343-355.
- Silber, J.S., D.G. Anderson, S.D. Daffner, B.T. Brislin, J.M. Leland, A.S. Hilibrand, A.R. Vaccaro, and T.J. Albert. 2003. Donor site morbidity after anterior iliac crest bone harvest for single-level anterior cervical discectomy and fusion. *Spine (Phila Pa 1976)*. 28:134-139.
- Simic, P., and S. Vukicevic. 2007. Bone morphogenetic proteins: from developmental signals to tissue regeneration. Conference on bone morphogenetic proteins. *EMBO Rep*. 8:327-331.
- Sohier, J., P. Corre, P. Weiss, and P. Layrolle. 2010. Hydrogel/calcium phosphate composites require specific properties for three-dimensional culture of human bone mesenchymal cells. *Acta Biomater*. 6:2932-2939.

- Sorkin, A., and M. von Zastrow. 2009. Endocytosis and signalling: intertwining molecular networks. *Nat Rev Mol Cell Biol.* 10:609-622.
- Srivastava, S., and N.A. Kotov. 2008. Composite Layer-by-Layer (LBL) assembly with inorganic nanoparticles and nanowires. *Acc Chem Res.* 41:1831-1841.
- Stevens, M.M. 2008. Biomaterials for bone tissue engineering. *Mater Today.* 11:18-25.
- Stevens, M.M., and J.H. George. 2005. Exploring and engineering the cell surface interface. *Science.* 310:1135-1138.
- ten Dijke, P., H. Yamashita, H. Ichijo, P. Franzen, M. Laiho, K. Miyazono, and C.H. Heldin. 1994a. Characterization of type I receptors for transforming growth factor-beta and activin. *Science.* 264:101-104.
- ten Dijke, P., H. Yamashita, T.K. Sampath, A.H. Reddi, M. Estevez, D.L. Riddle, H. Ichijo, C.H. Heldin, and K. Miyazono. 1994b. Identification of type I receptors for osteogenic protein-1 and bone morphogenetic protein-4. *J Biol Chem.* 269:16985-16988.
- Tsai, W.B., R.P. Chen, K.L. Wei, Y.R. Chen, T.Y. Liao, H.L. Liu, and J.Y. Lai. 2009. Polyelectrolyte multilayer films functionalized with peptides for promoting osteoblast functions. *Acta Biomater.* 5:3467-3477.
- Ulloa, R.M., J.P. Muschietti, M. Veron, H.N. Torres, and M.T. Tellez-Inon. 1995. Purification and characterization of a soluble nucleoside diphosphate kinase in *Trypanosoma cruzi*. *Mol Biochem Parasitol.* 70:119-129.
- Unger, R.E., S. Halstenberg, A. Sartoris, and C.J. Kirkpatrick. 2011. Human endothelial and osteoblast co-cultures on 3D biomaterials. *Methods Mol Biol.* 695:229-241.
- Unger, R.E., A. Sartoris, K. Peters, A. Motta, C. Migliaresi, M. Kunkel, U. Bulnheim, J. Rychly, and C.J. Kirkpatrick. 2007. Tissue-like self-assembly in cocultures of endothelial cells and osteoblasts and the formation of microcapillary-like structures on three-dimensional porous biomaterials. *Biomaterials.* 28:3965-3976.
- Urist, M.R. 1965. Bone: formation by autoinduction. *Science.* 150:893-899.
- van den Beucken, J.J., X.F. Walboomers, O.C. Boerman, M.R. Vos, N.A. Sommerdijk, T. Hayakawa, T. Fukushima, Y. Okahata, R.J. Nolte, and J.A. Jansen. 2006. Functionalization of multilayered DNA-coatings with bone morphogenetic protein 2. *J Control Release.* 113:63-72.
- Vazquez, C.P., T. Boudou, V. Dulong, C. Nicolas, C. Picart, and K. Glinel. 2009. Variation of polyelectrolyte film stiffness by photo-cross-linking: a new way to control cell adhesion. *Langmuir.* 25:3556-3563.
- Villars, F., B. Guillotin, T. Amedee, S. Dutoya, L. Bordenave, R. Bareille, and J. Amedee. 2002. Effect of HUVEC on human osteoprogenitor cell differentiation needs heterotypic gap junction communication. *Am J Physiol Cell Physiol.* 282:C775-785.
- von Einem, S., S. Erler, K. Bigl, B. Frerich, and E. Schwarz. 2011. The pro-form of BMP-2 exhibits a delayed and reduced activity when compared to mature BMP-2. *Growth Factors.* 29:63-71.
- Wagner, D.O., C. Sieber, R. Bhushan, J.H. Borgermann, D. Graf, and P. Knaus. 2010. BMPs: from bone to body morphogenetic proteins. *Sci Signal.* 3:mr1.
- Wang, E.A., V. Rosen, P. Cordes, R.M. Hewick, M.J. Kriz, D.P. Luxenberg, B.S. Sibley, and J.M. Wozney. 1988. Purification and characterization of other distinct bone-inducing factors. *Proc Natl Acad Sci U S A.* 85:9484-9488.
- Wang, K., C. Zhou, Y. Hong, and X. Zhang. 2012. A review of protein adsorption on bioceramics. *Interface Focus.* 2:259-277.
- Wang, W. 2005. Protein aggregation and its inhibition in biopharmaceutics. *Int J Pharm.* 289:1-30.
- Weiner, S., and H.D. Wagner. 1998. The Material Bone: Structure-Mechanical Function Relations. *Annu Rev Mater Sci.* 28:271-298.

- Wennerberg, A., and T. Albrektsson. 2009. Effects of titanium surface topography on bone integration: a systematic review. *Clin Oral Implants Res.* 20 Suppl 4:172-184.
- Wilson, J., G.H. Pigott, F.J. Schoen, and L.L. Hench. 1981. Toxicology and biocompatibility of bioglasses. *J Biomed Mater Res.* 15:805-817.
- Wilson, J.T., W. Cui, V. Kozlovskaya, E. Kharlampieva, D. Pan, Z. Qu, V.R. Krishnamurthy, J. Mets, V. Kumar, J. Wen, Y. Song, V.V. Tsukruk, and E.L. Chaikof. 2011. Cell surface engineering with polyelectrolyte multilayer thin films. *J Am Chem Soc.* 133:7054-7064.
- Wozney, J.M. 1992. The bone morphogenetic protein family and osteogenesis. *Mol Reprod Dev.* 32:160-167.
- Wozney, J.M., V. Rosen, A.J. Celeste, L.M. Mitsock, M.J. Whitters, R.W. Kriz, R.M. Hewick, and E.A. Wang. 1988. Novel regulators of bone formation: molecular clones and activities. *Science.* 242:1528-1534.
- Xia, W., C. Lindahl, J. Lausmaa, P. Borchardt, A. Ballo, P. Thomsen, and H. Engqvist. 2010. Biom mineralized strontium-substituted apatite/titanium dioxide coating on titanium surfaces. *Acta Biomater.* 6:1591-1600.
- Yaffe, D., and O. Saxel. 1977. Serial passaging and differentiation of myogenic cells isolated from dystrophic mouse muscle. *Nature.* 270:725-727.
- Yang, G.L., F.M. He, E. Song, J.A. Hu, X.X. Wang, and S.F. Zhao. 2010. In vivo comparison of bone formation on titanium implant surfaces coated with biomimetically deposited calcium phosphate or electrochemically deposited hydroxyapatite. *Int J Oral Maxillofac Implants.* 25:669-680.
- Yuan, H., H. Fernandes, P. Habibovic, J. de Boer, A.M. Barradas, W.R. Walsh, C.A. van Blitterswijk, and J.D. De Bruijn. 2011. 'Smart' biomaterials and osteoinductivity. *Nat Rev Rheumatol.* 7:c1; author reply c2.
- Zhang, H., J. Shih, J. Zhu, and N.A. Kotov. 2012. Layered nanocomposites from gold nanoparticles for neural prosthetic devices. *Nano Lett.* 12:3391-3398.
- Zhang, H., S. Wang, and B. Zhao. 2009. Histocompatibility of porous hydroxyapatite coating NiTi shape memory alloy. *Zhongguo Xiu Fu Chong Jian Wai Ke Za Zhi.* 23:468-472.
- Zhang, J., B. Senger, D. Vautier, C. Picart, P. Schaaf, J.C. Voegel, and P. Lavalley. 2005. Natural polyelectrolyte films based on layer-by layer deposition of collagen and hyaluronic acid. *Biomaterials.* 26:3353-3361.
- Zhang, W., C. Zhu, Y. Wu, D. Ye, S. Wang, D. Zou, X. Zhang, D.L. Kaplan, and X. Jiang. 2014. VEGF and BMP-2 promote bone regeneration by facilitating bone marrow stem cell homing and differentiation. *Eur Cell Mater.* 27:1-11; discussion 11-12.
- Zhao, D., K. Chang, T. Ebel, M. Qian, R. Willumeit, M. Yan, and F. Pyczak. 2013a. Microstructure and mechanical behavior of metal injection molded Ti-Nb binary alloys as biomedical material. *J Mech Behav Biomed.* 28:171-182.
- Zhao, Y., H.M. Wong, W. Wang, P. Li, Z. Xu, E.Y. Chong, C.H. Yan, K.W. Yeung, and P.K. Chu. 2013b. Cytocompatibility, osseointegration, and bioactivity of three-dimensional porous and nanostructured network on polyetheretherketone. *Biomaterials.* 34:9264-9277.

# Curriculum Vitae

## Flora GILDE

Born in Paris, France, December 17th, 1988

Portuguese

22A, rue Joseph Rey

38000 Grenoble

Tel : (+33) 06 52 59 37 57

E-mail: flora.gilde@gmail.com



## Education

2011 – 2014 **Grenoble Institute of Technology (Grenoble, France)**

*PhD, Biomaterials & Drug Delivery*

2010 – 2011 **Grenoble Institute of Technology (Grenoble, France)**

*Master 2, Biomaterials & Drug Delivery*

2006 – 2011 **University of Minho (Braga, Portugal)**

*Master degree in biomedical Engineering: Biomaterials, Rehabilitation and Biomechanics*

## Professional experience

2011 – 2014 **Grenoble INP, Laboratory of Materials and Physical Engineering, France**

*PhD thesis:*

Matrix-bound delivery of BMP-2 from a biomimetic film: protein structure, long-term stability and cellular uptake

2010 – 2011 **Grenoble INP, Laboratory of Materials and Physical Engineering, France**

*Master 2 (8 months internship):*

Structure and stability of poly (L-Lysine)/hyaluronan thin films as reservoirs for the bone morphogenetic protein-2

2009 - 2010 **3B's Research Group, Guimarães, Portugal**

*Master 1 (2 months internship):*

Preparation of bioactive membranes made of chitosan and alginate

## Languages

- **Portuguese:** mother tongue
- **French:** advanced level
- **English:** advanced level
- **Spanish:** to reactivate

## Hobbies

Backpacking and hiking, enjoying nature, cooking, dance and playing the piano.

## Publications

Gilde F, Fourel L, Guillot R, Paintrand I, Okada T, Boudou T, Albiges-Rizo C and Picart C. 2014. Matrix-bound delivery of BMP-2 to cells: internalization. *In preparation*.

Guillot R<sup>#</sup>, Gilde F<sup>#</sup>, Becquart P, Sailhan F, Lapeyrere A, Logeart-Avramoglou D, and Picart C. 2013. The stability of BMP loaded polyelectrolyte multilayer coatings on titanium. *Biomaterials*. 34:5737-5746

Caridade, SG, Monge C, Gilde F, Boudou T, Mano FJ, and Picart C. 2013. Free-standing polyelectrolyte membranes made of chitosan and alginate. *Biomacromolecules*. 14:1653-1660.

Gilde F, Maniti O, Guillot R, Mano JF, Logeart-Avramoglou D, Sailhan F, and Picart C. 2012. Secondary structure of rhBMP-2 in a protective biopolymeric carrier material. *Biomacromolecules*. 13:3620-3626.

## Conferences

### Oral communications:

- ESB 2014 “26<sup>th</sup> European Conference on biomaterials”, 30 August – 4 September, 2014, Liverpool, UK
- 1<sup>st</sup> ERC Biomim meeting “At the Frontier between Materials and Biology”, 10-12 April, 2013, Grenoble, France

### Posters:

- BIOMAT, “Assises Nationales de la Recherche en Biomatériaux”, 19 - 20 Mai, 2014, Autrans, France
- ESF conference, “Biological Surfaces and Interfaces”, 30 June - 5 July, 2013, Catalonia, Spain
- ERC Grantees Conference, “Frontier Research in Chemistry”, 22 - 24 November, 2012, Strasbourg, France
- GDR 3070: “Physique de la cellule au tissu”, 22 – 24 Octobre, 2012, Autrans, France
- Nanosciences Foundation days, 2011, 2012, Grenoble, France

## Abstract

The natural surface of bulk prostheses materials is not always suitable for successful osteointegration of implants. Therefore, improving the surface to render it osteoconductive and osteoinductive is needed. The controlled delivery of osteoinductive bone morphogenetic proteins (BMPs) from the surface of implantable materials would enable faster and better bone formation around the implant. In particular, BMP-2 plays an important role in the early phase of differentiation of stem cells in bone cells. The coating of natural polymers that have a high affinity for BMP-2 would enable BMP retention and localized delivery at the implant surface. Using the layer-by-layer technique, we have developed a coating made of the biopolymers hyaluronan and poly(L-Lysine), which acts as a reservoir to trap BMP-2 and to present them to cells in a "matrix-bound" manner. The *in vitro* bioactivity and *in vivo* osteoinductive properties of BMP-2-loaded films have previously been proved. In this work, the aim is to further understand the interaction of the BMP-2 with the film and the uptake of BMP-2 by the cells. First, the secondary structure of matrix-bound BMP-2 was studied and compared to its structure in solution. Second, the impact of drying, long term storage and sterilization on film structure and bioactivity were assessed. Finally, we investigated if and how matrix-bound BMP-2 is internalized by the cells from the different cross-linked films, the internalization route and its relation to BMP-2 signaling.

## Résumé

La surface naturelle des prothèses n'est pas toujours idéale pour l'obtention d'une bonne ostéo-intégration. Par conséquent, l'amélioration des propriétés de surface pour les rendre ostéo-conductrices ou ostéo-inductrices est souhaitable. La délivrance contrôlée de protéines ostéo-inductrices de la famille des *bone morphogenetic proteins* (BMPs) par la surface des matériaux implantables permettrait une formation osseuse optimisée et plus rapide autour de l'implant. En particulier, la BMP-2 est importante dans la phase initiale de la différenciation vers l'os. En raison de leur similarité avec les tissus naturels, l'utilisation des revêtements de biopolymères qui ont une bonne affinité avec les molécules bioactives semble prometteuse pour le chargement et la délivrance de la BMP-2. Notre équipe a déjà mis au point un film à base des biopolymères hyaluronane et de poly(L-lysine), en utilisant la technique d'assemblage couche par couche. Ce film constitue un réservoir qui permet de présenter la BMP-2 "liée à la matrice". La bioactivité *in vitro* et les propriétés ostéo-inductrices *in vivo* de ces films ont déjà prouvées. Dans ce travail, nous avons cherché à mieux comprendre l'interaction de la BMP-2 avec le film et l'interaction des cellules avec la BMP-2. Tout d'abord, nous avons étudié la structure de la BMP-2 piégée dans les films et nous l'avons comparé à celle en solution; puis nous avons évalué l'impact du séchage, du stockage à long terme et de la stérilisation sur la structure du film et sa bioactivité. Enfin, nous avons étudié l'internalisation de la BMP-2 par les cellules en fonction de la réticulation du film et avons étudié la relation entre internalisation et voies de signalisation.